

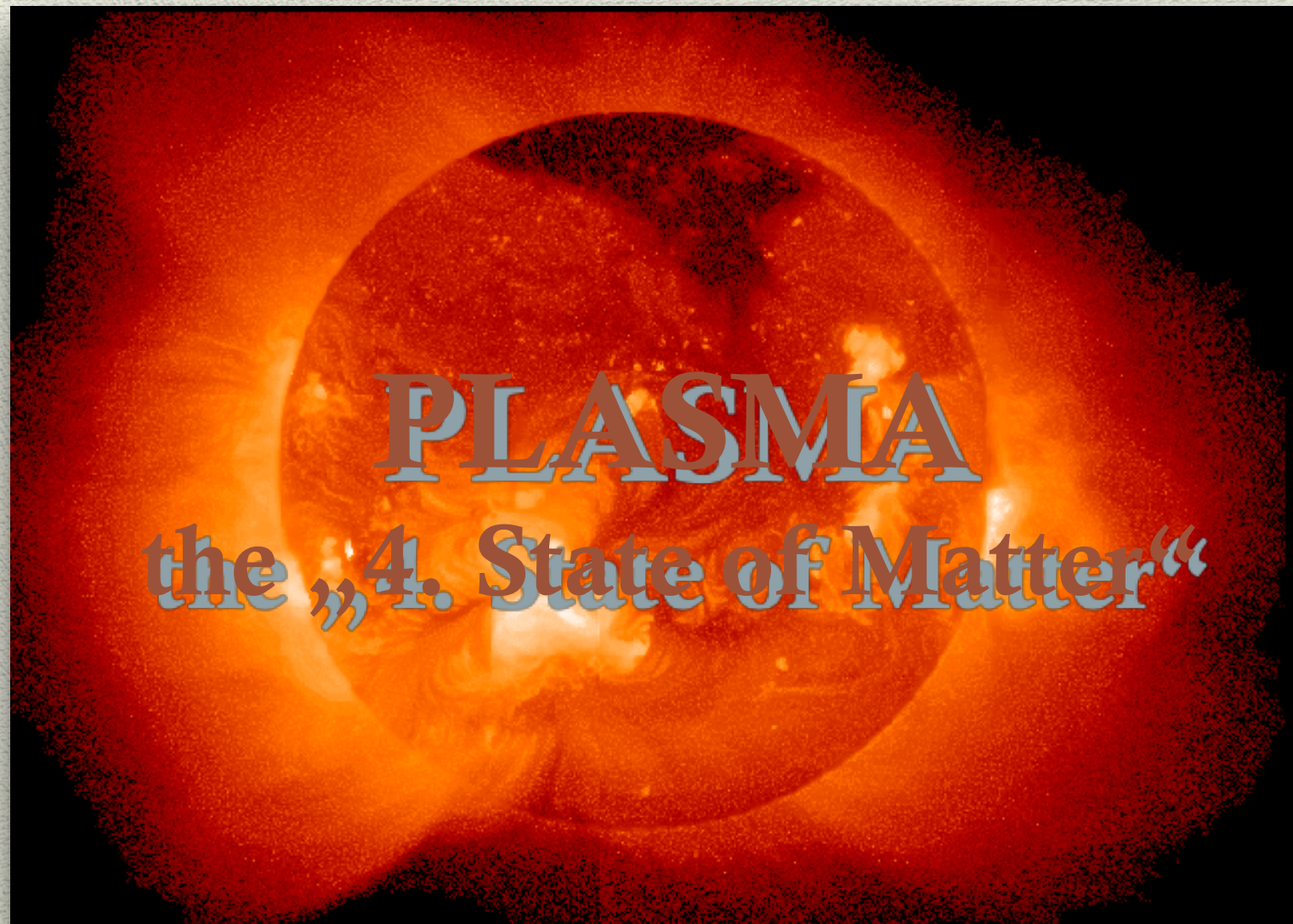
Plasmas for
Astrophysics,
Nuclear
Decays
Observation and
Radiation for
Archaeometry

David Mascali,



Laboratori Nazionali del Sud - 18 Feb. 2019

Physics and Technology of magnetized plasmas



Some Applications

Light

(see lamps und projector)

Surface Hardening



Plasma Monitor (Television)

large, well resolving, flat



cold
plasma

Surface Refinement

Plasma treated roof
of the cathedral
„Christ the Saviour“
in Moscow. Steel tiles
covered with films
of Titanium Nitride
and diamond-like carbon



Main Plasma Constituents

- positively charged ions
- electrons
- neutrals

Key Plasma Properties

- quasineutrality
- collective behavior

Electron Temperature and Distribution Functions

Weakly ionized plasma is a mixture of different gases:
neutral gas, ion gas and electron gas.

Under the action of electromagnetic fields electrons gain much more energy from the EM-field than ions. Their mean energy exceeds by far the mean energy of the ions and the neutrals. Thus

$$T_e \gg T_+, T_n$$

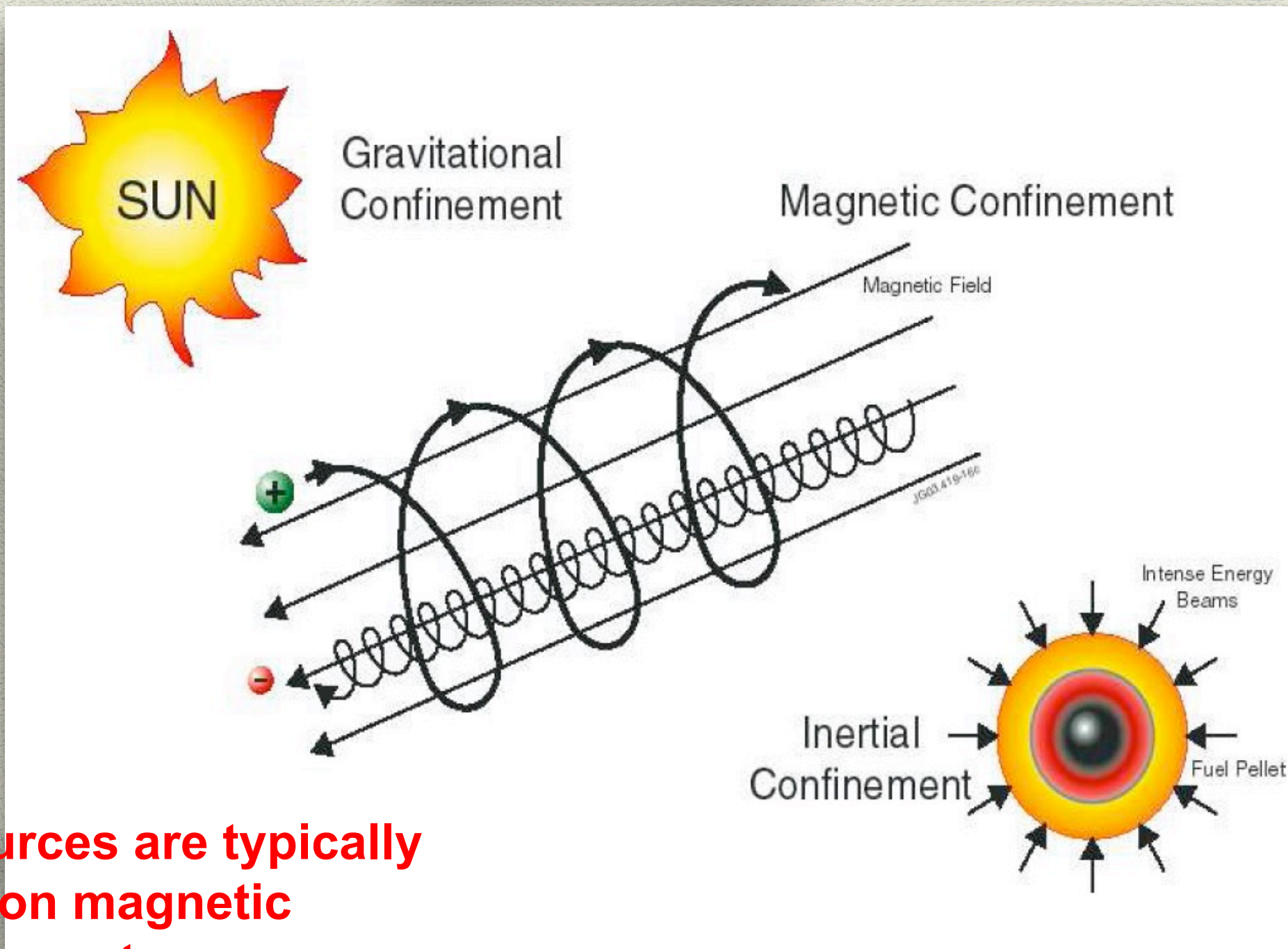
In plasma temperatures are measured in eV:

$$kT = 1\text{eV corresponds to } T = 11600 \text{ K}$$

Typical values: $kT_e = 1... 10^4 \text{ eV}$ for electrons (i.e. $10^4 - 10^8 \text{ }^\circ\text{K !!}$)

$$kT_+ = 0.03...1\text{eV for ions}$$

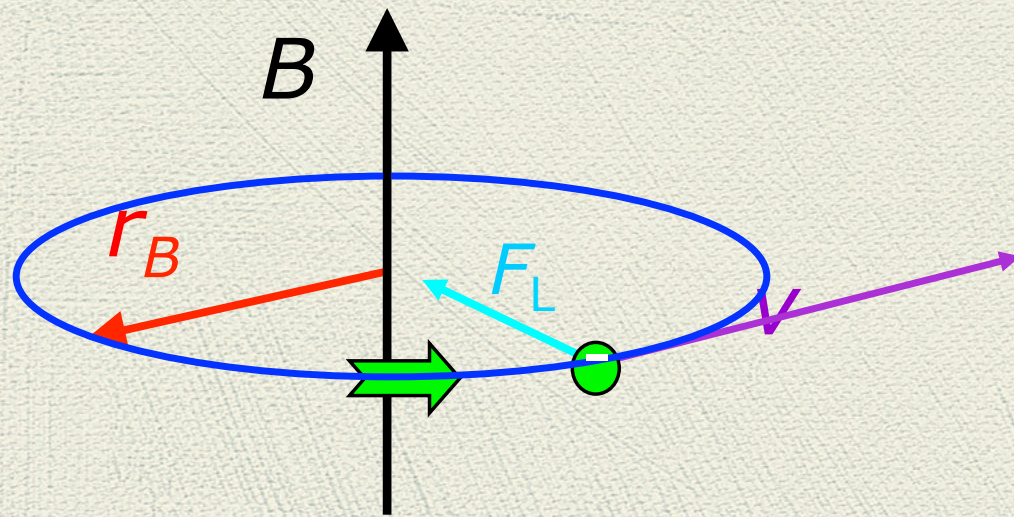
How do plasmas can be confined?



Ion sources are typically based on magnetic confinement

Gyration of ions and electrons under the action of a static magnetic field

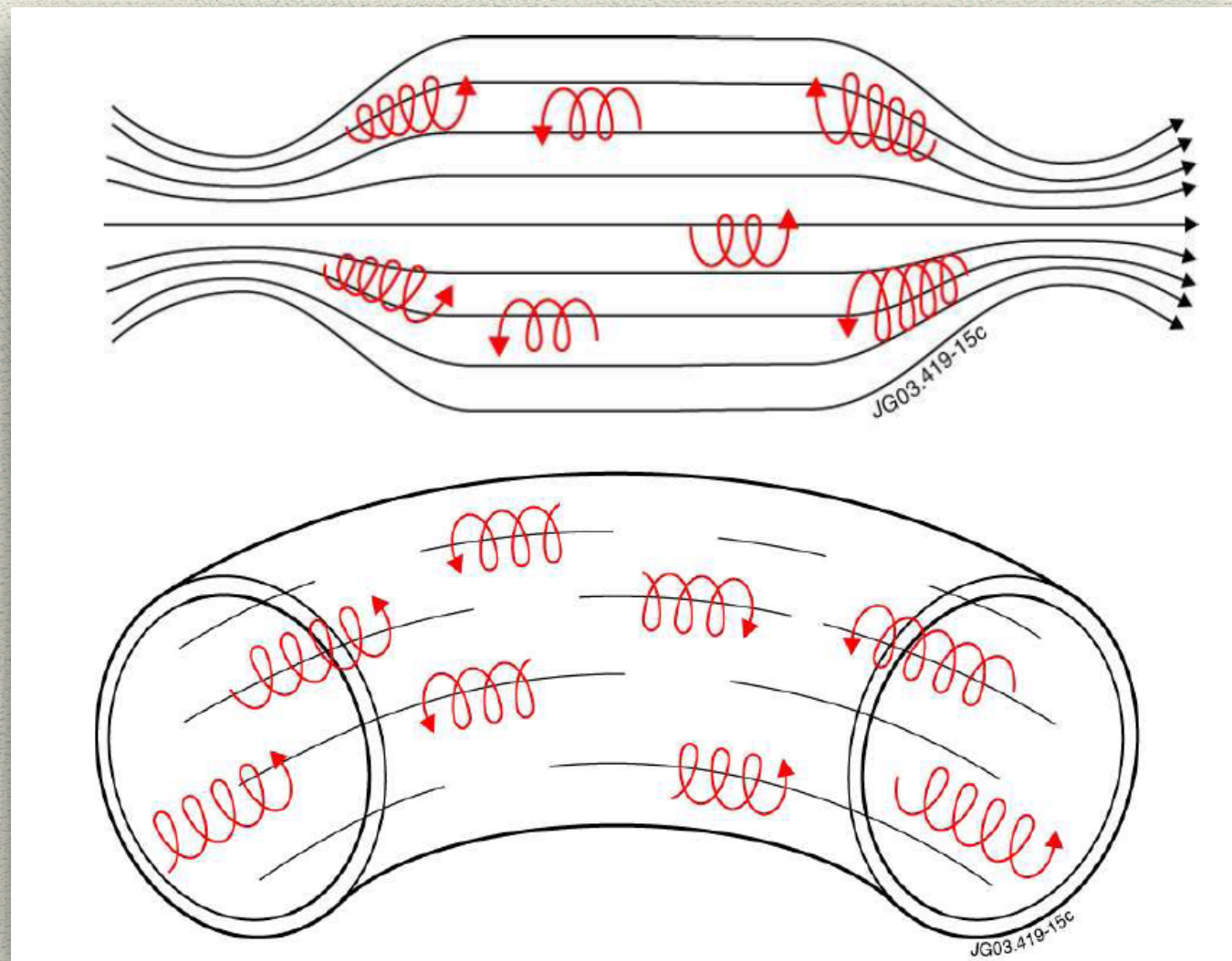
- ❖ The Lorentz force \mathbf{F}_L exerted by a static magnetic field of induction B on particles of mass m bearing an elementary charge e causes a circular motion.
- ❖ The radius (cyclotron radius) r_B of the circular trajectory is given by $r_B = mv/eB$
- ❖ The corresponding cyclotron frequency ω_B does not depend on the particle velocity v : $\omega_B = eB/m$



$$\mathbf{F}_L = q\mathbf{v} \times \mathbf{B}$$

Magnetic Confinement

Magnetic fields intrinsically force charged particles to reduce freedom degrees: electrons spiralyze around the field lines and can be trapped for several ms in mirror machines or toroidal structures.



MIRROR STRUCTURES

have axial symmetry and can be produced by sequences of room temperature or SC coils. They are commonly used in ion sources field

TOROIDAL CONFINEMENT

is typical of Fusion Machines like TOKAMAKS or STELLARATORS

The ideal confinement requires some stringent conditions on plasma equilibrium and stability

Plasma can also be viewed as fluids. Therefore the confinement and its equilibrium and stability can be investigated by looking to the equilibrium between the plasma kinetic pressure and the magnetic (confining) field pressure.

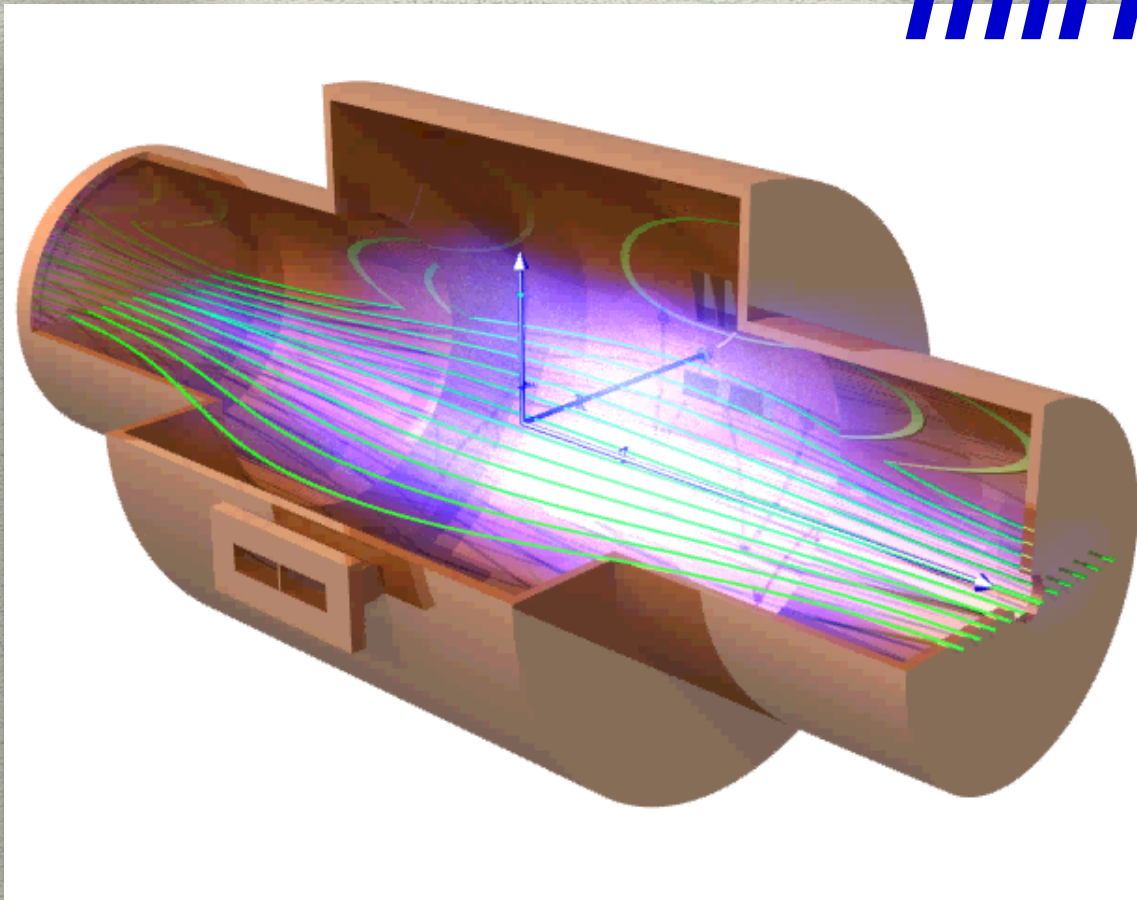
$$p + \frac{B^2}{2\mu_0} = \text{costante}$$

The stability of the confinement can be studied as a function of the β parameter, which is the ratio between the kinetic and magnetic pressures.

The condition for a magnetically stable plasma is that $\beta \ll 1$

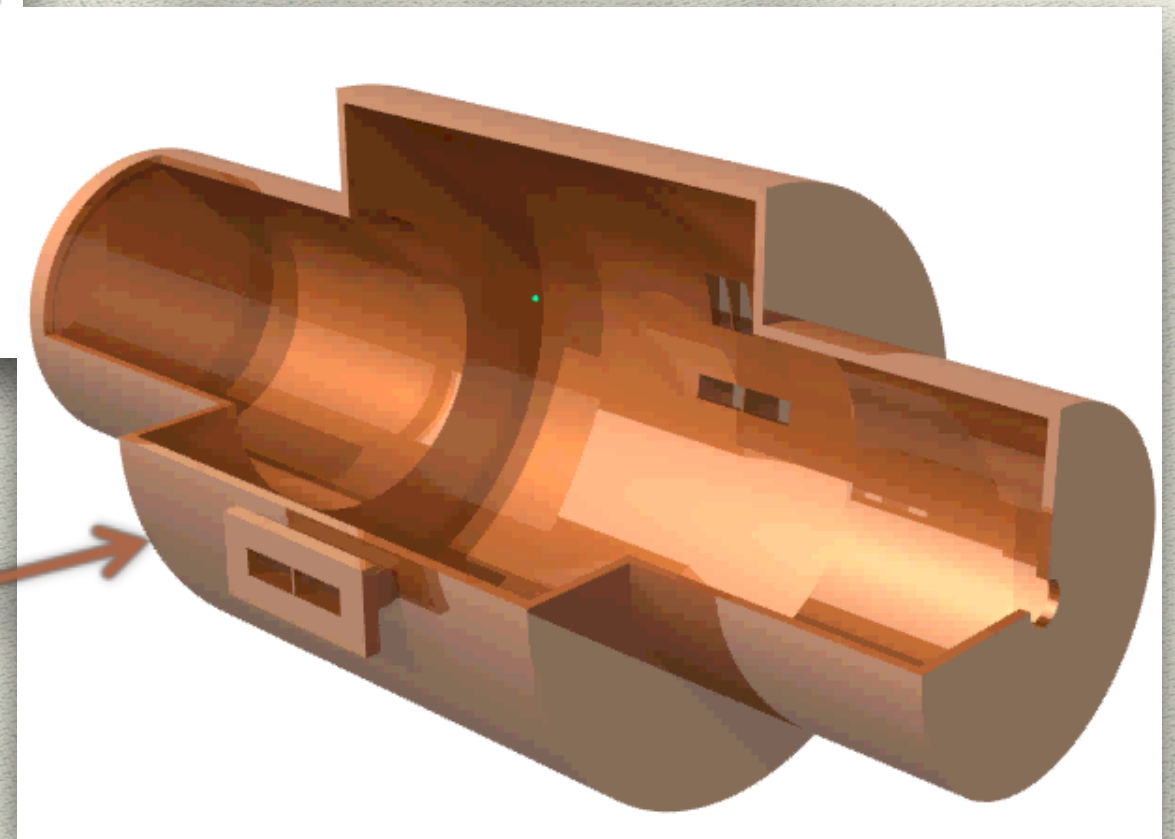
$$\beta \equiv \frac{\sum nkT}{\frac{B^2}{2\mu_0}}$$

Principles of magnetic mirrors

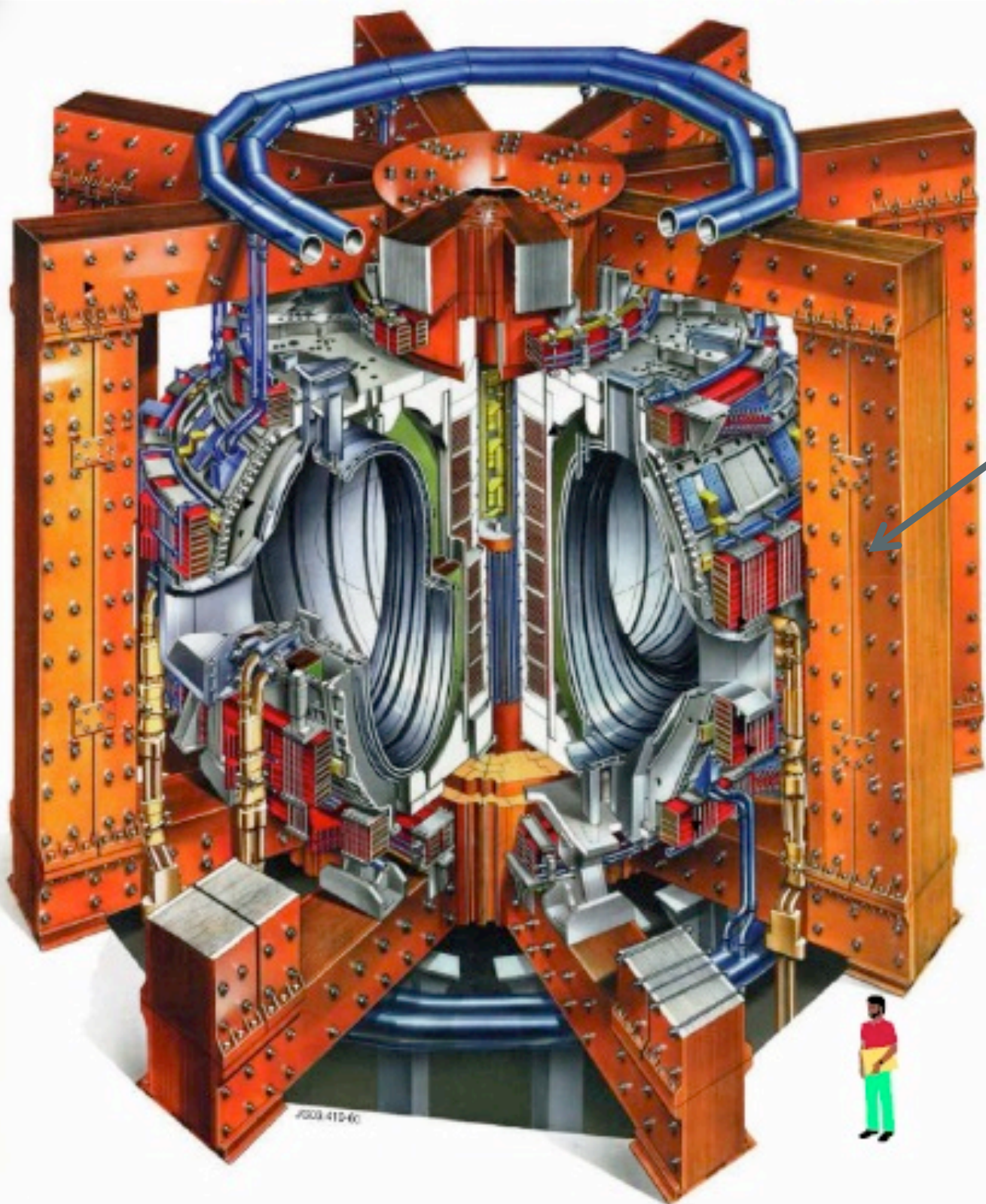


Particles trajectories in plasmas are affected by several drifts, due to spontaneous or induced E fields, B lines curvature, B gradient, gravity, etc...

Particles rebound inside the trap and are contemporaneously affected by the "phi" drift around the magnetic axis, due to the B curvature and axial gradient

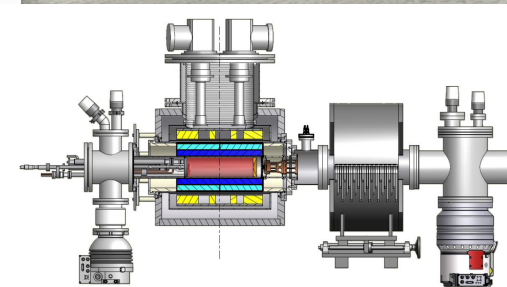


JET: il Tokamak Europeo

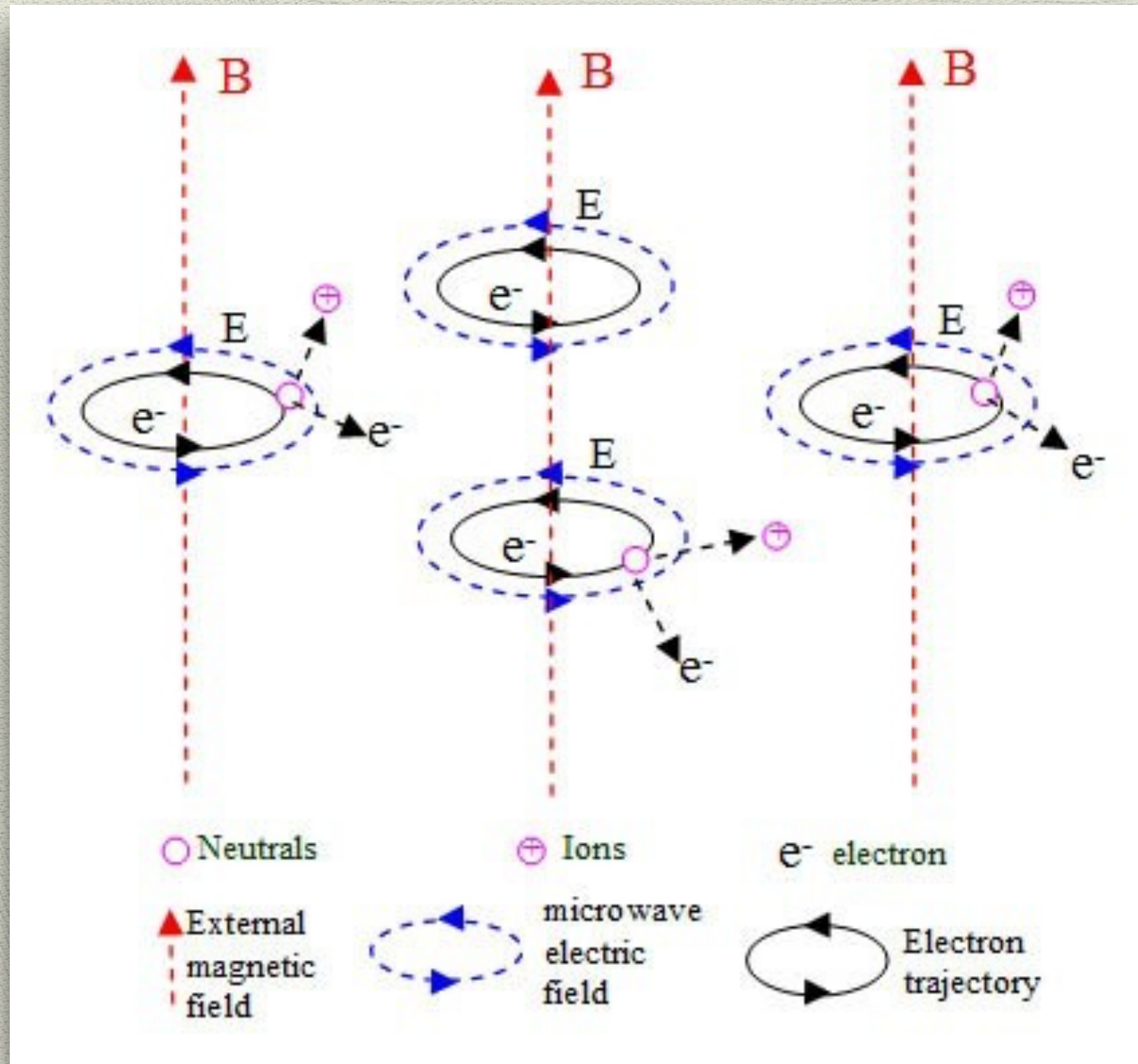


JET Tokamak for nuclear fusion (energy production)

AISHA: an extremely compact plasma machine



The plasma heating via Electron Cyclotron Resonance



LNS plasma team topics

Ion Beams
Production

Advanced
Sensors R&D

RF probes

Wavelet-Analysis

High-Resolution
X-ray Spectroscopy

Fundamental
plasma
investigation

Ultra Compact Proton Source
& negative noble-gas ions
injector

Optical Emission
Spectroscopy

RF Polarimetry

Plasmas for
Astrophysics,
Nuclear
Decays
Observation and
Radiation for
Archaeometry



INFN-LNS plasma-based machines

Name	Type	Trap	Species	I	$n_e - T_e$
<i>SERSE</i> CS Injector	ECR	B-min S.C.	from H to Pb	$O^{6+} \sim 500 \mu A$ $Ar^{16+} \sim 20 \mu A$	$n_e \sim 10^{13} \text{ cm}^{-3}$ $T_e^{warm} \sim 1 \div 10 \text{ keV}$ $T_e^{hot} \sim 100 \text{ keV}$
<i>CAESAR</i> CS Injector	ECR	B-min N.C.	Ne, Ar	H, O, N, $O^{6+} \sim 80 \mu A$ $Ar^{14+} \sim 20 \mu A$	$n_e \sim 10^{12} \text{ cm}^{-3}$ $T_e^{warm} \sim 0.5 \div 5 \text{ keV}$ $T_e^{hot} \sim 50 \text{ keV}$
<i>PS-ESS</i>	MDIS	B-flat N.C.	Protons, also H^{2+} , D	$\sim 100 \text{ mA}$	$n_e \sim 10^{12} \text{ cm}^{-3}$ $T_e \sim 15 \div 25 \text{ eV}$
<i>FPT</i> Test-bench	Trap	Bottle B-flat Beach	gaseous elements		$n_e \sim 10^{12} \div 10^{13} \text{ cm}^{-3}$ $T_e \sim 15 \div 25 \text{ eV}$
<i>AISHa</i> Hadrontherapy machine	ECR	B-min S.C.	C, Li, O, Ar	$C^{4+} \sim 800 \mu A$ $O^{6+} \sim 800 \mu A$	$n_e \sim 10^{12} \div 10^{13} \text{ cm}^{-3}$ $T_e \sim 15 \div 25 \text{ eV}$
<i>VIS</i>	MDIS	B-flat S.C.	H, H^{2+} , D, He	$H^+ \sim 60 \text{ mA}$ $He^+ \sim 40 \text{ mA}$	$n_e \sim 10^{12} \div 10^{13} \text{ cm}^{-3}$ $T_e \sim 15 \div 25 \text{ eV}$

Catania: a fertile network of "plasma-users"



100 m

High power proton accelerator for spallation

ESS accelerator

Design Drivers:

High Average Beam Power

5 MW

High Peak Beam Power

125 MW

High Availability

> 95%

Key parameters:

-2.86 ms pulses

-2 GeV

-62.5 mA

-14 Hz

-Protons (H⁺)

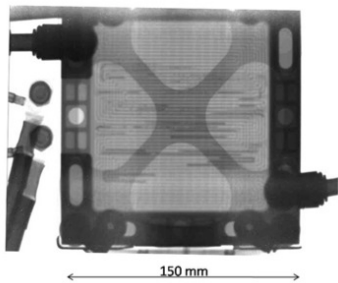
-Low losses

-Low heat loss cryostats for minimum energy consumption

-Flexible design for future upgrades

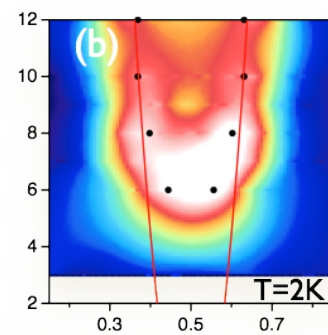
Boosting neutron science for fundamental physics and applications

Charge neutral deeply penetrating



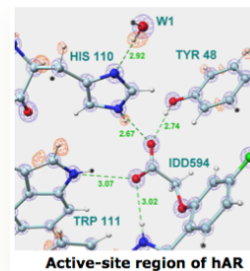
Li motion in fuel cells

S=1/2 spin probe directly magnetism



Solve the puzzle of High-Tc superconductivity

Nuclear scattering sensitive to light elements and isotopes



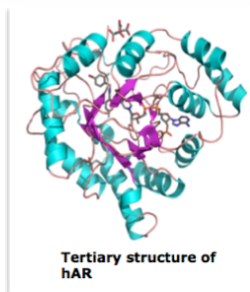
Active sites in proteins



Help build electric cars



Efficient high speed trains



Tertiary structure of hAR

Better drugs



The proton source for ESS accelerator

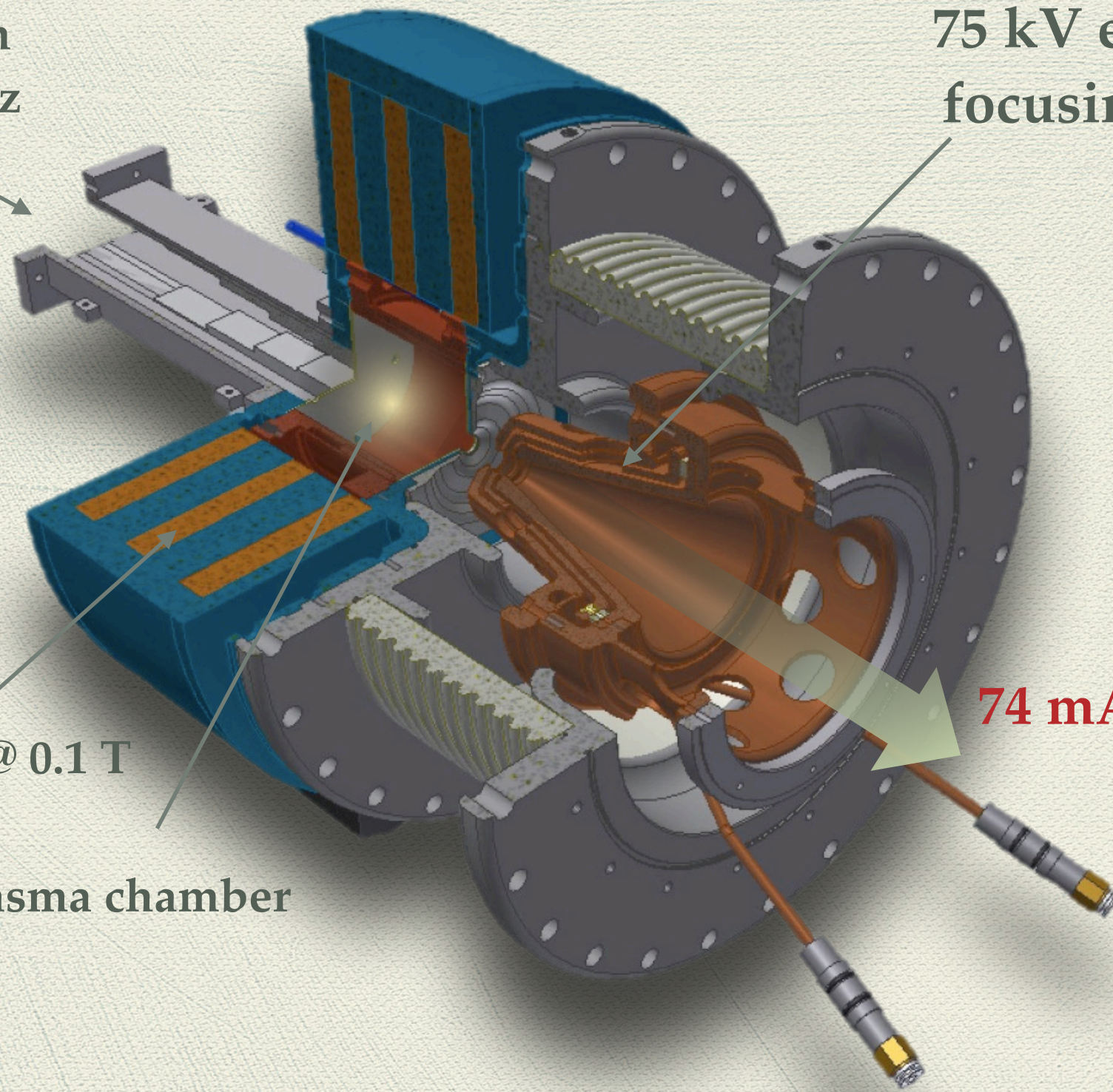
1 kW RF injection system at 2.45 GHz

75 kV extraction/focusing system

Magnetic system @ 0.1 T

Plasma chamber

74 mA proton beam

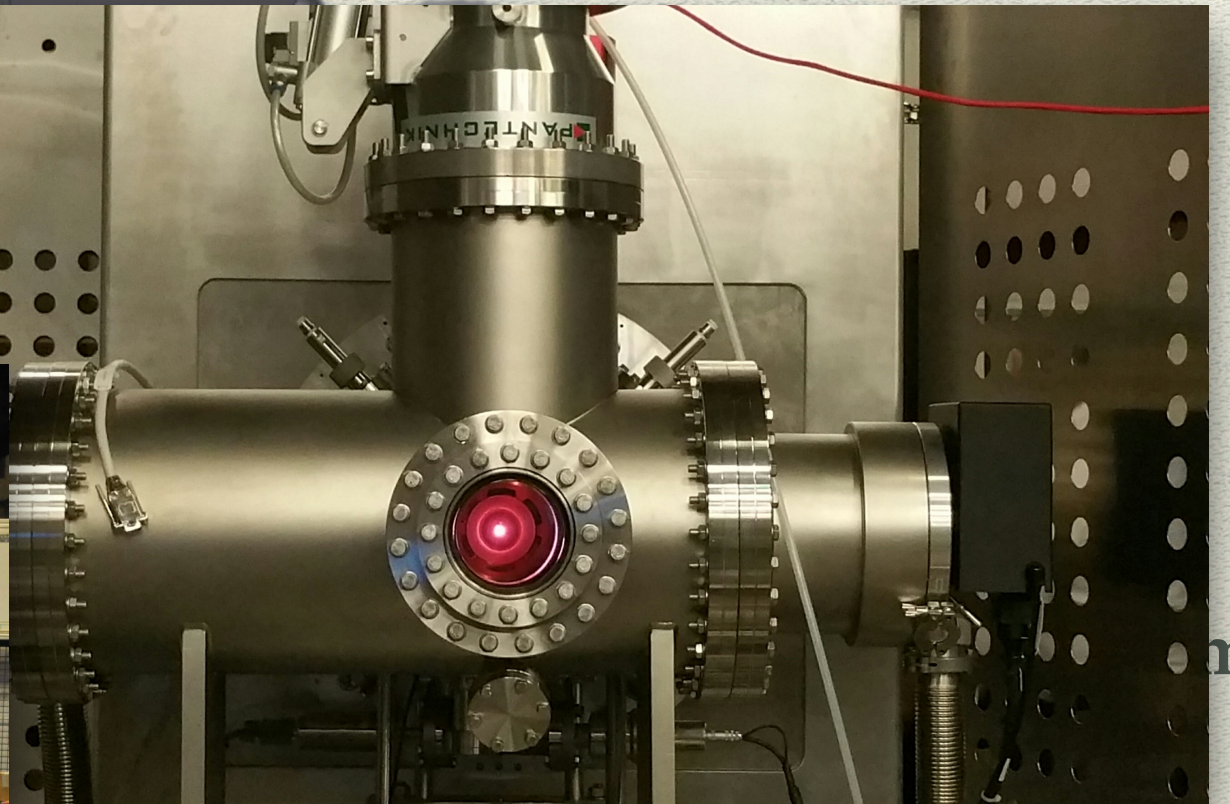
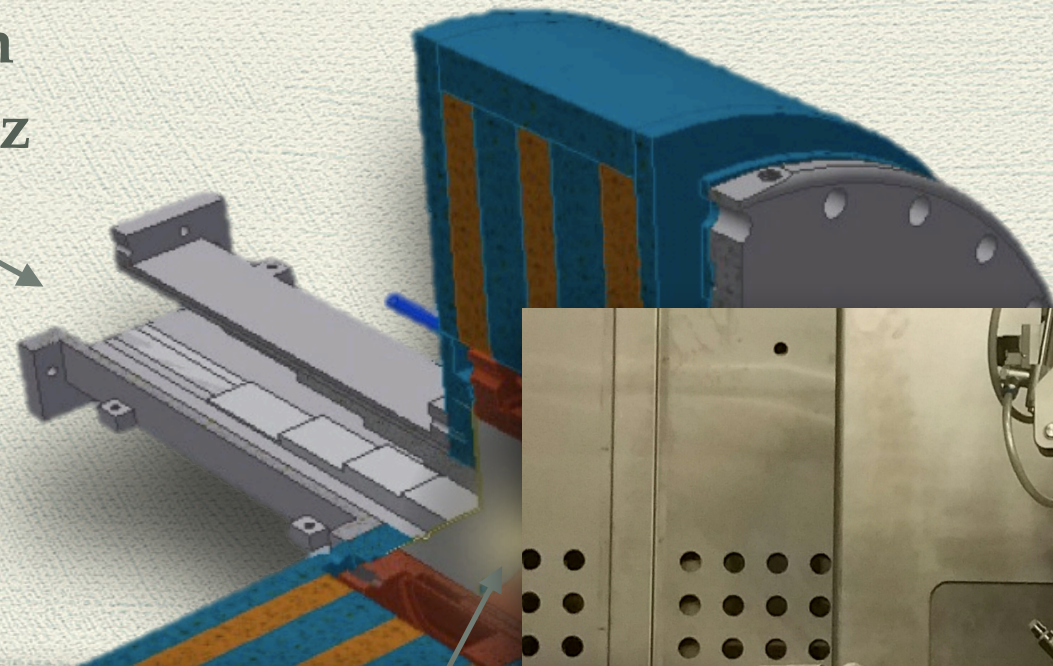




The proton source for ESS accelerator

1 kW RF injection system at 2.45 GHz

75 kV ext. system



100 mA proton curr. - 0.2 pi mm mrad reached!!



POR – U.E. funds for regional development

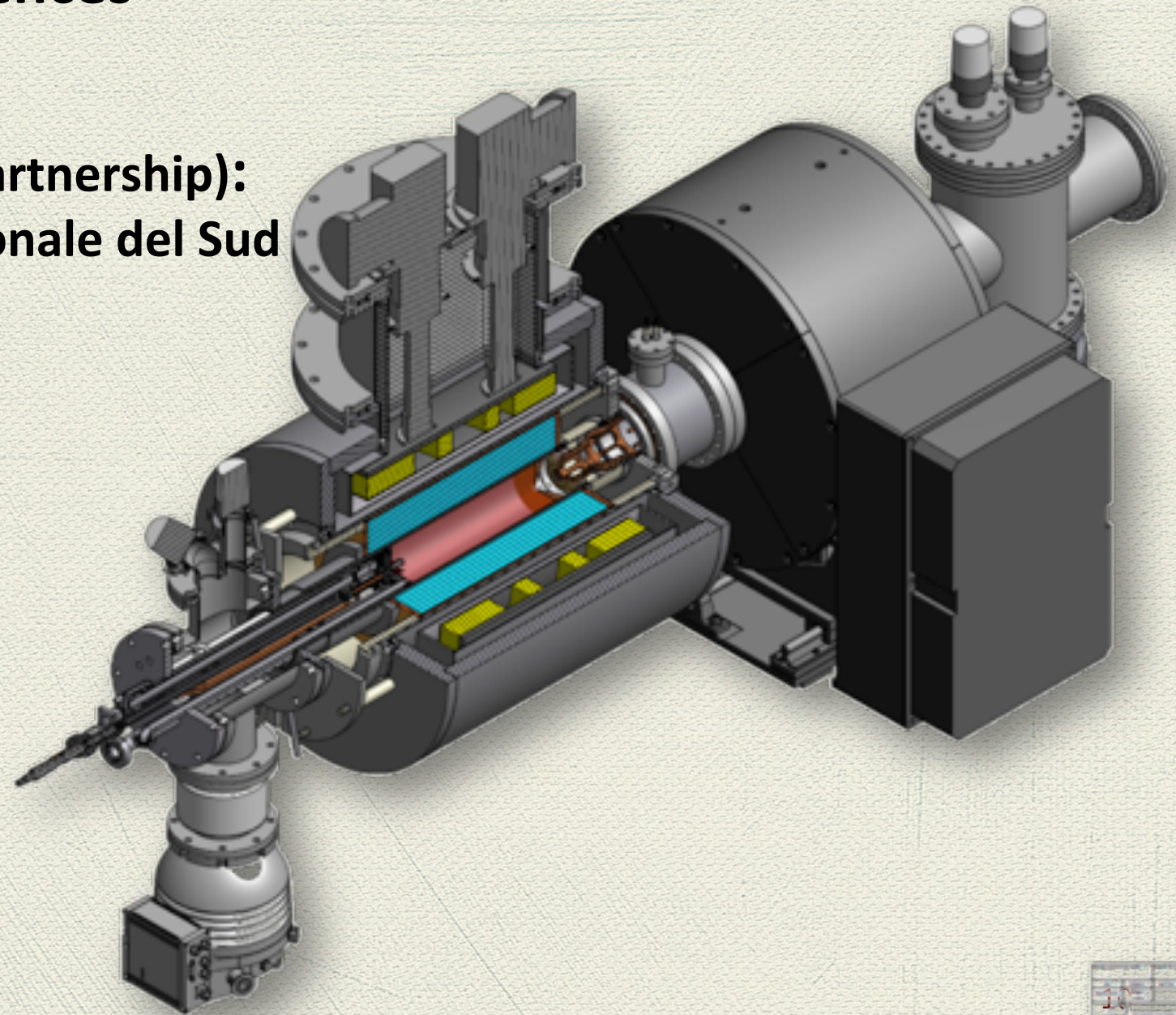


Regione Siciliana

Topics: Health and Life Sciences

Proponents (public-private partnership):

- INFN-Laboratori Nazionale del Sud
- Hitec2000 srl
- C3SL srl
- Unico srl



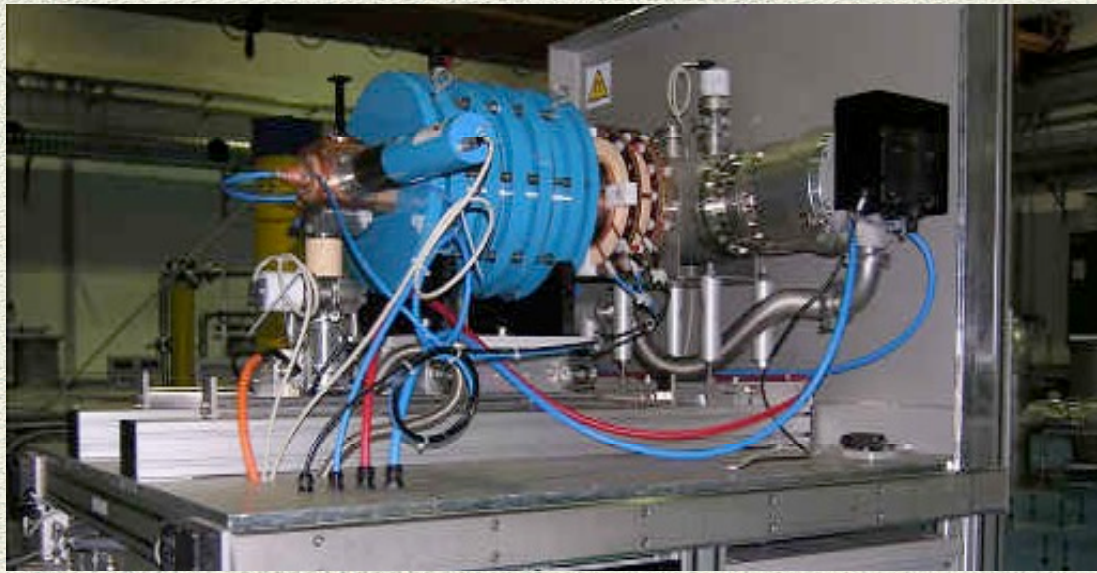
AISHa





The GOAL: make a step forward w.r.t. PK-SUPERNANOGEN for CNAO and other hadron therapy facilities

Measured performances



Ions	Current (request) [μA]	Current (avail.) [μA]	After improvements by INFN-LNS [μA]	Emittance (request) π mm.mrad	Emittance (new extractor) π mm.mrad	Stability [99,8%]
C ⁴⁺	200	200	250	0.75	0.56	36 h
H ₂ ⁺	1000	1000		0.75	0.42	2 h
H ₃ ⁺	700	600	1000	0.75	0.67	8 h
He ⁺	500	500		0.75	0.60	2 h

Significant improvements have been provided by INFN-LNS: frequency tuning effect, gas control, extractor reliability, etc. but further improvements are not possible and different set of requirements are done for the treatments by therapy experts.



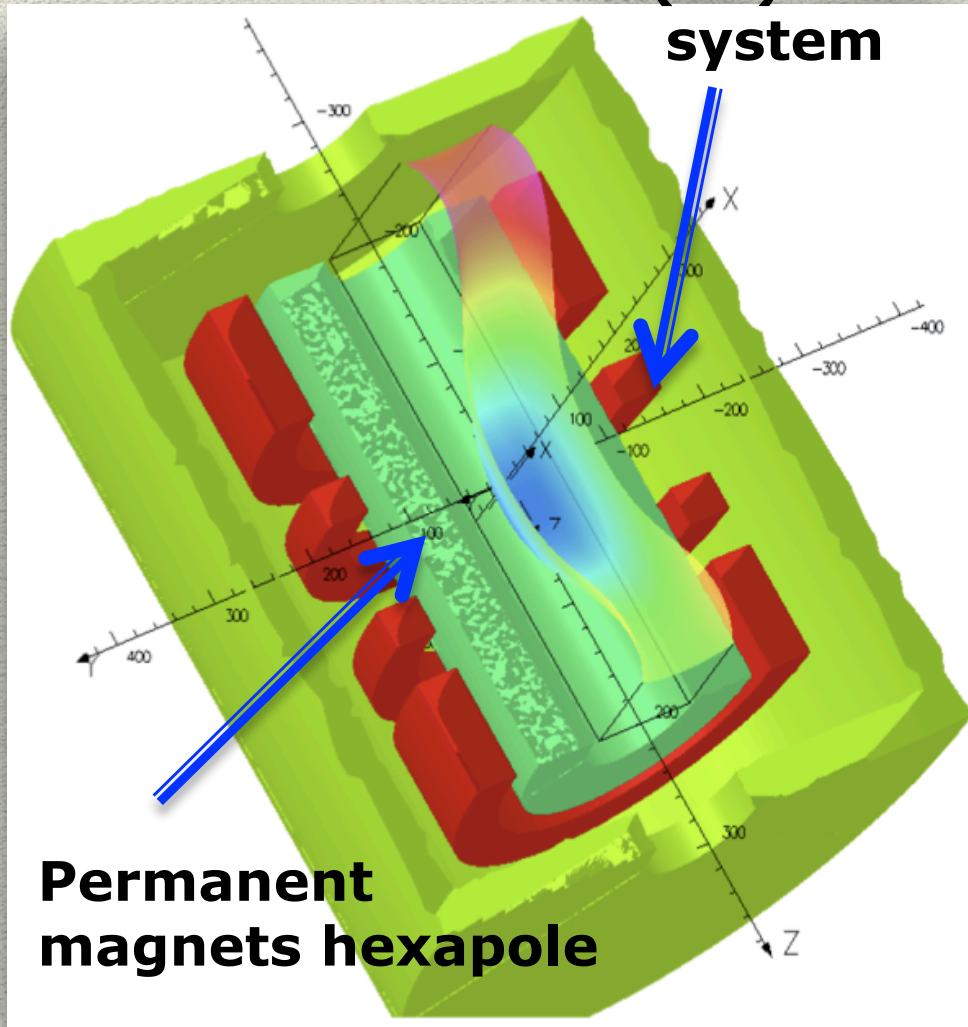
AISHa



AISHA

Advanced Ion Source for HAdrontherapy

4 (SC) coils system



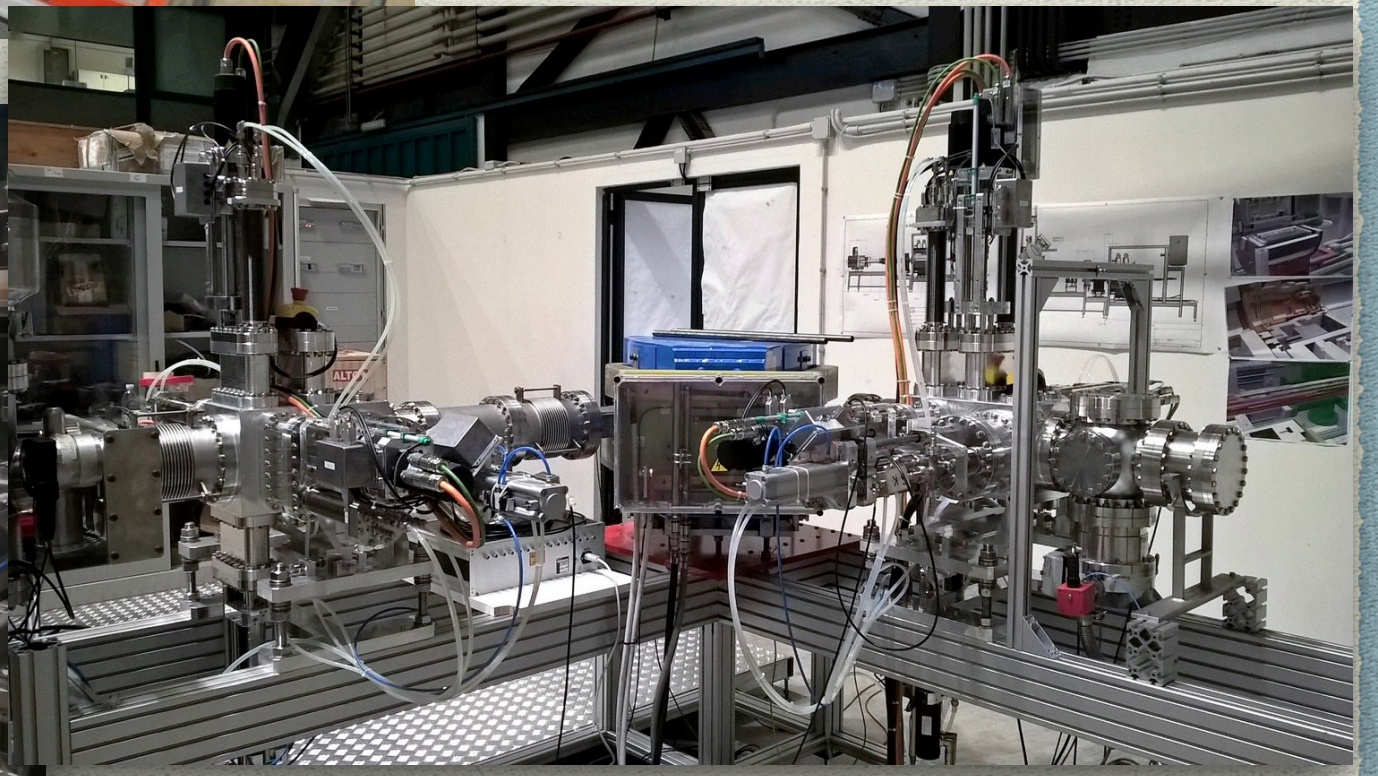
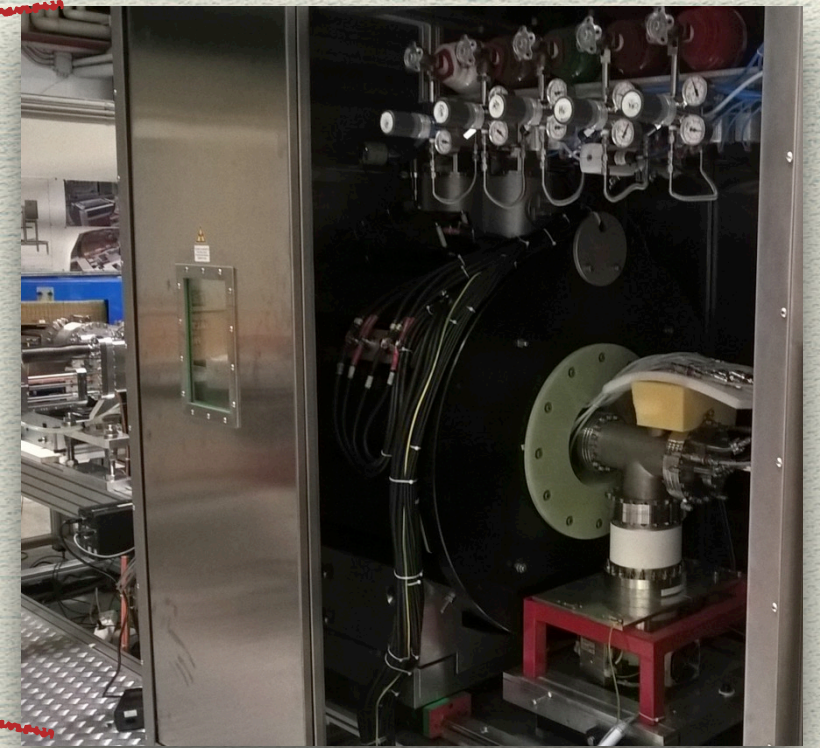
Permanent magnets hexapole

AISHA is a hybrid ECRIS: the radial confining field is obtained by means of a permanent magnet hexapole, while the axial field is obtained with a **Helium-free superconducting system**.

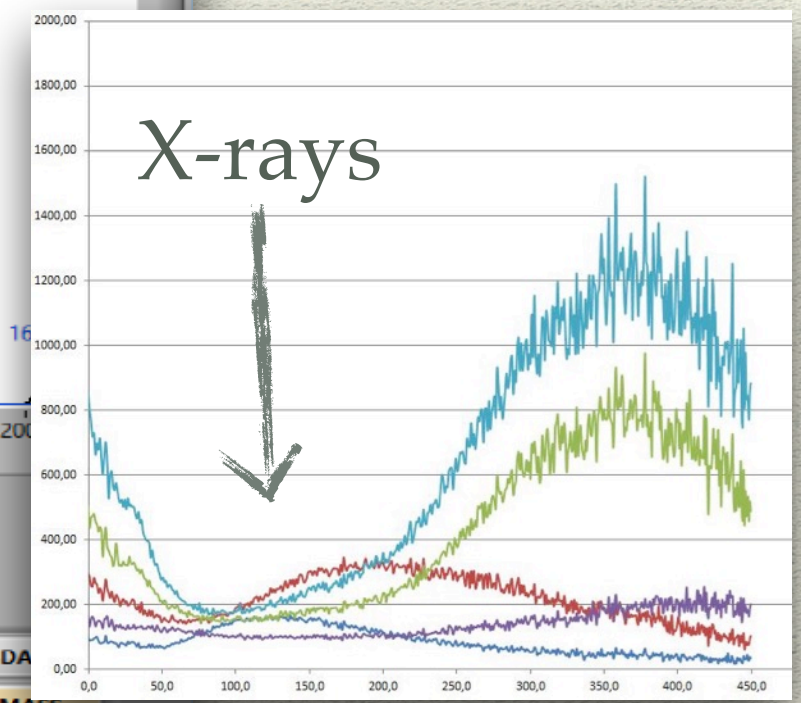
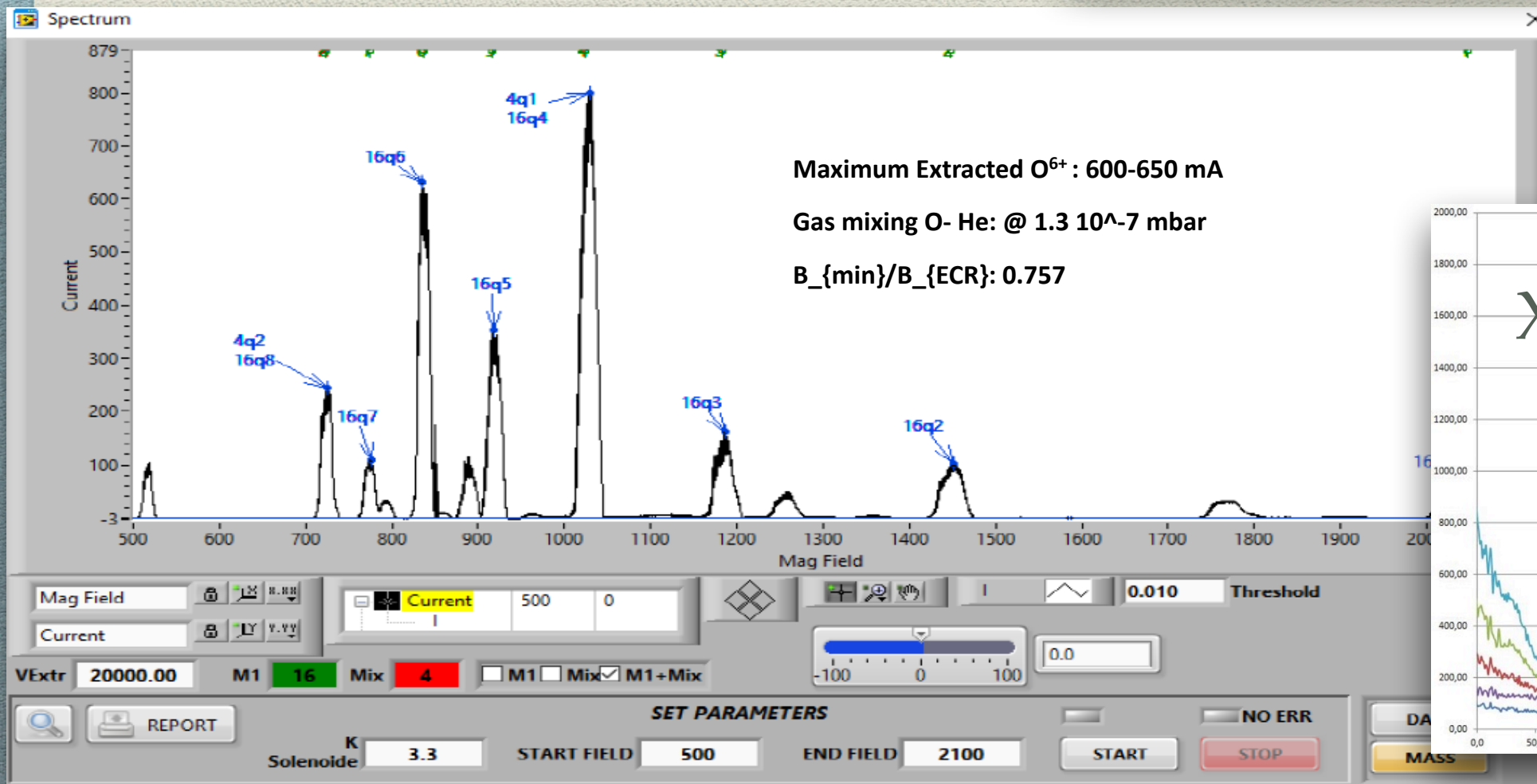
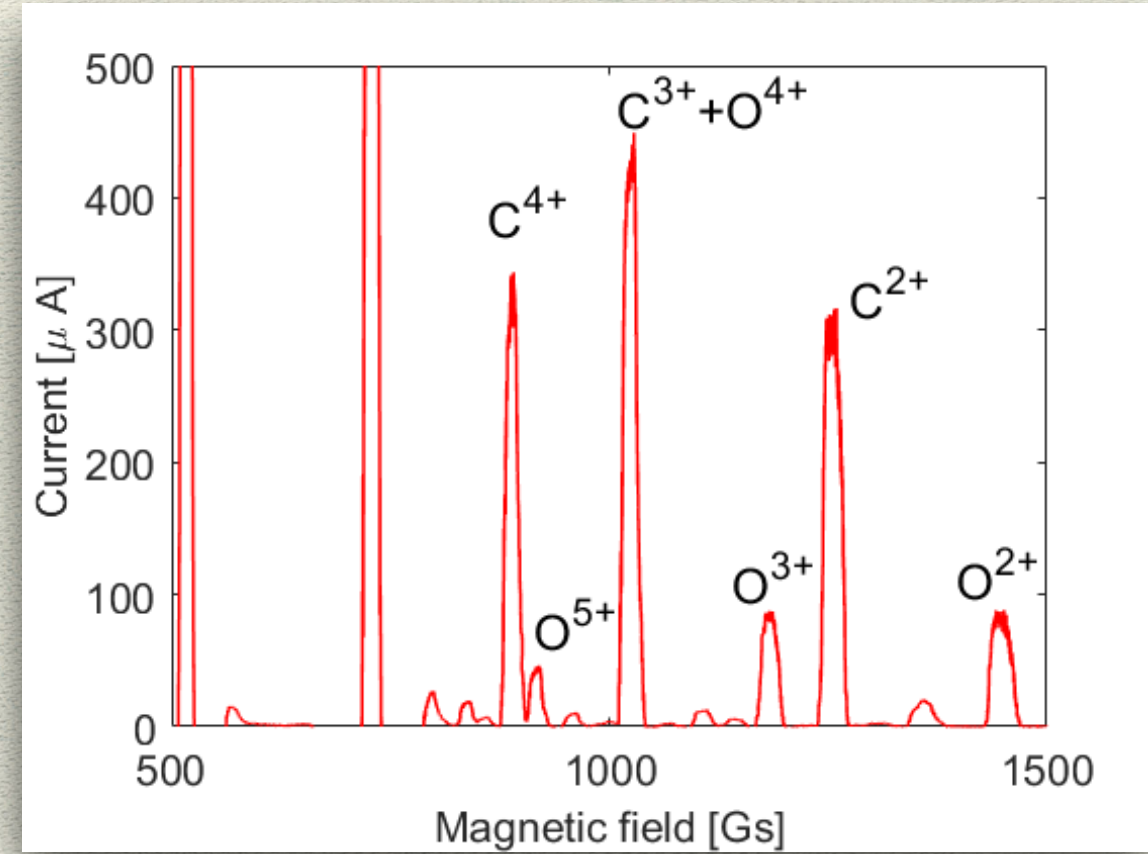
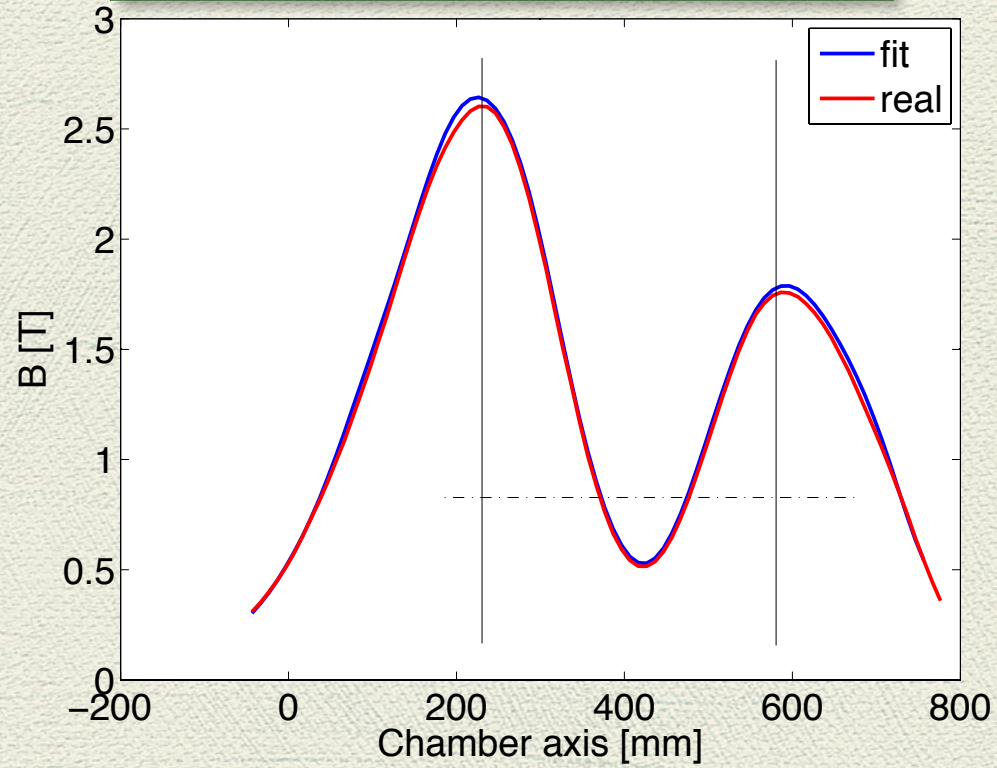
The **operating frequency of 18 GHz will permit** to maximize the plasma density by employing commercial microwave tubes meeting the needs of the installation in hospital environments.

Radial field	1.3 T
Axial field	2.7 T - 0.4 T - 1.6 T
Operating frequencies	17.3 GHz – 21.5 GHz
Operating power	1.5 + 1.5 kW (max)
Extraction voltage	40 kV (max)
Chamber diameter / length	Ø 92 mm / 360 mm
LHe	Free
Warm bore diameter	274 mm
Source weight	1400 kg

AISHa



First Spectra



LNS plasma team topics

**Ion Beams
Production**

Advanced

Sensors R&D

RF probes

Wavelet-Analysis

**Fundamental
plasma
investigation**

*Ultra Compact Proton Source
& negative noble-gas ions
injector*

*High-Resolution
X-ray Spectroscopy*

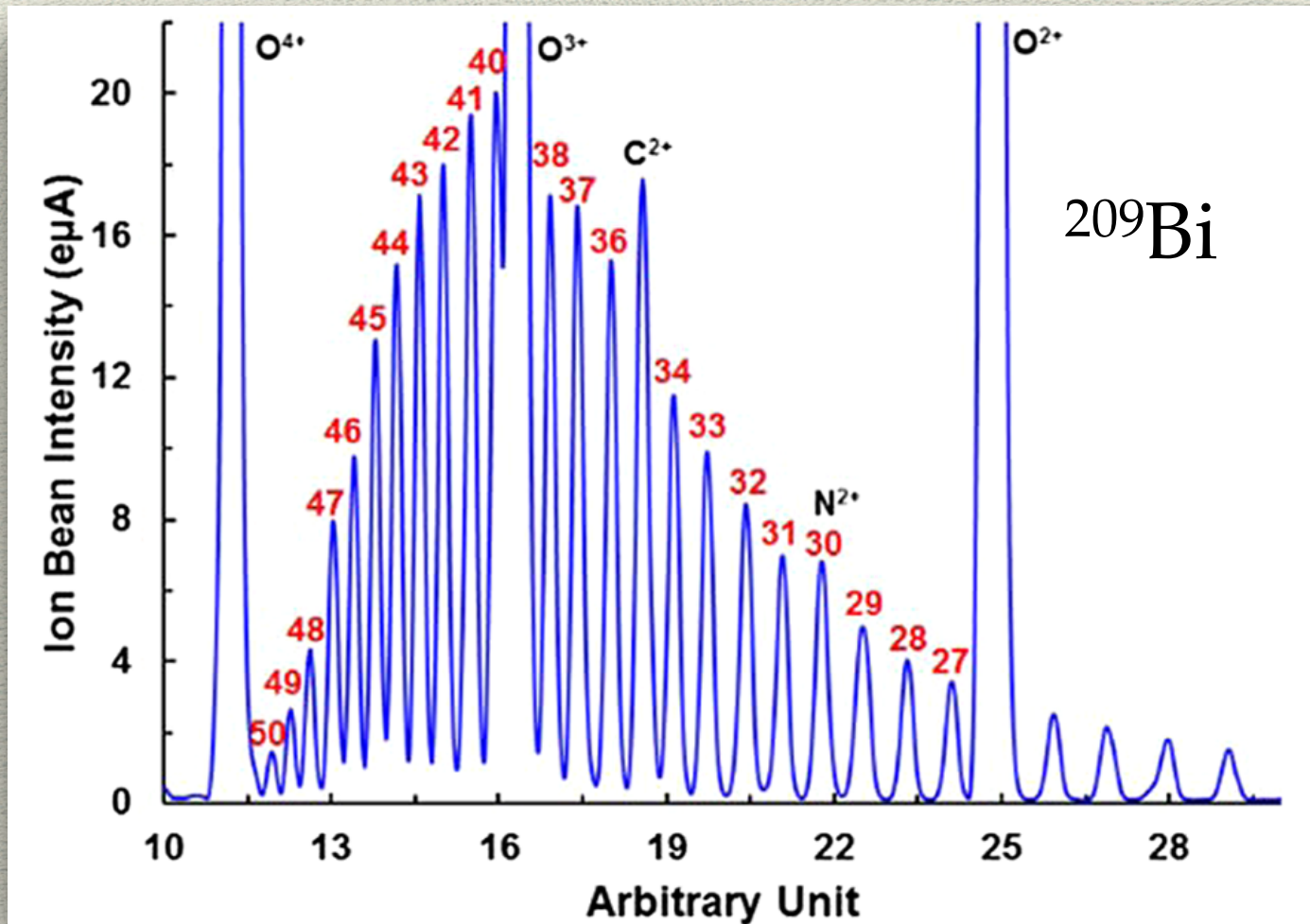
*Optical Emission
Spectroscopy*

RF Polarimetry

*Plasmas for
Astrophysics,
Nuclear
Decays
Observation and
Radiation for
Archaeometry*



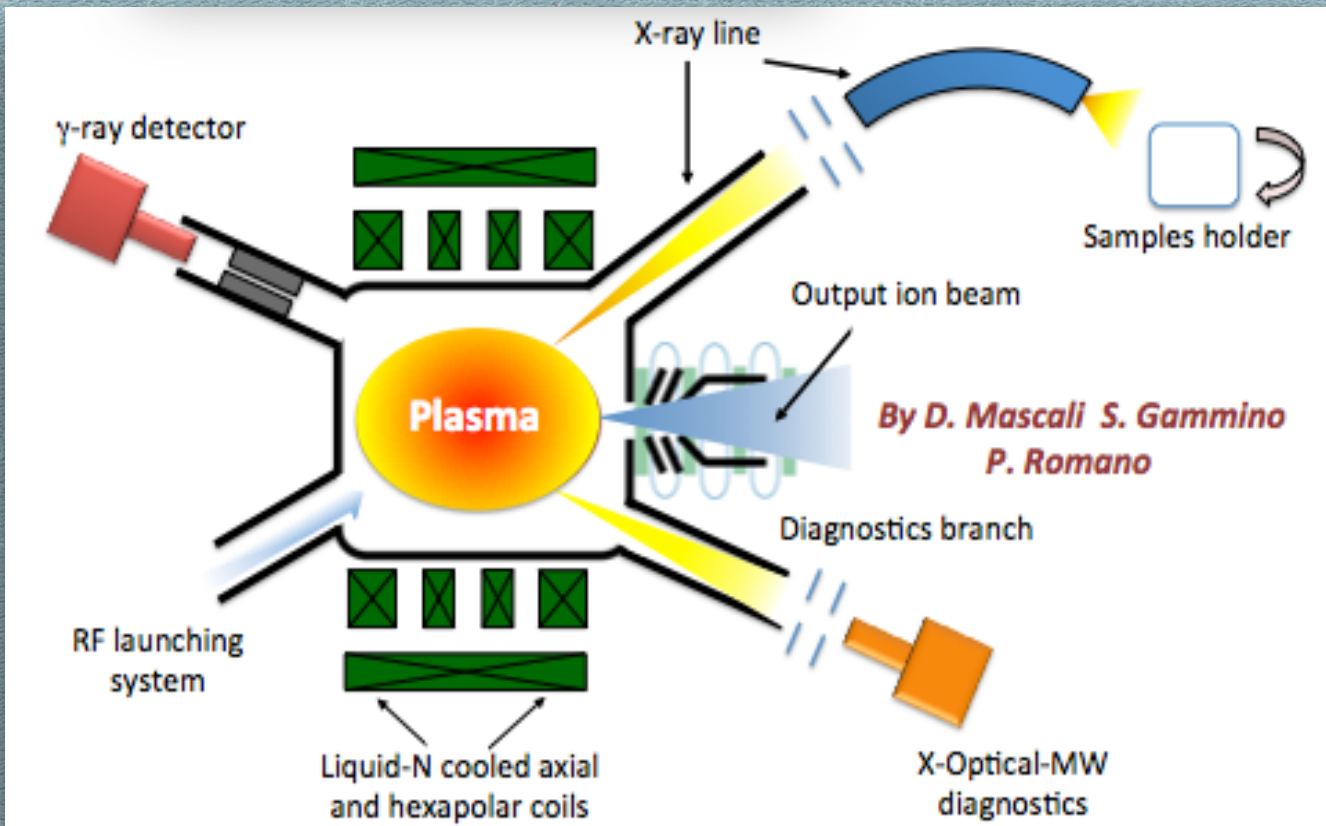
Confinement of highly charged ions in a magnetoplasma



According to the plasma density, temperature and confinement time, a given charge state distribution can be maintained in a dynamical equilibrium for hours or even days!!

SECRAL source at IMP - Lanzhou, China

1. Plasma can be obtained by (almost) any element, including rare isotopes
2. The Charge State Distribution can be modulated according to the plasma density and temperature
3. The decay-products can be tagged by γ -rays or by XRF on accumulation targets



Plasmas for
Astrophysics,
Nuclear
Decays
Observation and
Radiation for
Archaeometry

S-process

^{85}Kr [$T_{1/2} = 10.76$ y, **s-process**, γ @514 keV]

^{176}Lu [$T_{1/2} = 38$ Gy, (**CosmoChronometers**) γ @ 202.88 & 307 keV]

^{187}Re [$T_{1/2} = 50$ Gy, (**CosmoChronometers**), no $\gamma \rightarrow ^{187}\text{Os}$.]

^{87}Rb [$T_{1/2} = 48$ Gy, (**CosmoChronometers**), no $\gamma \rightarrow ^{87}\text{Sr}$.]

^7Be [$T_{1/2} = 53$ d, (**BBN, solar neutrino**) γ @477.6 keV.]

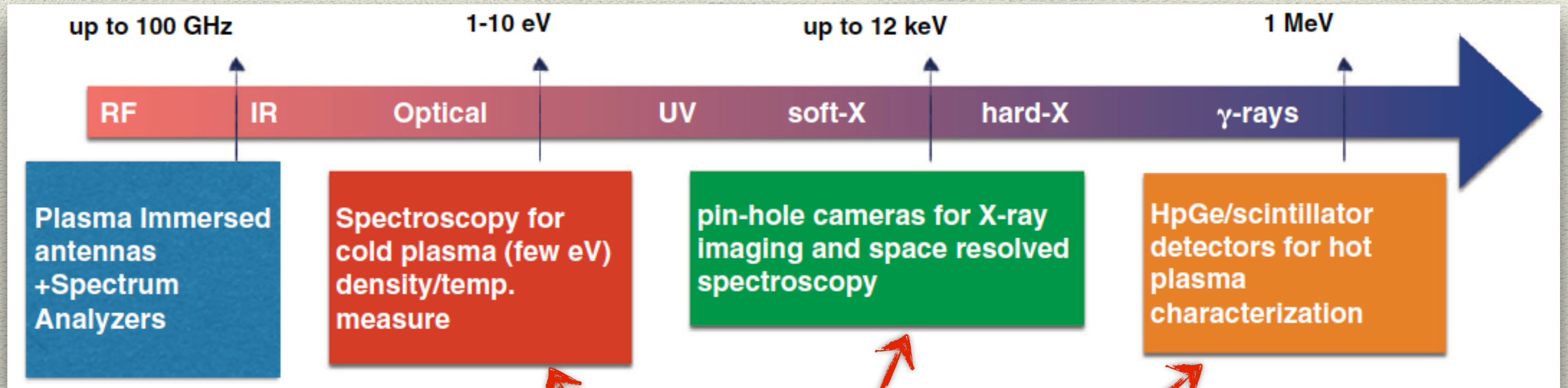
CosmoChronometers

Magnetoplasmas
 in laboratory

*Opacities for MM
 physics*

Let's trap beta-decaying radionuclides in magnetoplasma, thus studying if and how the lifetime is affected by the atomic charge state and by the "environment"

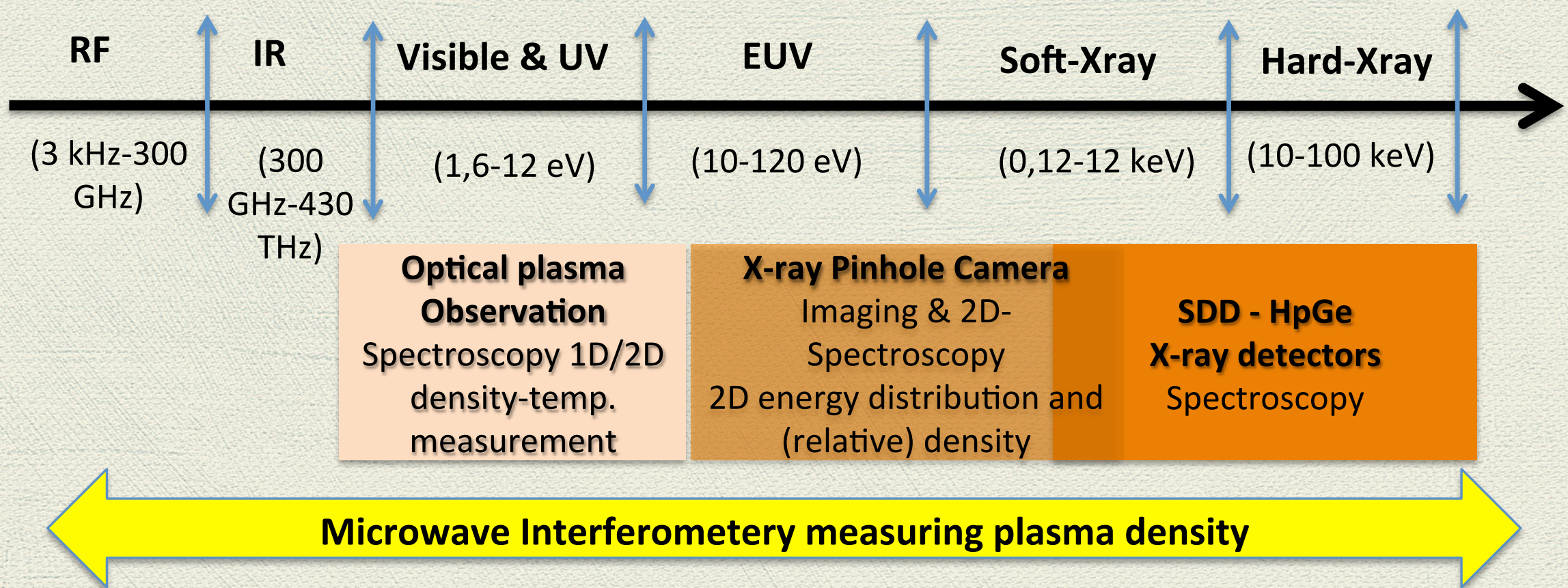
Non-intrusive plasma diagnostics methods



Measuring the plasma density in different energy regimes: density, temperature and plasma structure evaluation under different operative parameters



Non-intrusive plasma diagnostics methods

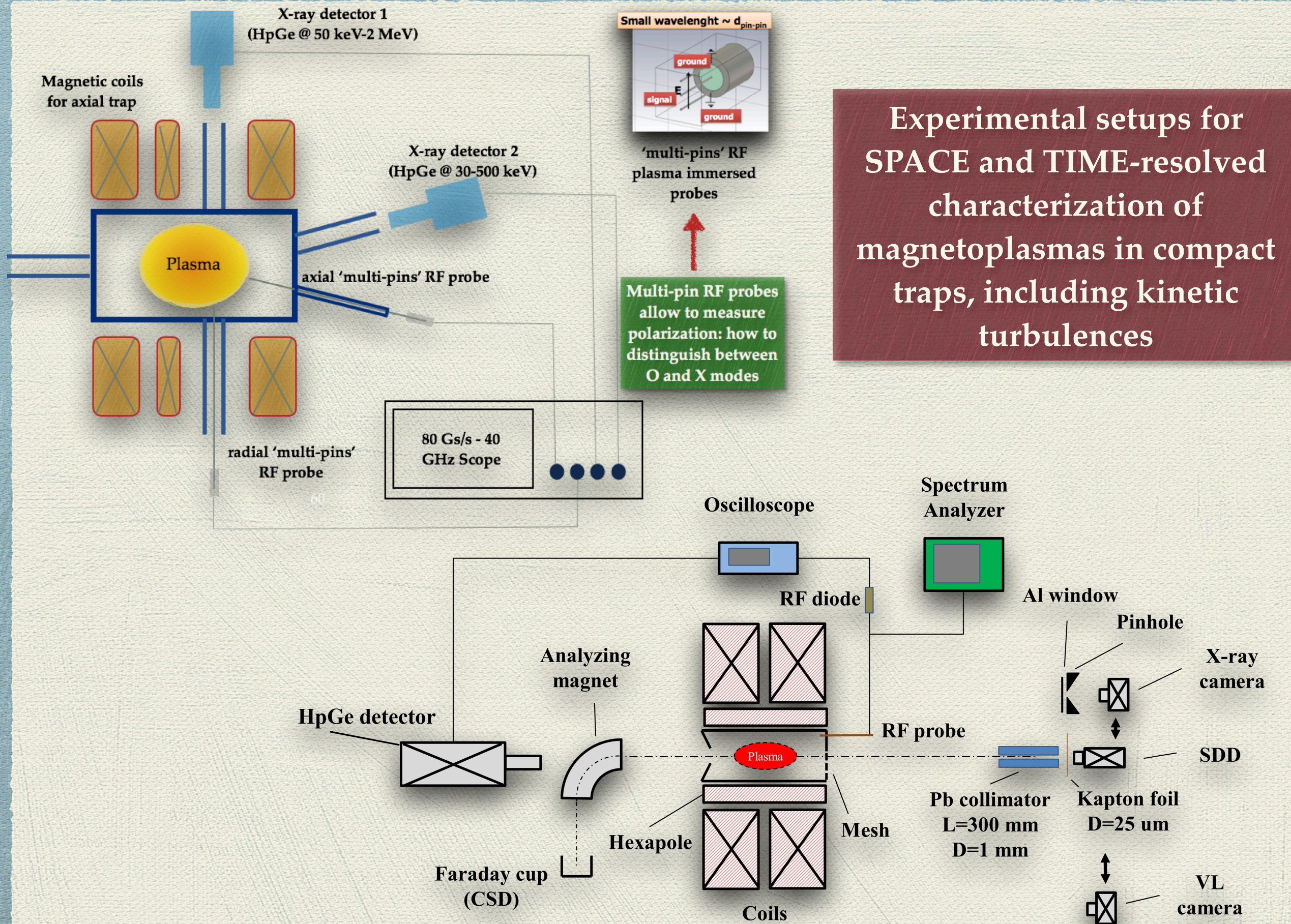


We need a tool able to measure density of electrons with an externally injected "probing" radiation (no perturbation since $P_{\text{probing}}/P_{\text{exciting}} < 1\%$)

→ Density measurement technique no-longer based on plasma emission but on "response-on-transmission" of microwaves through the plasma



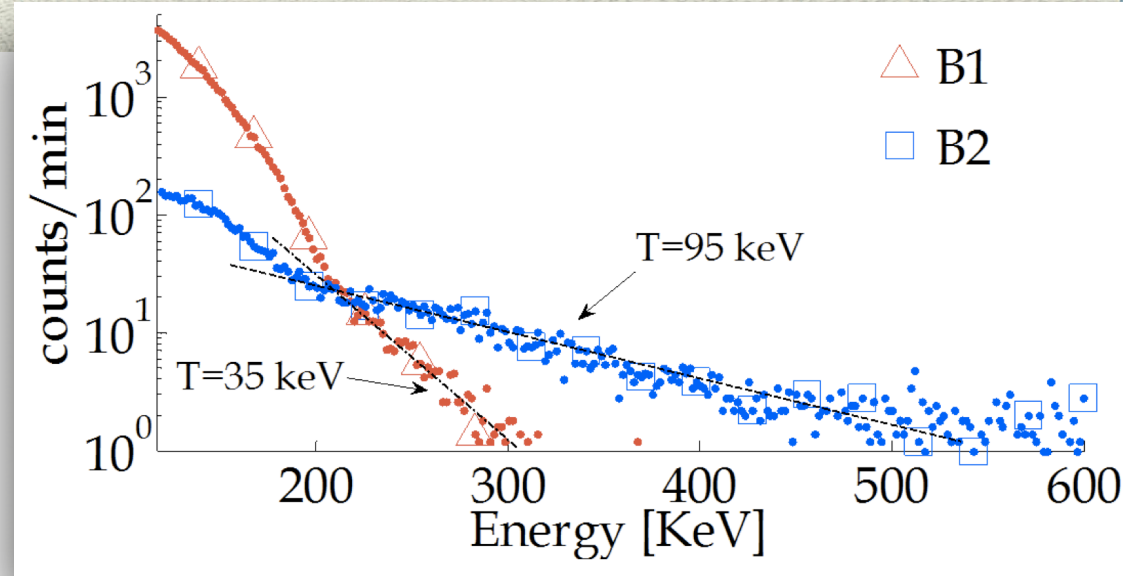
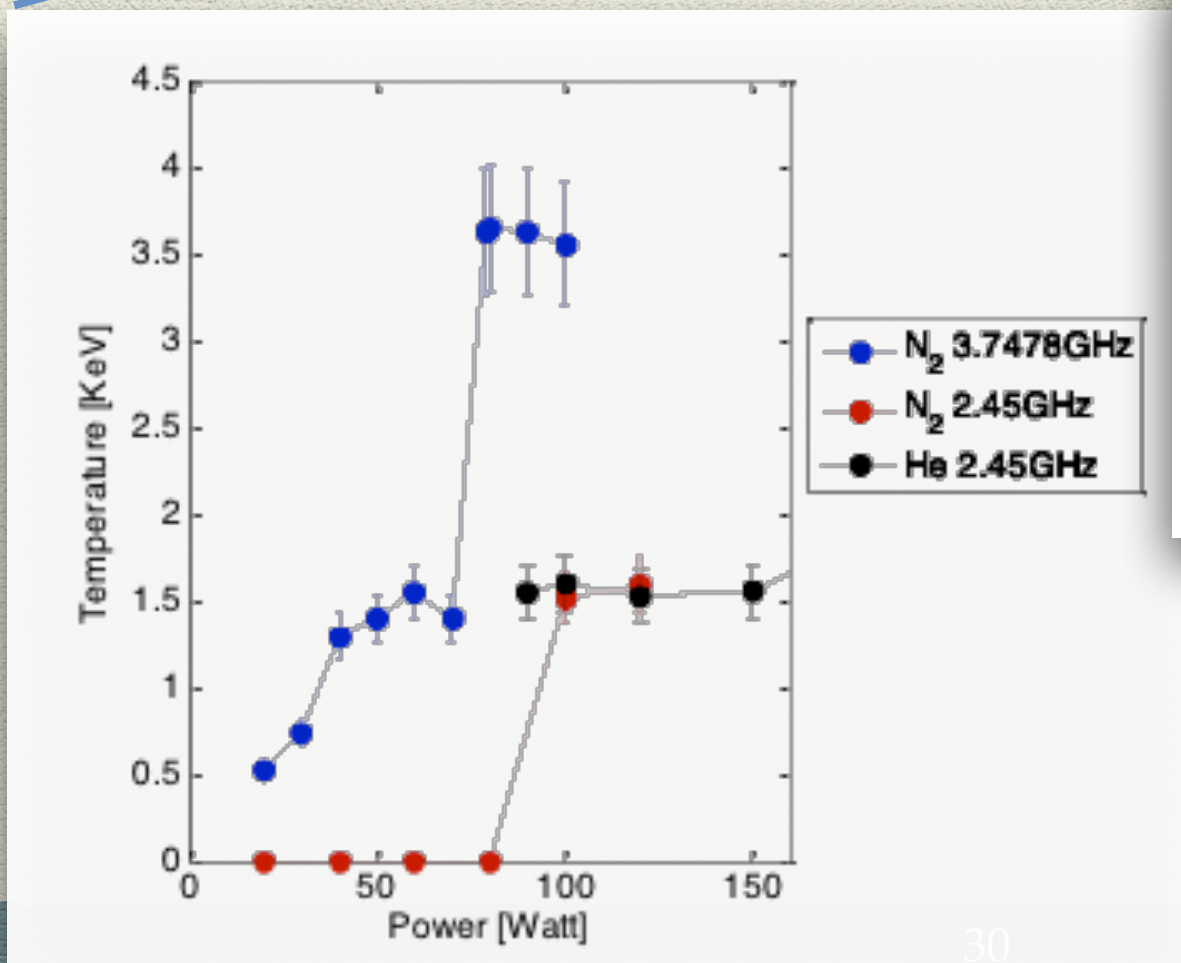
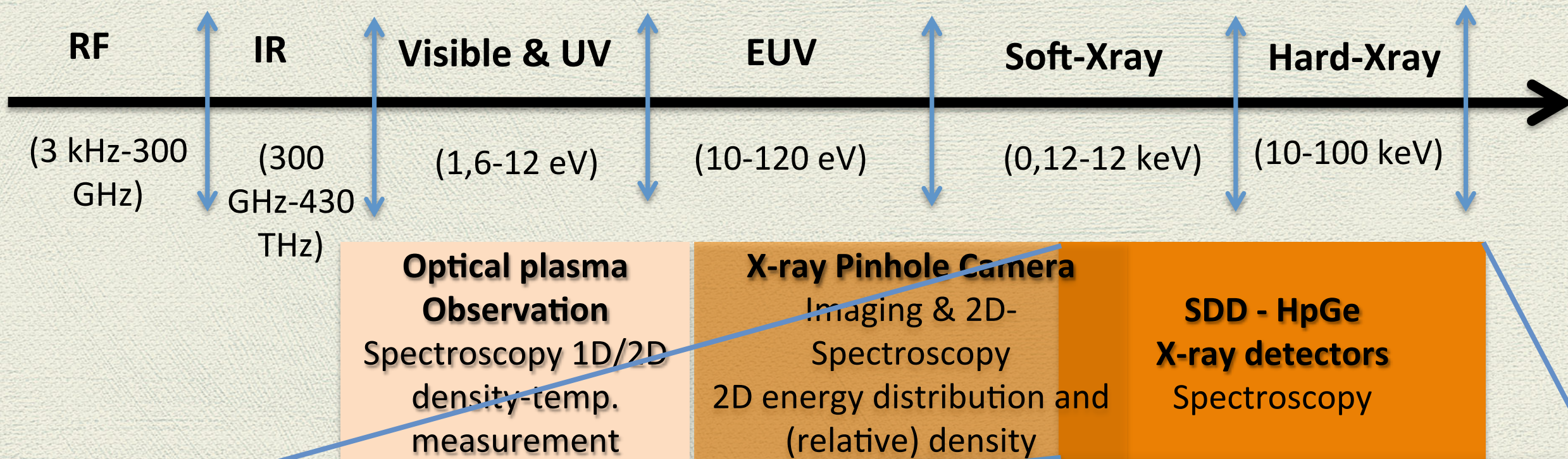
MICROWAVE INTERFEROMETRY



Experimental setups for SPACE and TIME-resolved characterization of magnetoplasmas in compact traps, including kinetic turbulences

[see also E. Naselli et al. poster presentation, this conf.]

Non-intrusive plasma diagnostics methods





Correlating X-ray fluxes, plasma density and $\langle q \rangle$: volumetric measurements

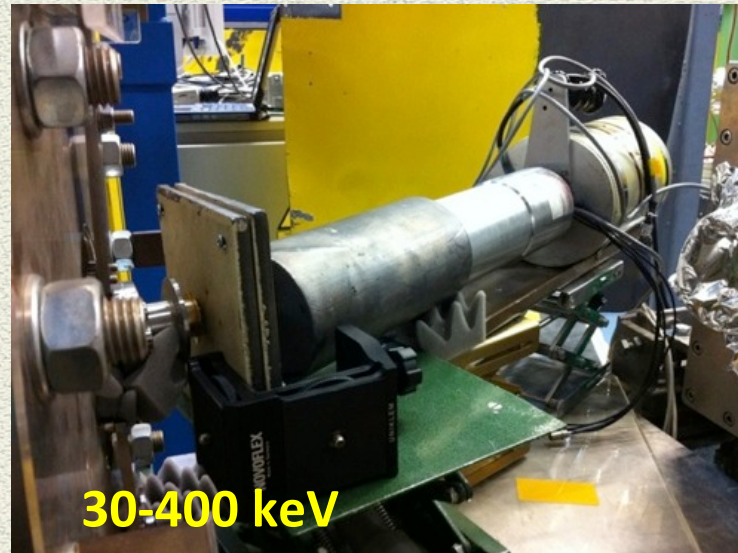
Measurements at GSI (March 2013):

impact of the pumping wave frequency on the X-ray spectra for either intermediate and high energy levels



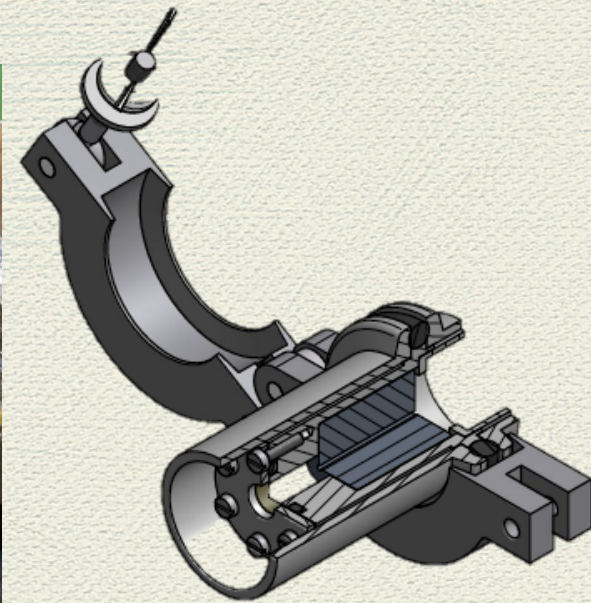
2.5-30 keV

SDD detector for warm electron component

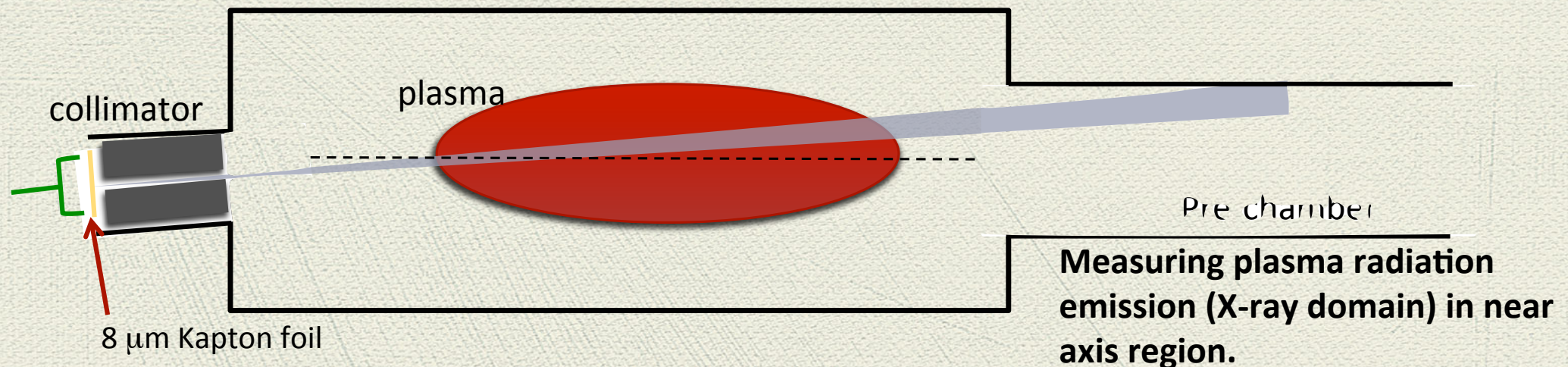


30-400 keV

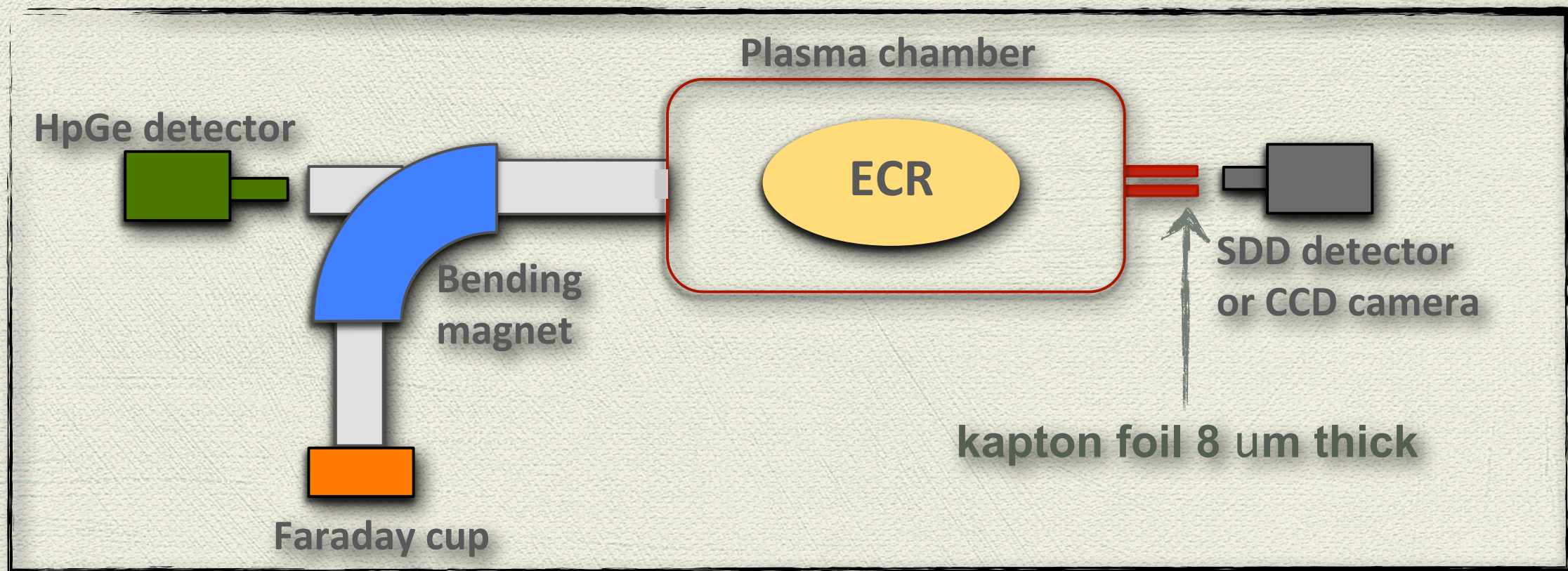
HpGe detector for hot electron component



Collimation system for the detection of the plasma-core (only) X-radiation.



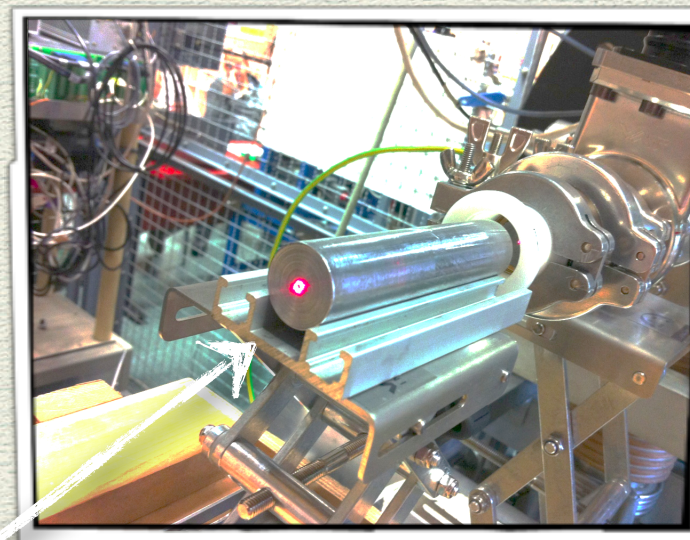
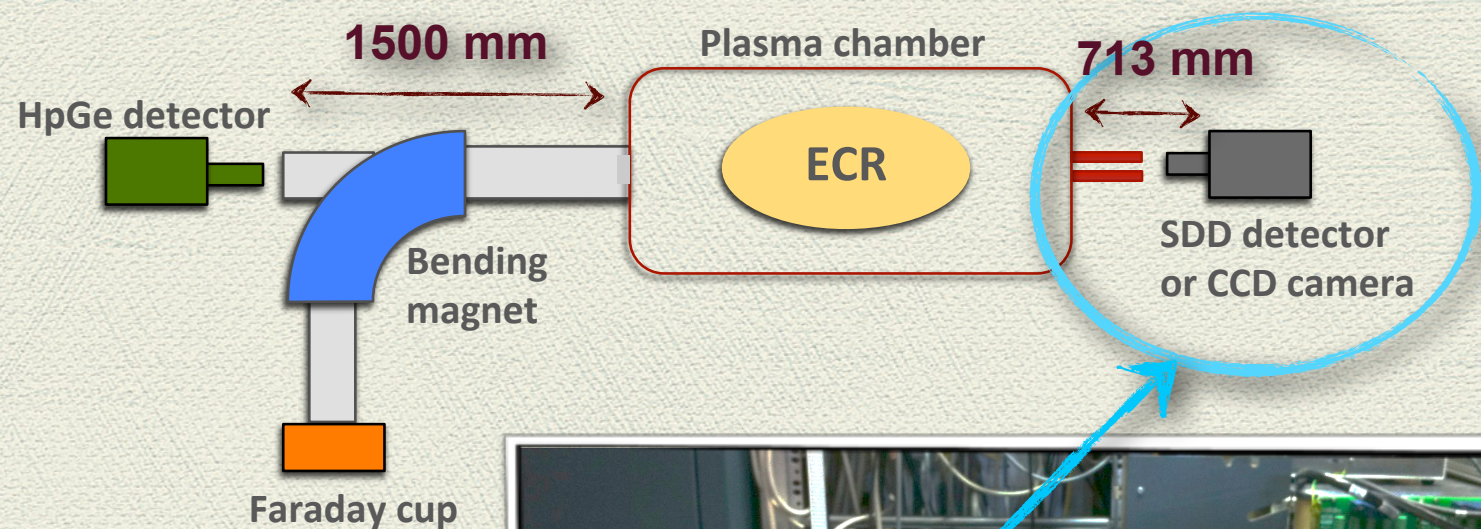
Experimental setup for simultaneous measurement of density, temperature and CSD



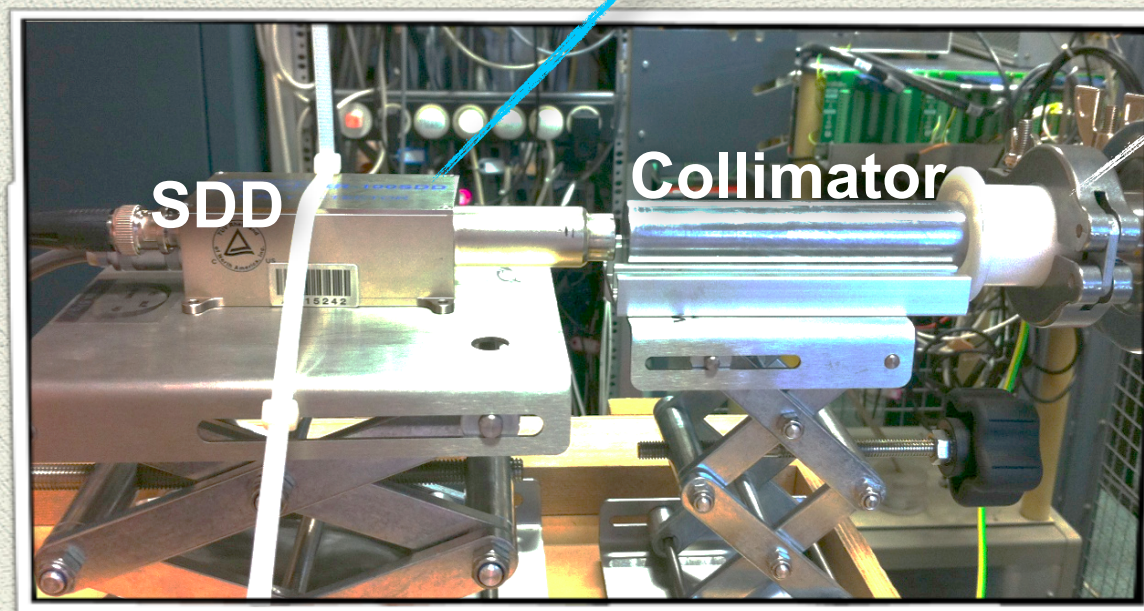
- ◆ Three detectors were used for a broad characterization of the EEDF:
 - HpGe for "hot electrons" $E > 30 \text{ keV}$
 - SDD for "warm electrons" $2 < E < 30 \text{ keV}$
 - CCD camera for imaging and 2D resolved spectroscopy $1 < E < 10 \text{ keV}$



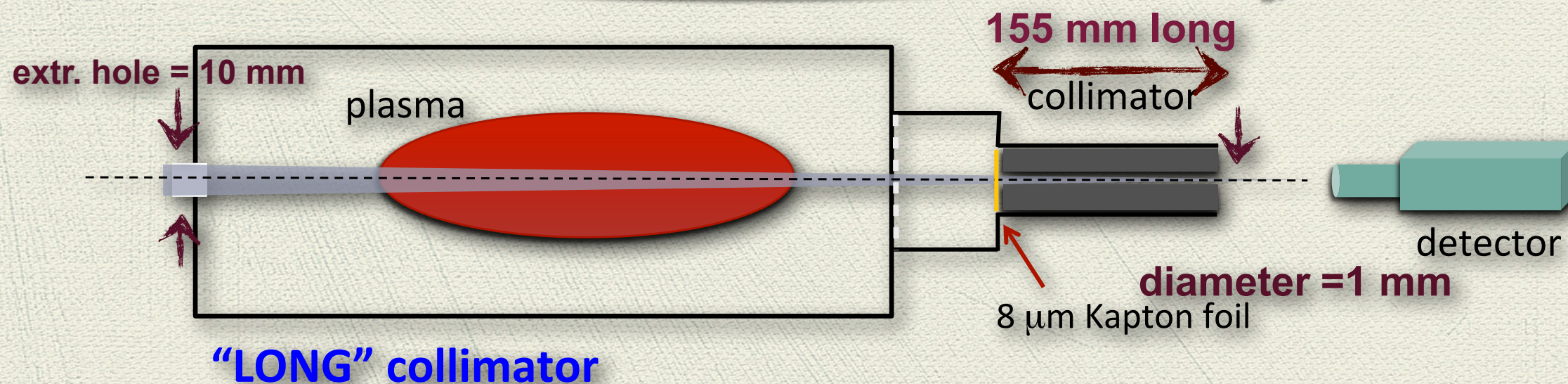
SDD - Setup @ ATOMKI Hungarian Acc. of Sciences



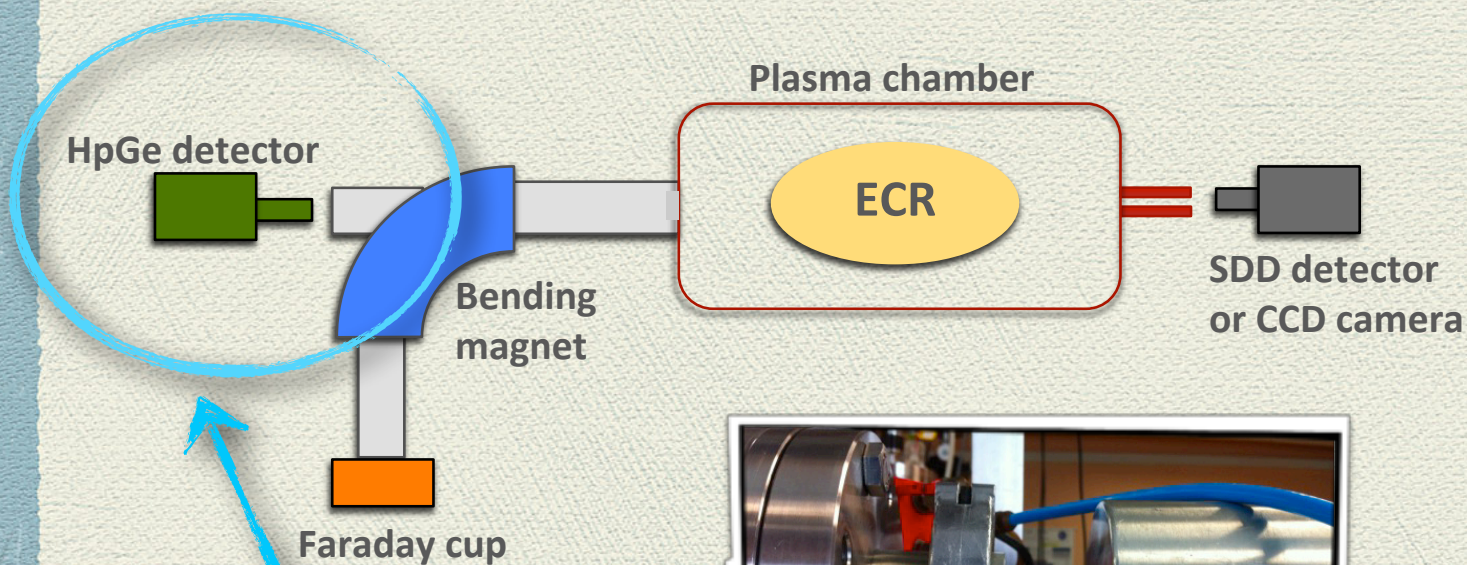
Collimator alignment



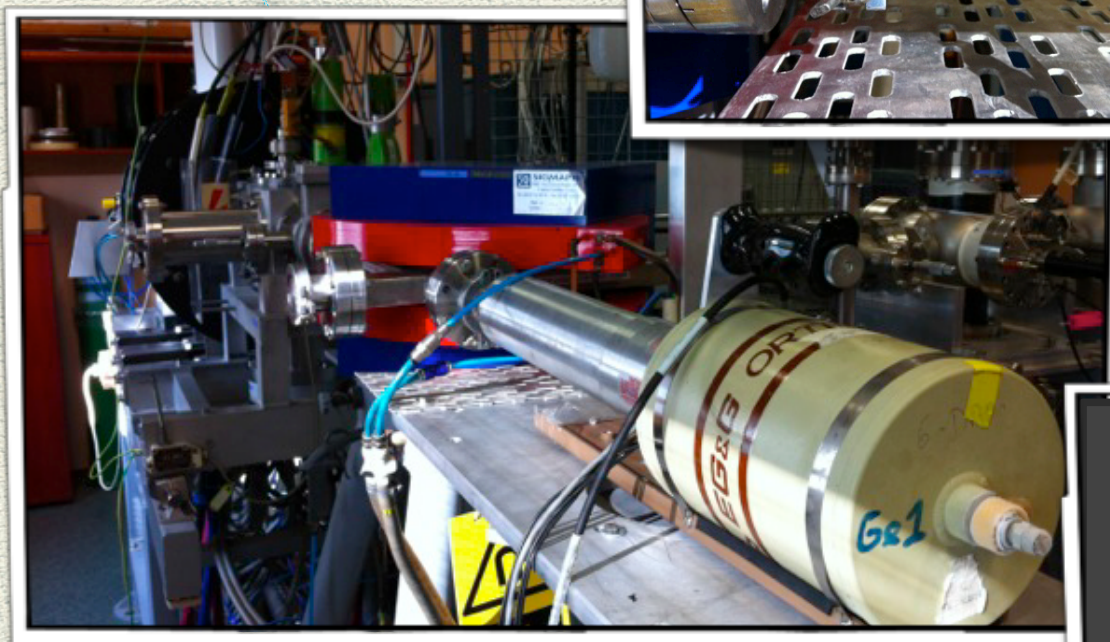
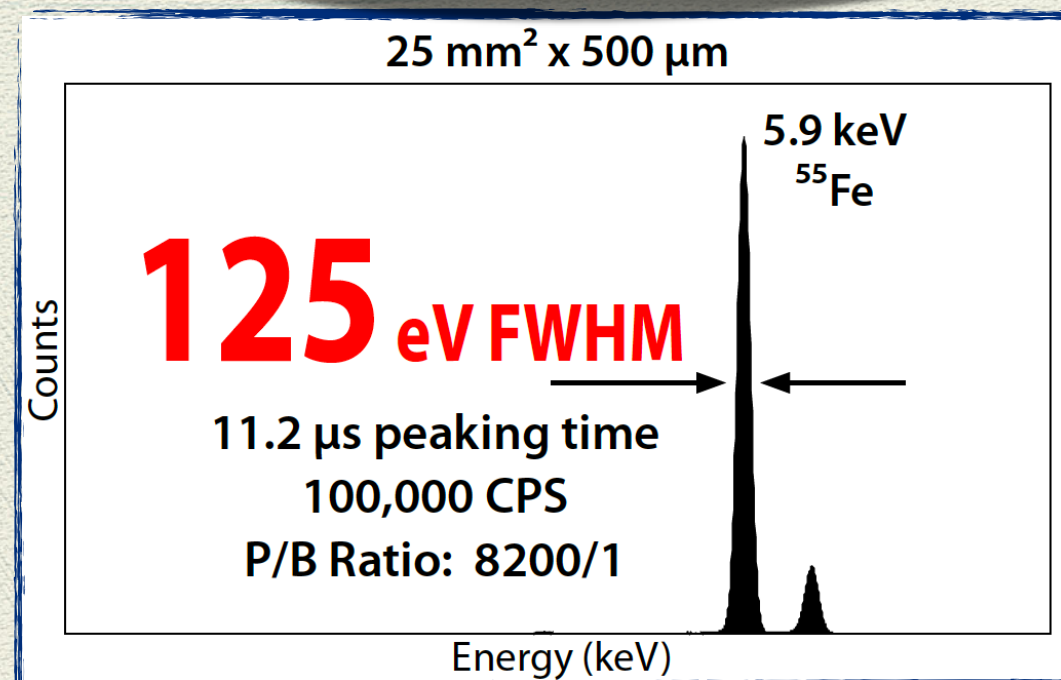
Bulk lead 155 mm long drilled collimator for near axis inspection



SDD and HpGe Set-up



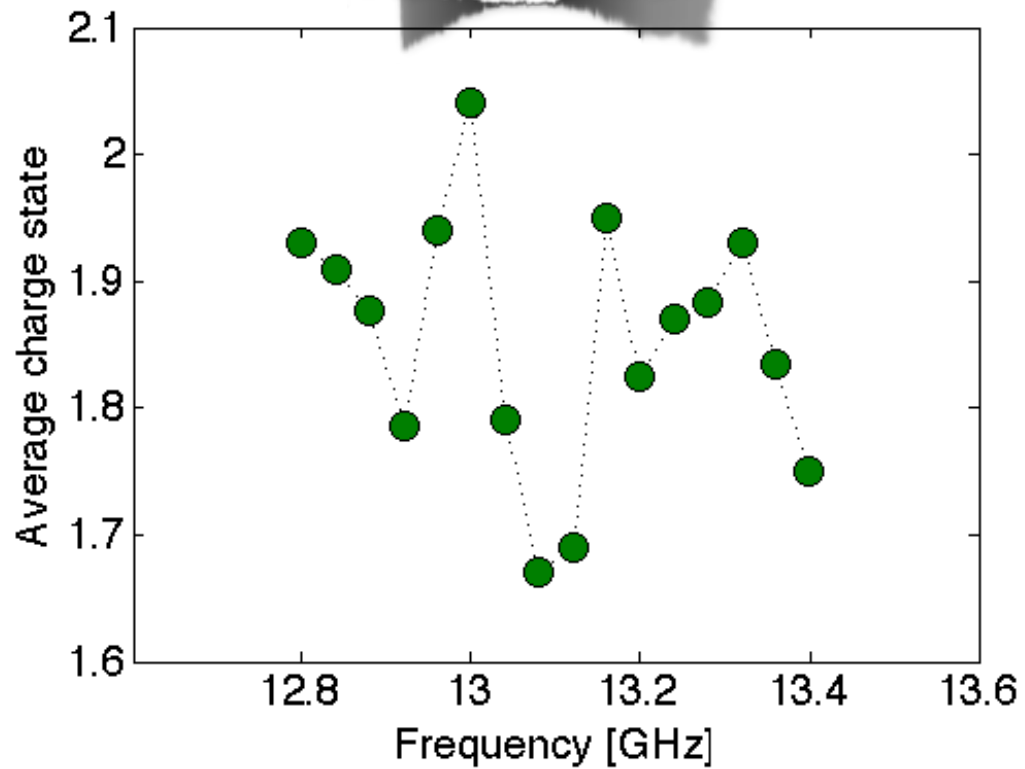
SDD - Silicon Drift Detector (SDD - 80 mm² active area) for measuring **warm X-rays** in the 2.5-30 keV domain.



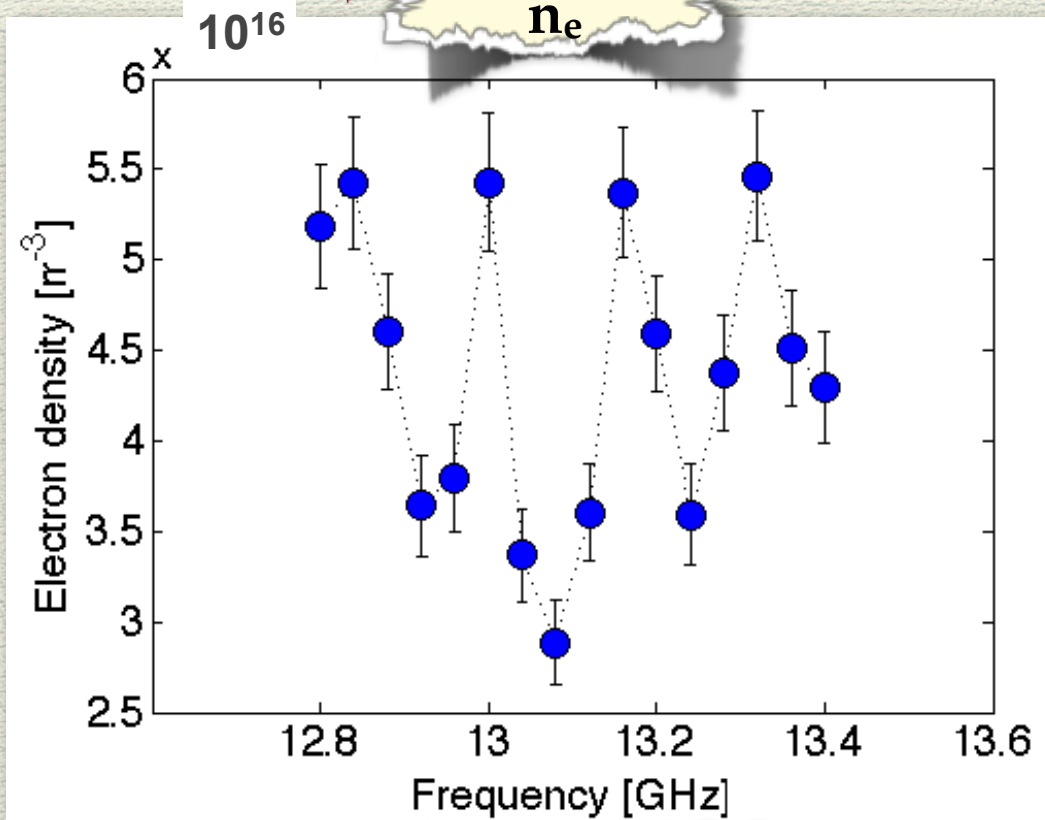
HpGe - HeGe Detector (3000 mm²) active area for measuring **hot X-rays** in the energy domain 30-400 keV

(SDD) F.T.E. study

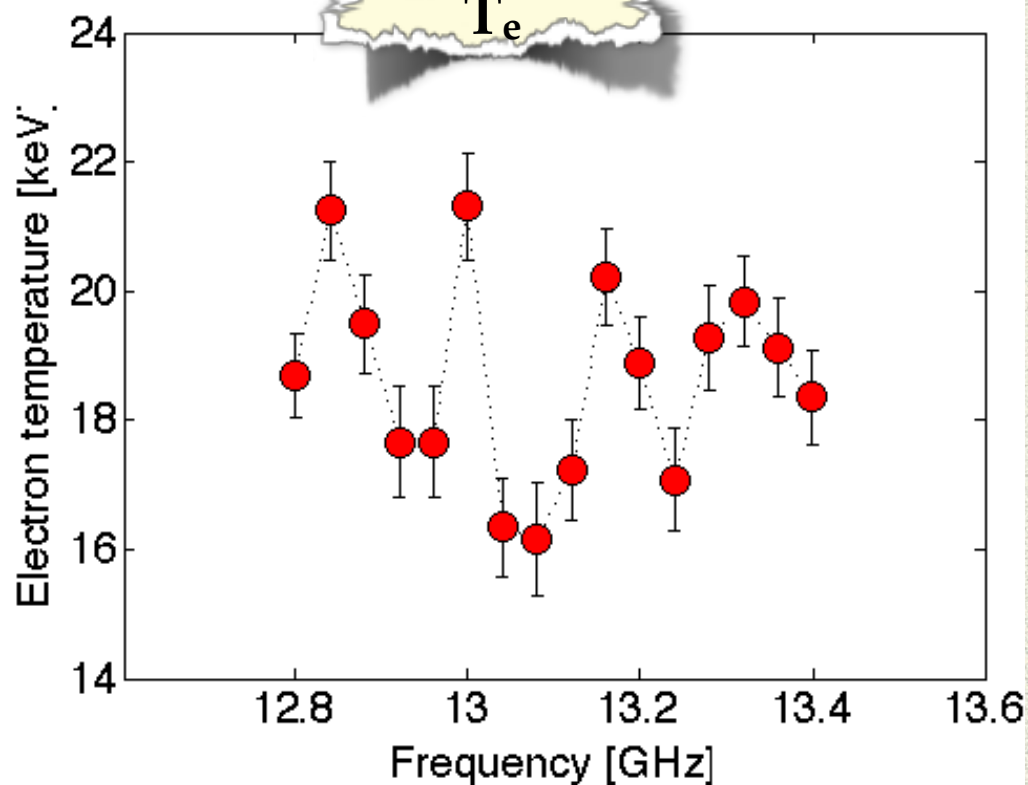
$\langle q \rangle$



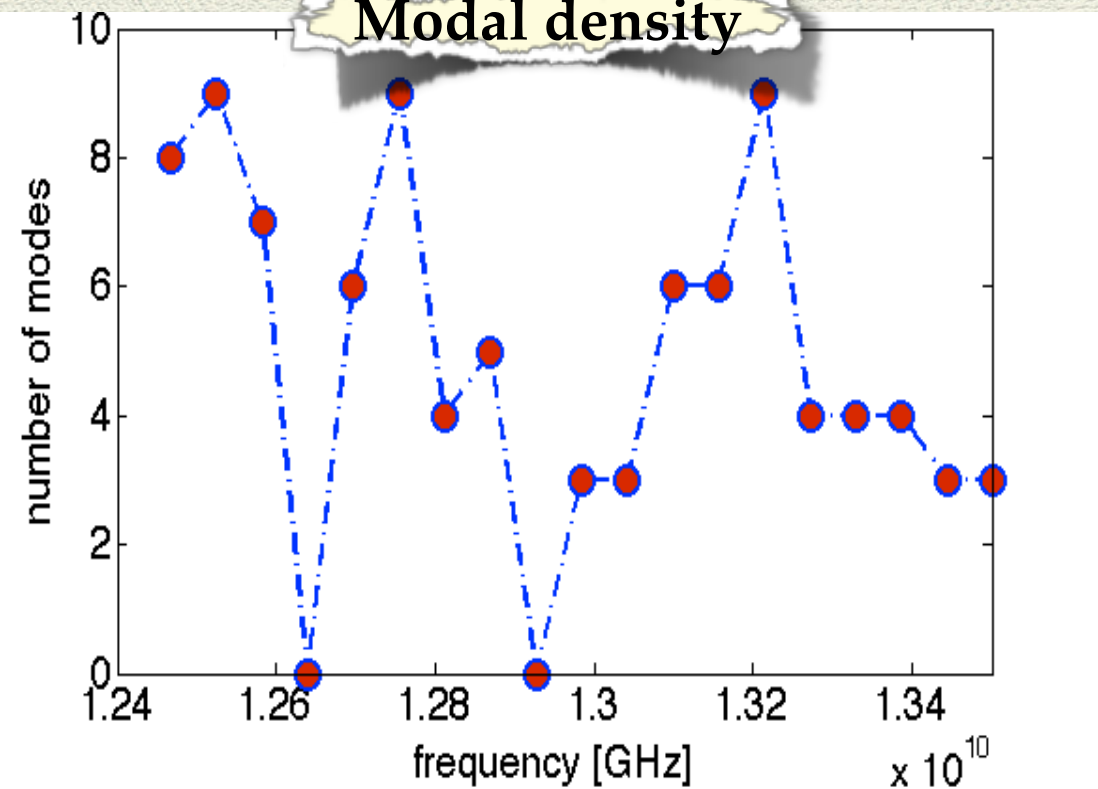
n_e



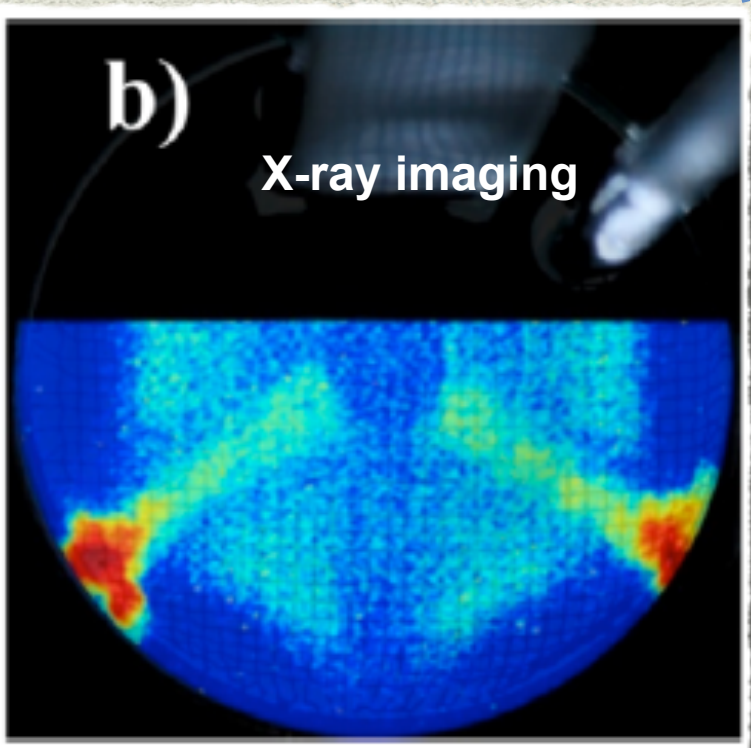
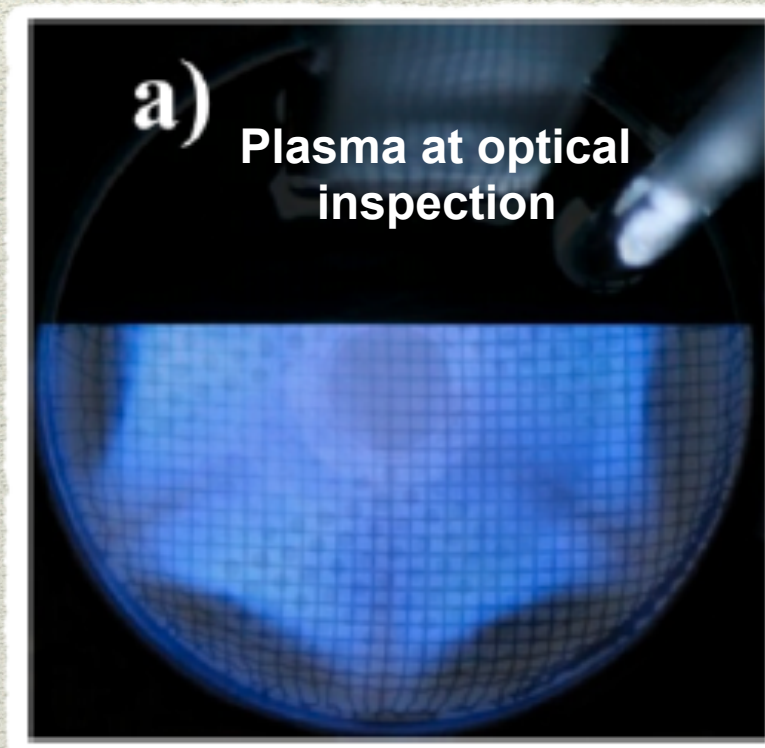
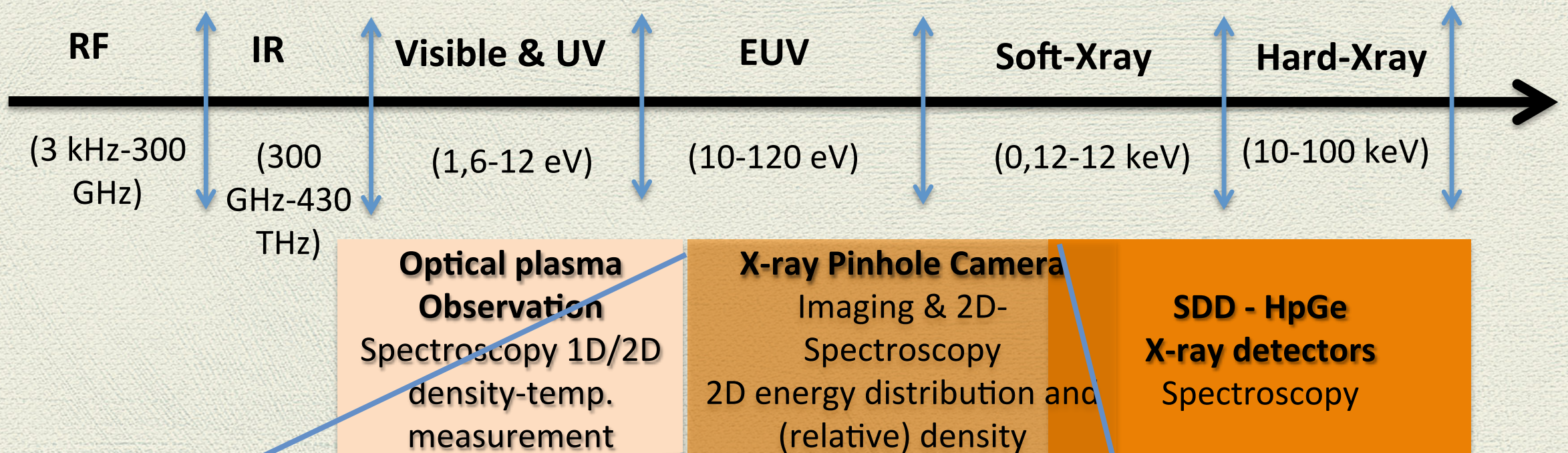
T_e



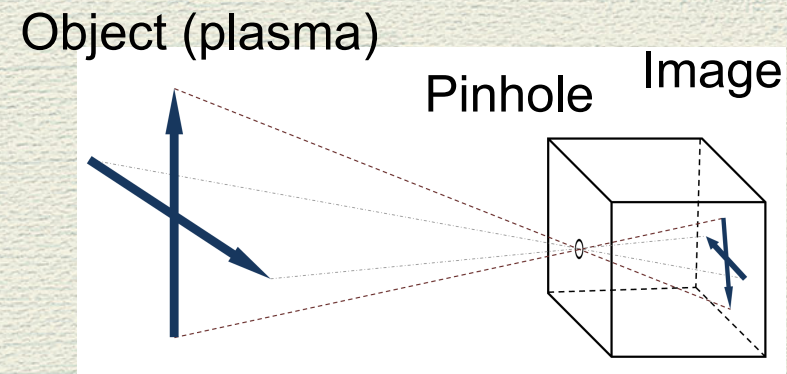
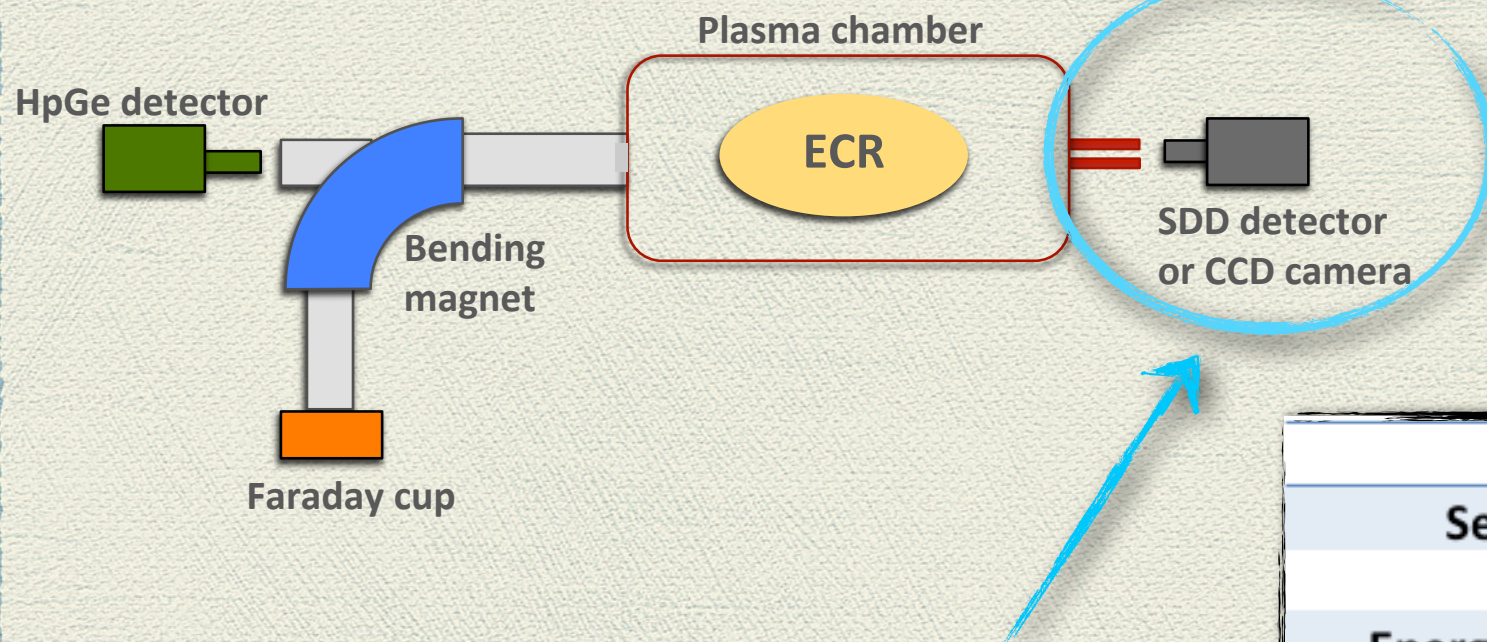
Modal density



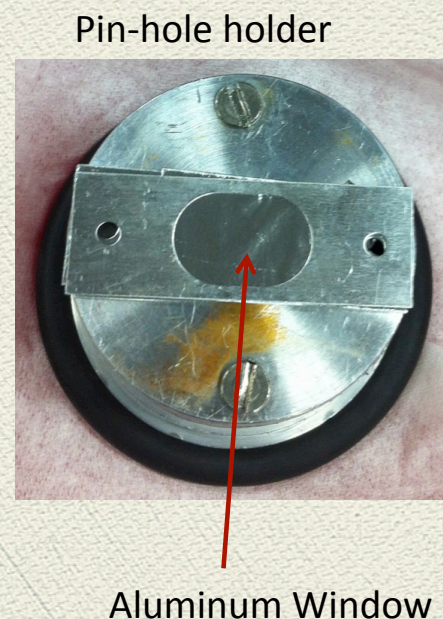
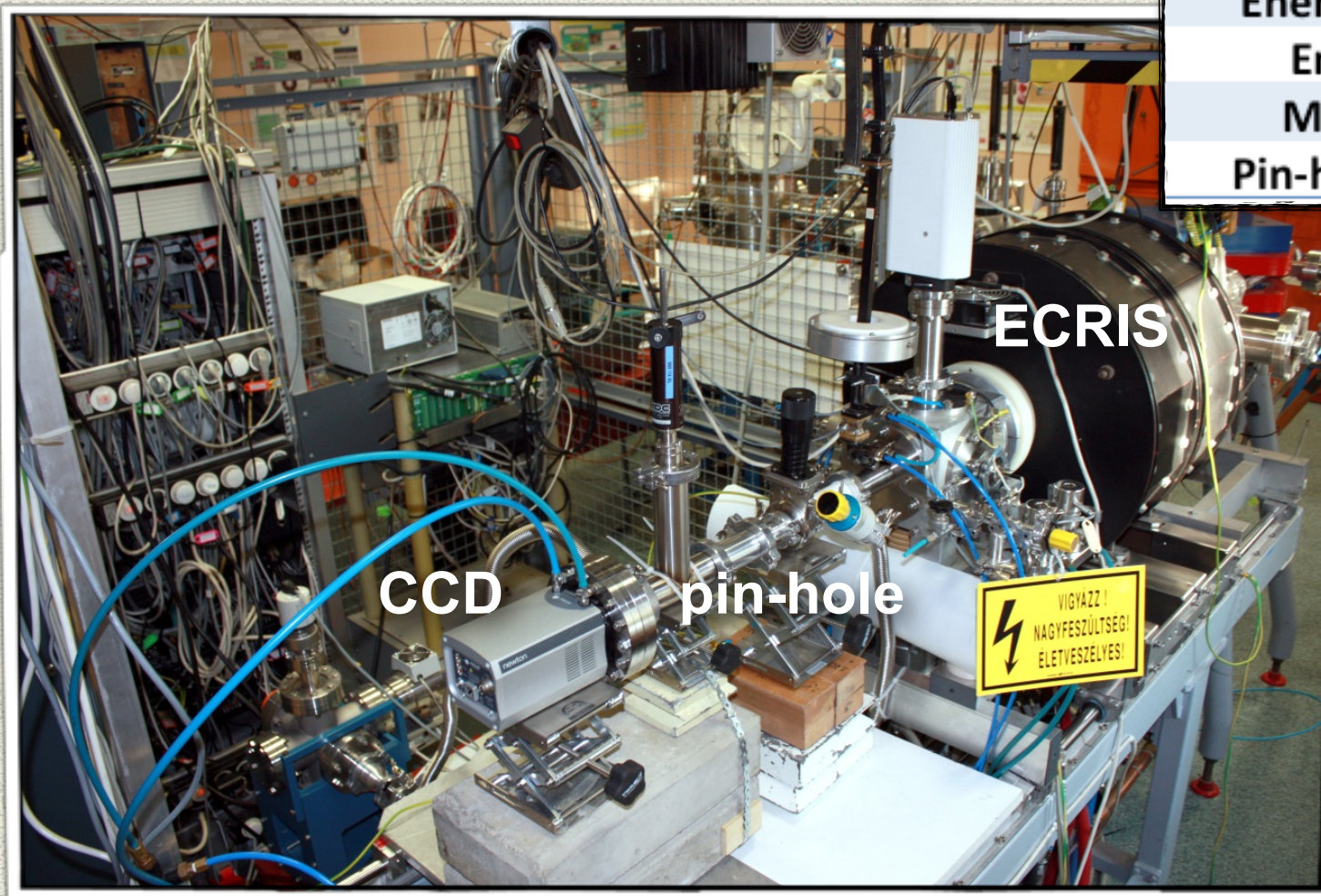
Non-intrusive plasma diagnostics methods



CCD camera Set-up

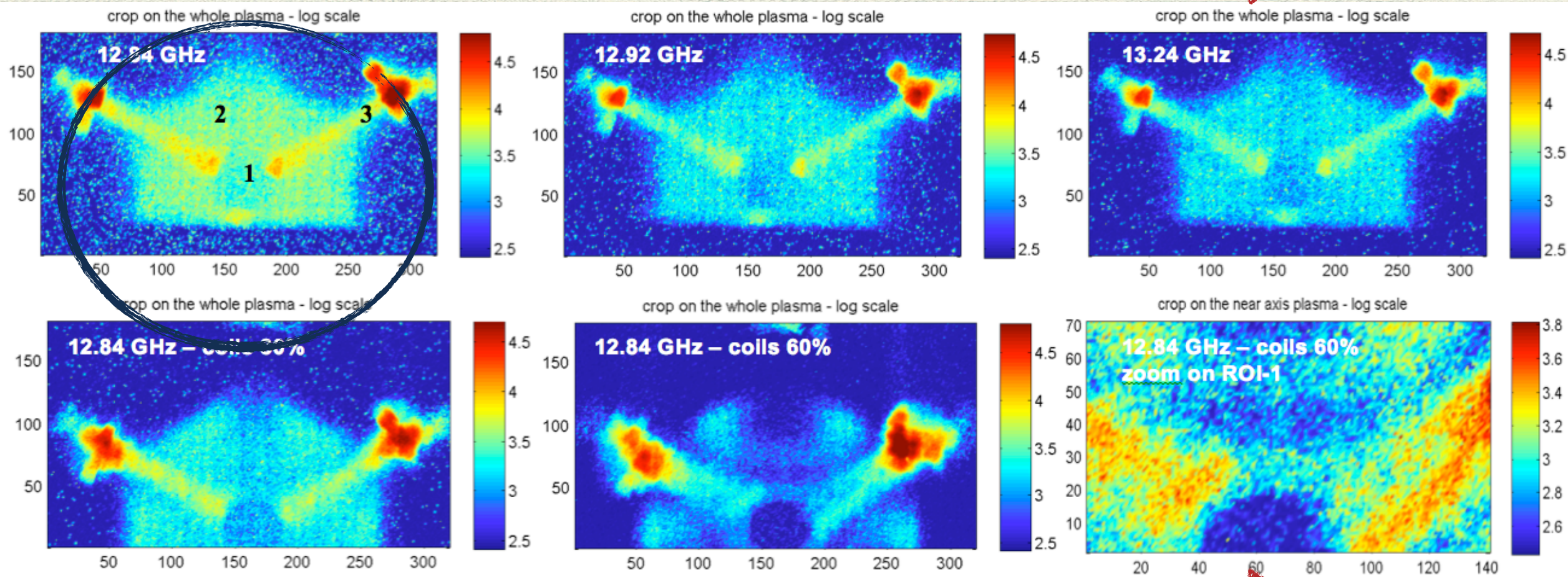


Model	Andor Technology - Newton
Sensor size	27.6 mm x 6.9 mm
Pixels	1024 x 255 (0.3 MP)
Energy Resolution	150 eV
Energy range	1-10 keV
Magnification	0.082-0.124-0.158
Pin-hole diameters	75 μ m and 100 μ m (W and Pb)

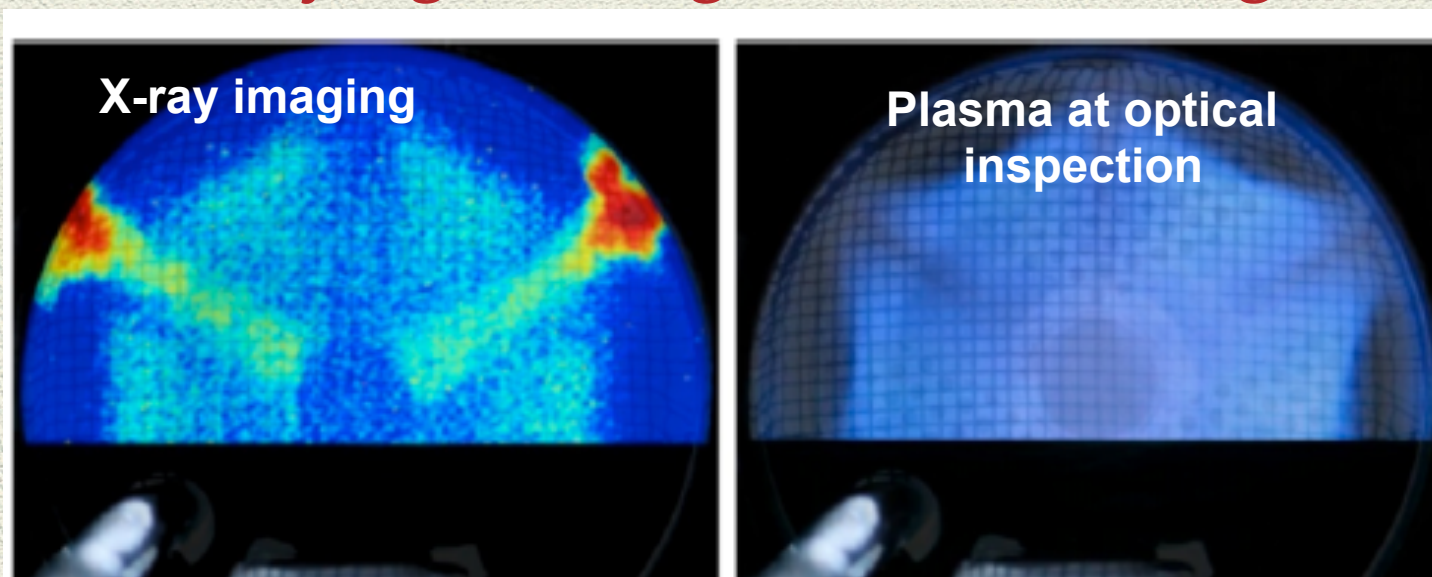


X-ray imaging

Varying the pumping wave frequency (F.T.E.)



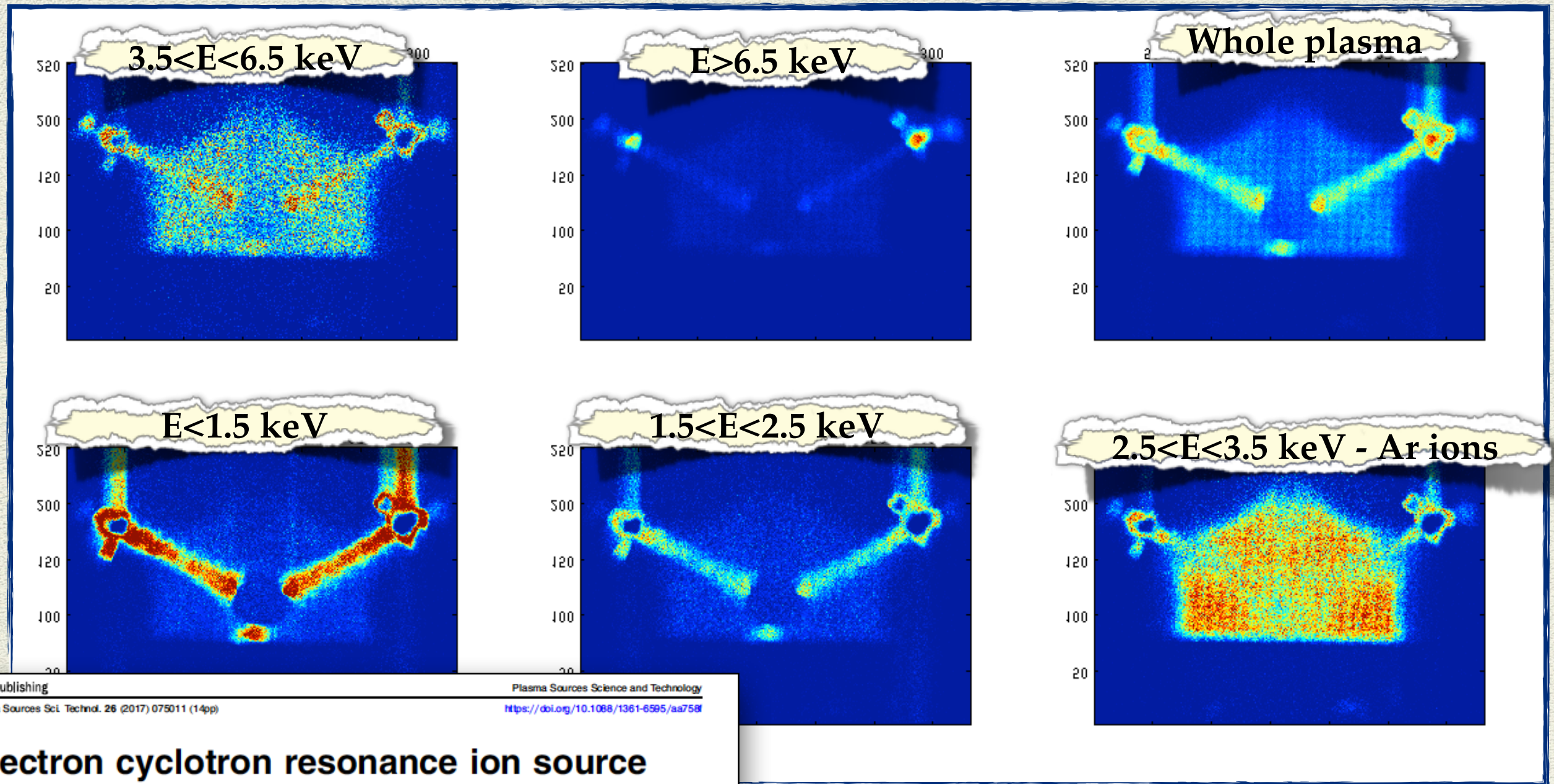
Varying the magnetic field strength



Plasma inspection after energy filtering

13.24 GHz - distribution at different energies

(equalized pseudocolor maps)



IOP Publishing
Plasma Sources Sci. Technol. 26 (2017) 075011 (14pp)

Plasma Sources Science and Technology
<https://doi.org/10.1088/1361-6595/aa758f>

**Electron cyclotron resonance ion source
plasma characterization by energy
dispersive x-ray imaging**

See S. Biri's talk for last news and experiments!!

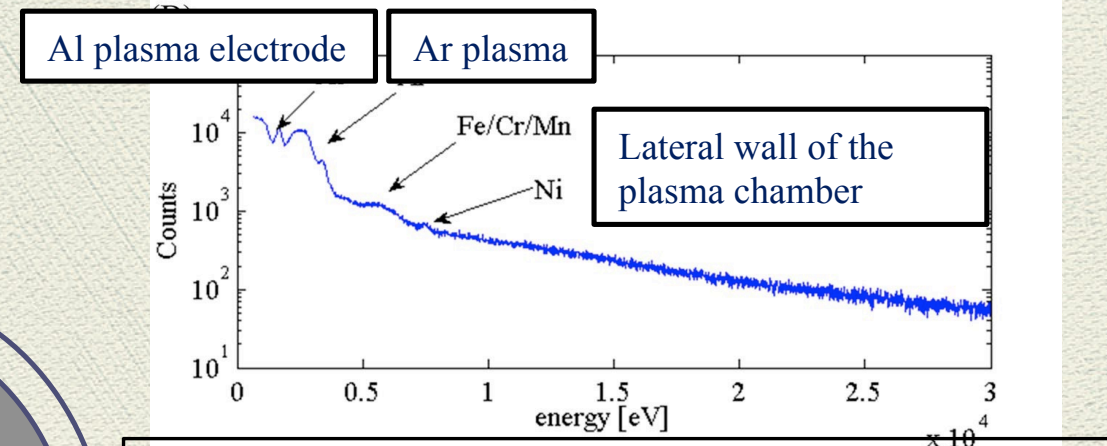
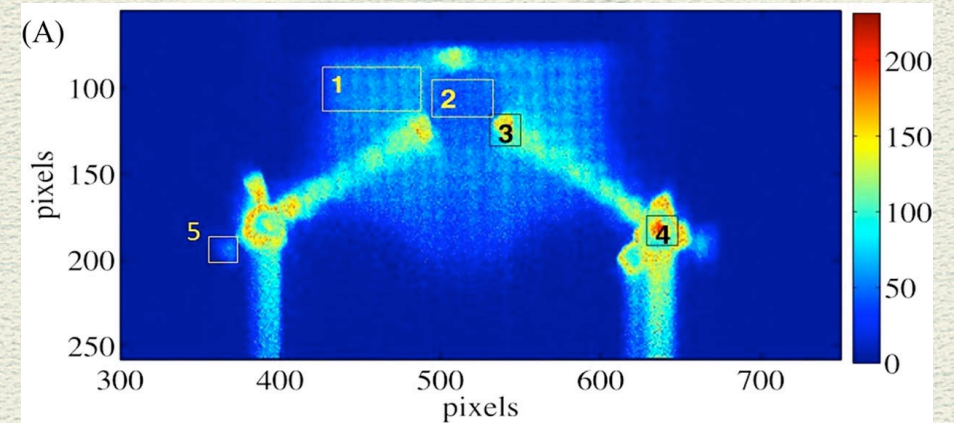
R Rácz^{1,5}, D Mascali², S Biri¹, C Caliri², G Castro², A Galatà³,
S Gammino², L Neri², J Pálinkás¹, F P Romano⁴ and G Torrisci²

Advanced design of the plasma chamber walls oriented to **spatially-resolved X-ray spectroscopy**

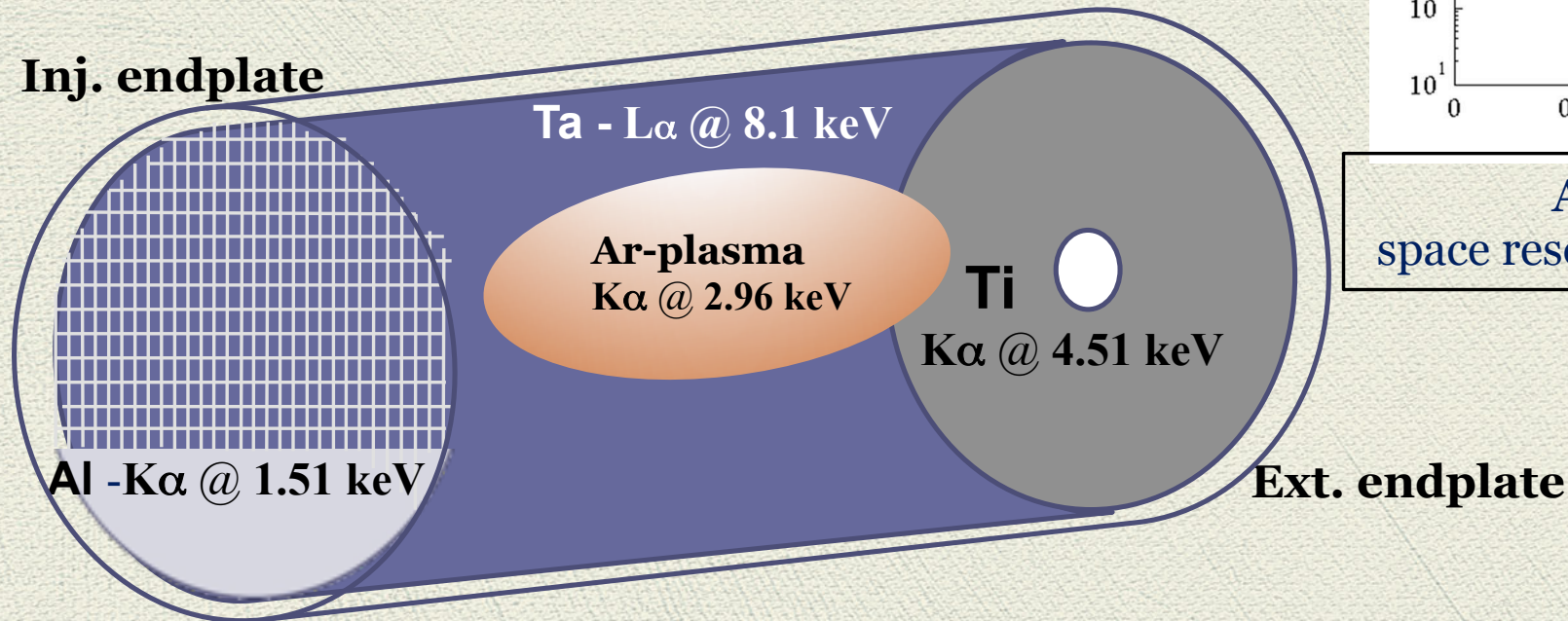
Measurements in 2014 show that fluorescence lines can be used to get info about where the electrons collide on the chamber walls!

Now, in order to have well separated component of the emitted X-ray:
 → **special design of plasma chamber for studying confinement dynamics** (plasma vs. losses X-radiation emission)

X-ray image from 2014 experiment



Already in 2014 PhC X-ray space resolved-spectroscopy was performed

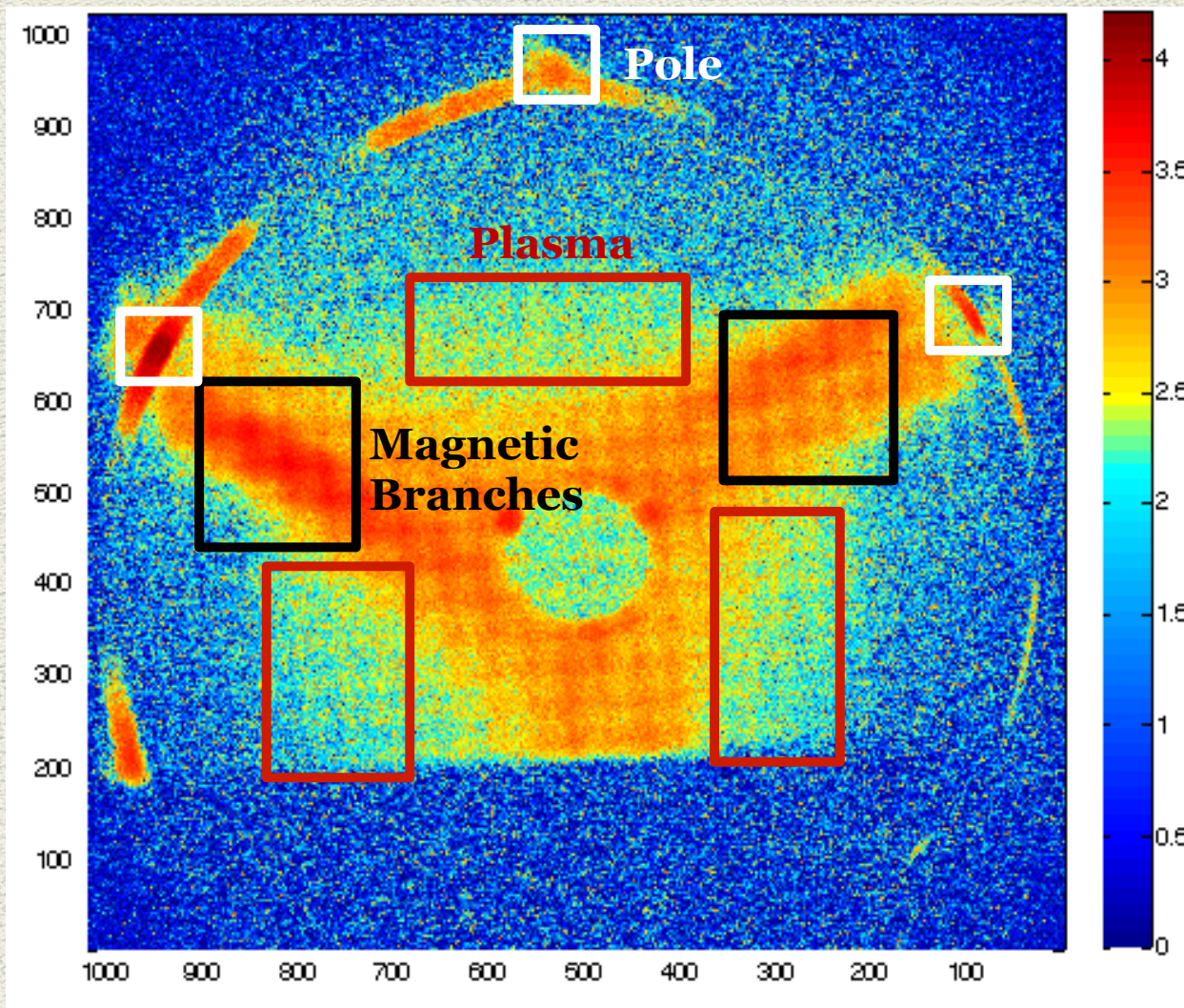


R. Racz et al. *Plasma Sources Science and Technology*, Vol. 26, No. 7
 D. Mascali et al., *Review of Scientific Instruments* **87**, 02A510 (2016)

Advanced design of the plasma chamber walls oriented to **spatially-resolved X-ray spectroscopy**

High-spatial resolution, time integrated images with an **exposure time of 50 sec**

→ Counts estimated in each ROI rely to $n \cdot E$, i.e. including both photon flux and energy content



X-rays coming from magnetic branches consist of mostly fluorescence from Ti

X-rays coming from plasma are mostly due to ionized $K\alpha$ Argon lines

X-rays coming from poles are mostly due to radial losses impinging on the Ta liner

Flux in Branches+Poles=**LOSSES**
Flux in red rectangles: **PLASMA**

Decoupling of n vs E will be possible only after the spectral analysis (already acquired but not yet elaborated)

Comparison with self-consistent simulations

Solving the **time-dependent Vlasov equation**, including single particle collisions

$$\frac{\partial f_\alpha}{\partial t} + \vec{v} \cdot \vec{\nabla} f_\alpha + \frac{q_\alpha}{m_\alpha} \left(\vec{E} + \frac{\vec{v} \times \vec{B}}{c} \right) \cdot \vec{\nabla}_v f_\alpha = 0$$

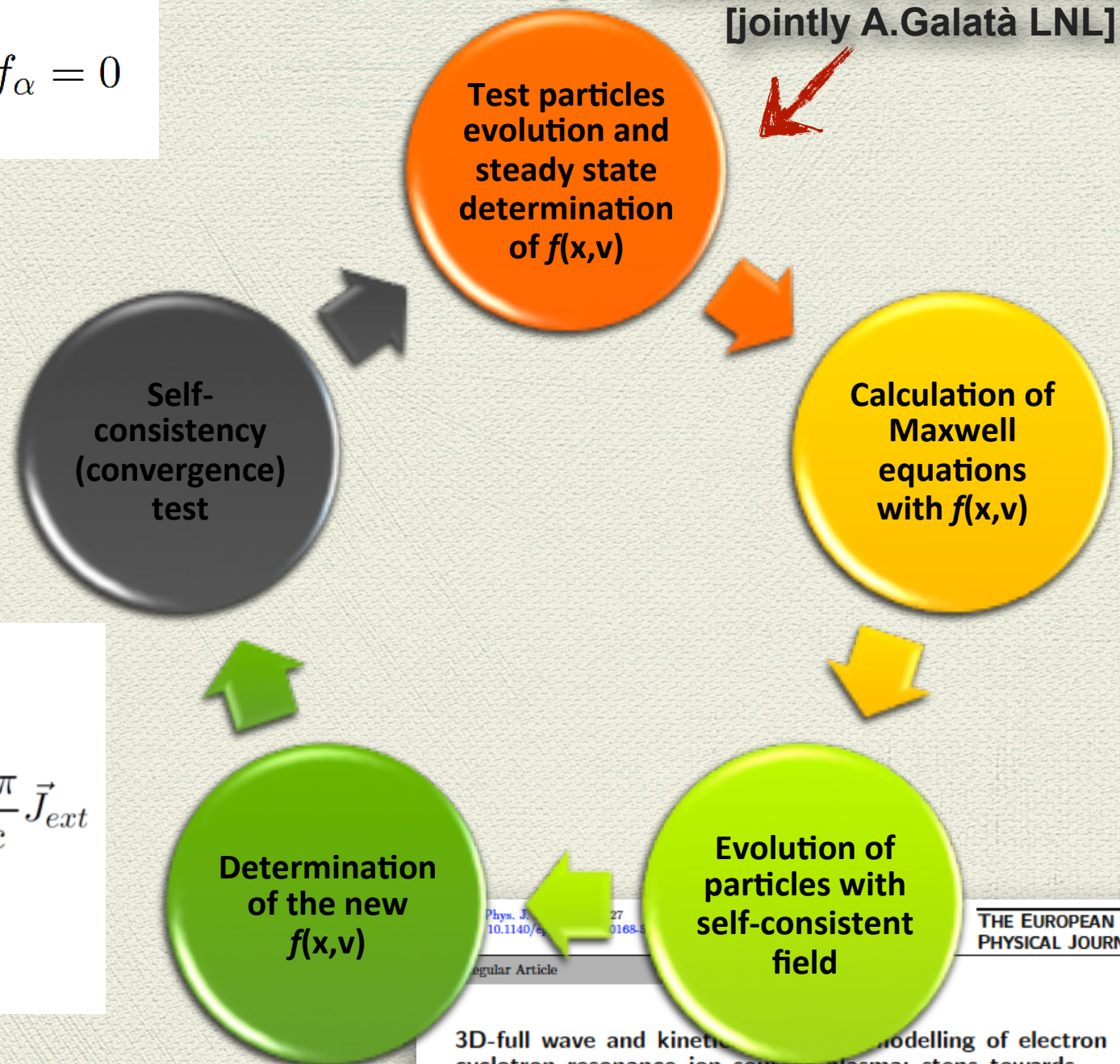
$$\frac{d\vec{v}}{dt} = \frac{q}{m_0 \gamma} \left[\vec{E} + \vec{v} \times B - \frac{\vec{v} \cdot \vec{E}}{c^2} \vec{v} \right]$$

Collisions by Langevin method
[jointly A.Galatà LNL]

Step-by-step current

Step-by-step plasma density

$$\begin{aligned} \vec{\nabla} \cdot \vec{E} &= 4\pi \sum_\alpha \bar{n}_\alpha q_\alpha \int f_\alpha d\vec{v} + 4\pi \rho_{ext} \\ \vec{\nabla} \times \vec{B} &= \frac{1}{c} \frac{\partial \vec{E}}{\partial t} + \frac{4\pi}{c} \sum_\alpha \bar{n}_\alpha q_\alpha \int \vec{v} f_\alpha d\vec{v} + \frac{4\pi}{c} \vec{J}_{ext} \\ \vec{\nabla} \times \vec{E} &= -\frac{1}{c} \frac{\partial \vec{B}}{\partial t} \end{aligned}$$



Phys. J. 27
10.1140/epj/s10168-18-00168-5
Regular Article

THE EUROPEAN
PHYSICAL JOURNAL D

3D-full wave and kinetic modelling of electron cyclotron resonance ion sources plasma: steps towards self-consistency*

David Mascali¹, Giuseppe Torrisci^{1,2,*}, Lorenzo Neri¹, Gino Sorbello^{1,3}, Giuseppe Castro¹, Luigi Celona¹, and Santo Gammino¹

Comparison with self-consistent simulations

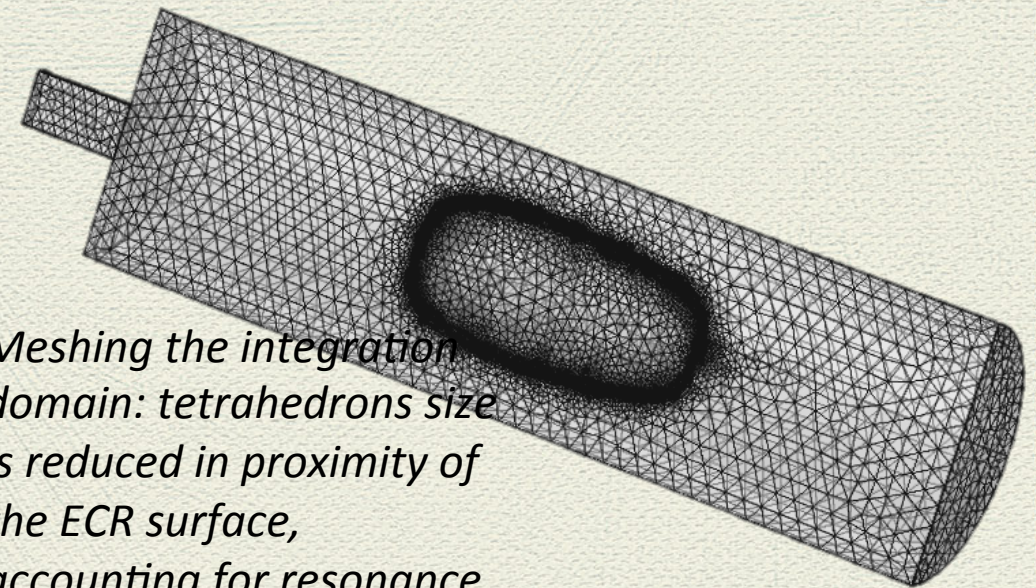
Solution of Maxwell's equations in **COMSOL** using MUMPS direct solver

Full anisotropic dielectric tensor for the magnetized plasma computed in **MATLAB**

Electromagnetic field in ECRIS Plasma

$$\nabla \times \nabla \times \mathbf{E} - \frac{\omega^2}{c^2} \overline{\overline{\epsilon_r}} \cdot \mathbf{E} = 0$$

Wave equation with tensorial permittivity

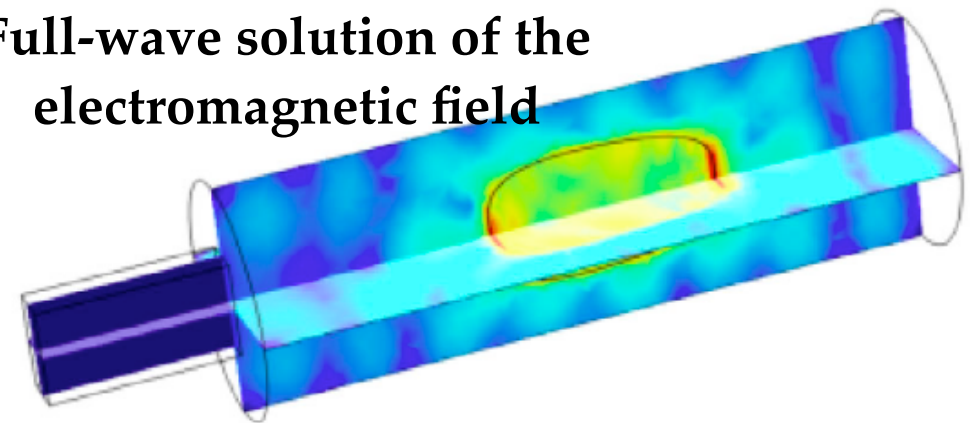


Meshing the integration domain: tetrahedrons size is reduced in proximity of the ECR surface, accounting for resonance.

$$\overline{\overline{\epsilon}} = \epsilon_0 \overline{\overline{\epsilon_r}} = \epsilon_0 \left(\overline{\overline{\epsilon'}} - i \overline{\overline{\epsilon''}} \right) = \epsilon_0 \left(\overline{\overline{I}} - \frac{i \overline{\overline{\sigma}}}{\omega \epsilon_0} \right)$$

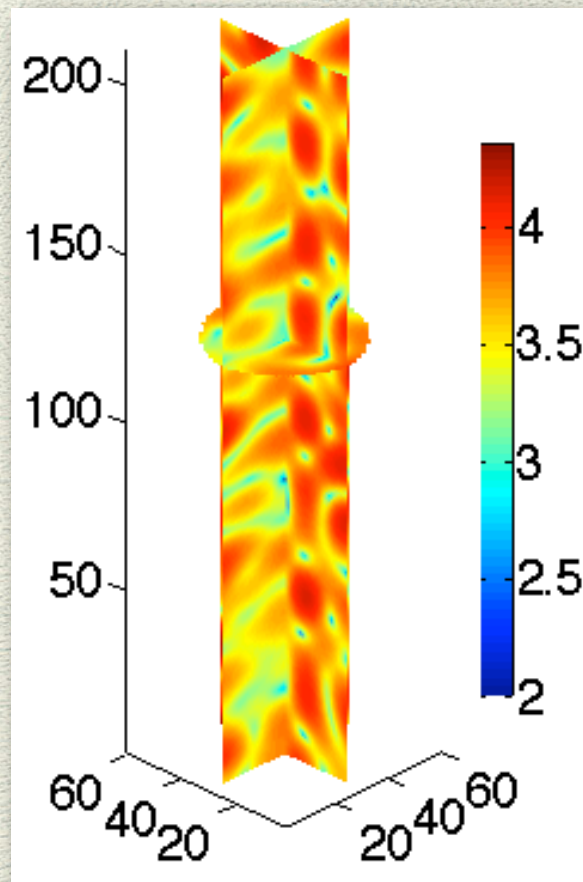
$$= \epsilon_0 \begin{bmatrix} 1 + i \frac{\omega_p^2}{\omega} \frac{a_x}{\Delta} & i \frac{\omega_p^2}{\omega} \frac{c_z + d_{xy}}{\Delta} & i \frac{\omega_p^2}{\omega} \frac{-c_y + d_{xz}}{\Delta} \\ i \frac{\omega_p^2}{\omega} \frac{-c_z + d_{xy}}{\Delta} & 1 + \frac{i \omega_p^2}{\omega} \frac{a_y}{\Delta} & i \frac{\omega_p^2}{\omega} \frac{c_x + d_{yz}}{\Delta} \\ i \frac{\omega_p^2}{\omega} \frac{c_y + d_{xz}}{\Delta} & i \frac{\omega_p^2}{\omega} \frac{-c_x + d_{zy}}{\Delta} & 1 + i \frac{\omega_p^2}{\omega} \frac{a_z}{\Delta} \end{bmatrix}$$

Full-wave solution of the electromagnetic field

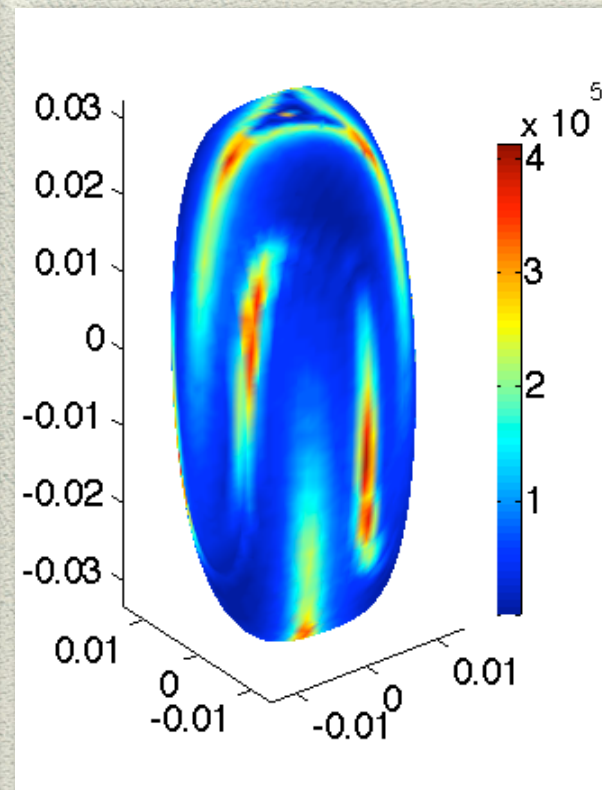


Full-3D non homogeneous dielectric permittivity
Tensor depends on local density and B-field

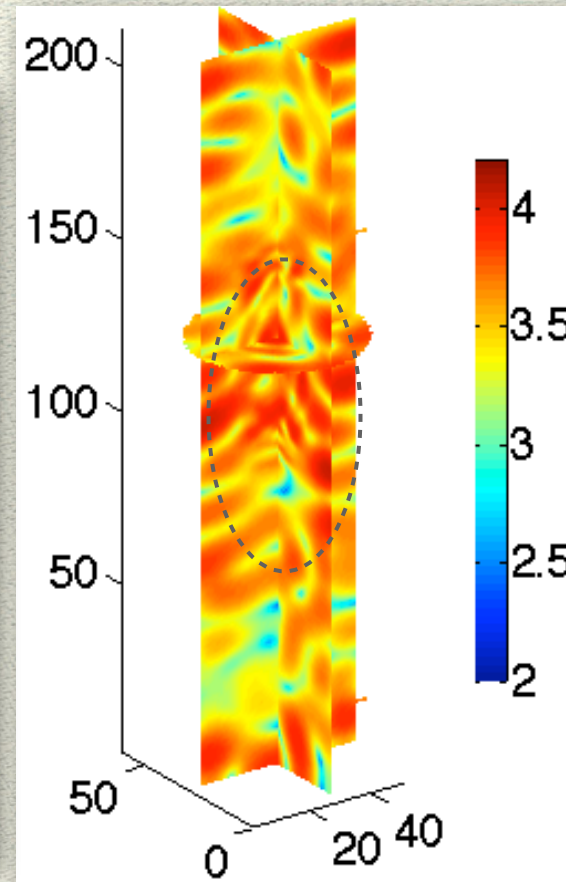
Searching self-consistency



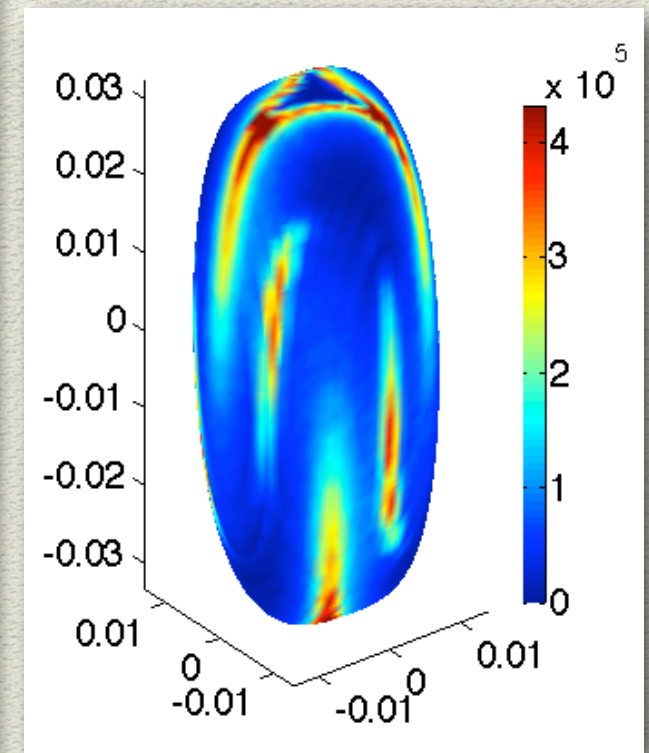
Freq. dom. solution
step 0
(vacuum cavity)



Particle Tracking
step 1
(vacuum
field+plasmoid-halo
initial density distr.)



Freq. dom. solution
step 1
(70% density from
plasmoid halo
model+30% step-1
density structure)

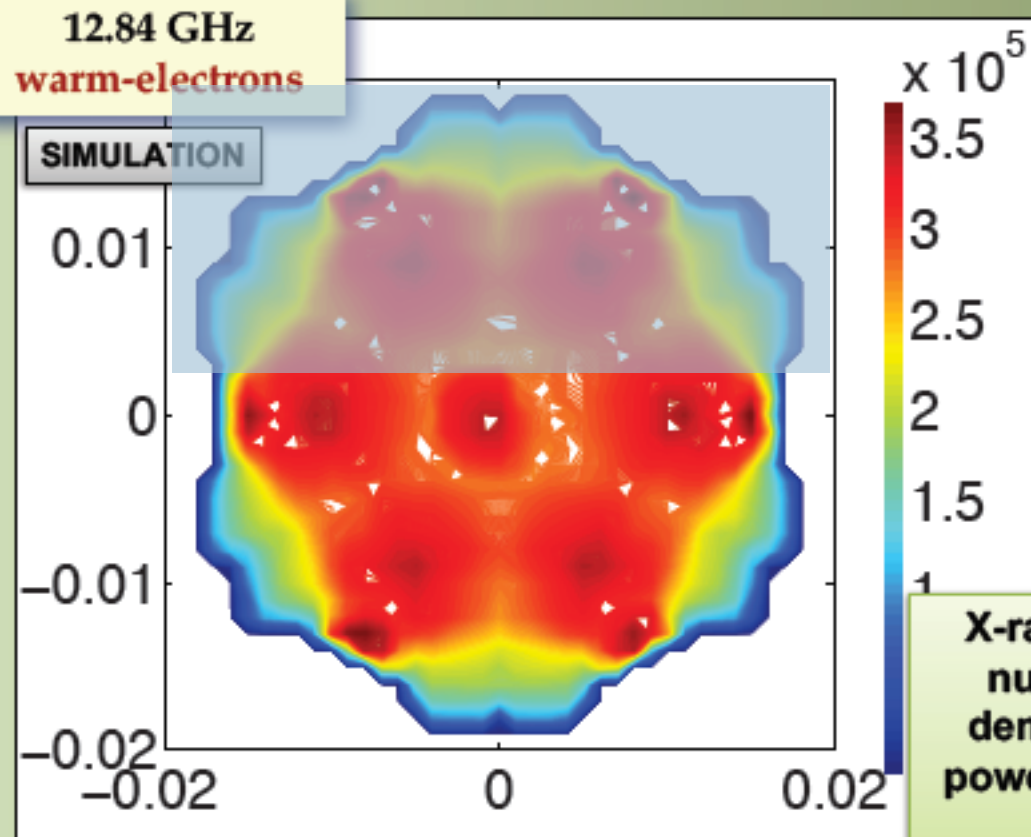


Particle Tracking
step 2
(70% vacuum field +
30% step-1 full-wave
calculated field)

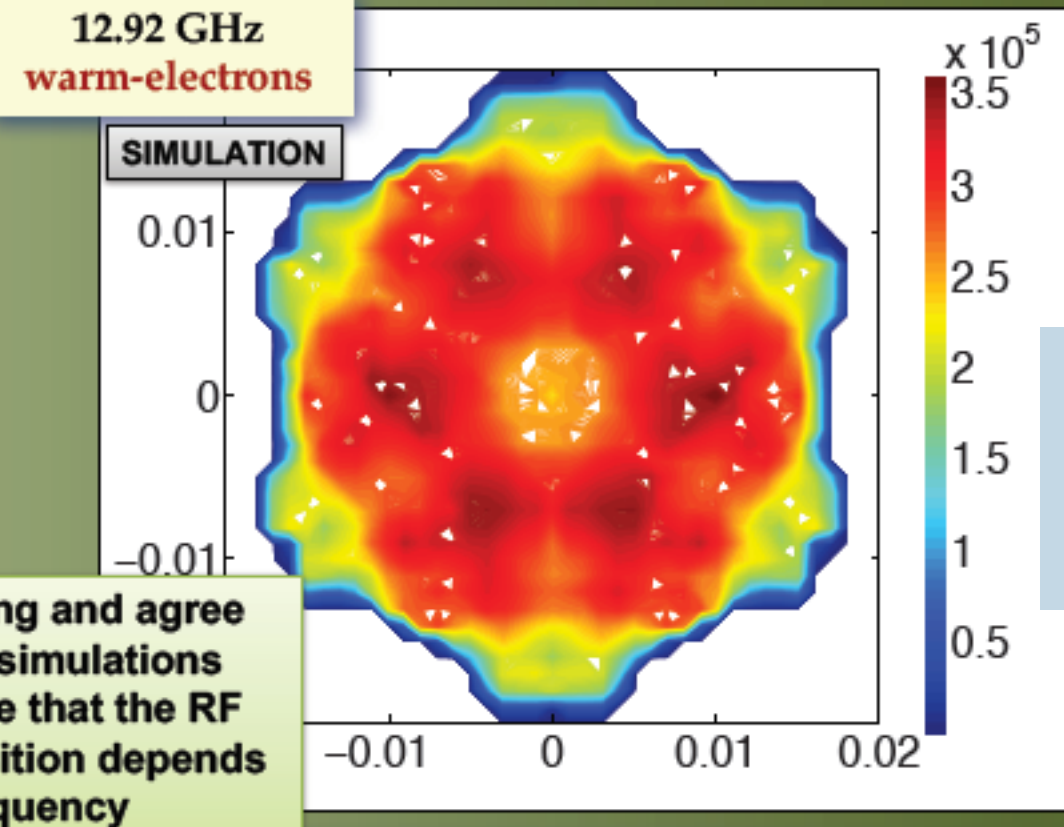
Comparison to self-consistent simulations

12.84 and 12.92 GHz

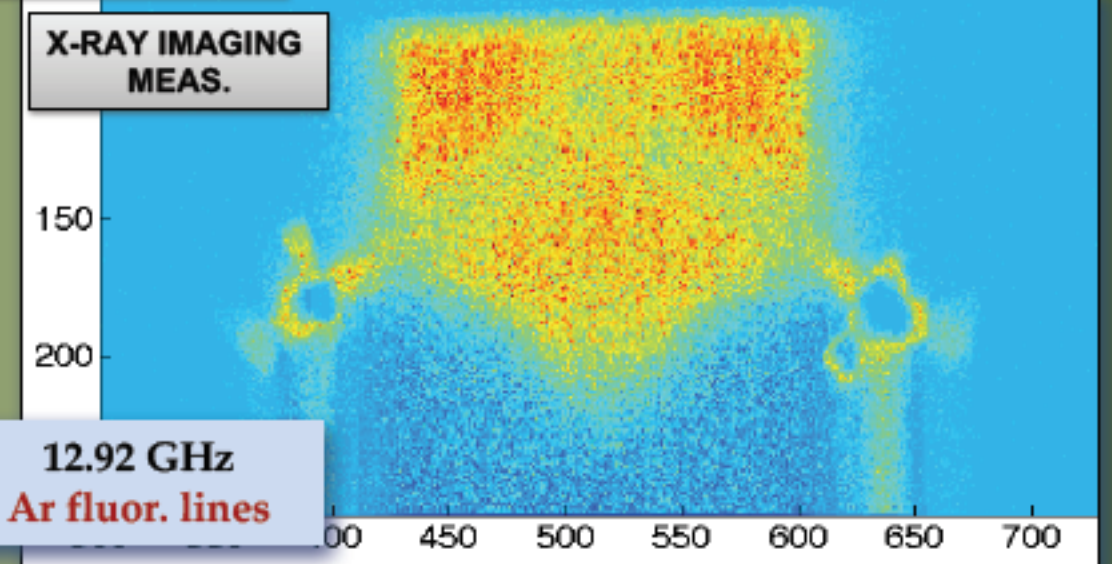
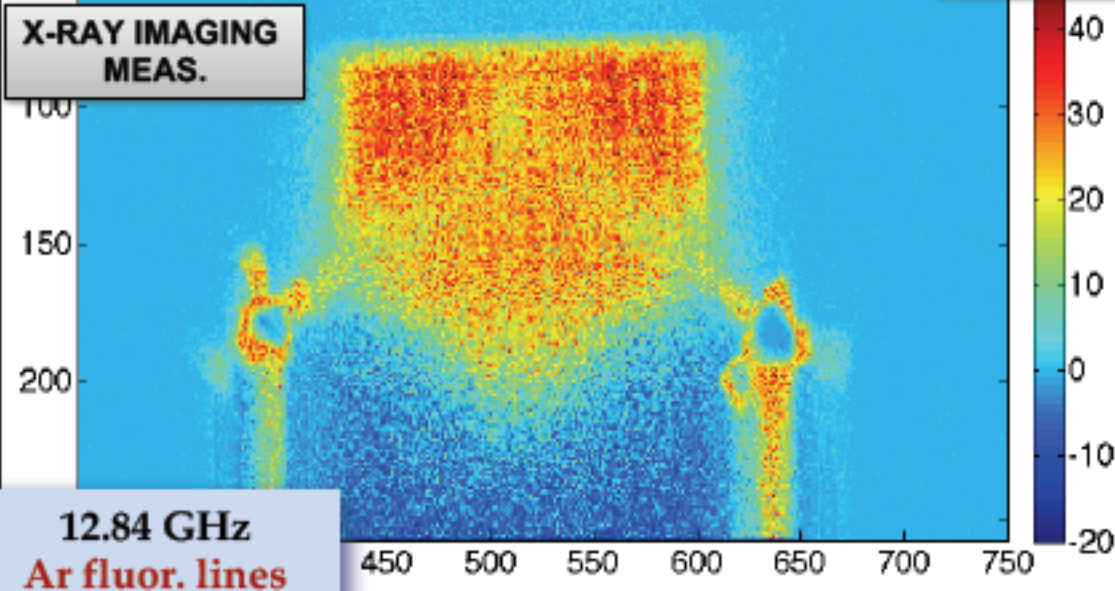
Energy density in 2-12 keV range on xy plane z=0
@12,84 GHz



Energy density in 2-12 keV range on xy plane z=0
@12,92 GHz



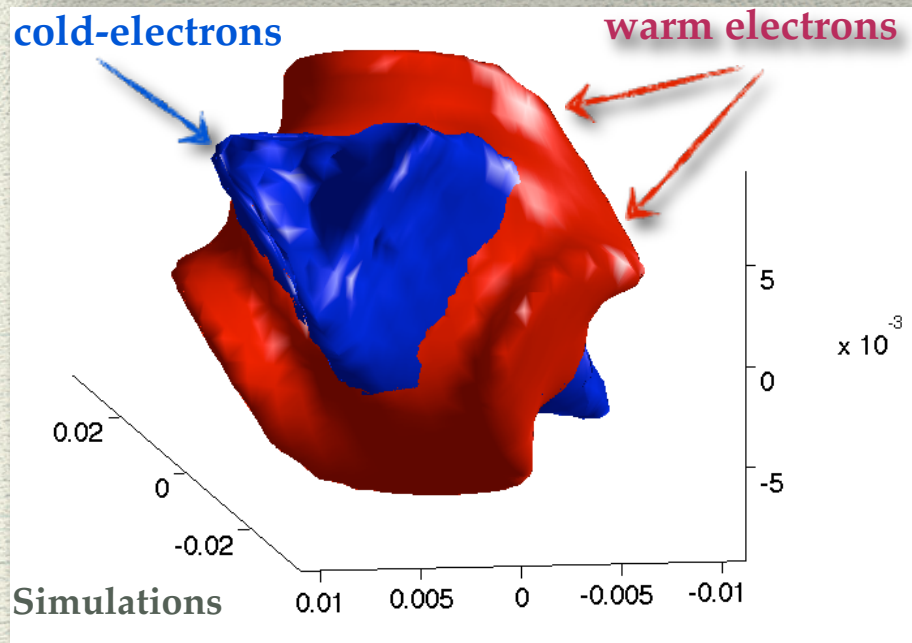
X-ray imaging and agree numerical simulations demonstrate that the RF power deposition depends of frequency



Including ionization

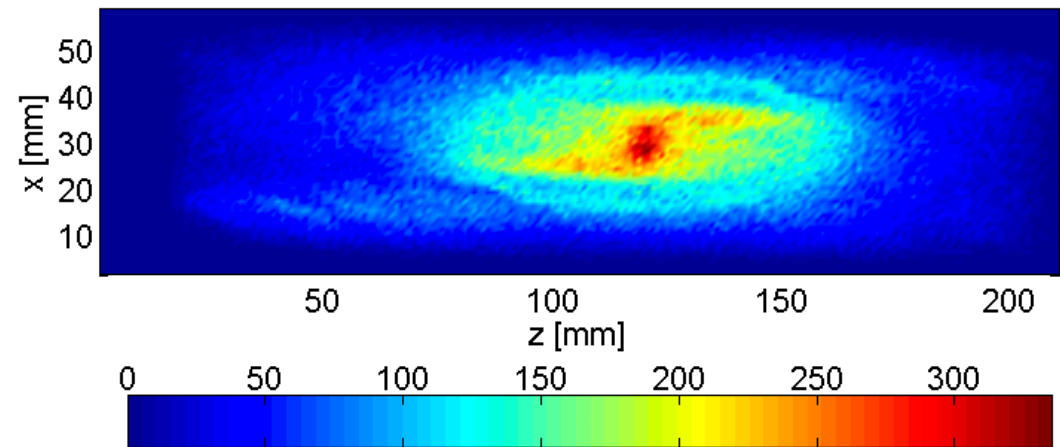
$$\frac{\nu_{ion i \rightarrow i+1}}{n_e} = \sum_{j=1}^N \frac{a_{ij} q_{ij}}{T_e^{3/2}} \left\{ \frac{1}{P_{ij}/T_e} E_1(P_{ij}/T_e) - \frac{b_{ij} e^{c_{ij}}}{P_{ij}/T_e + c_{ij}} E_1(P_{ij}/T_e + c_{ij}) \right\}$$

Lotz formula for multi-step ionisation

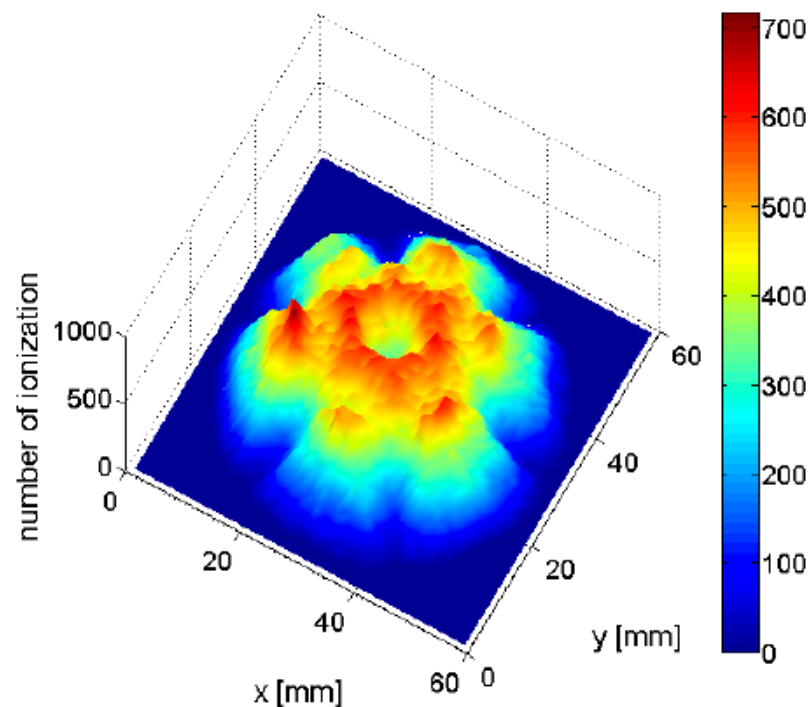


Starting from 3D distribution of electrons in the plasma, maps of ions distribution can be obtained

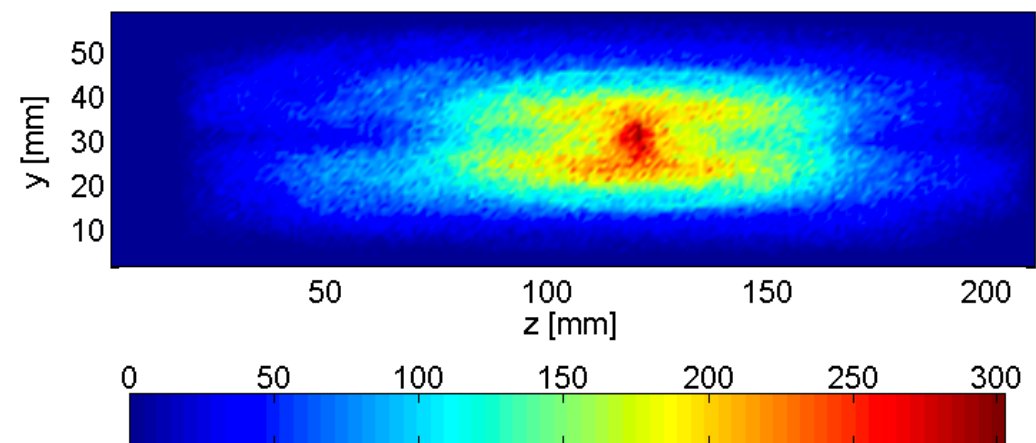
Projection on xz plane of ionization map for O



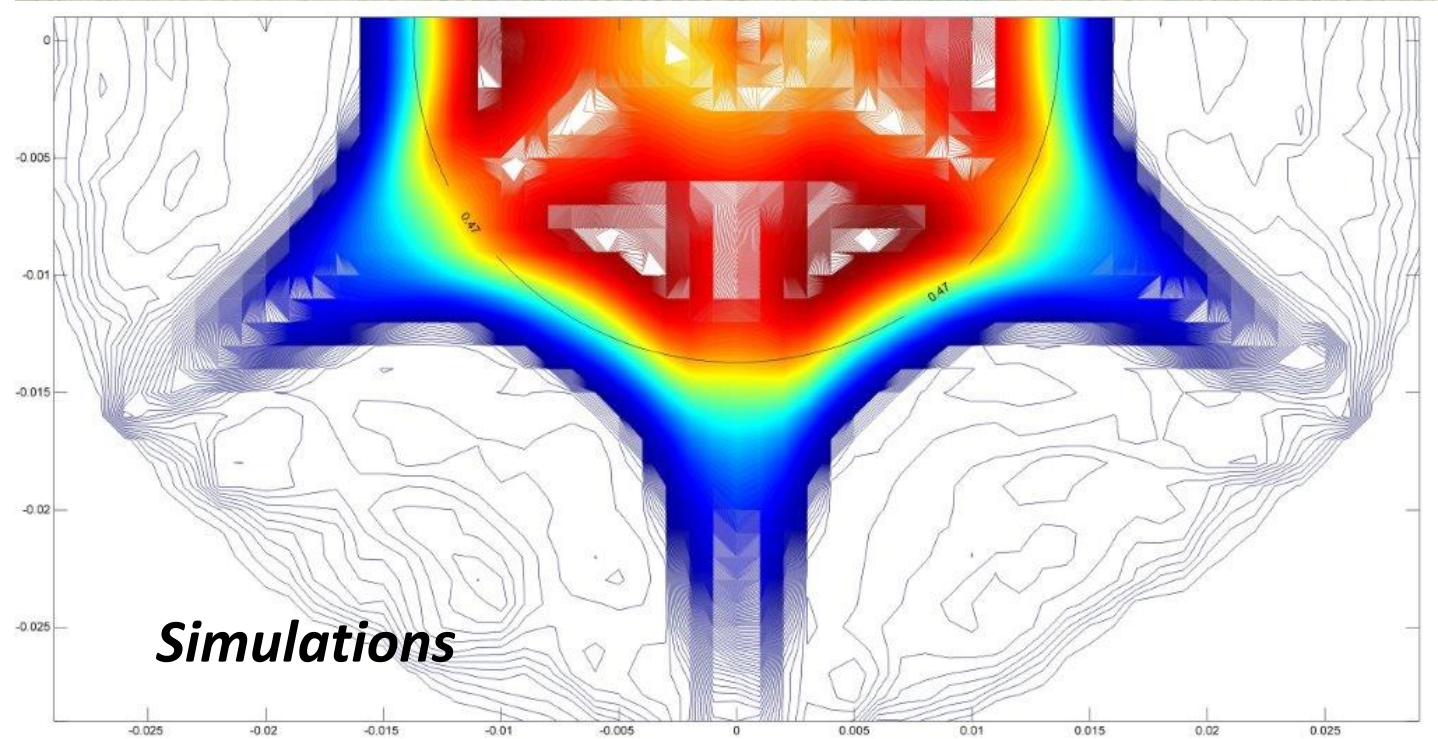
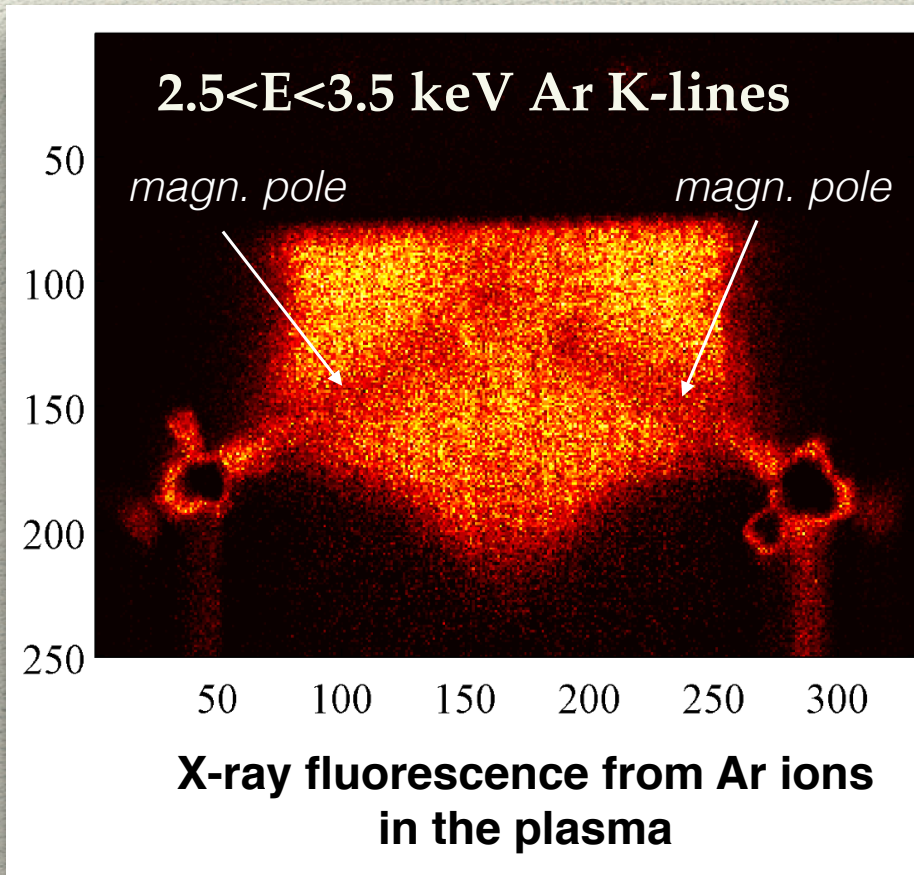
Projection on xy plane of ionization map for Ar



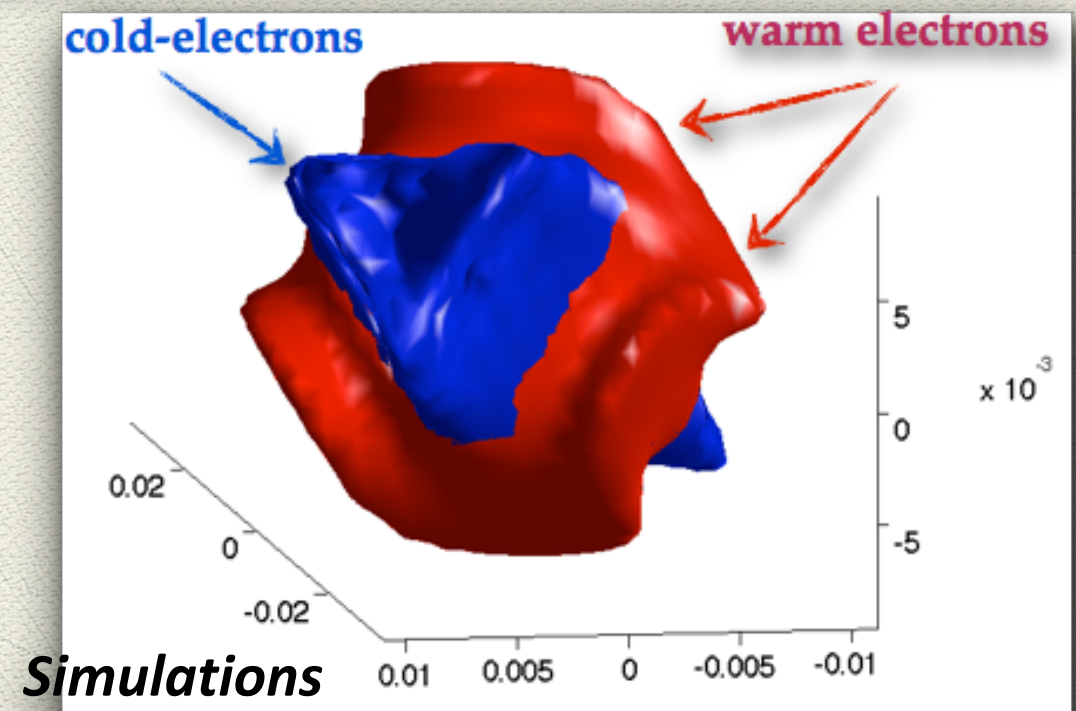
Projection on yz plane of ionization map for O



X-ray imaging and 3D plasma modelling



3D self-consistent simulations very well reproduce energy content distribution of the plasma, which in turn fits with experimental detected displacement of Argon ions



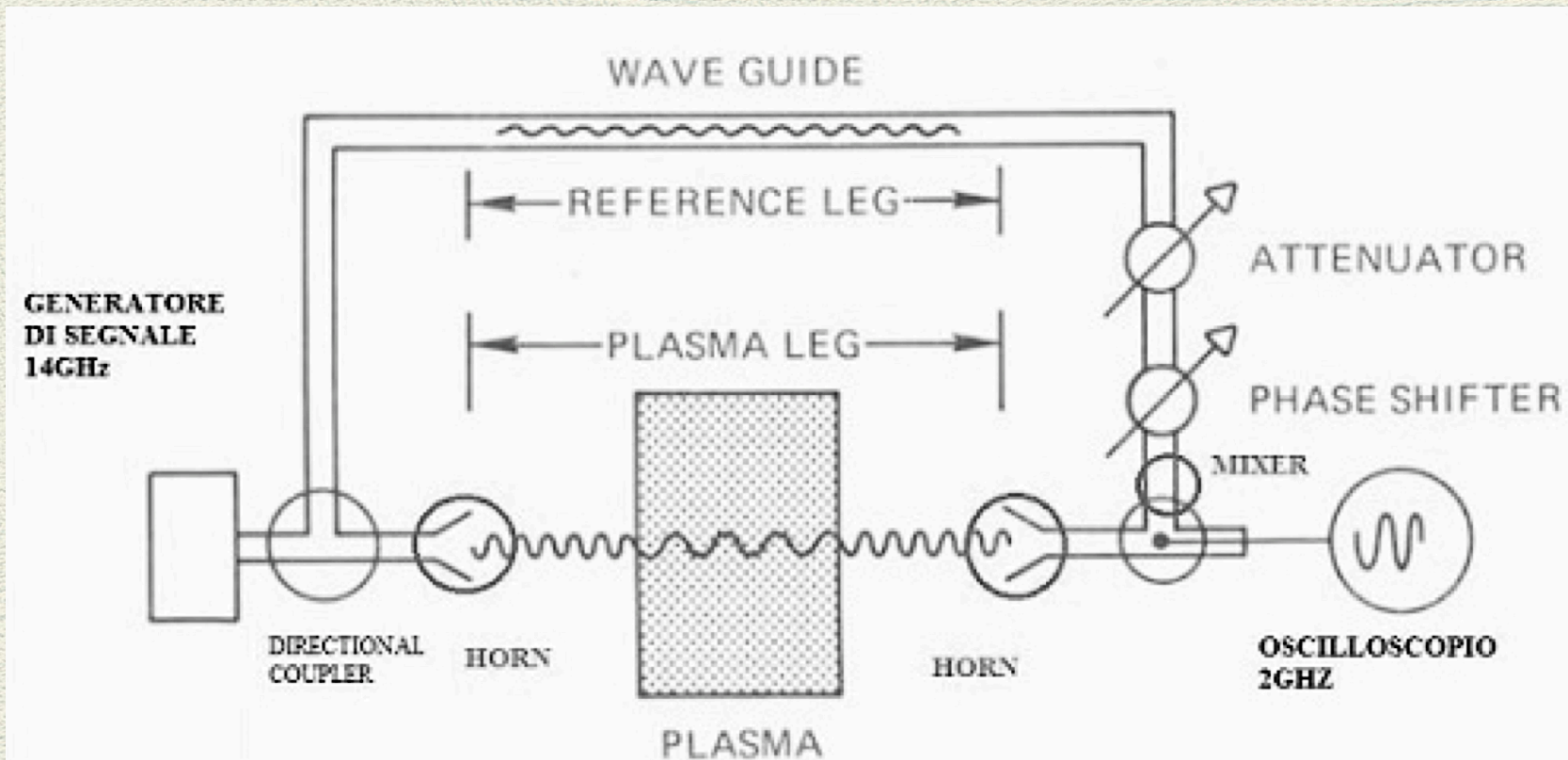
Probing the plasma density in all the energy domains



VESPRI

VERY Sensitive evaluation of Plasma density by micROWAVE Interferometry

Probing the plasma density in all the energy domains



Classical Scheme of Interferometer

How to calculate the density n of the plasma

$$\Delta\varphi = \frac{\omega}{c} \left[1 - \left(1 - \frac{\omega_p^2}{\omega^2} \right)^{\frac{1}{2}} \right] L \quad \longrightarrow \quad \omega_p^2 = \frac{4\pi n e^2}{m \epsilon_0} \quad \longrightarrow$$

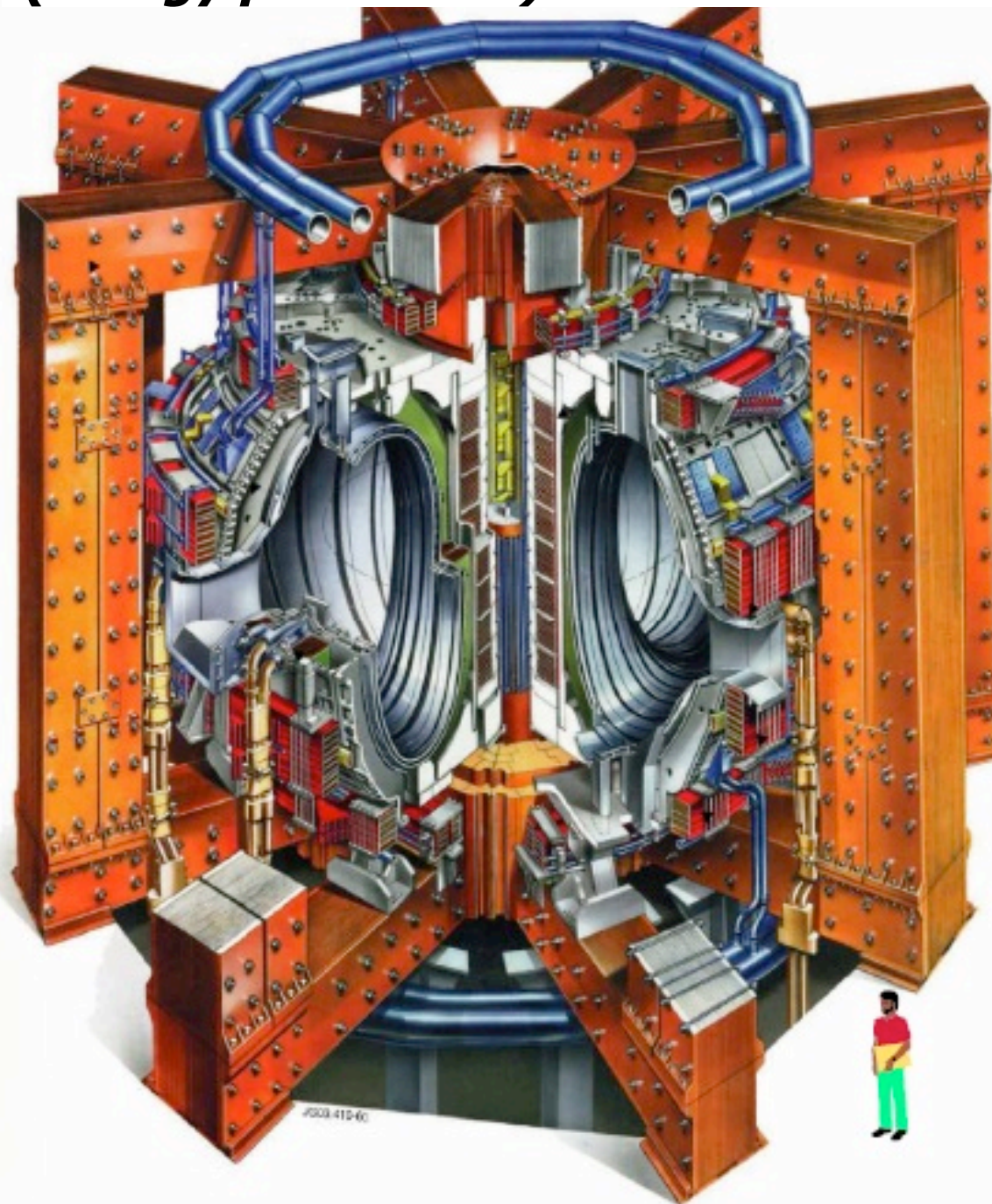
In plasmas the phase variation depends on the "natural plasma frequency"

The plasma frequency depends on the density

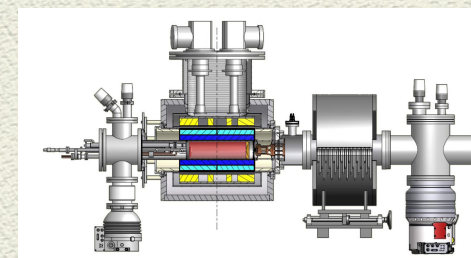
Microwave interferometry measures plasma density through a measurement of phase shift.

The main challenge: "downsizing"

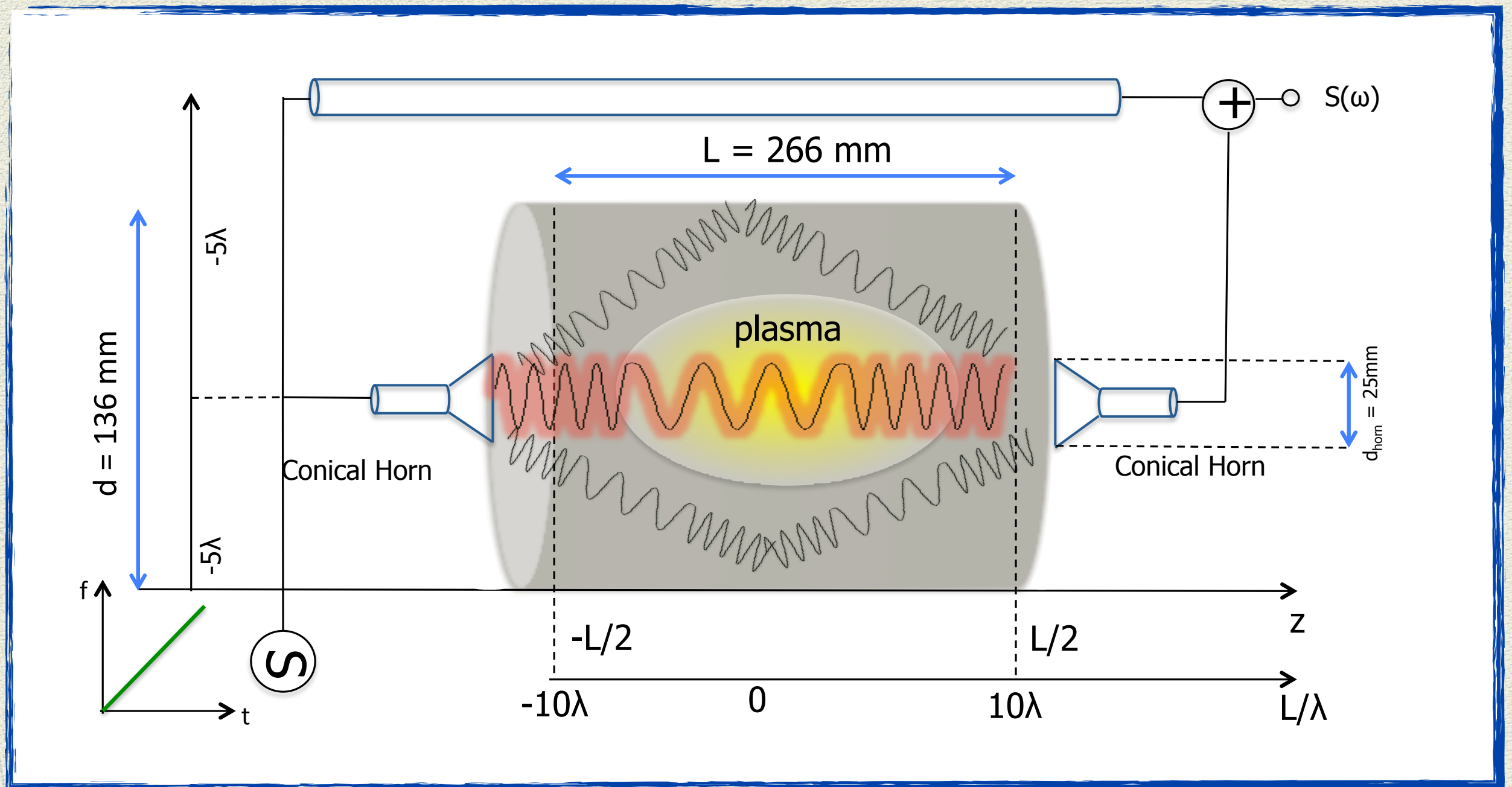
**JET Tokamak for nuclear fusion
(energy production)**



**ECR ION Source:
extremely compact
plasma machine**



Probing the plasma density in all the energy domains

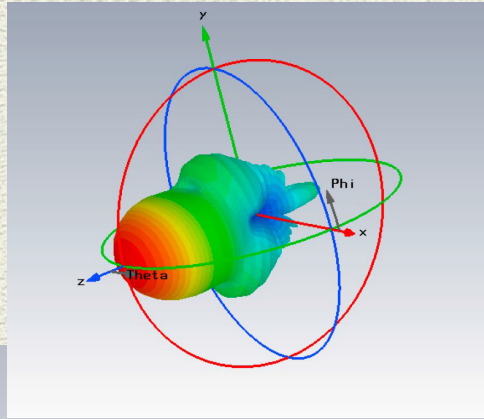


Drawbacks

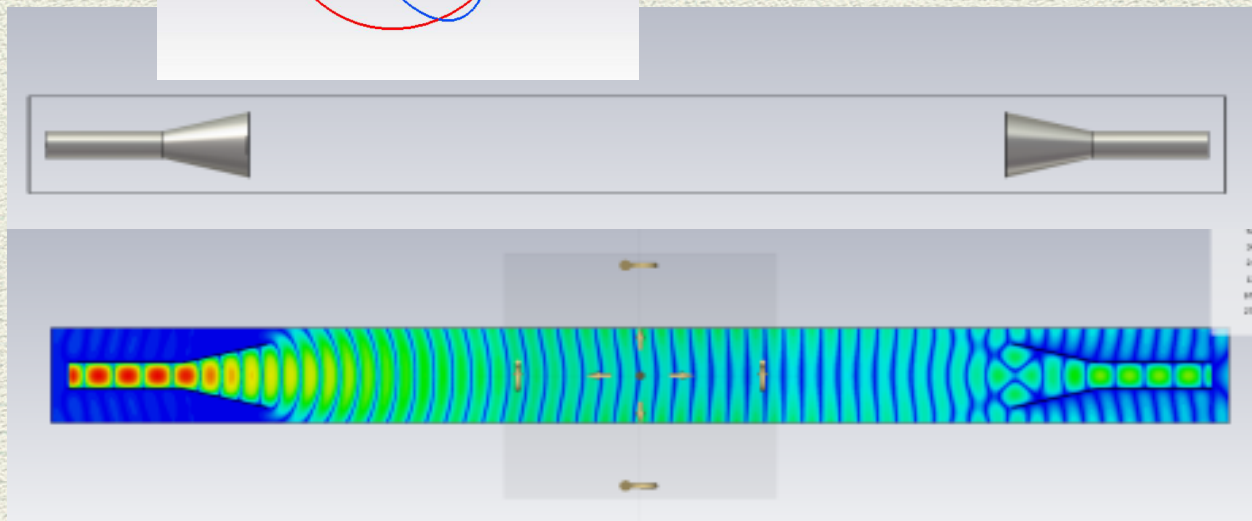


- Limited ECRIS access probing port
- Multi-paths introduce spurious signals

Interferometry in ECRIS: simulations

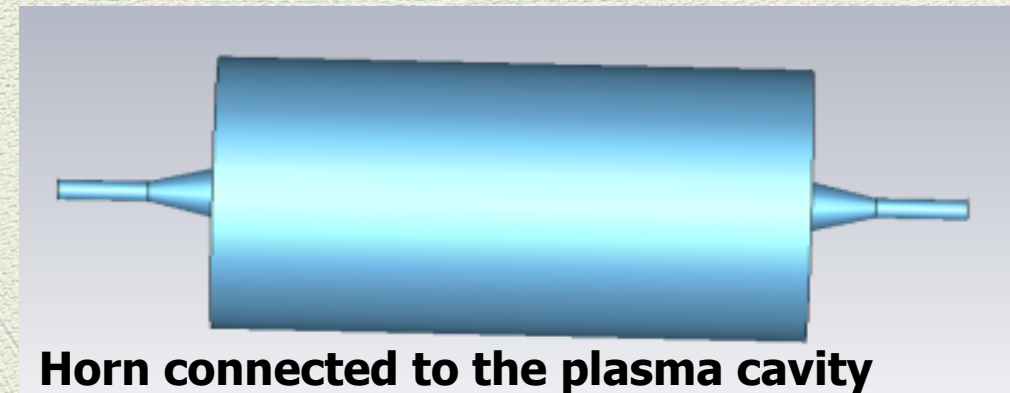


•Antenna directivity

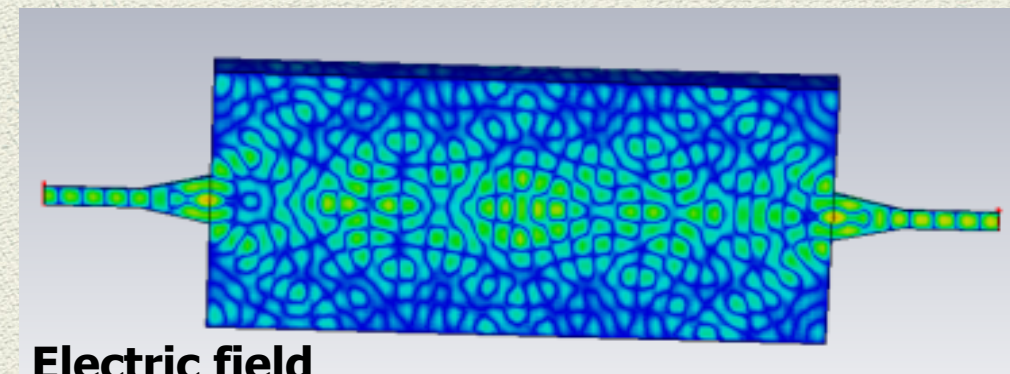


Horn-to-horn transmission for antennas facing each other in vacuum

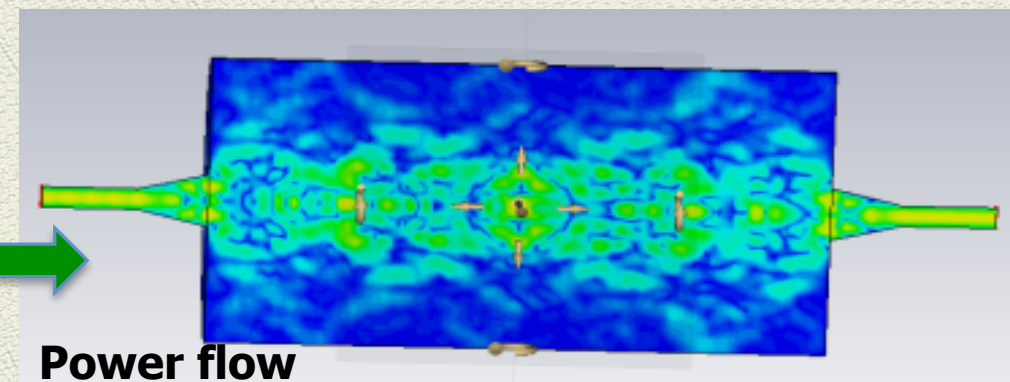
Numerical simulations (COMSOL+CST) put in evidence cavity walls effects



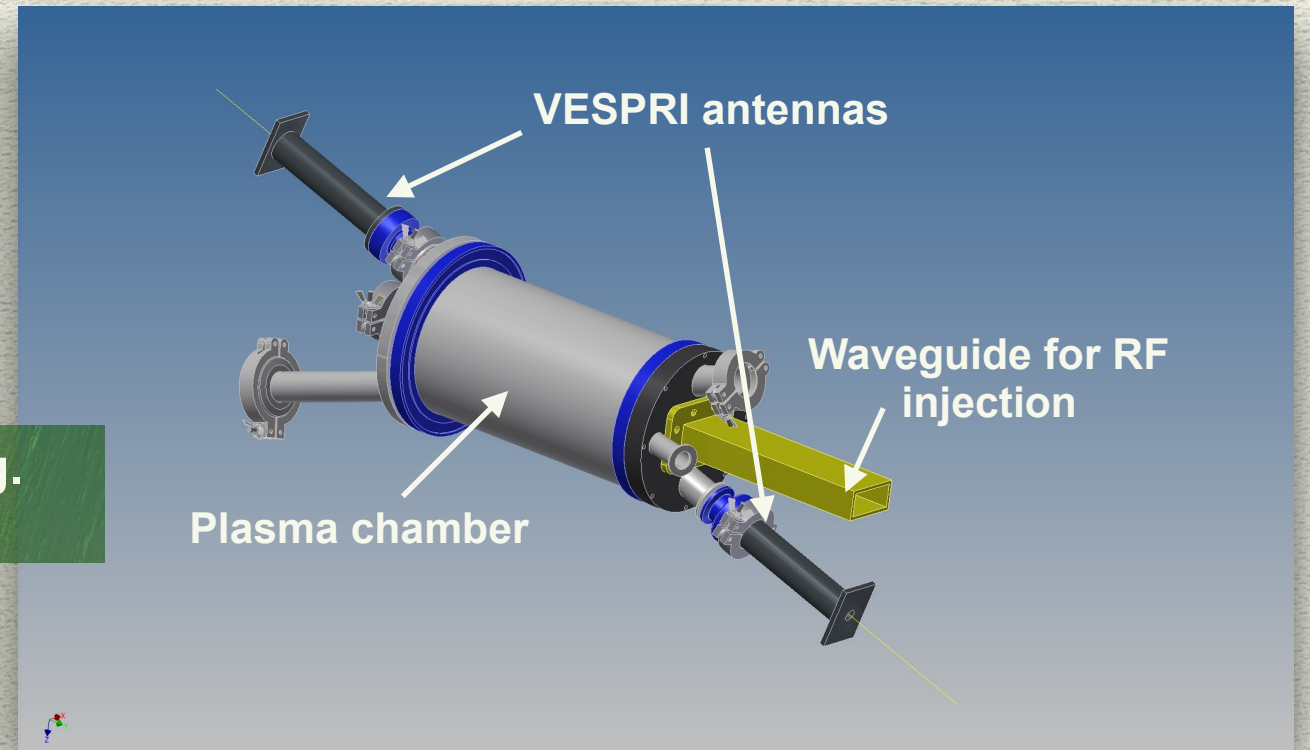
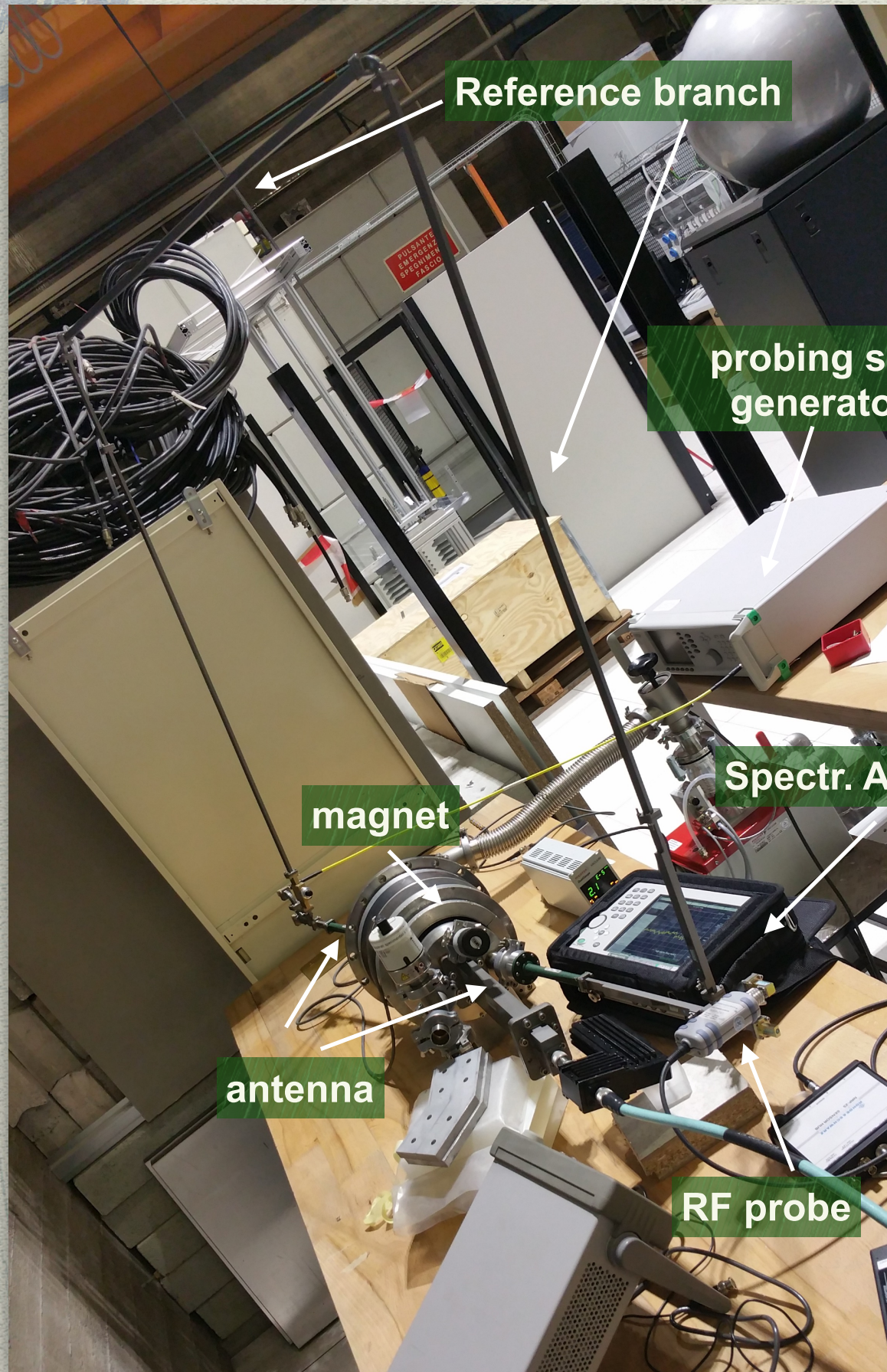
Horn connected to the plasma cavity



Electric field

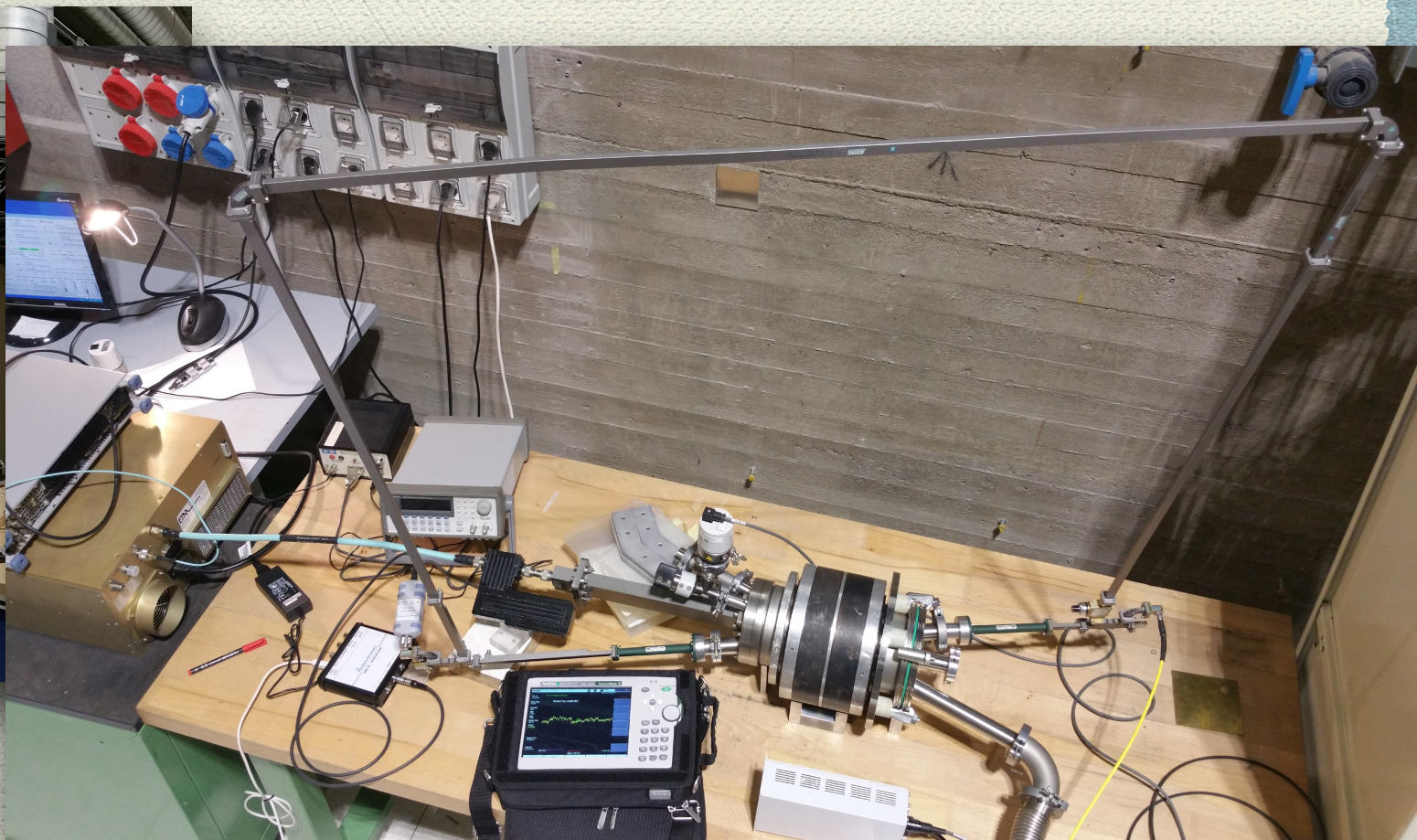
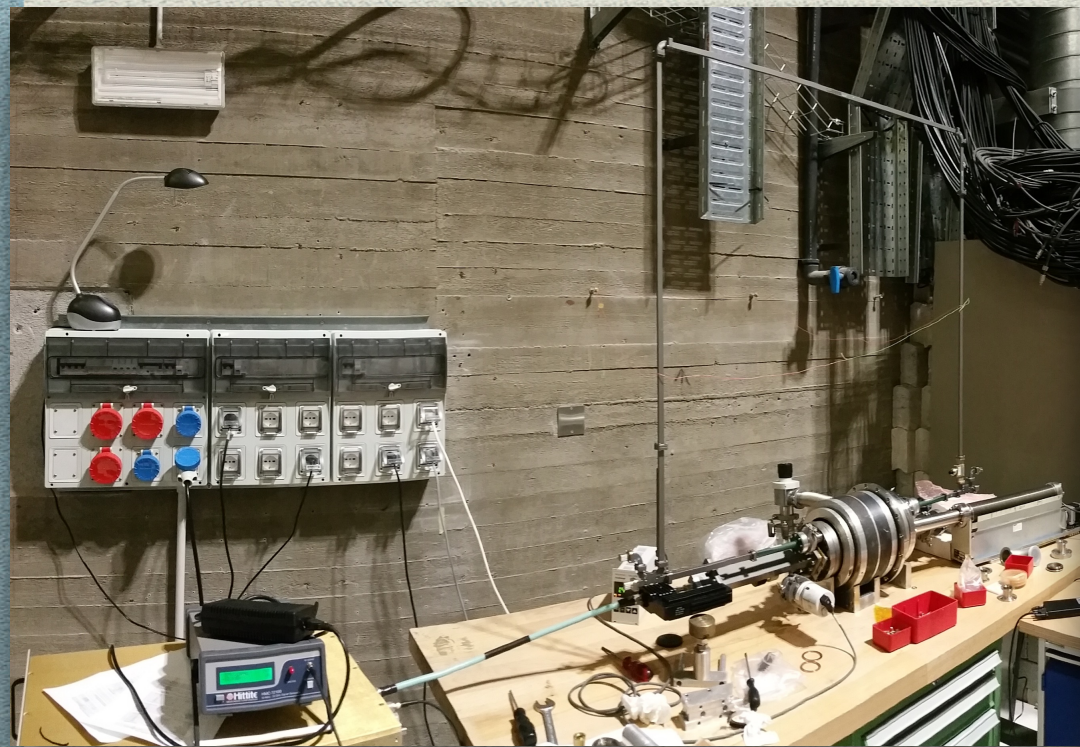
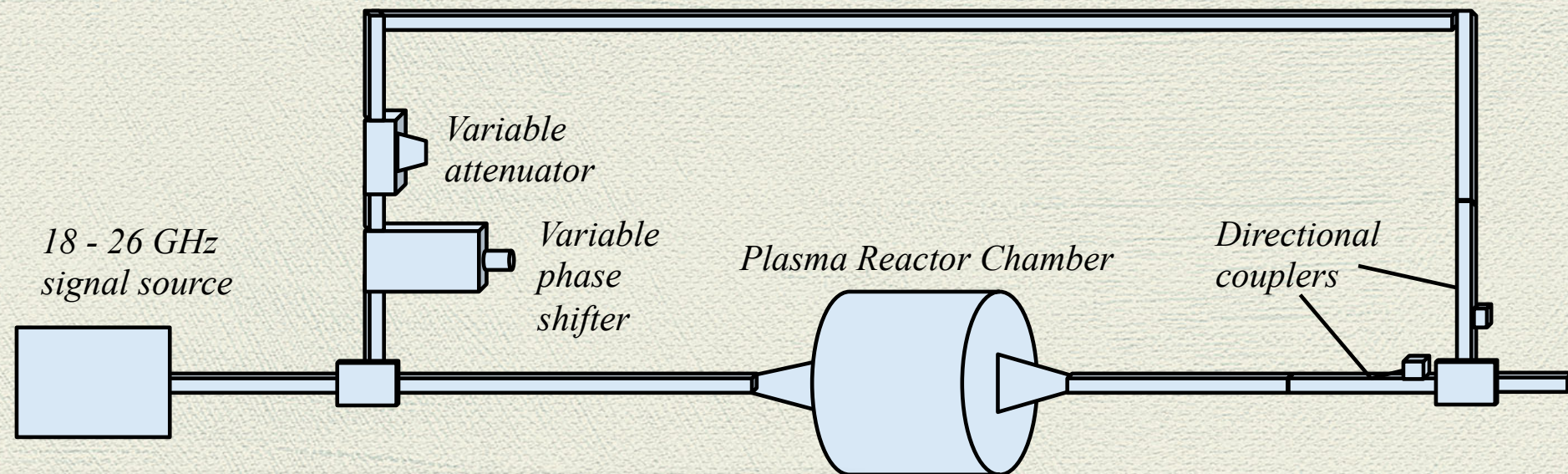


Power flow

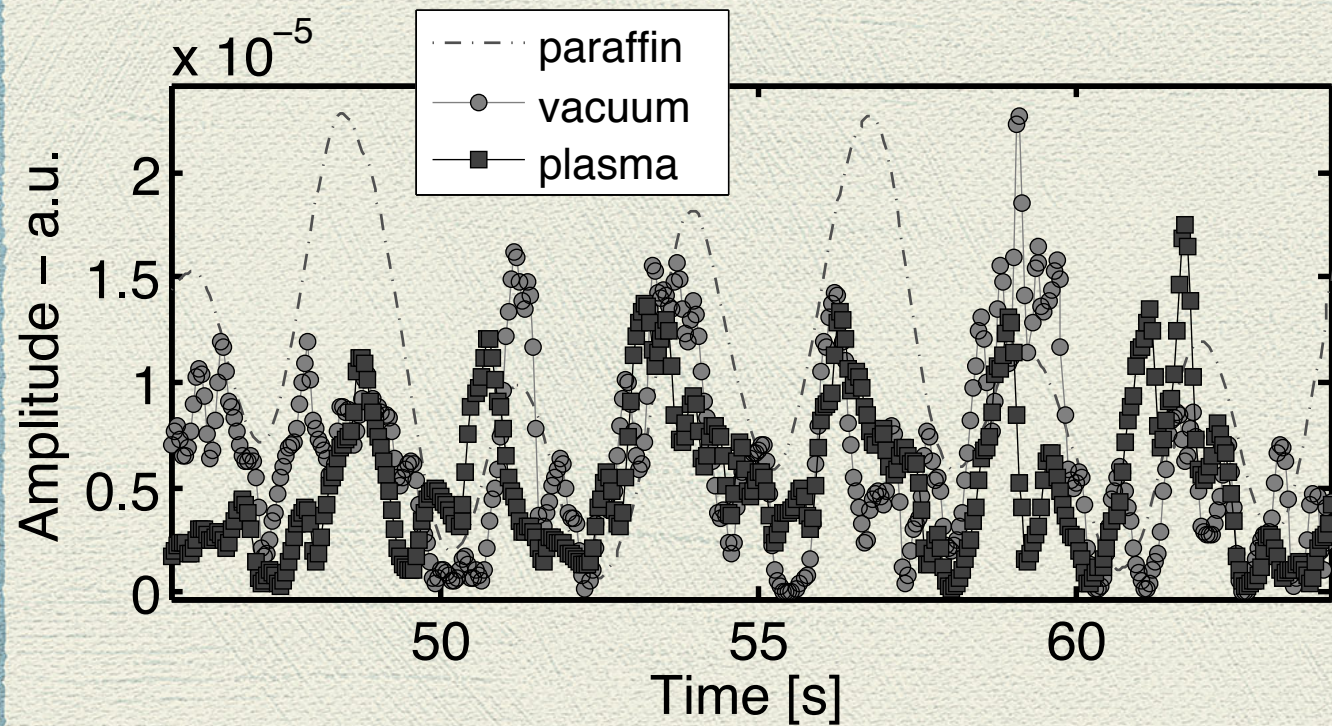


Interferometry
in ECRIS:
measuring of plasma
density inside the
cavity of the LNS
plasma reactor

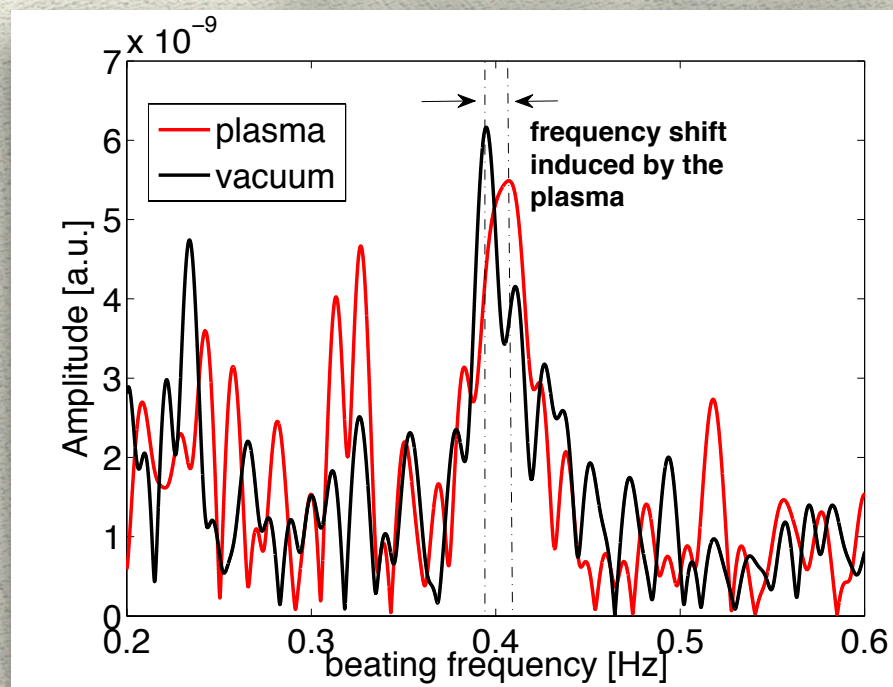
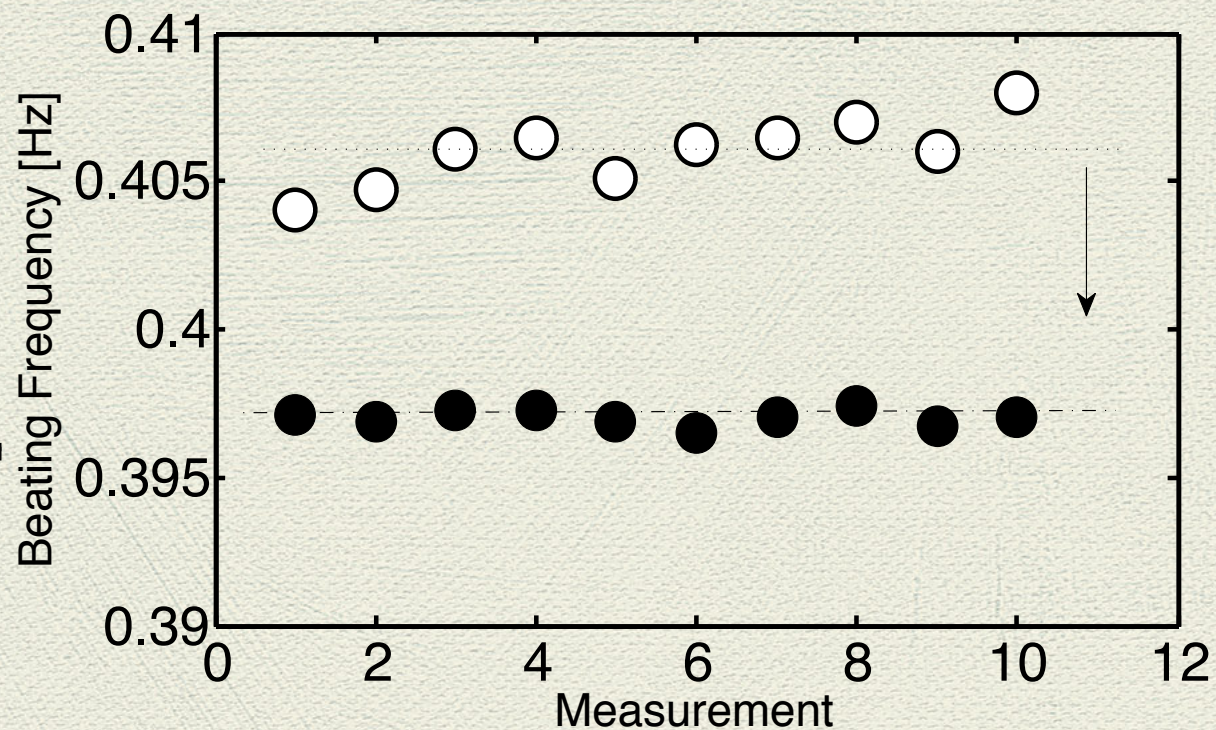
Interferometry in ECRIS: the frequency sweep method



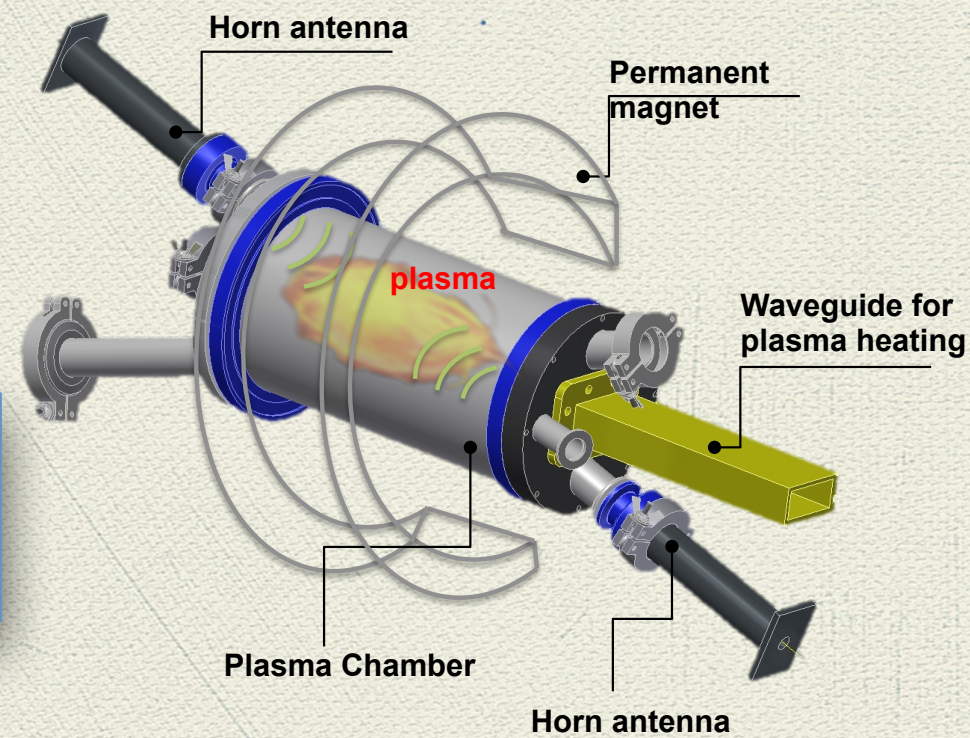
Interferometry in ECRIS: the measurements in plasma



FFT spectrum with plasma vs vacuum

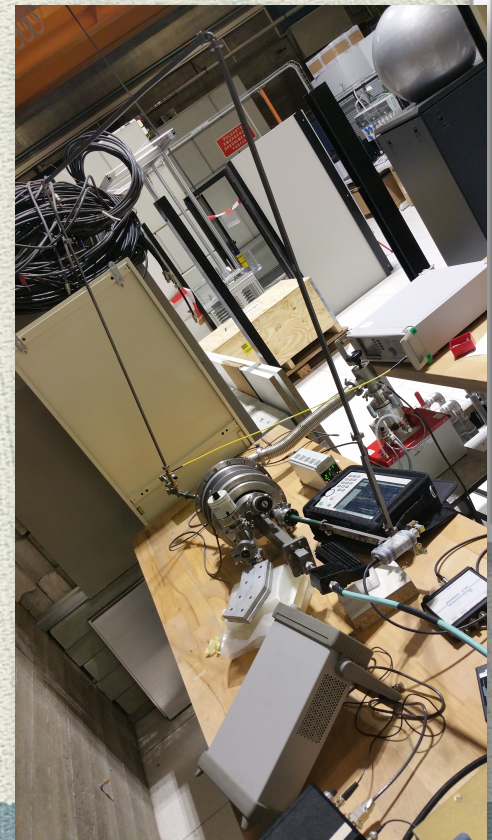
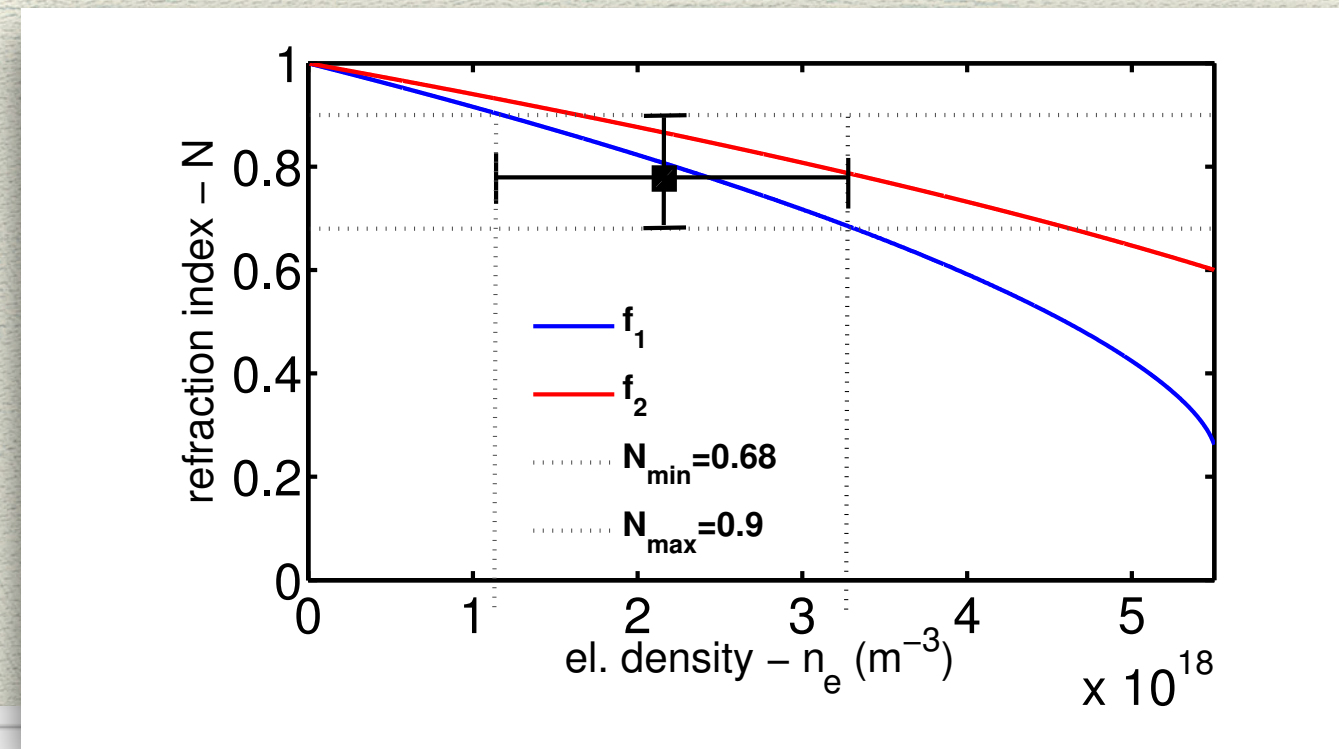
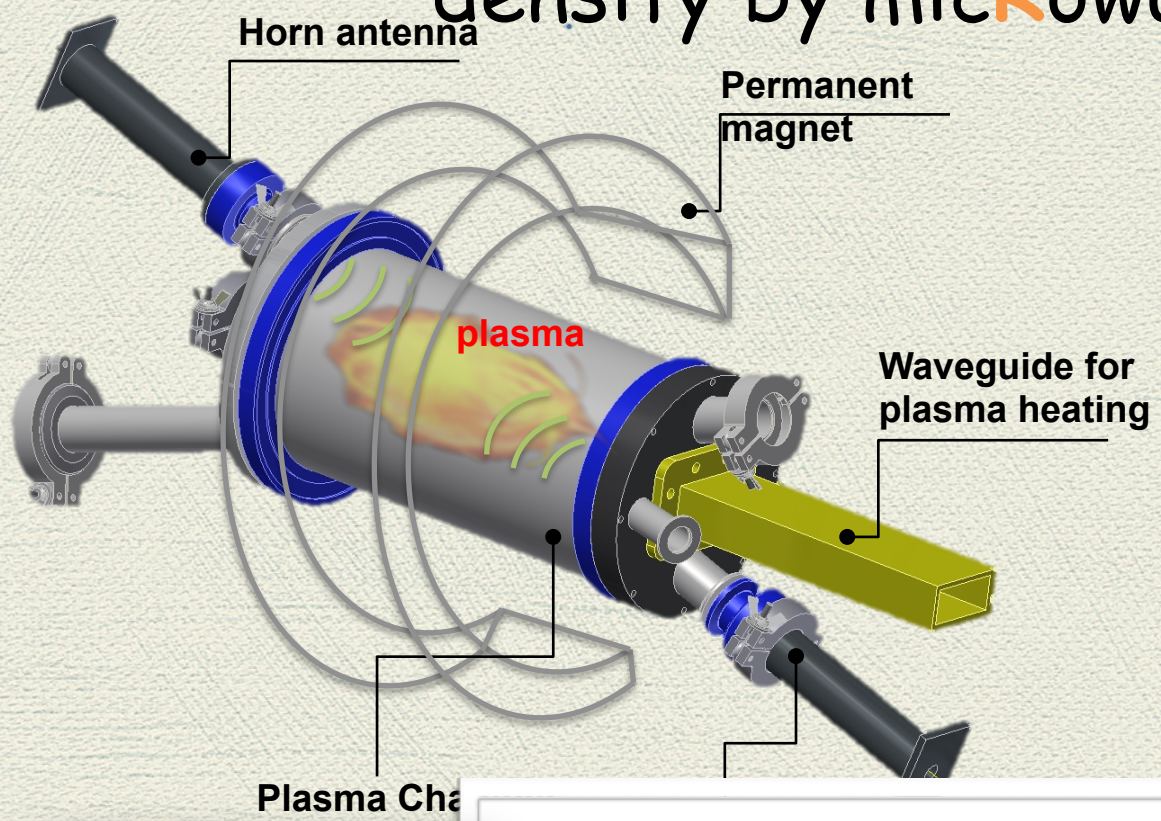


[G. Torrisi et al. "A Novel Microwave Frequency Sweep Interferometer for ECR Plasma Electron Density Measurements", accepted for oral presentation at EuMW2016 and publication on IEEE Xplore]



VESPRI

VERY Sensitive evaluation of Plasma density by micROWave Interferometry



1 REVIEW OF SCIENTIFIC INSTRUMENTS 87, 000000 (2016)

2 **The first measurement of plasma density in an ECRIS-like device by means**

3 **of a frequency-sweep microwave interferometer**

4 **D. Mascali,^{1,a)} G. Torrì,¹ O. Leonardi,¹ G. Sorbello,^{1,2} G. Castro,¹ L. G. Celona,¹**

5 **R. Miracoli,³ R. Agnello,¹ and S. Gammino¹**

6 ¹INFN - Laboratori Nazionali del Sud, 95123 Catania, Italy

7 ²Università di Catania, Dipartimento di Ingegneria Elettrica Eletttronica e Informatica, 95125 Catania, Italy

8 ³ESS Bilbao, 48170 Zamudio, Spain

9 (Received 29 June 2016; accepted 15 September 2016; published online 15 September 2016)

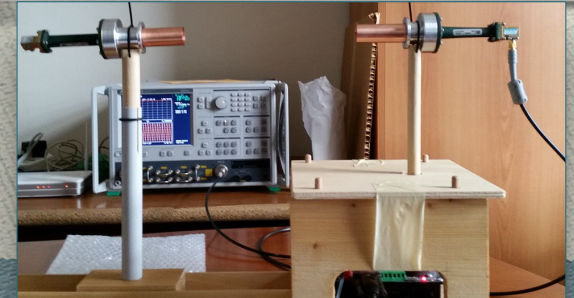


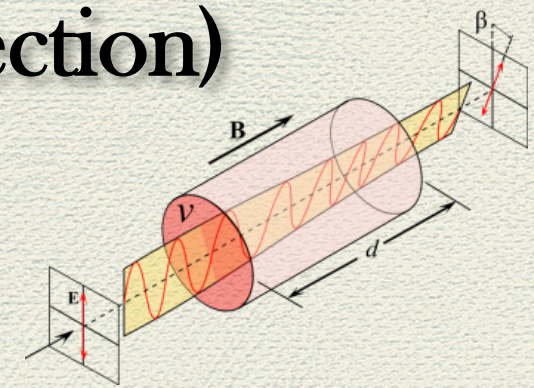
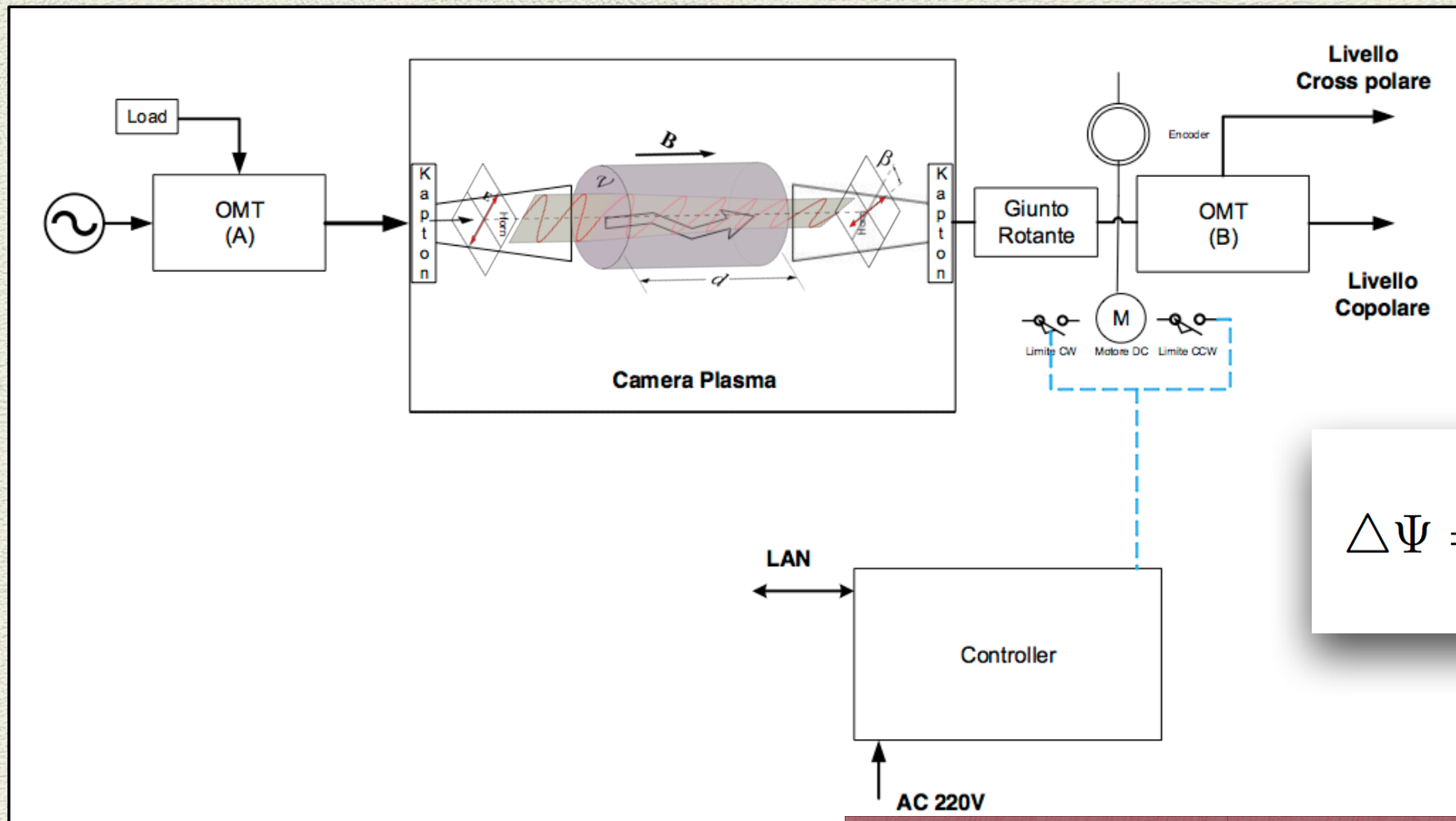
TABLE I. Horn-to-horn signal beating frequencies and corresponding indexes of refraction. Comparison among the three cases: empty, paraffin, plasma filled cavity.

Medium	P_{RF} [W]	ω_{beat} [rad/sec]	refr. index N
Empty Cavity	0	$2\pi * 0.397$	1 ^a
Bulk Paraffin	0	$2\pi * 0.380$	1.43 ^b
Plasma	150	$2\pi * 0.407$	0.79 ± 0.11^c

^a assumed by definition for the absolute calibration.
^b in agreement with the literature value $N_{20GHz} \simeq 1.45$.
^c Error evaluation in a series of ten measurements.

Faraday rotation measurements

Next step Polarimetry (Faraday rotation detection)



$$\Delta\Psi = \frac{e^3\lambda^2}{2\pi m_e^2 c^4} \int_0^L n_e(l) B_{\parallel}(l) dl$$

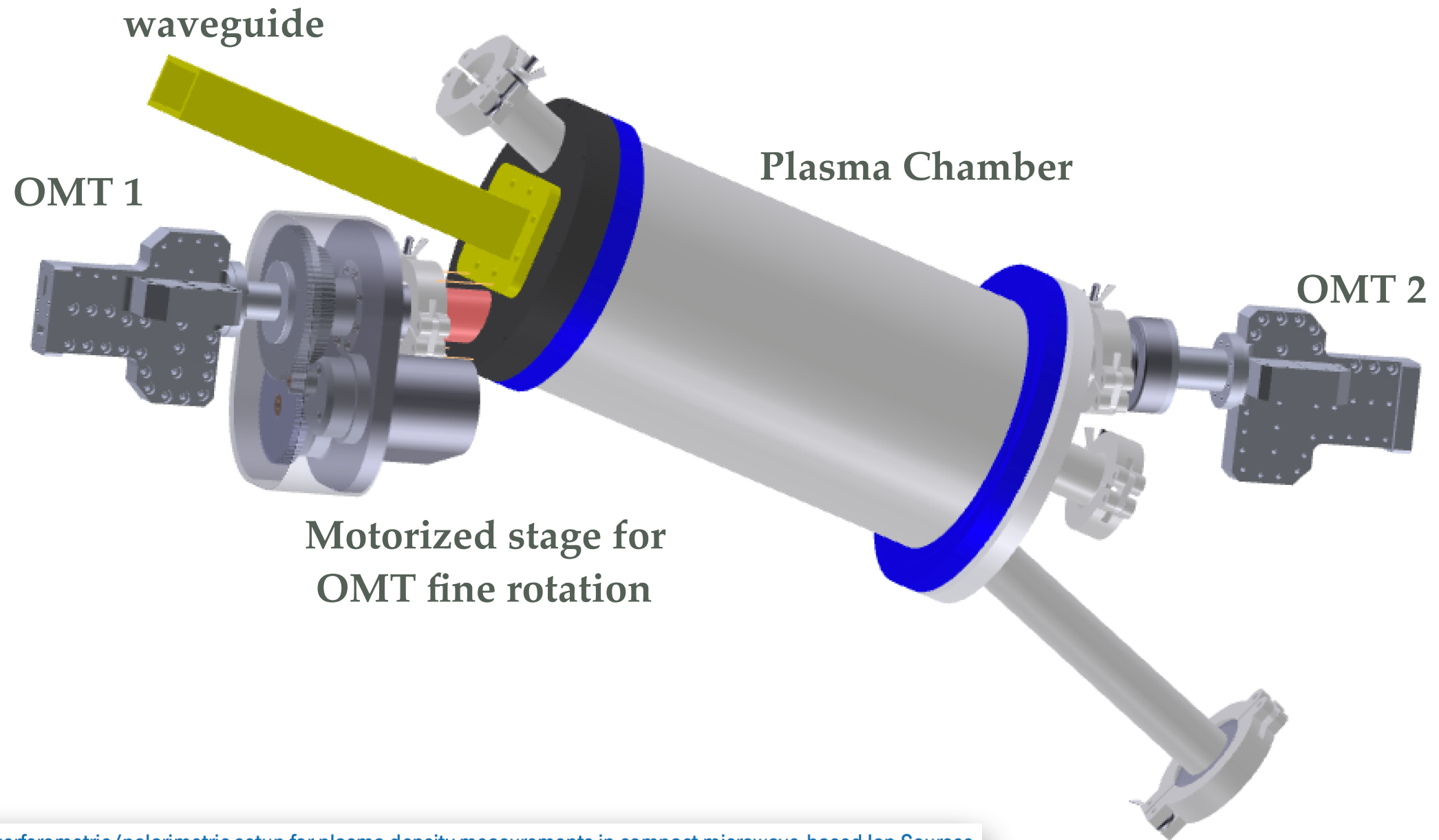
Setup Block Diagram

The polarimetric system has been designed jointly with SICIL-Sat s.r.l. (satellite communications)

INFN

Faraday rotation measurements

Final Design of the OMT-based system



A new interferometric/polarimetric setup for plasma density measurements in compact microwave-based Ion Sources

G. Torrisi, E. Naselli, D. Mascali, G. Castro, L. Celona, G. Sorbello and S. Gammino

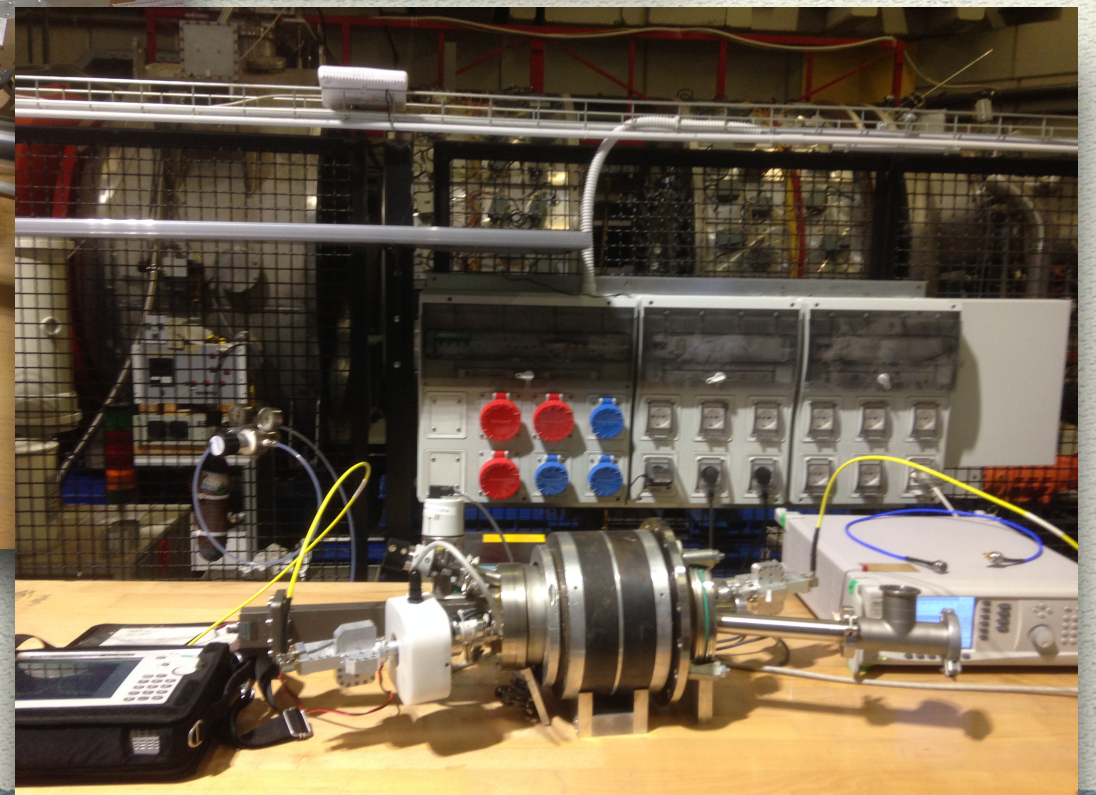
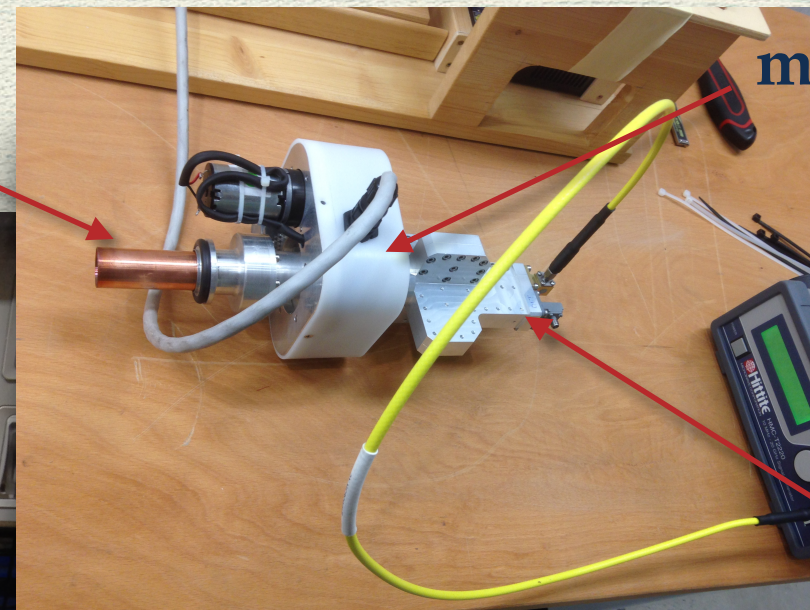
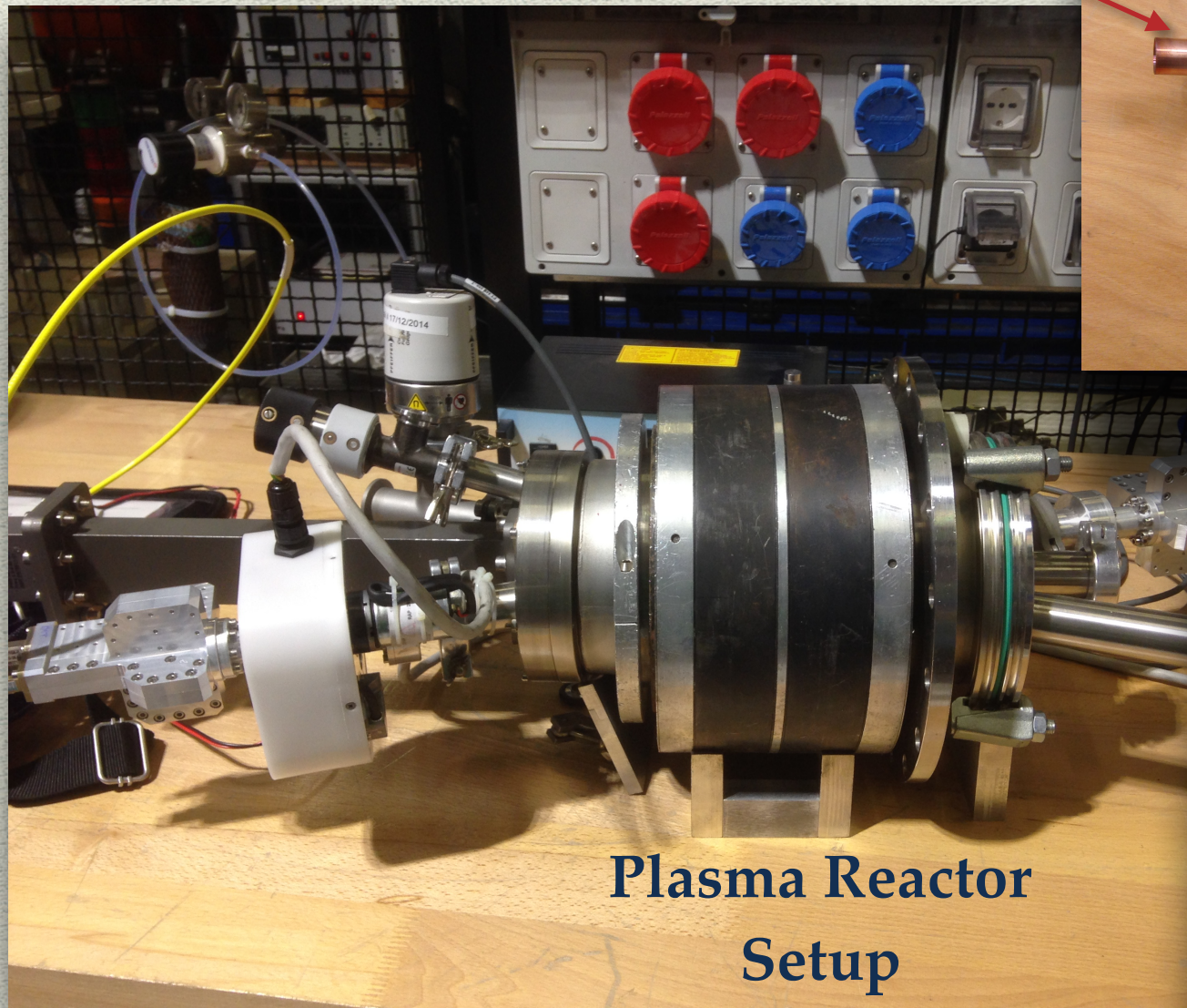
2017 *J. Inst.* **12** C10003 <https://doi.org/10.1088/1748-0221/12/10/C10003>

Faraday rotation measurements Installation of the OMT-based system

Antenna

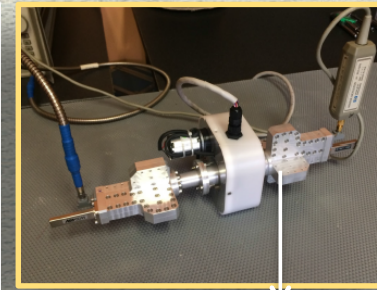
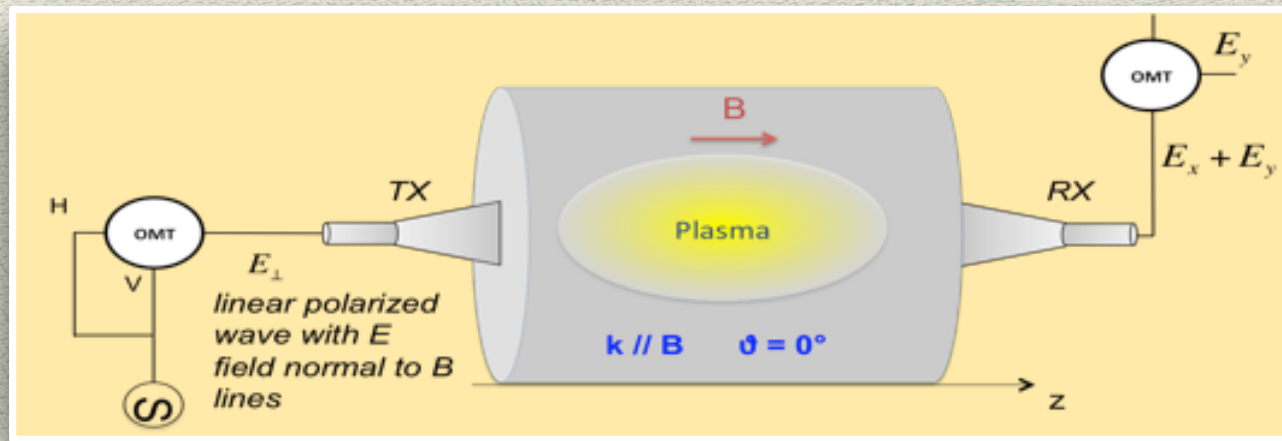
motorized stage

OMT



Faraday rotation measurements

Original Analysis method development



OrthoMode Transducer (OMT)

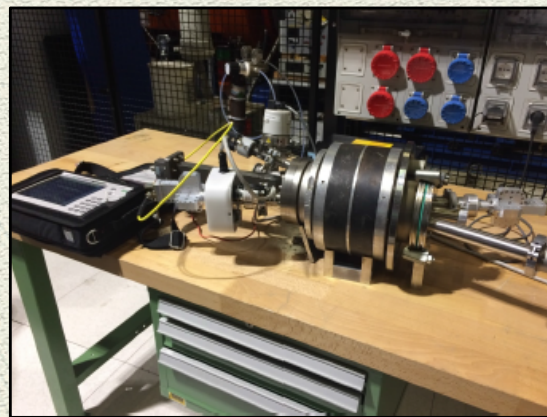
• Microwave range 18 GHz ÷ 26.5 GHz

• Test-bench: Plasma Reactor

L=26.6 cm
d=13.6 cm
B≈0.1 T

$$\lambda/L \ll 1$$

→ Undesired plasma chamber/Cavity effects



$$\beta = \frac{q_e^3}{8\pi^2 c^3 m_e^2 \epsilon_0} B d n_e \lambda^2$$

→ Spurious components rejection: Malus law-based selection

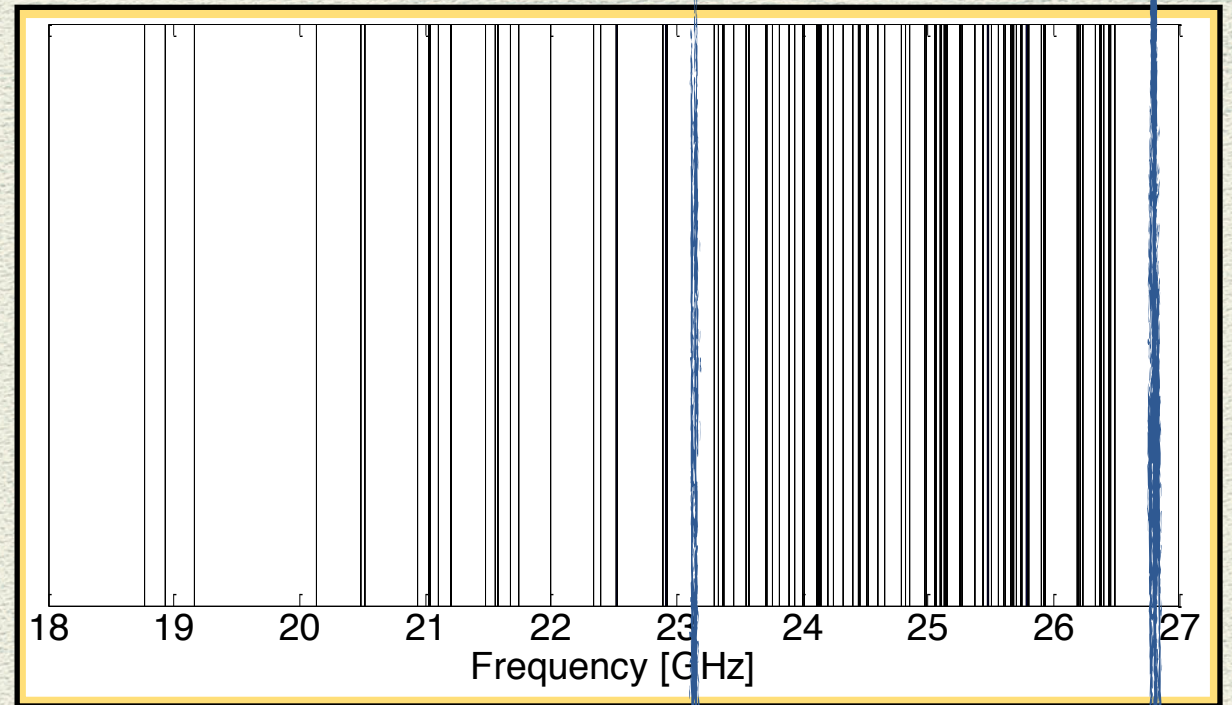
$$P = P_0 \cos^2 \vartheta + b$$

- Free-space
- Empty cavity
- Plasma-filled cavity

$$\left. \begin{aligned} \vartheta_{P_{\max}} &= 0^\circ \\ \vartheta_{P_{\min}} &= 90^\circ \end{aligned} \right\}$$

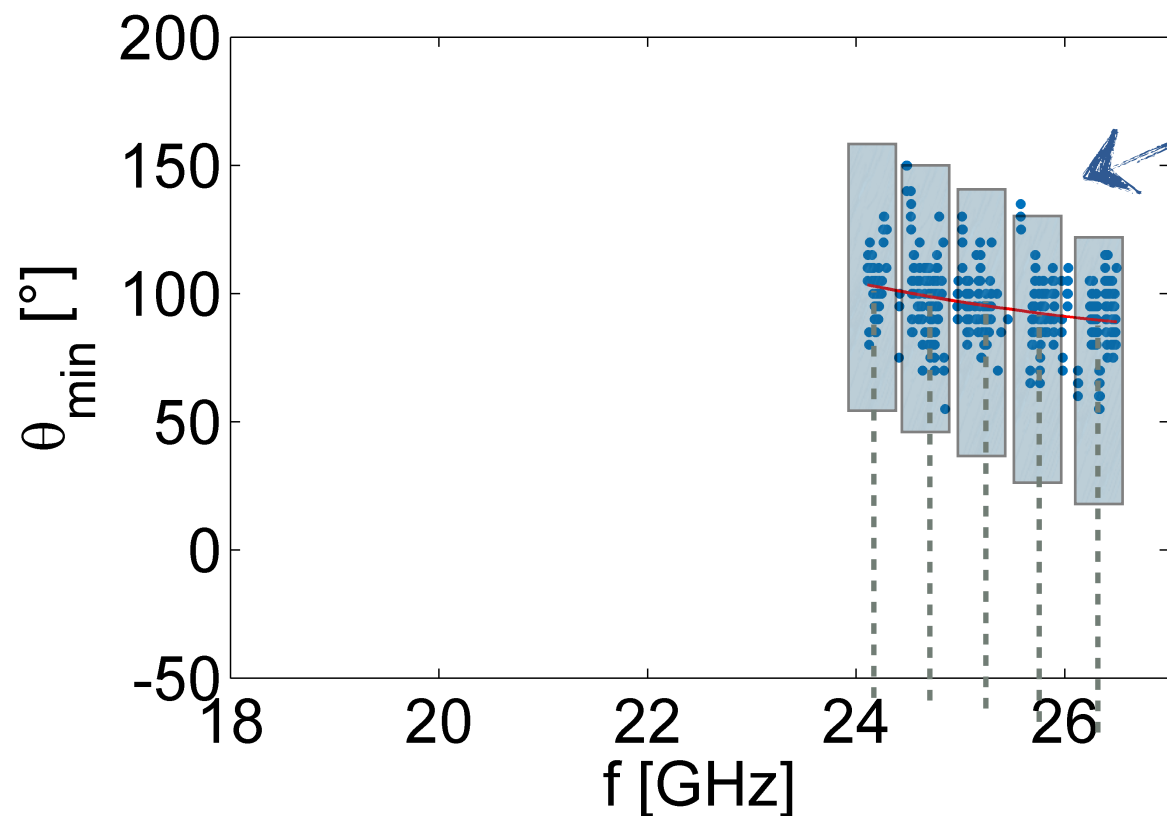
$$\left. \begin{aligned} \vartheta_{P_{\max}} &= \beta_{\text{Faraday}} \\ \vartheta_{P_{\min}} &= 90^\circ + \beta_{\text{Faraday}} \end{aligned} \right\}$$

Faraday rotation
measurements
CUT on the frequencies
unaffected by the
cavity



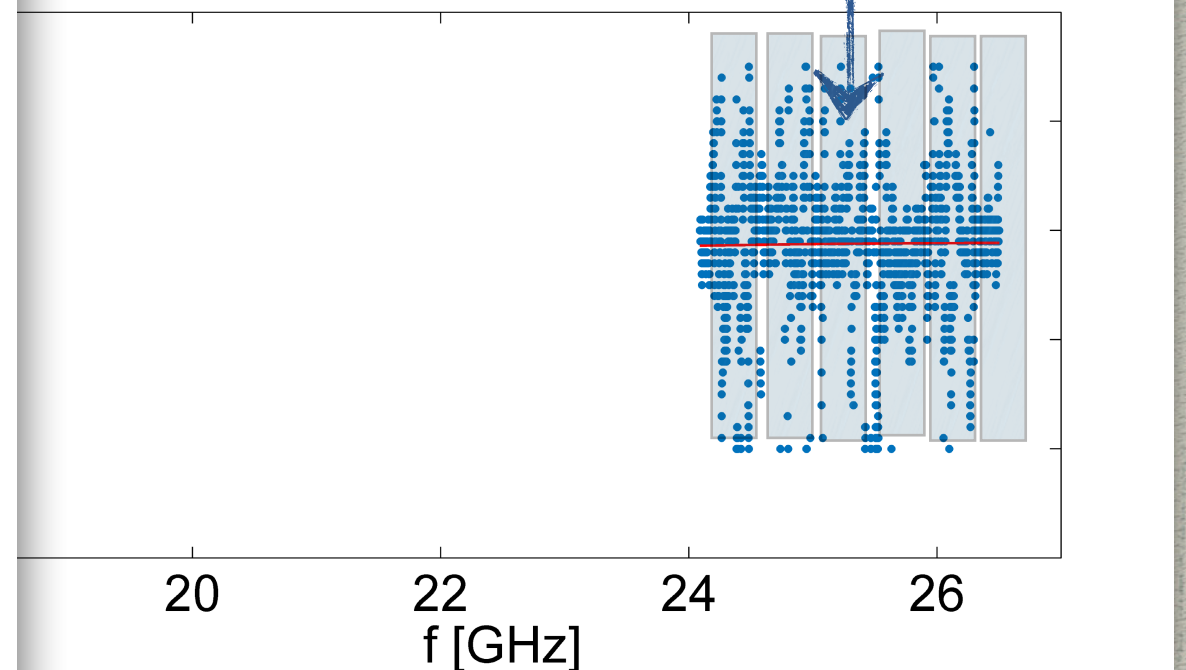
Plasma-filled cavity

Malus law-based selection: $R=0.95$



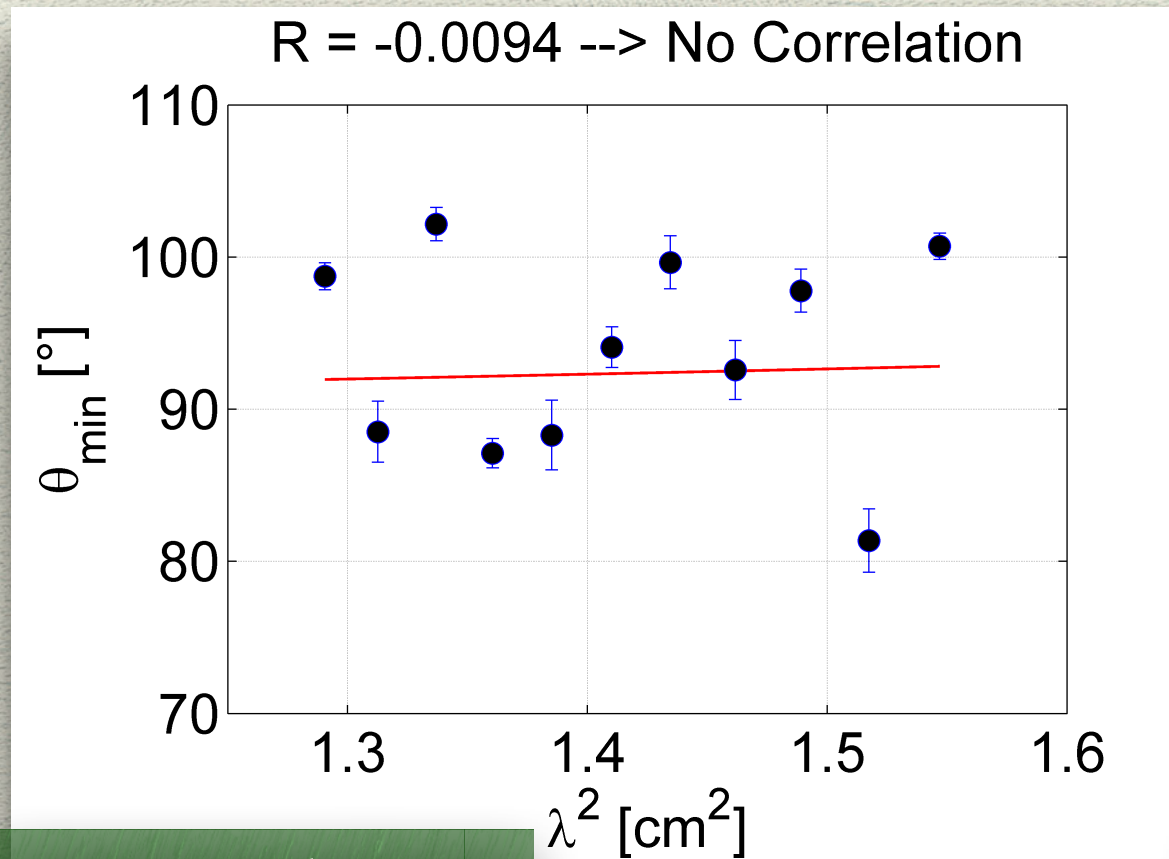
Empty cavity

Malus law-based selection: $R=0.95$

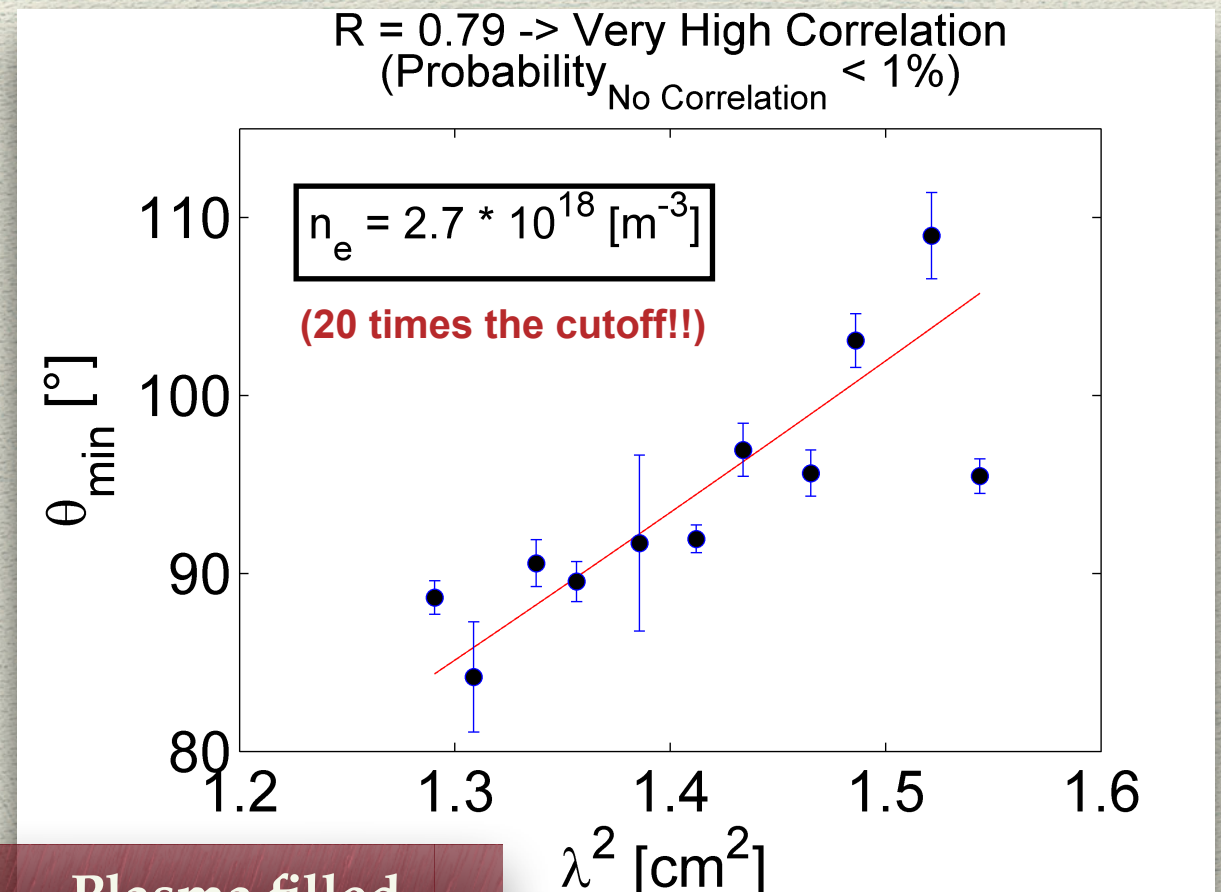


Faraday rotation measurements

Fitting procedure



Empty Plasma Chamber



Plasma filled Chamber

Experimental data have been **fitted** with statistical consistence **by a λ^2 law**, in agreement with Faraday rotation dependence on the probing wave-length

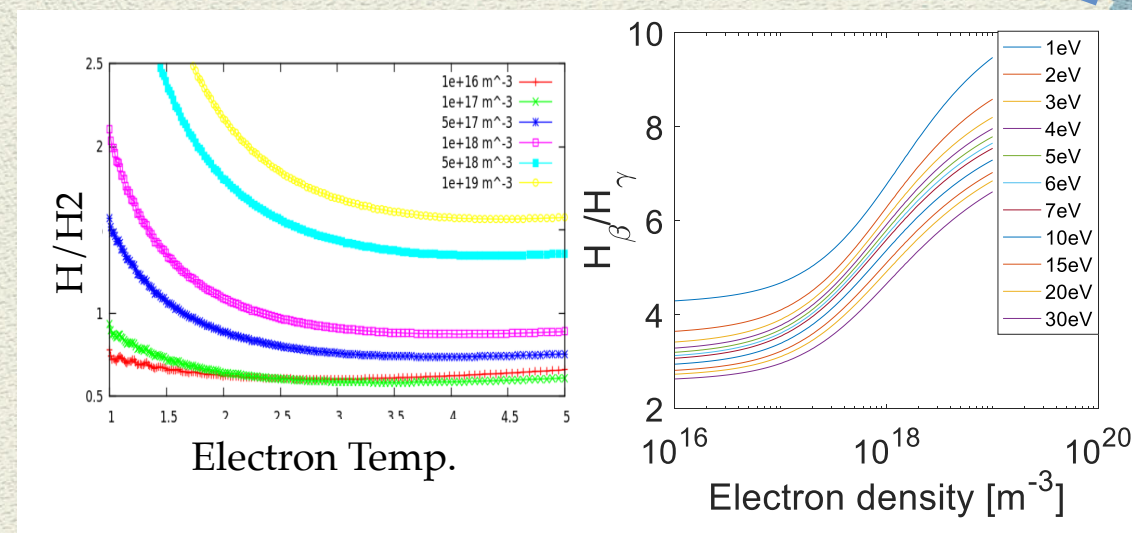
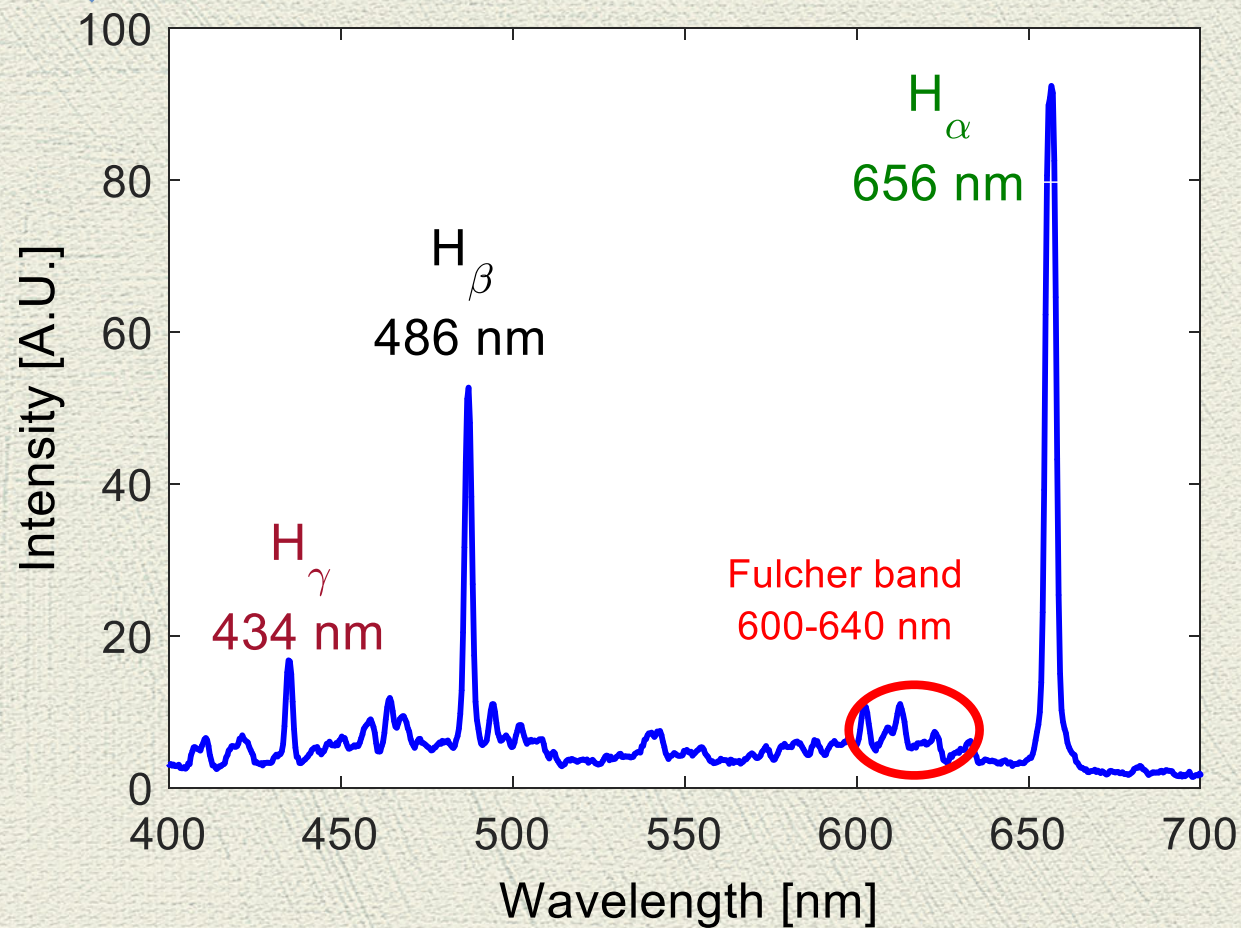
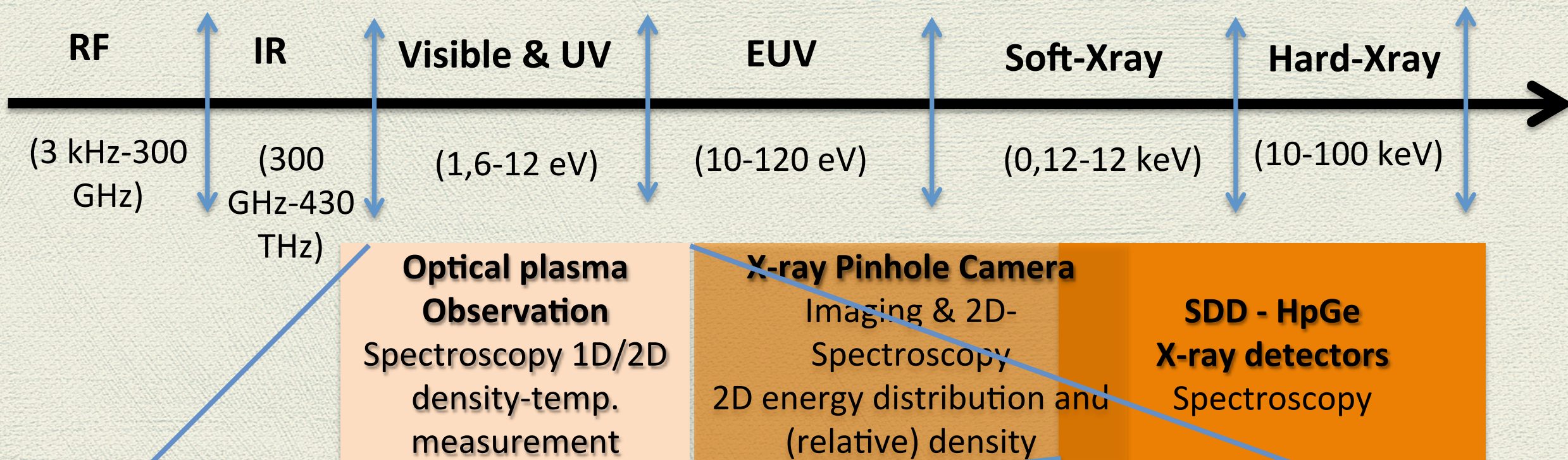
$$\theta = \frac{q_e^3}{8\pi^2 c^3 m_e^2 \epsilon_0} B d n_e \lambda^2$$

↑ Magnetic field
 ↑ plasma density

↓ wavelength

READY for
Multidiagnostics
operations!!

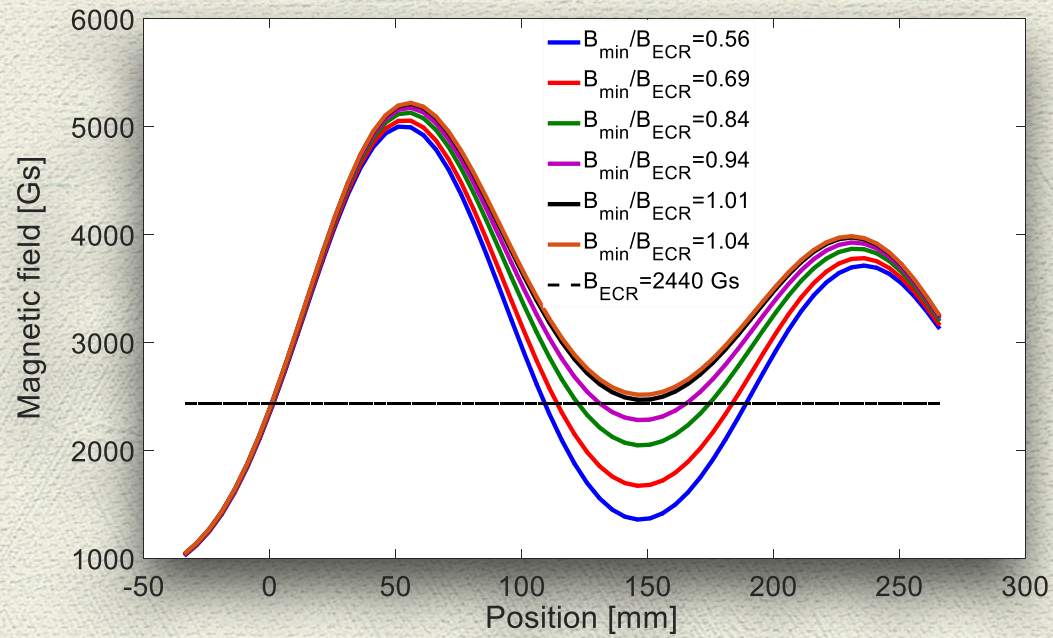
Non-intrusive plasma diagnostics methods



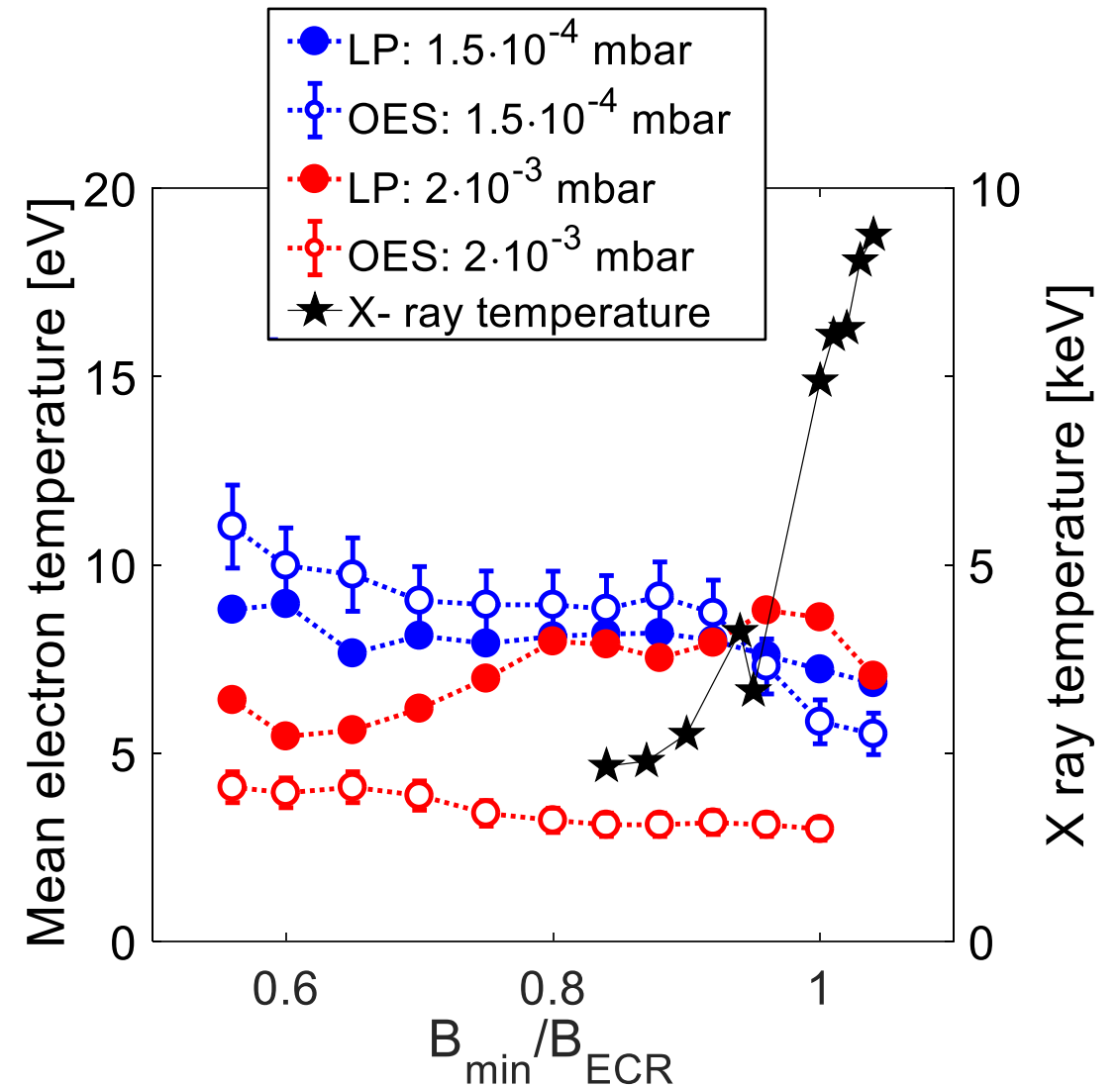
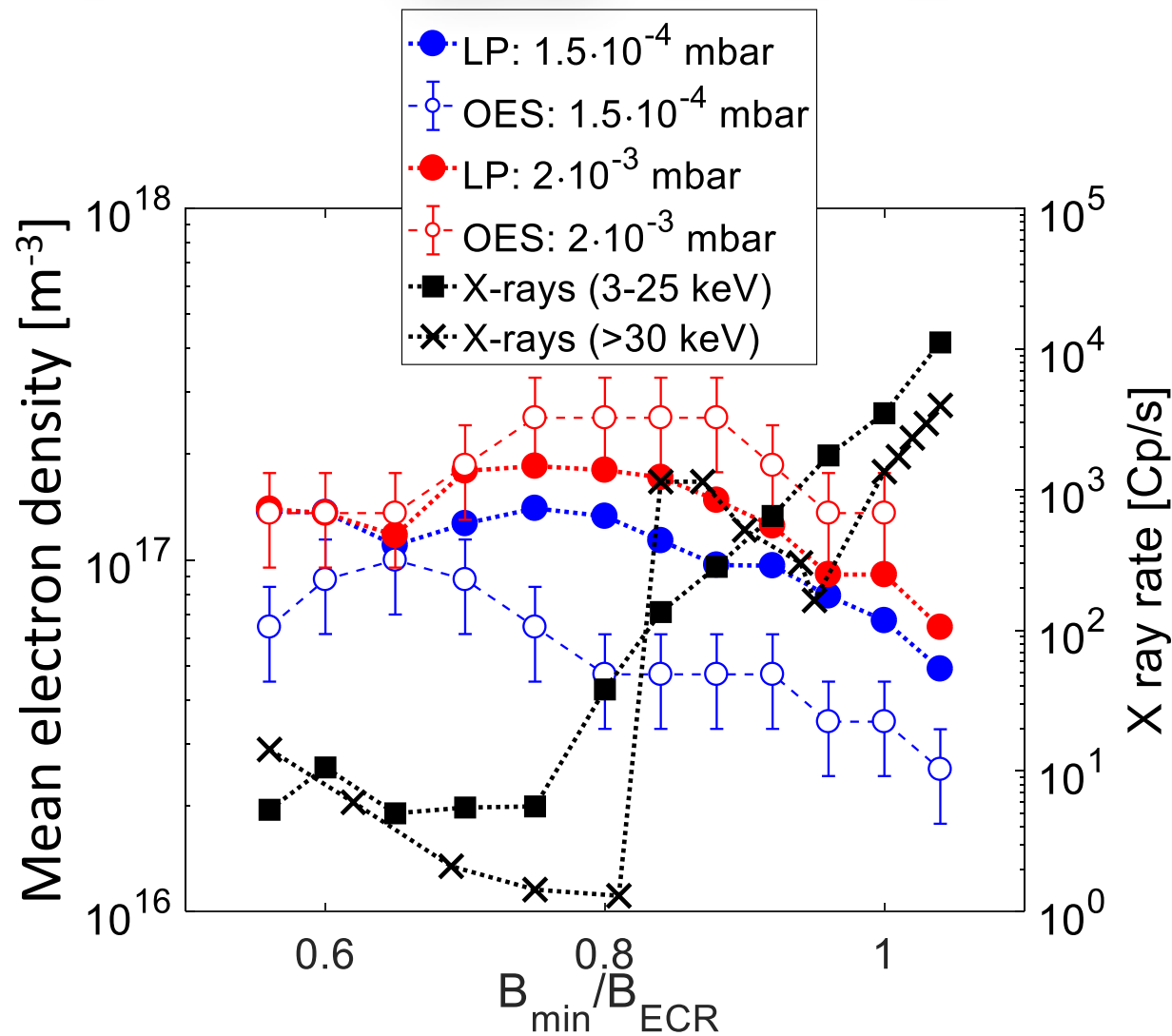
U. Fantz, Plasma Sources Sci. Technol. 15, p. S137 (2006).

Multidiagnostics including OES

recently presented at ICIS17-Geneva

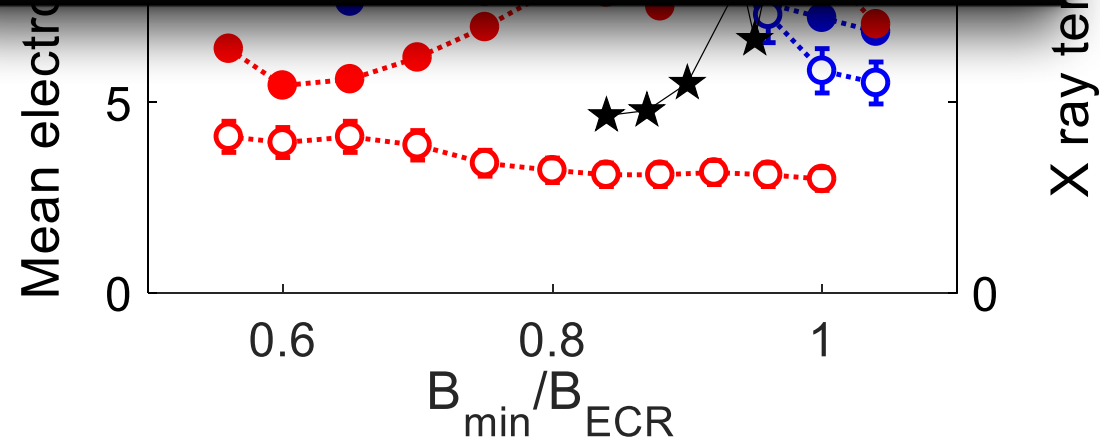
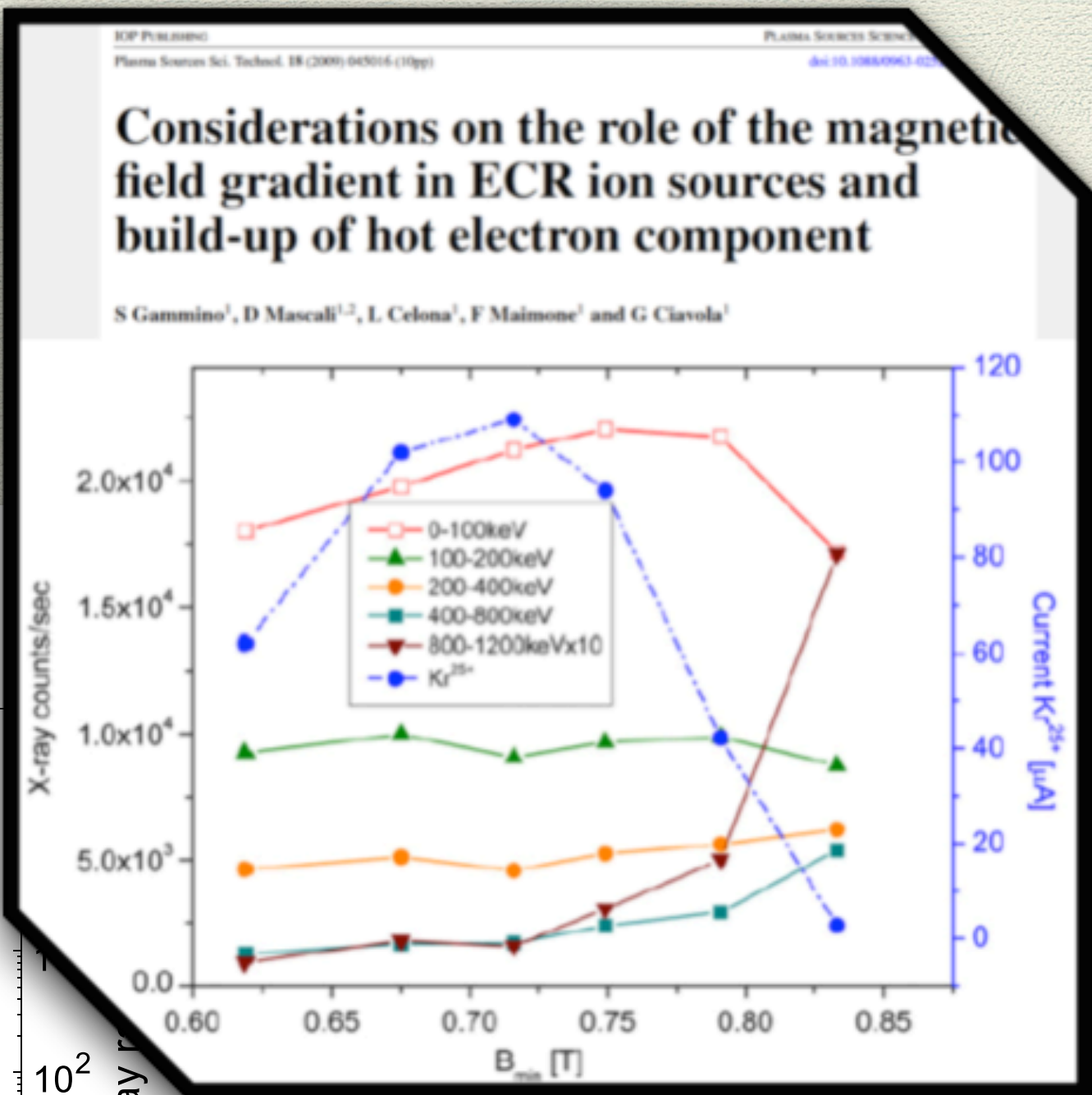
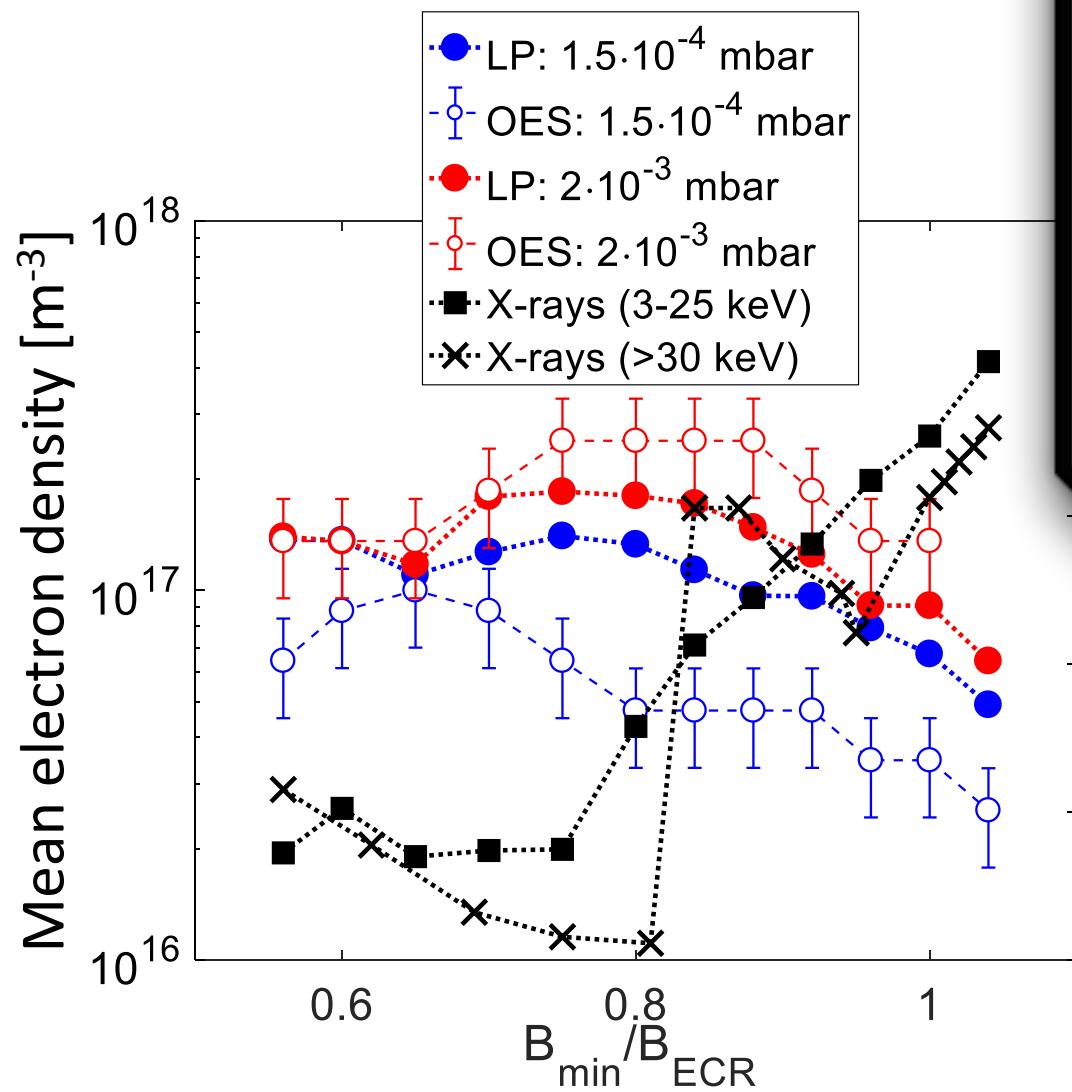


Data seem to say temperature and abundances of warm/hot electrons depend mostly from axial gradients

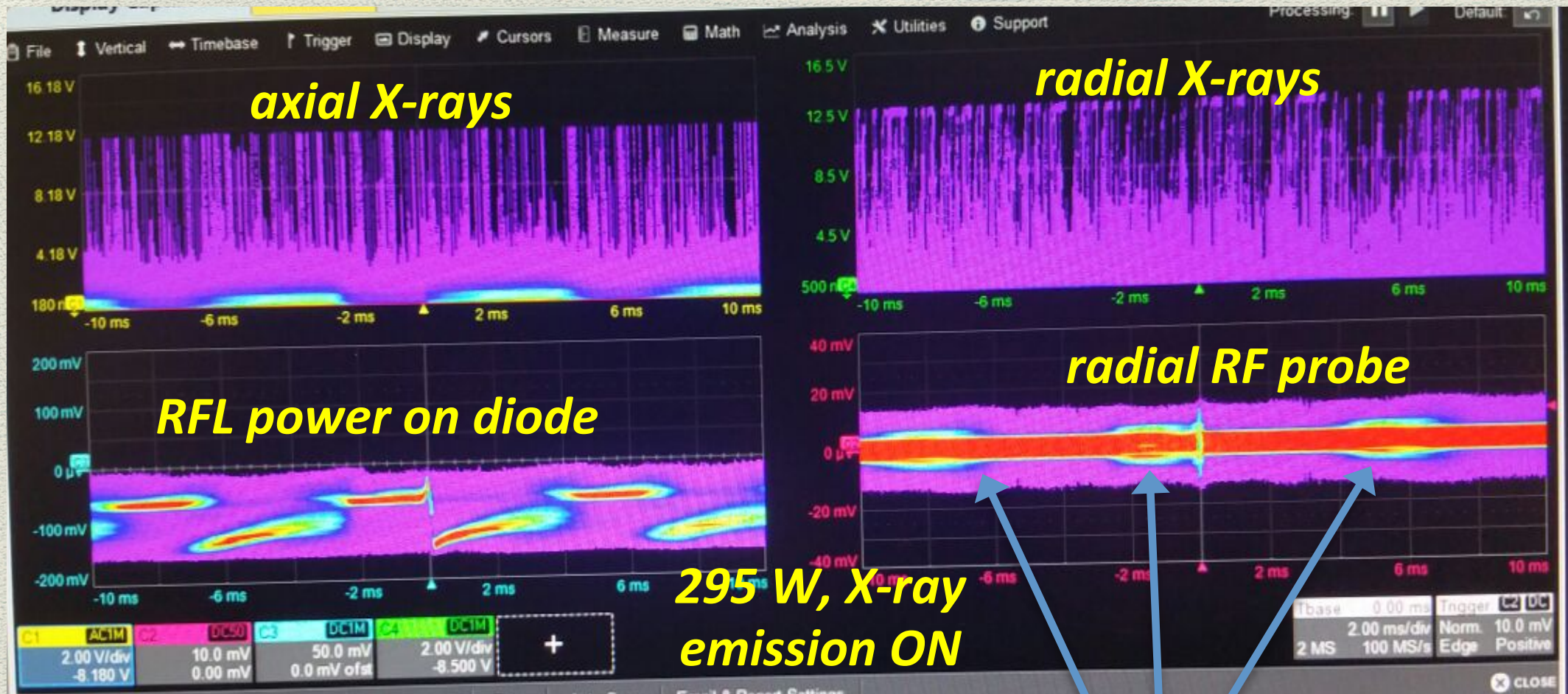


Multidiagnostics including OES

It helps to explain the scaling laws and rule of thumbs of existing ECR.



Probing turbulent plasma regimes (CYCLOTRON MASER INST.) in a **Time-Resolved** way



Radio-Bursts

Kinetic instabilities in a mirror-confined plasma sustained by high-power microwave radiation

A. G. Shalashov, M. E. Viktorov, D. A. Mansfeld, and S. V. Golubev

Citation: *Physics of Plasmas* 24, 032111 (2017);

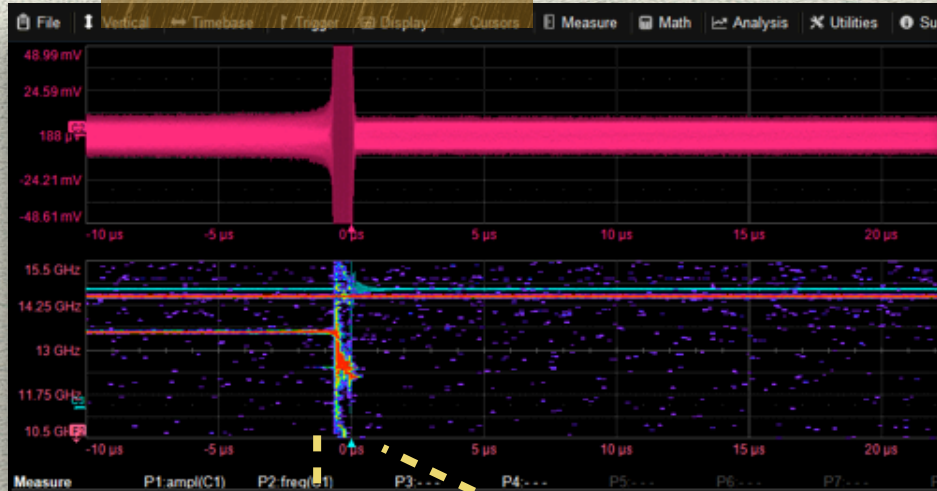
IOP Publishing Plasma Sources Science and Technology
Plasma Sources Sci. Technol. 23 (2014) 025020 (8pp) doi:10.1088/0963-0252/23/2/025020

Beam current oscillations driven by cyclotron instabilities in a minimum- B electron cyclotron resonance ion source plasma

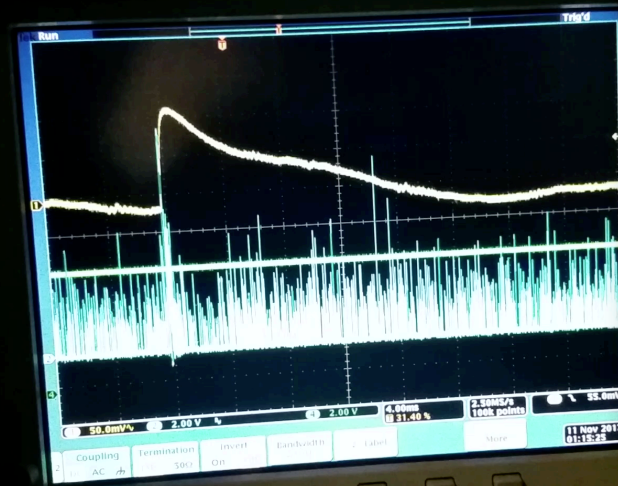
O Tarvainen¹, I Izotov², D Mansfeld², V Skalyga^{2,3}, S Golubev^{2,3}, T Kalvas¹, H Koivisto¹, J Komppula¹, R Kronholm¹, J Lailainen¹ and V Toivanen⁴

Time Resolved Characterization at the LPSC Charge Breeder

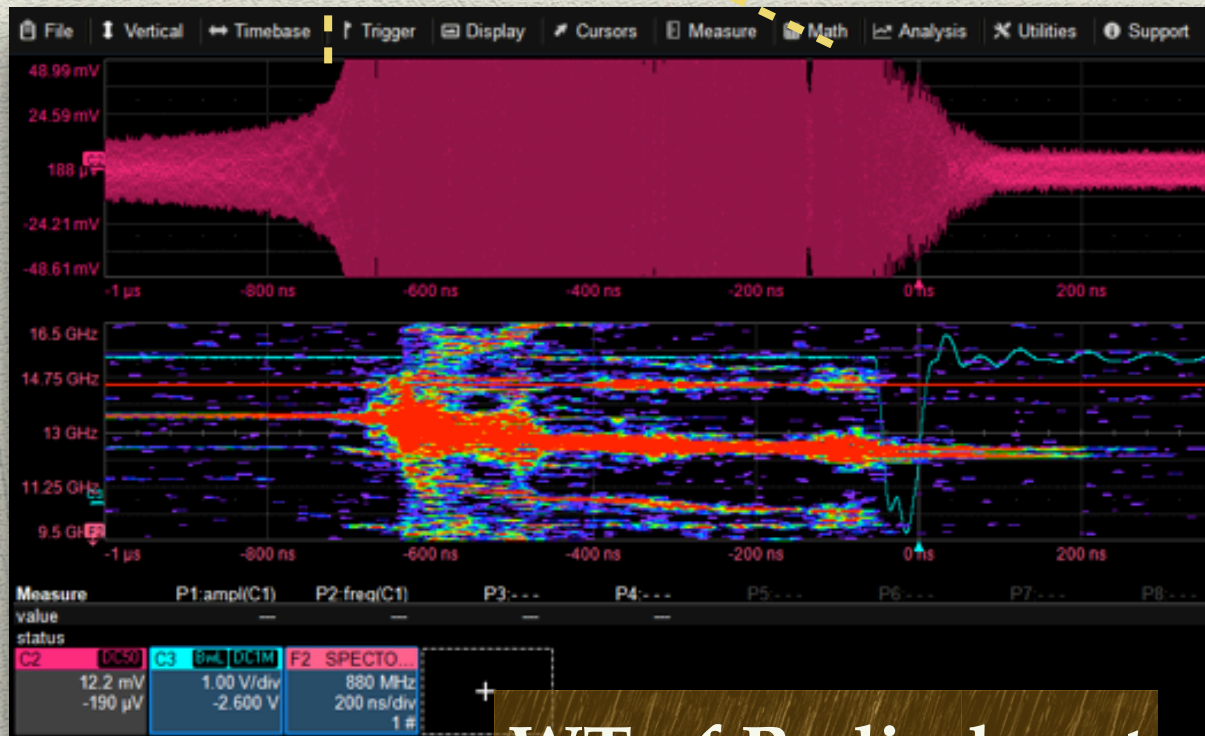
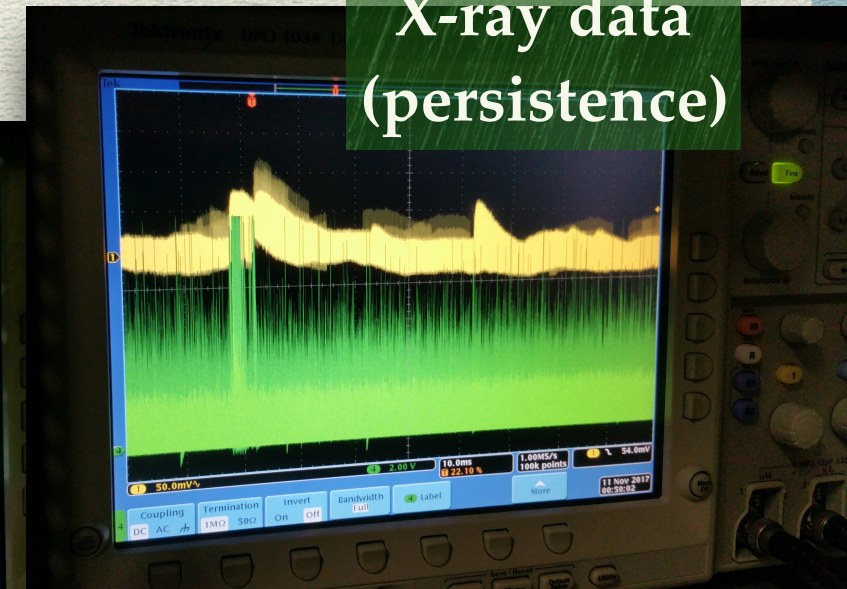
Radio-burst



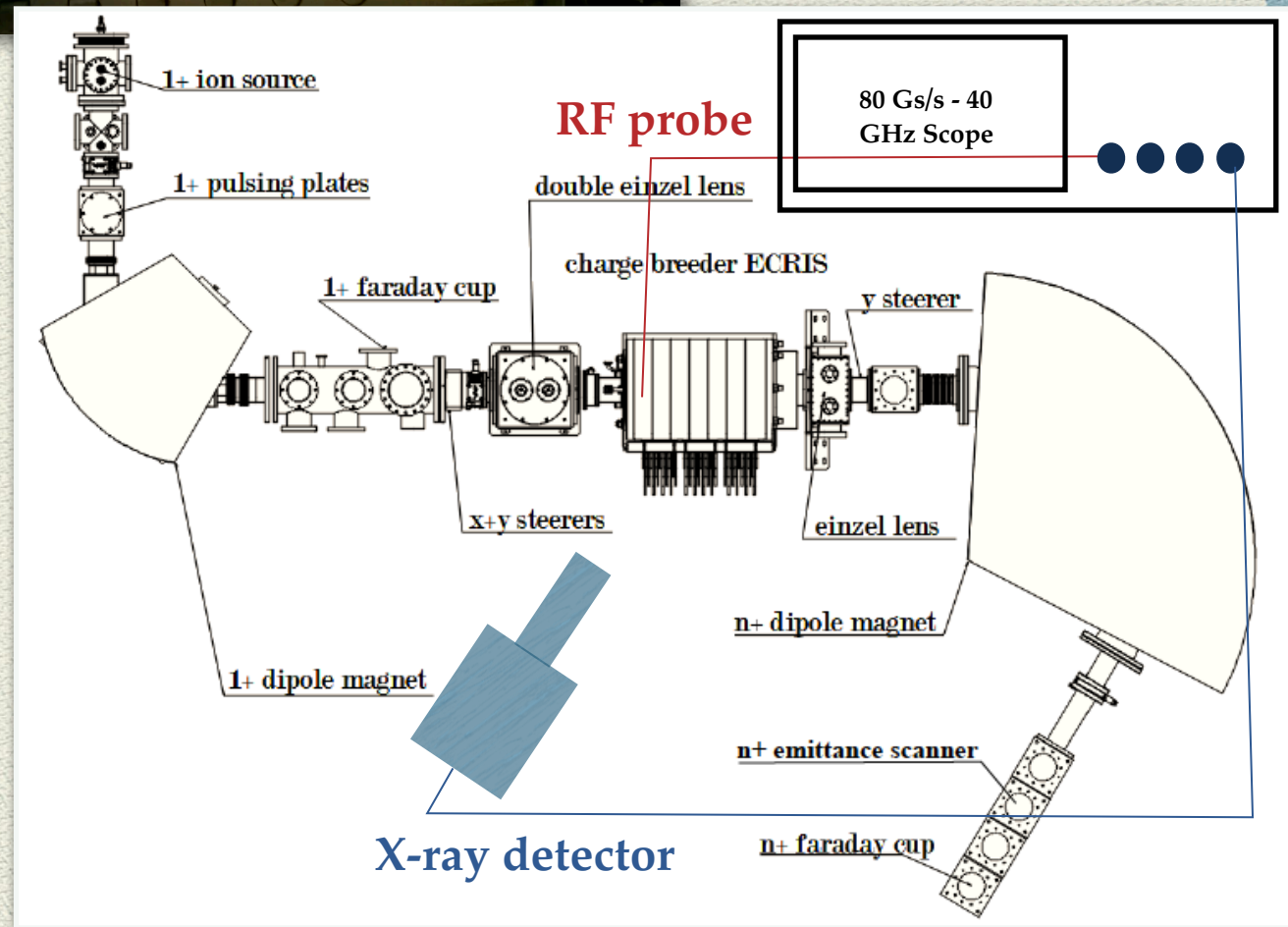
X-ray data



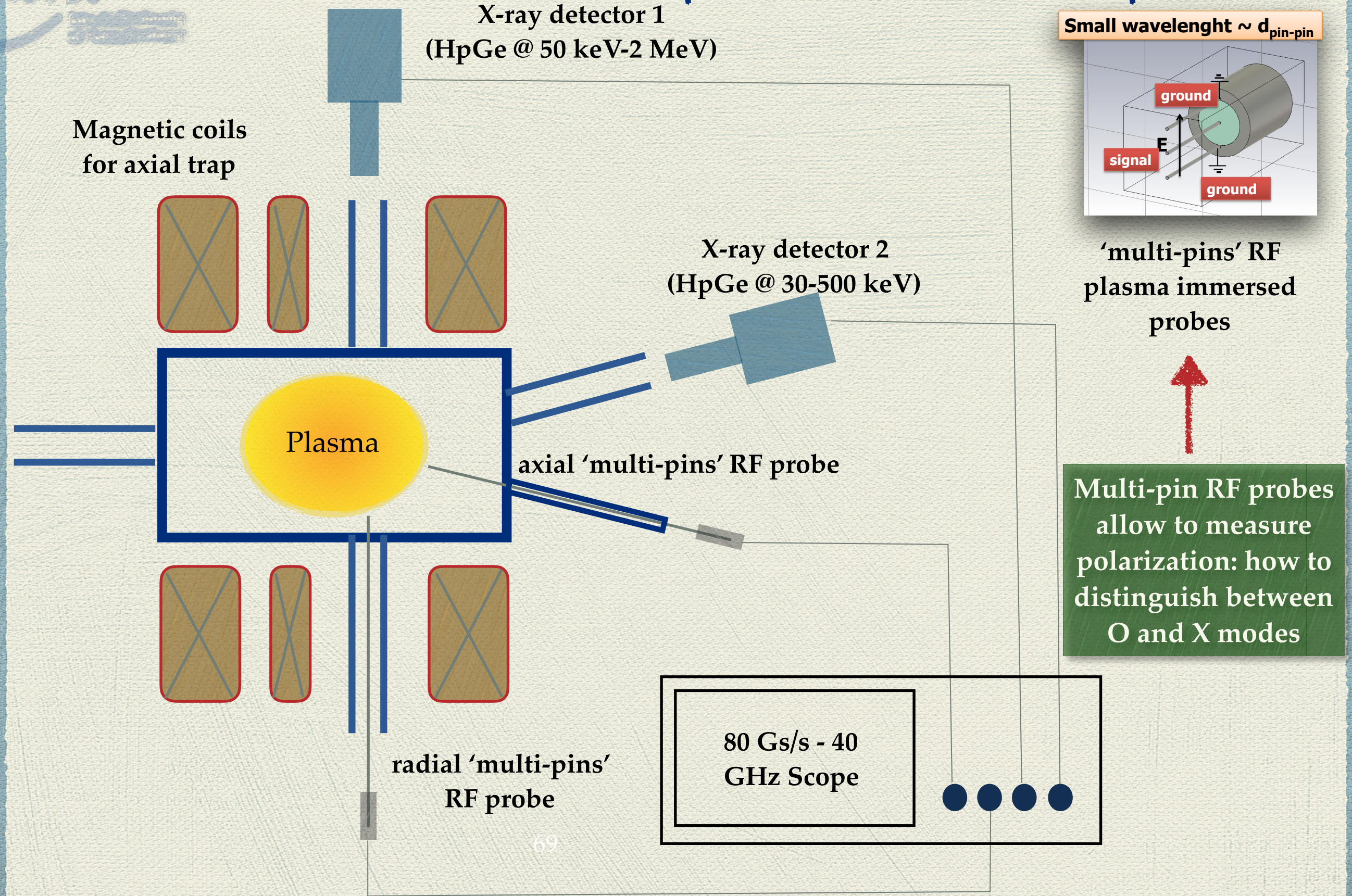
X-ray data (persistence)



WT of Radio-burst



Experimental setup @ LNS

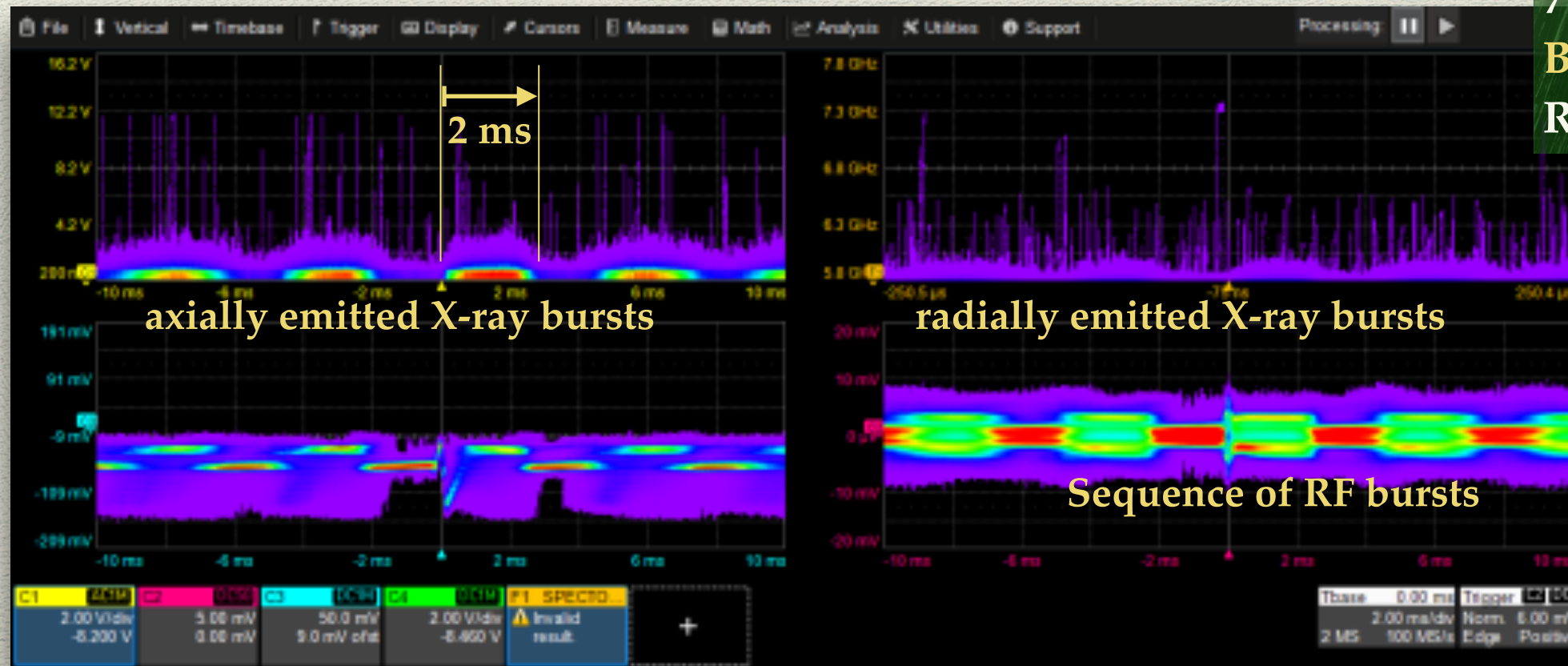


INSTABILITY ONSET DEPENDS FROM THE AXIAL TRAP'S SCALE-LENGTH ONLY!! (L parameter)

7 GHz

$B_{min}/B_{cr} = 0.8$

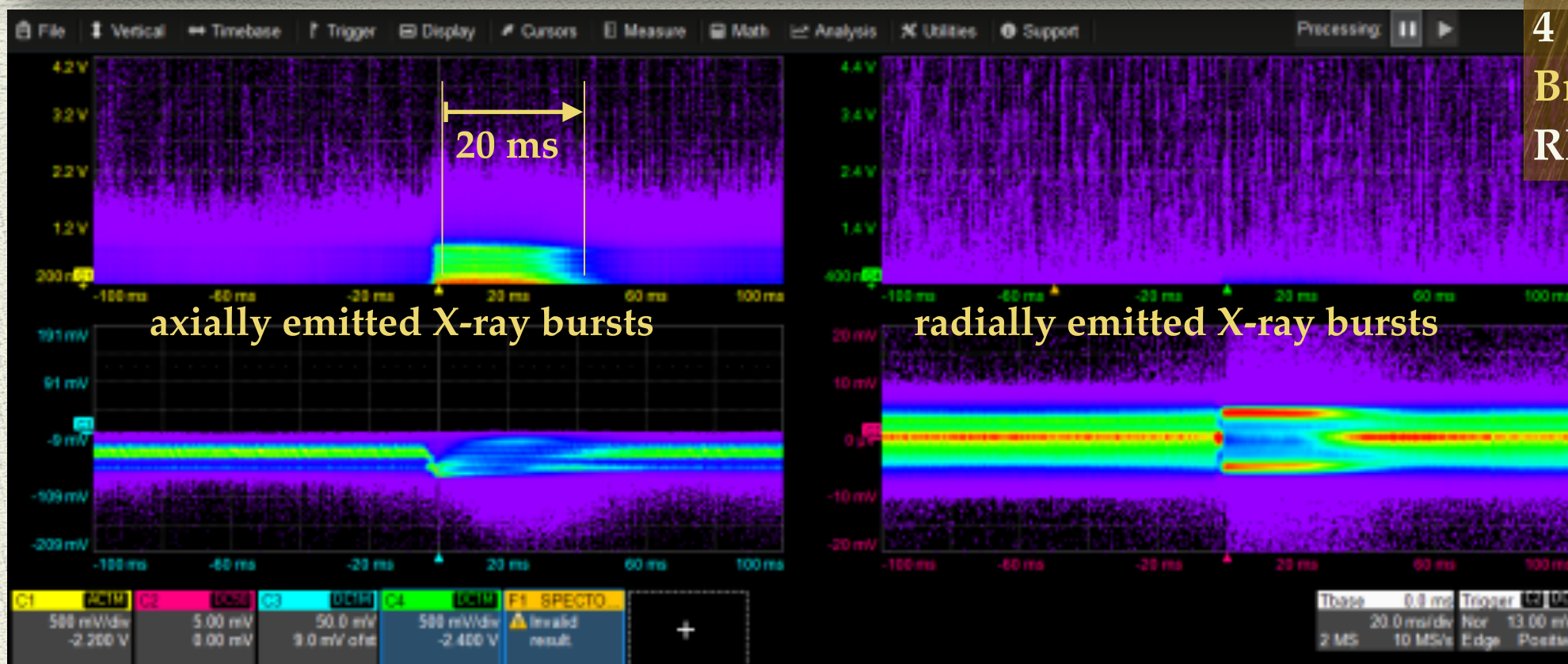
RF power = 250 W



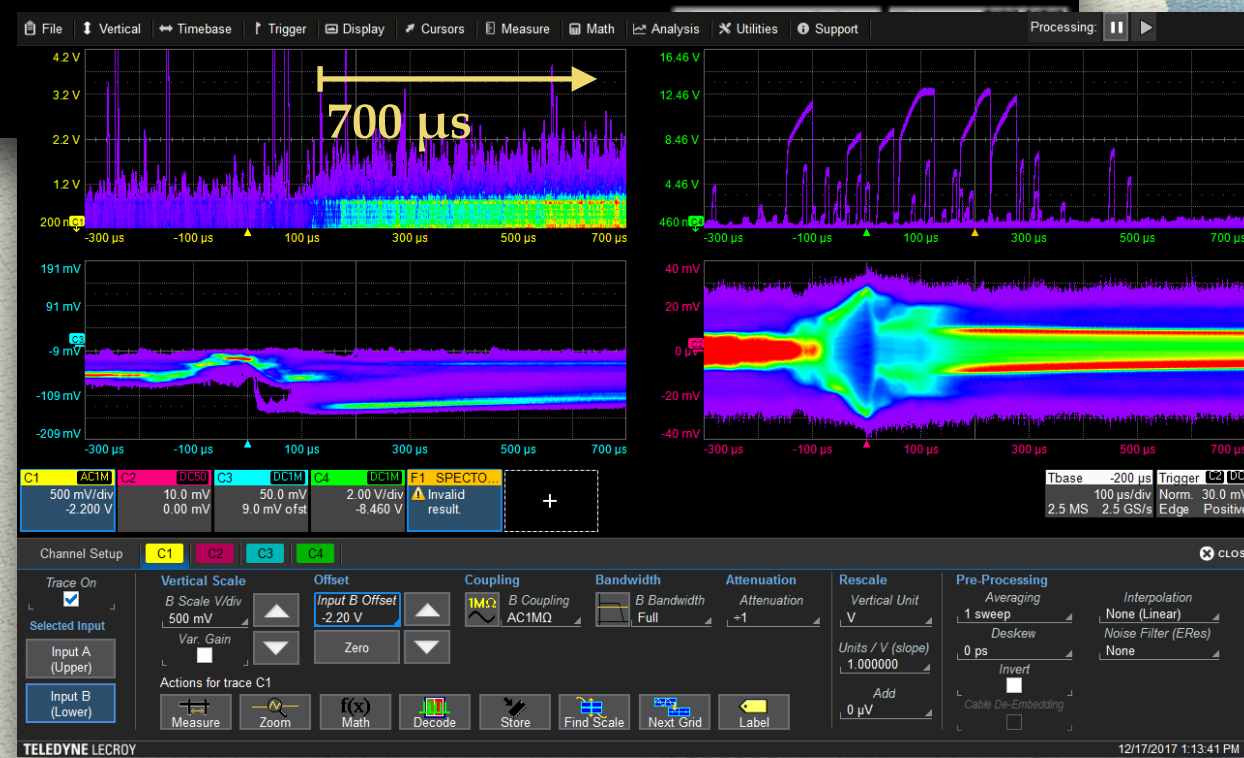
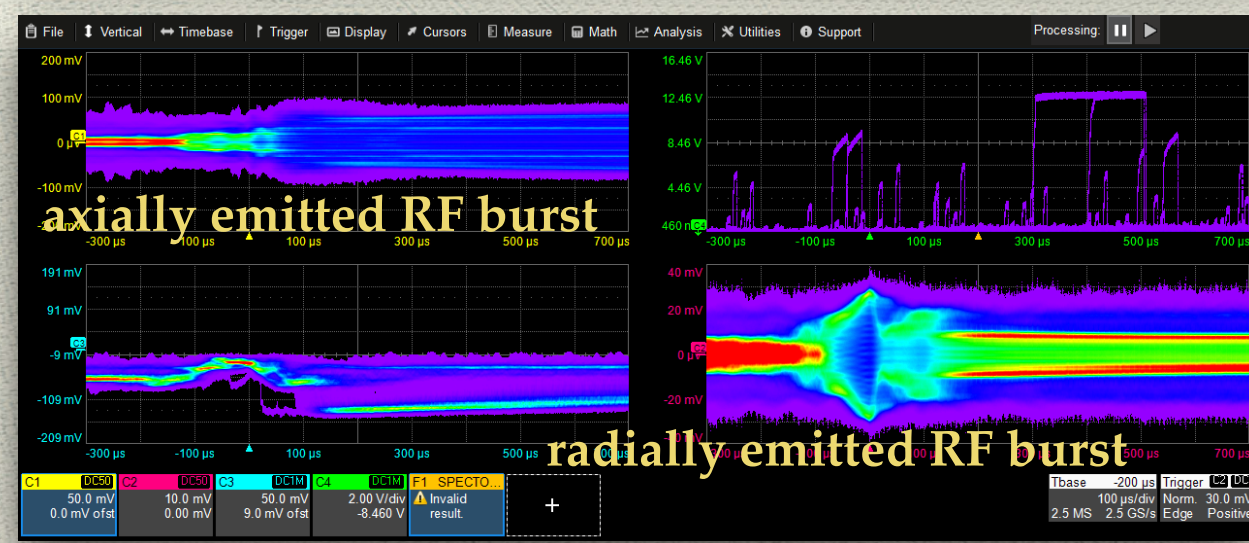
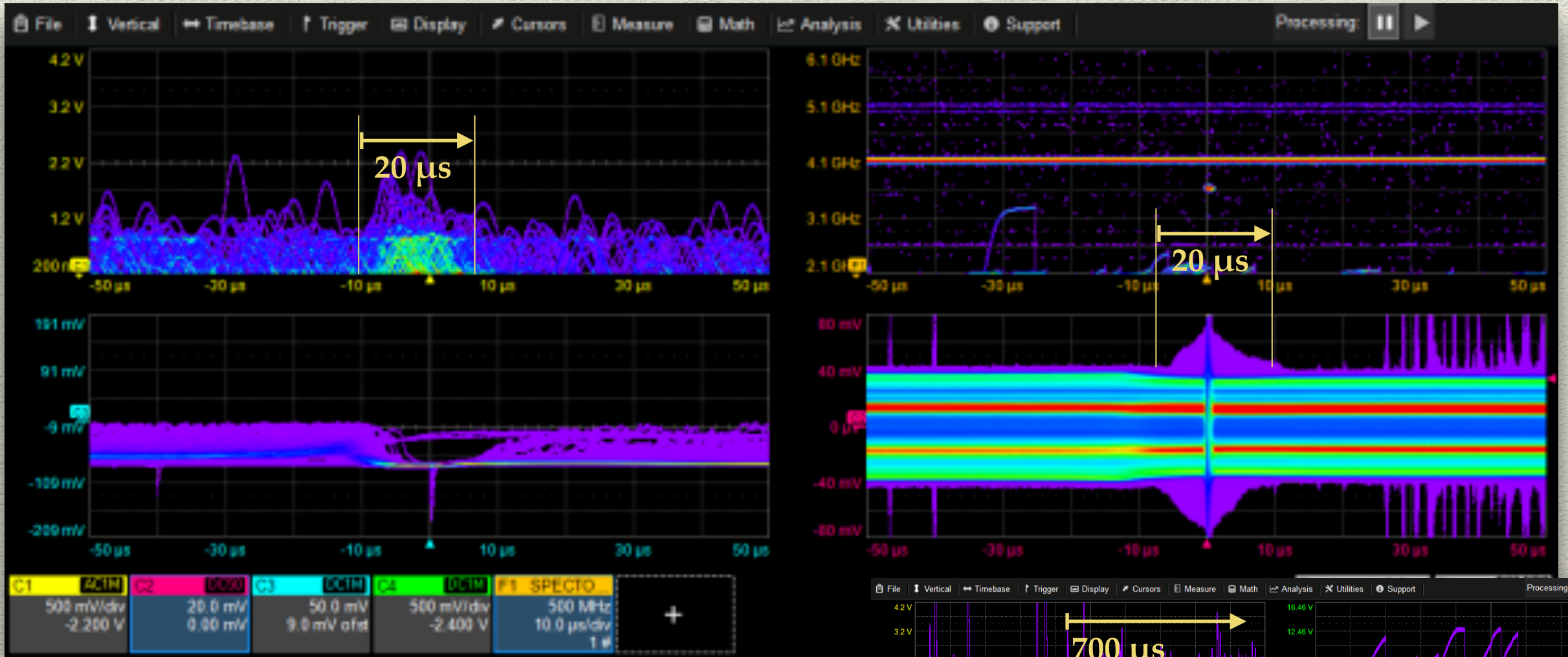
4 GHz

$B_{min}/B_{cr} = 0.95$

RF power = 250 W

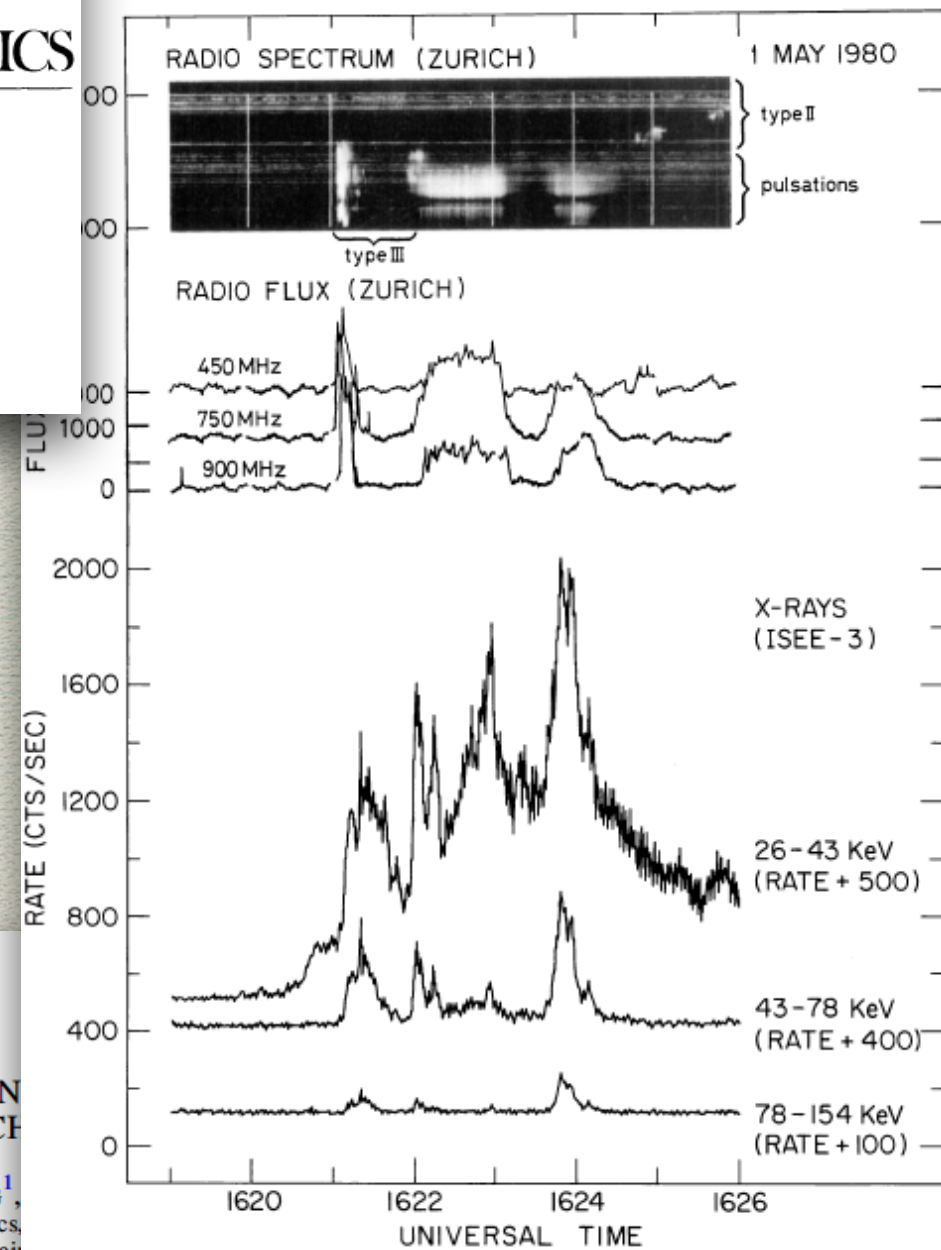
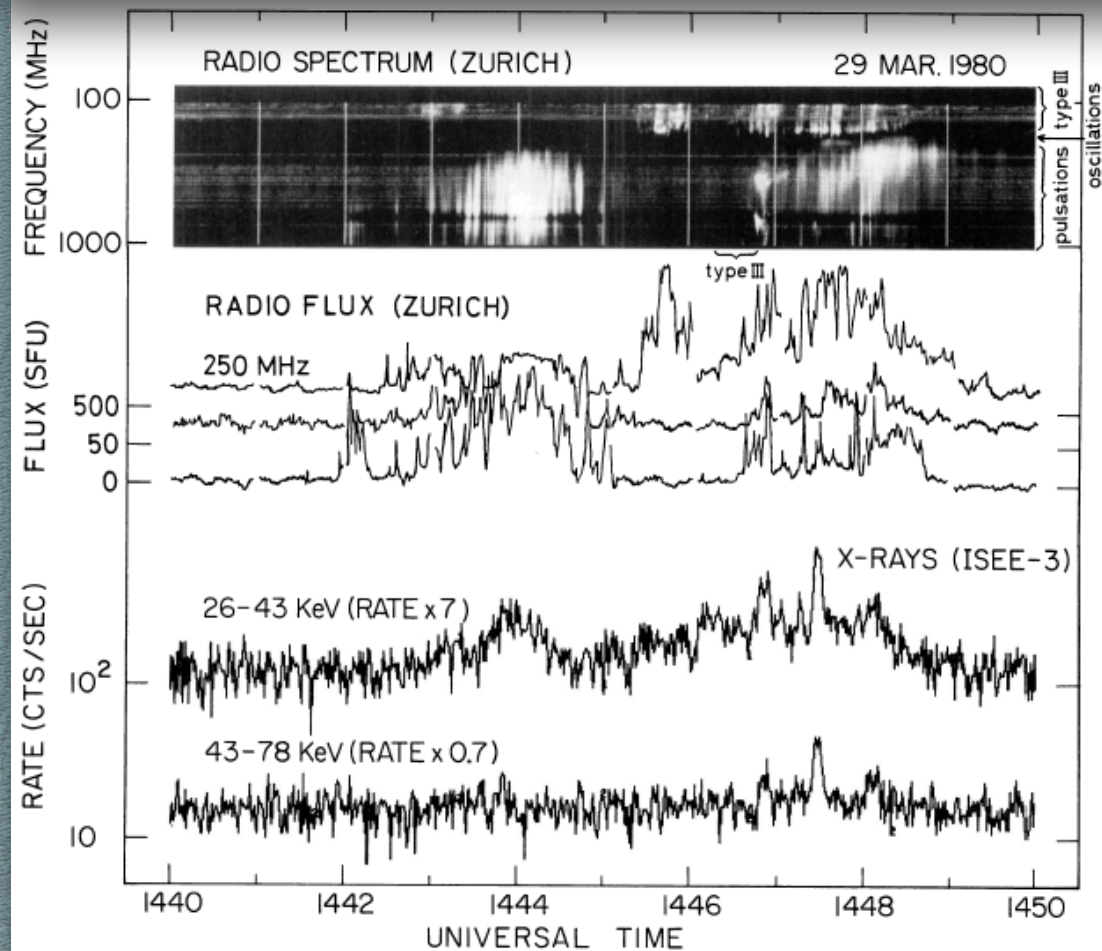


IN ADDITION TO THE "DELAYED" EMISSION OF X-RAY BURSTS, NORMALLY RELATED TO "PRECIPITATION" OF ELECTRONS FROM THE TRAP, SIMULTANEOUS EMISSION OF X-RAYS HAS BEEN OBSERVED IN THE RF BURST TIMESCALE



Correlation of solar radio pulsations with hard X-ray emission

M.J. Aschwanden*, A.O. Benz¹, and S.R. Kane²



ASTROPHYSICAL JOURNAL, 822:58 (8pp), 2016 May 10
The American Astronomical Society. All rights reserved.

CYCLOTRON MASER EMISSION PITCH

G. Q. ZHAO¹, H. Q. FENG¹,
¹Institute of Space Physics,
²Purple Mountain

³Xinjiang Astronomical Observatory, CAS, Urumqi 830011, China
Received 2016 January 25; accepted 2016 March 6; published 2016 May 5

A&A 370, 1000–1003 (2001)
DOI: 10.1051/0004-6361:20010290
© ESO 2001

Astronomy
&
Astrophysics

Coherent cyclotron maser radiation from UV Ceti

R. Bingham^{1,2,3}, R. A. Cairns³, and B. J. Kellett¹

Fertile network of collaborations



INFN-LNS
Plasma studies

INFN-LNL
Beam-plasma studies

INFN-LNS
Nucl. Exp. aspects

INFN-Pg
Theory

INFN-other section
interested (Bo, Ts, Ge)



University of Michigan
University of Cambridge



Collaborations

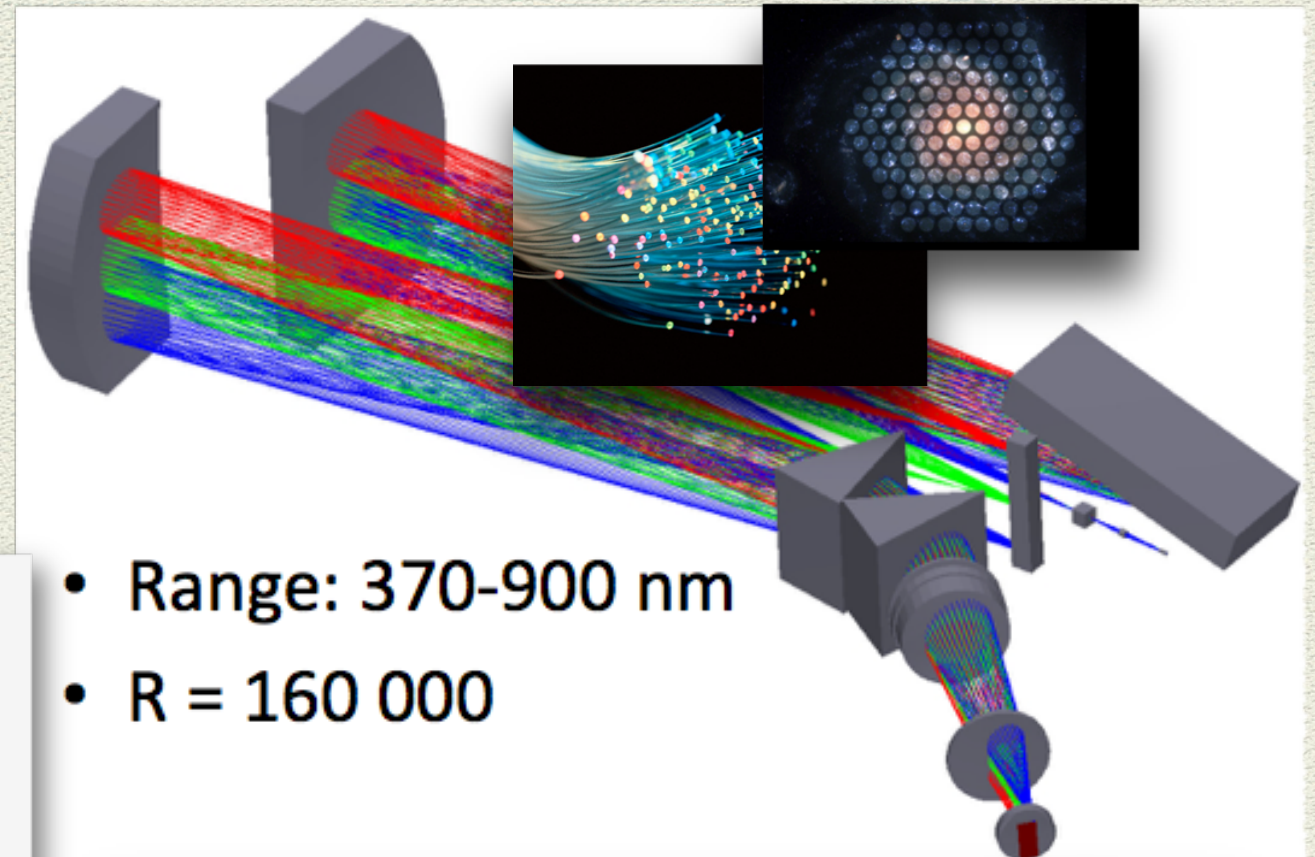


Official declaration
of interest



SpectroPolarimetry for C.S.D. on-line measure

Spettrografo Alta Risoluzione Galileo



- Range: 370-900 nm
- R = 160 000

PANDORA@Work

INFN-INAF MoU
in progress

the first MoU to
be signed by the two institutions

CSN III and V



Starting a new synergy with
Astronomy/Astrophysics!!!

SARG has been transferred to
LNS from T.N.G. in La Palma,
Canary Islands



Spettrografo
Alta
Risoluzione
Galileo

- 370-900 nm
- $R = 160\,000$
- Full Stokes Capability
(Leone et al. 2003, SPIE, 4843, 465)



SARG@TNG, Canary Islands, has been one of the most powerful spectropolarimetry for the observation of magnetized stars' atmospheres

SARG@LNS, February 2018 → Now in the installation phase



SpectroPolarimetry for C.S.D. on-line measurements

Optical Emission Spectroscopy is already widely used worldwide to measure plasma density and temperature...

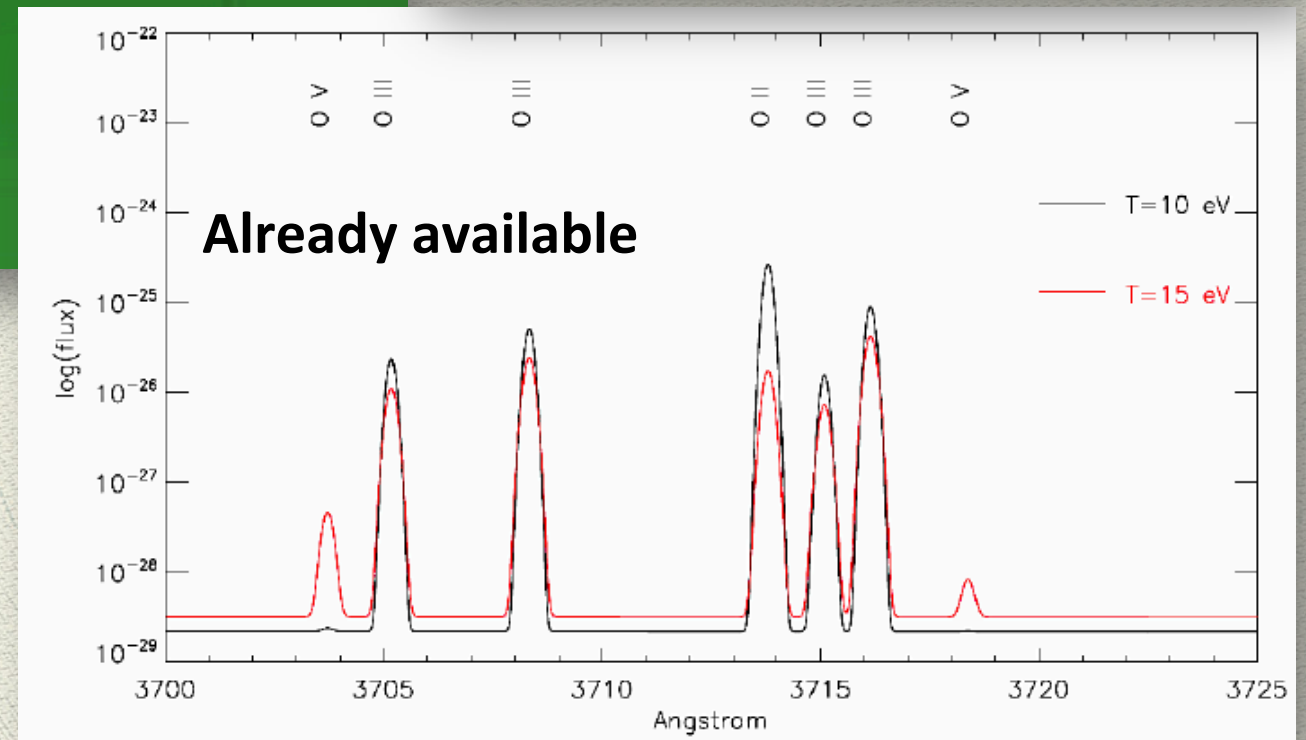
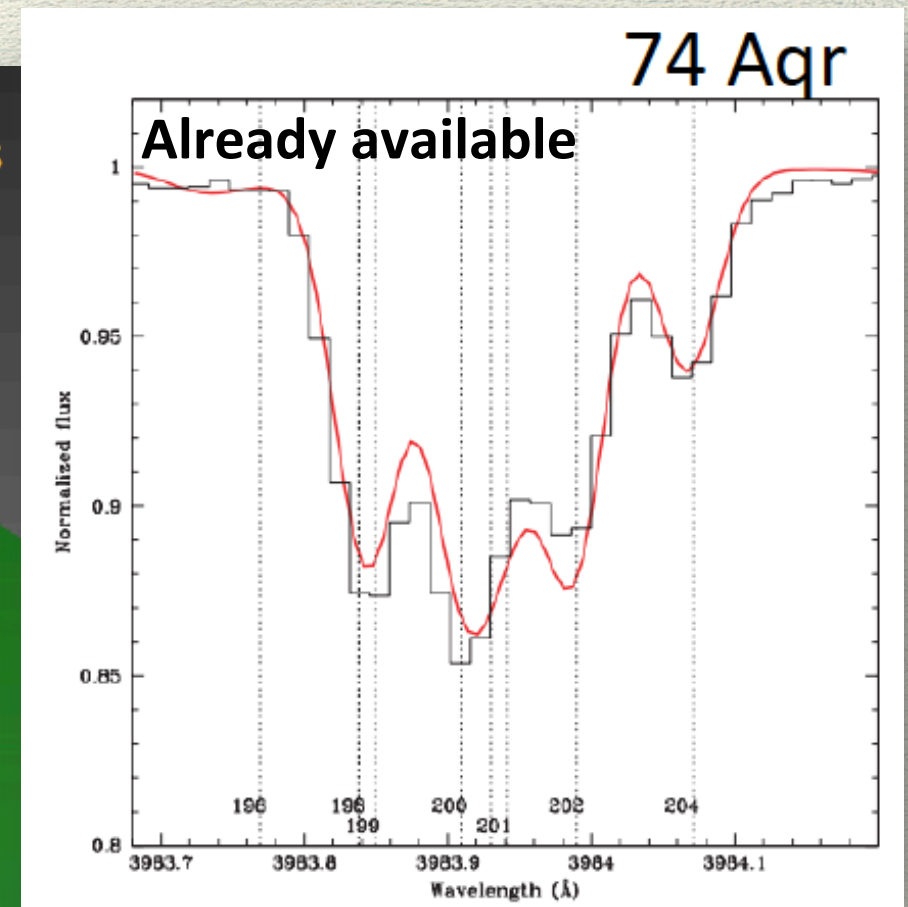
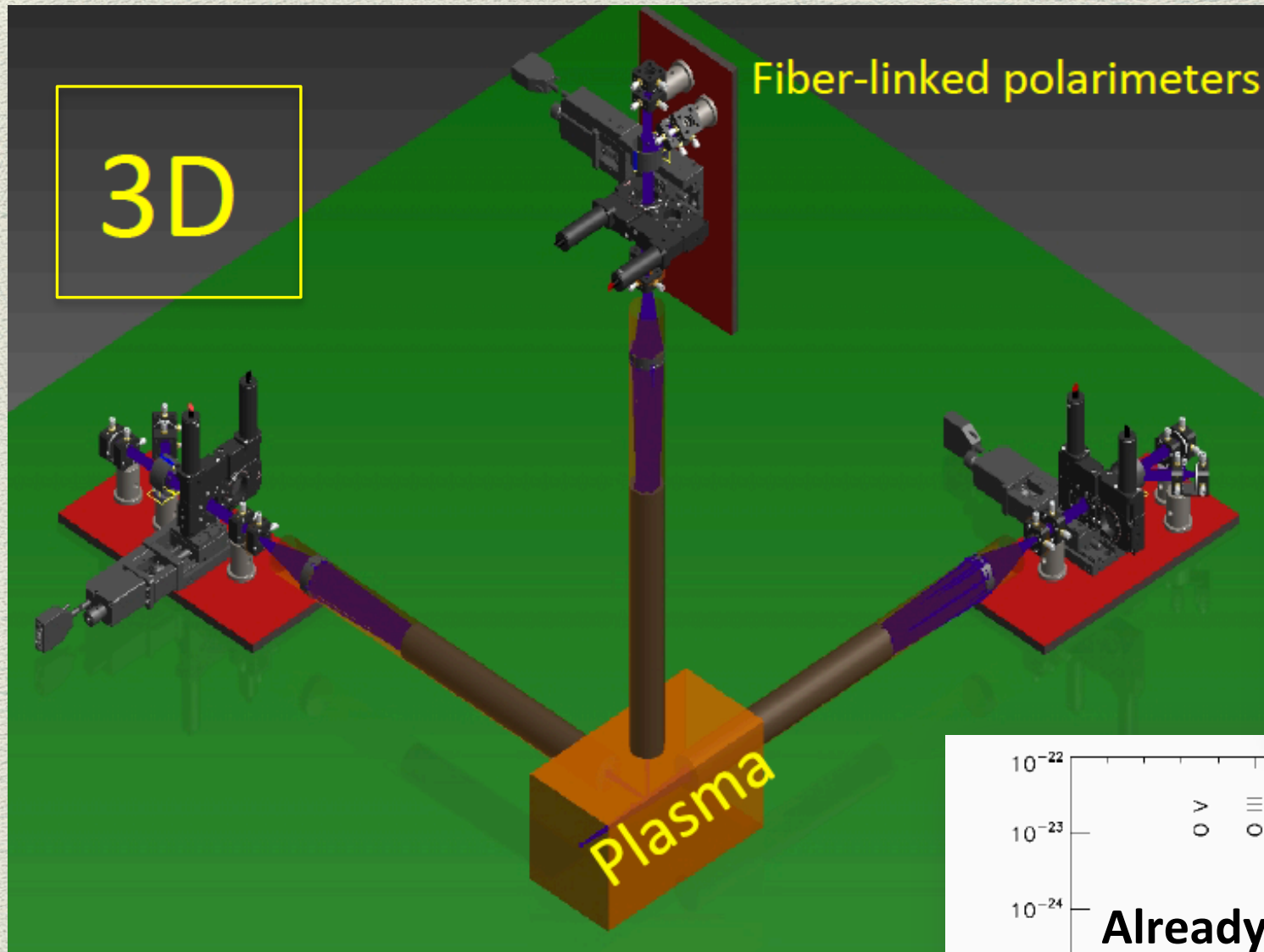
BUT...

The effect of the magnetic field is rarely taken into account. It may affect in a relevant way line-ratios, etc.

→ SPECTROPOLARIMETRY is needed!

Collaboration with Cambridge Univ. and University of Michigan started to integrate astrophysical databases to ECR plasmas

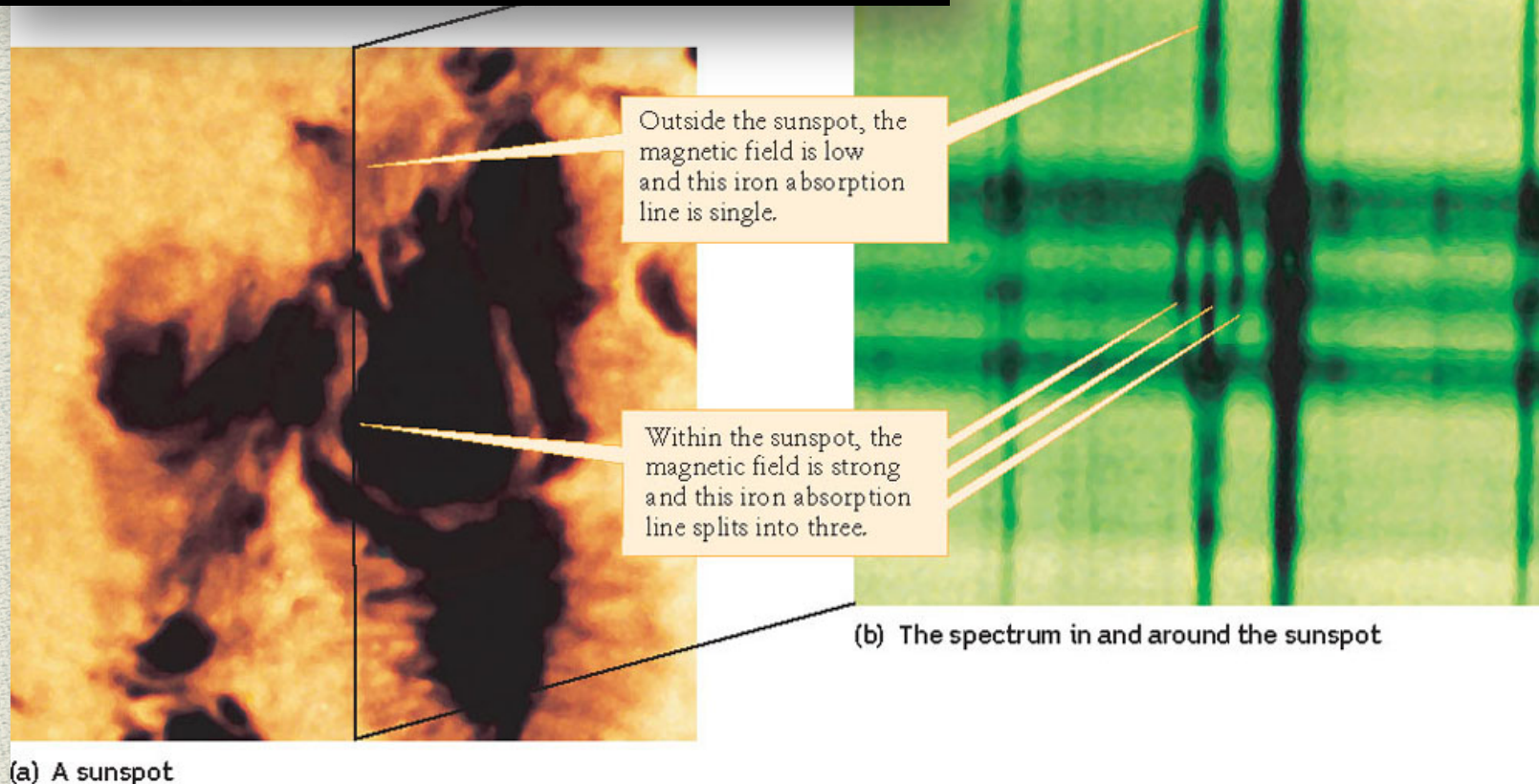
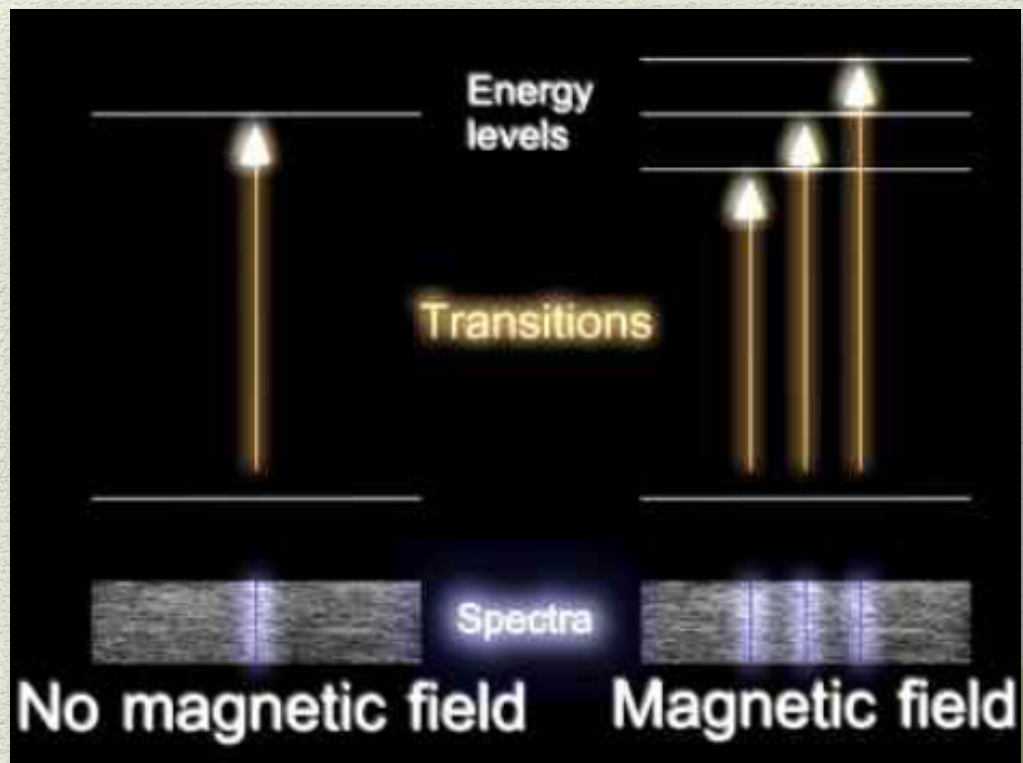
SpectroPolarimetry for C.S.D. on-line measurements



UPGRADE of SARG for allowing 3D **plasma tomography** is needed!!

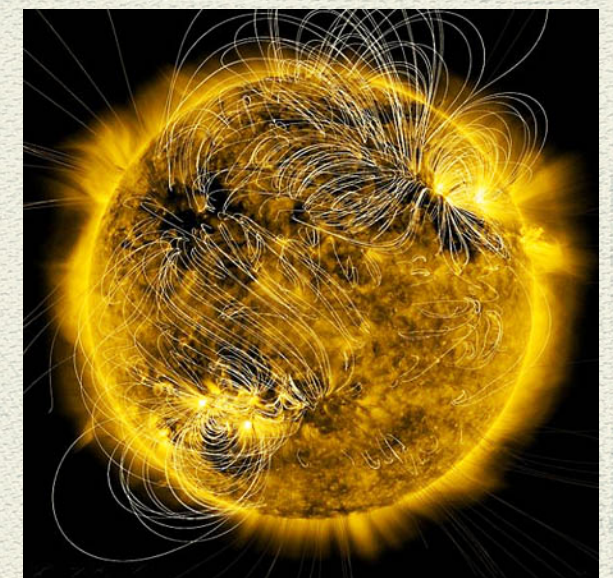
PANDORA's fall-out for Cosmic Magnetic Fields

Since George Ellery Hale (1908) we measure *LS-coupling* magnetic fields



(a) A sunspot

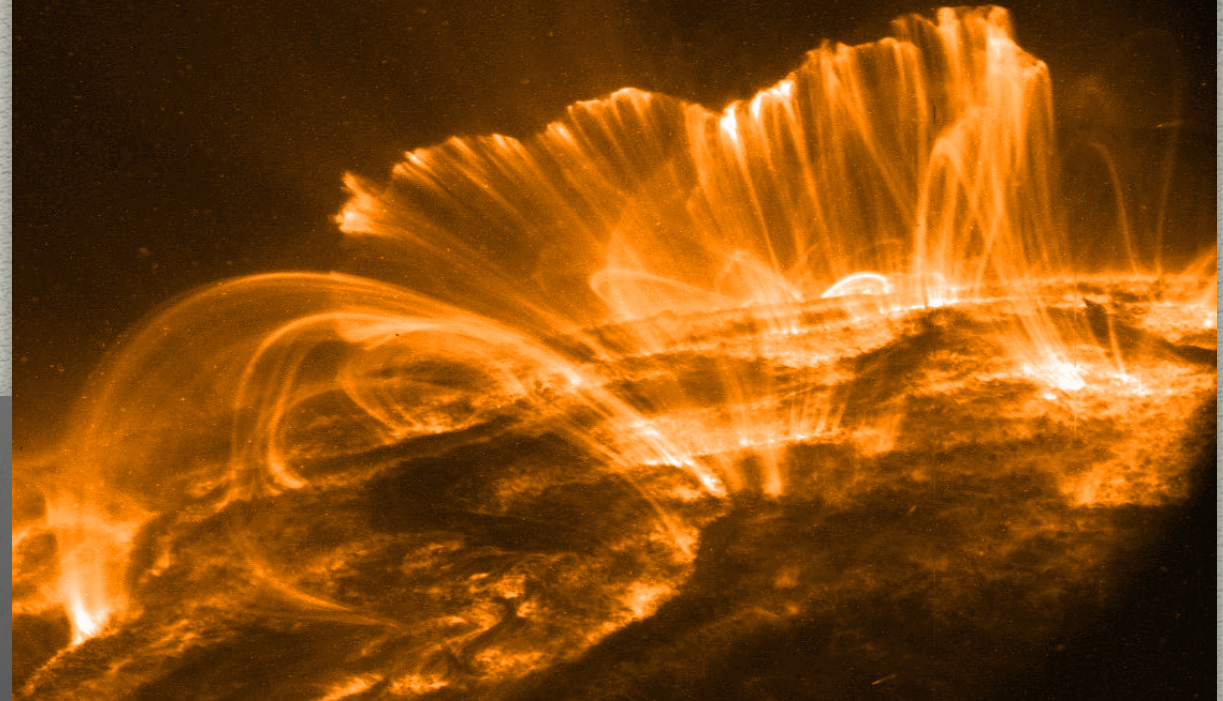
(b) The spectrum in and around the sunspot



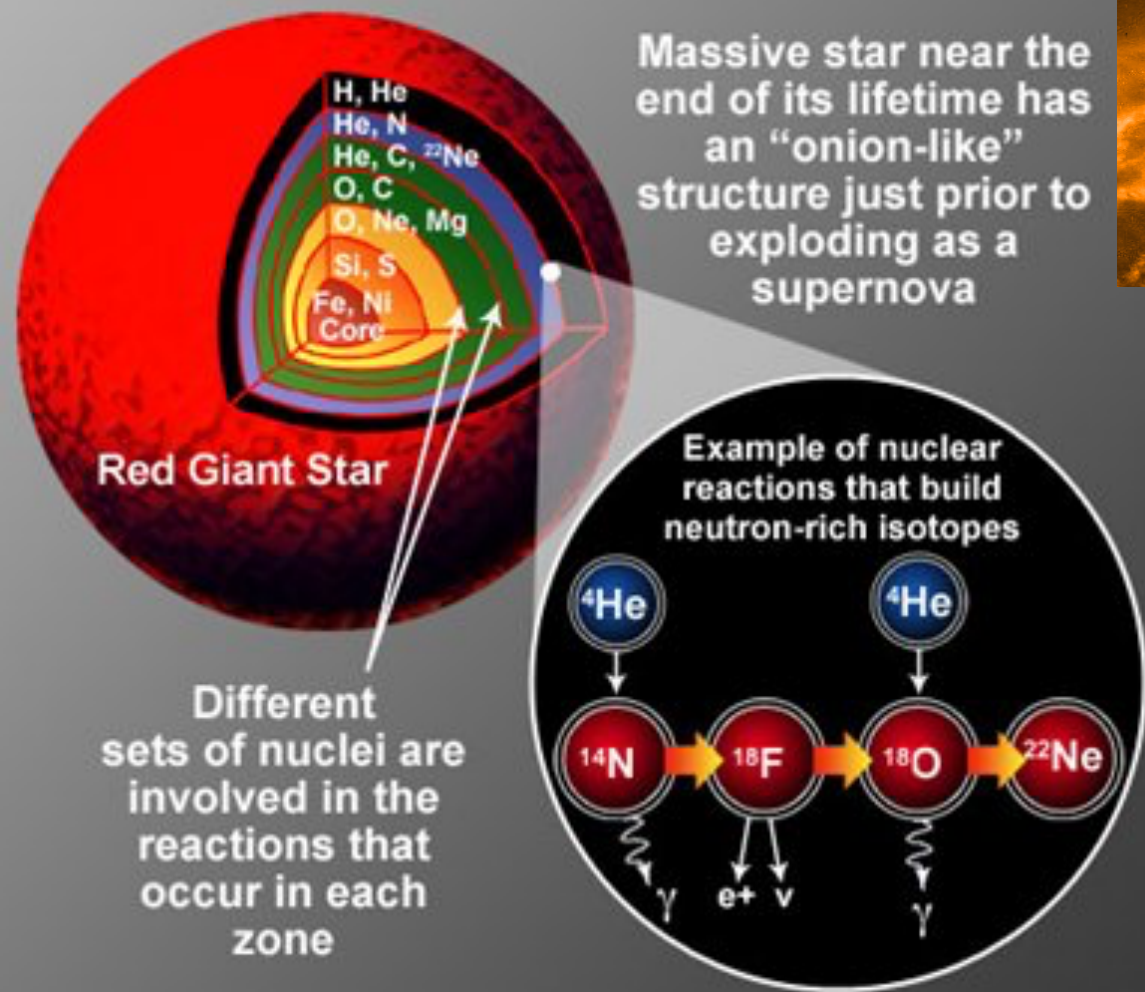
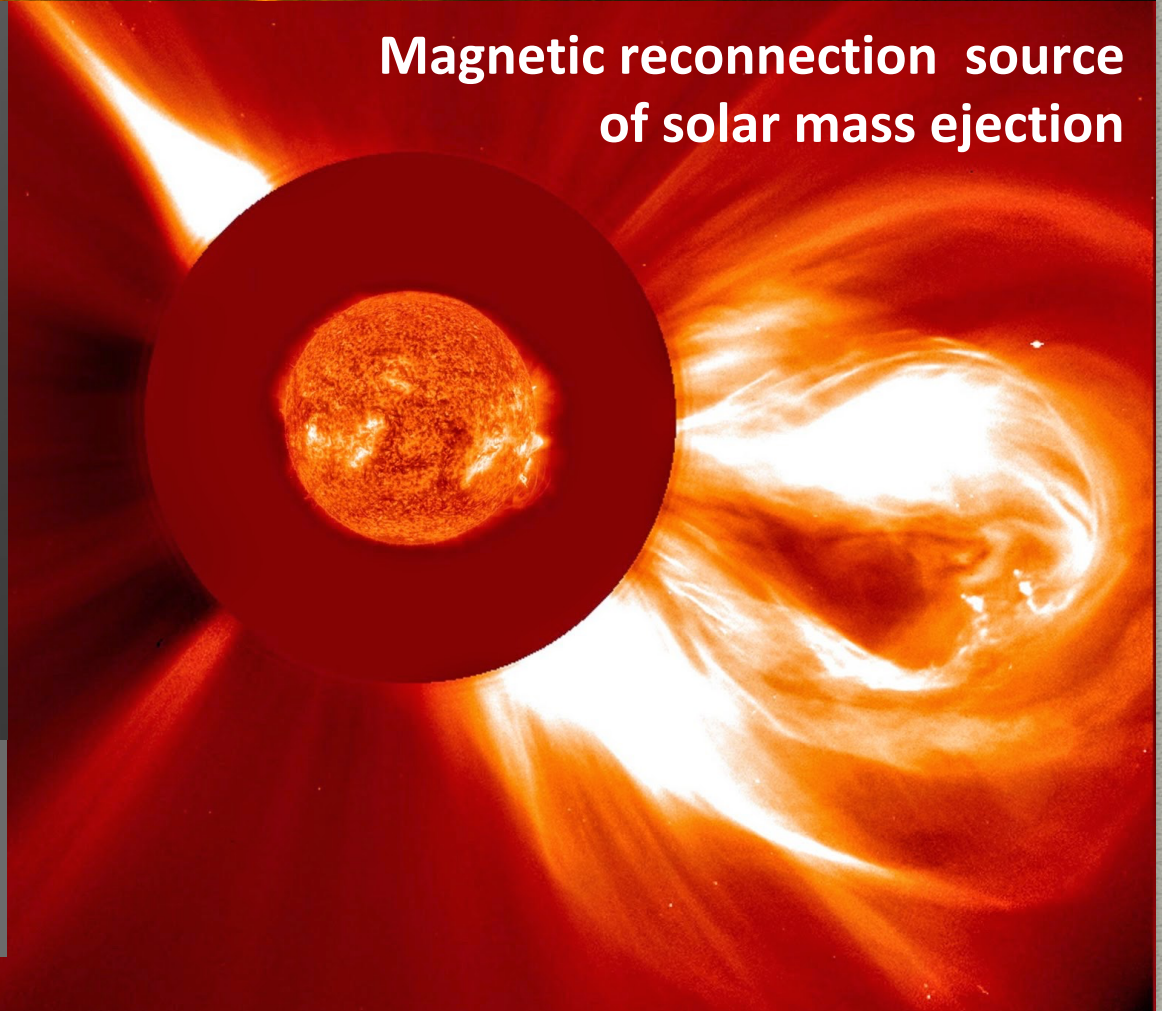
Building In-laboratory **DATABASE** of Landé factors

First-light PANDORA Astrophysics

Alfvén waves source for coronal heating



Magnetic reconnection source of solar mass ejection



Nuclear reactions for Stellar Structure and Chemical evolution

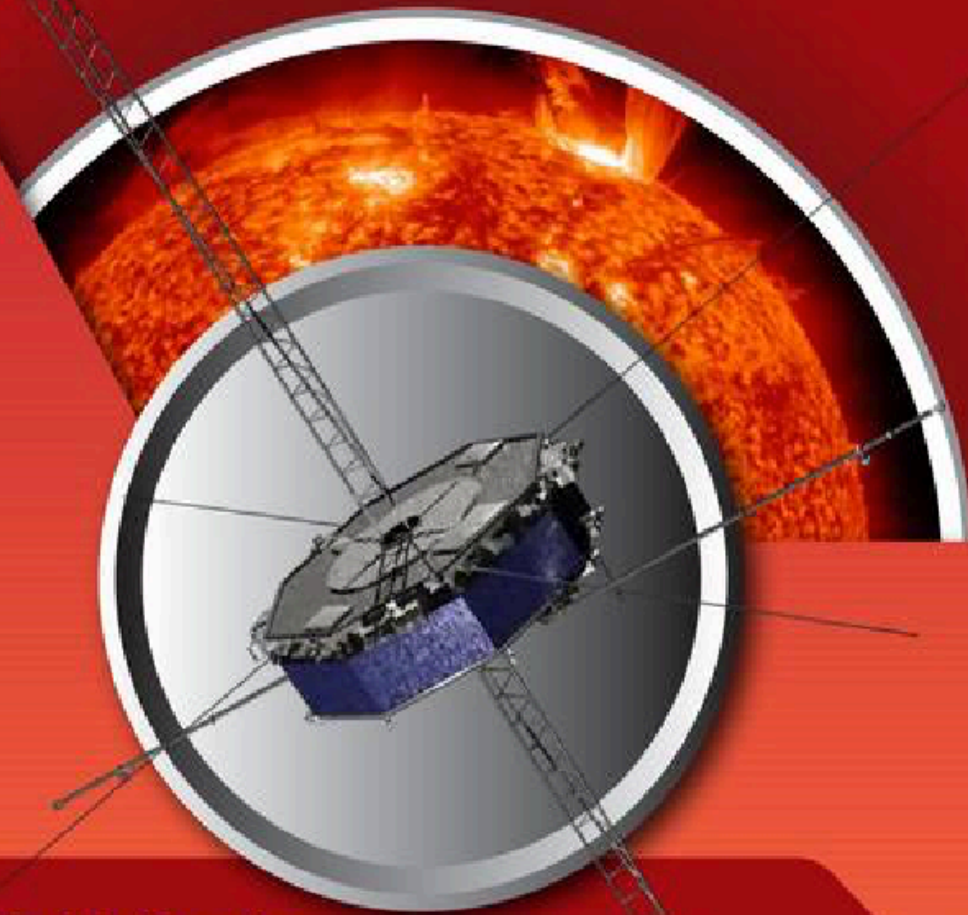
National Aeronautics and Space Administration



MAGNETIC RECONNECTION

Magnetic fields go in, energy comes out. Magnetic reconnection is a fundamental process of nature that happens all across our universe.

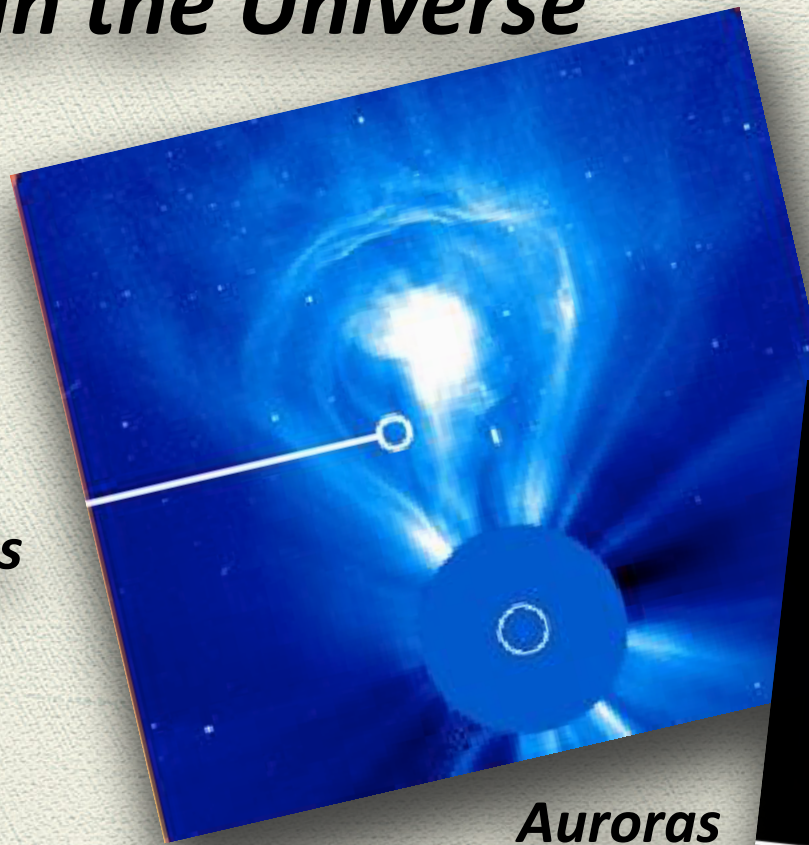
NASA's Magnetospheric Multiscale, or MMS, mission studies magnetic reconnection near Earth so we can understand it everywhere.



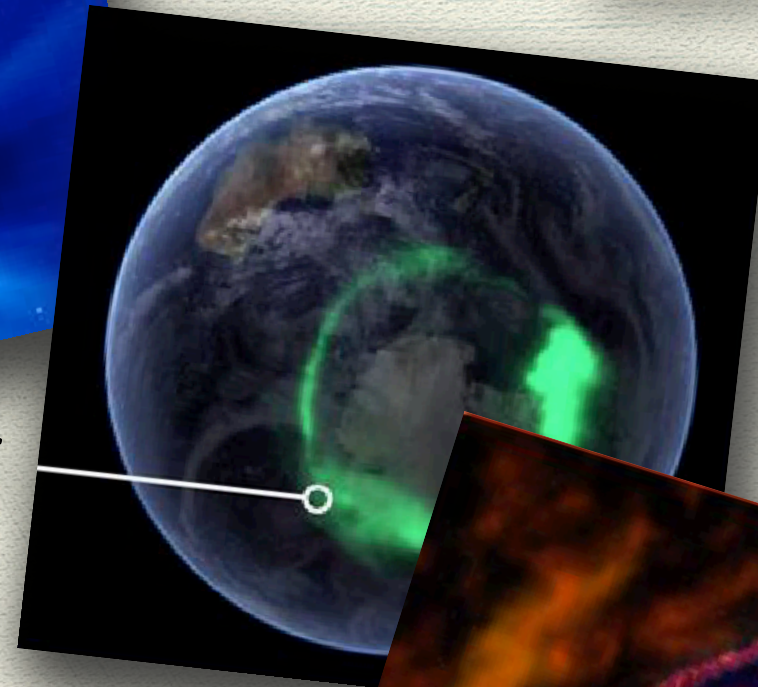
Magnetic Reconnection occurrence in the Universe

*PANDORA's
fall-out for
Observative
Astrophysics*

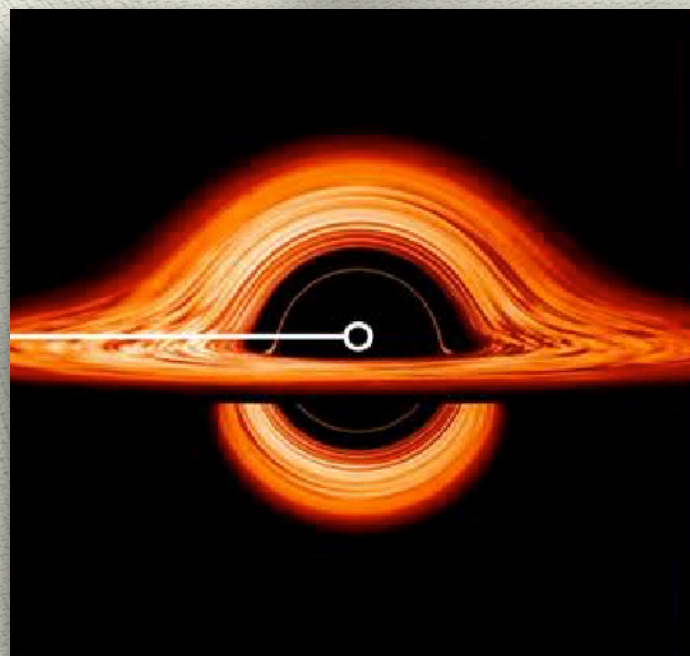
*Coronal mass
ejection*



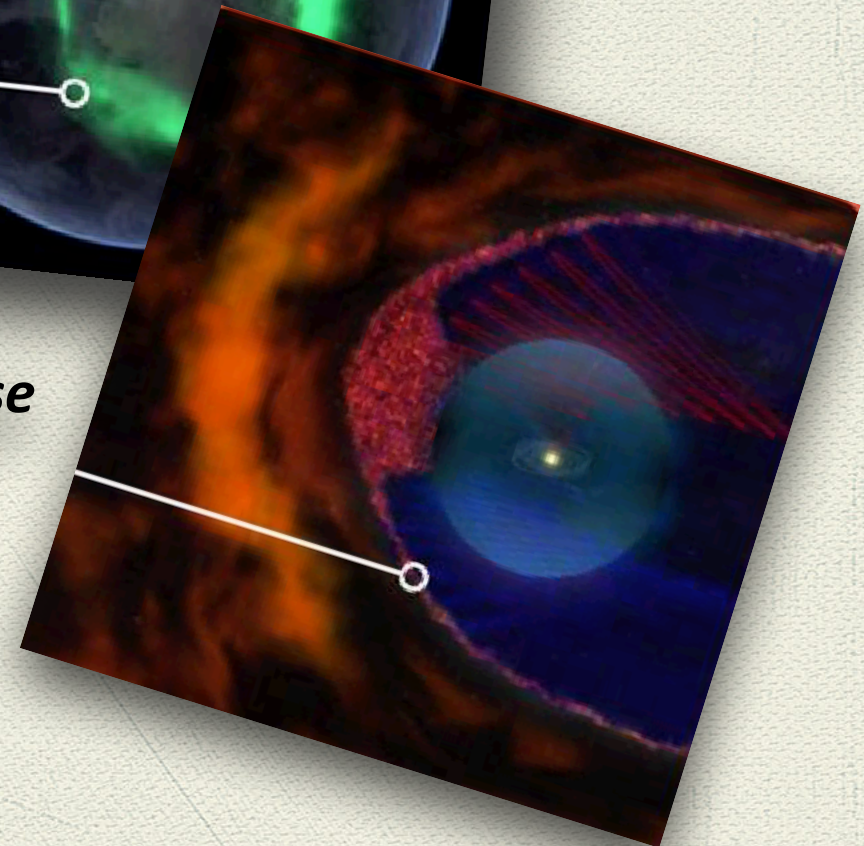
Auroras



Black holes



Heliopause



Spectroscopic identification of r-process nucleosynthesis in a double neutron-star merger

E. Pian¹, P. D'Avanzo², S. Benetti³, M. Branchesi^{4,5}, E. Brocato⁶, S. Campana², E. Cappellaro³, S. Covino², V. D'Elia^{6,7}, J. P. U. Fynbo⁸, F. Getman⁹, G. Ghirlanda², G. Ghisellini², A. Grado⁹, G. Greco^{10,11}, J. Hjorth⁸, C. Kouveliotou¹², A. Levan¹³, L. Limatola⁹, D. Malesani⁸, P. A. Mazzali^{14,15}, A. Melandri², P. Møller¹⁶, L. Nicastro¹, E. Palazzi¹, S. Piranomonte⁶, A. Rossi¹, S. Rosswog¹⁷, M. Ruffert¹⁸, S. Saviane¹⁹, S. Schady²⁰, S. S. Shupe²¹, S. S. Shupe²², S. S. Shupe²³, S. S. Shupe²⁴, S. S. Shupe²⁵, S. S. Shupe²⁶, S. S. Shupe²⁷, S. S. Shupe²⁸, S. S. Shupe²⁹, S. S. Shupe³⁰, S. S. Shupe³¹, S. S. Shupe³², S. S. Shupe³³, S. S. Shupe³⁴, S. S. Shupe³⁵, S. S. Shupe³⁶, S. S. Shupe³⁷, S. S. Shupe³⁸, S. S. Shupe³⁹, S. S. Shupe⁴⁰, S. S. Shupe⁴¹, S. S. Shupe⁴², S. S. Shupe⁴³, S. S. Shupe⁴⁴, S. S. Shupe⁴⁵, S. S. Shupe⁴⁶, S. S. Shupe⁴⁷, S. S. Shupe⁴⁸, S. S. Shupe⁴⁹, S. S. Shupe⁵⁰, S. S. Shupe⁵¹, S. S. Shupe⁵², S. S. Shupe⁵³, S. S. Shupe⁵⁴, S. S. Shupe⁵⁵, S. S. Shupe⁵⁶, S. S. Shupe⁵⁷, S. S. Shupe⁵⁸, S. S. Shupe⁵⁹, S. S. Shupe⁶⁰, S. S. Shupe⁶¹, S. S. Shupe⁶², S. S. Shupe⁶³, S. S. Shupe⁶⁴, S. S. Shupe⁶⁵, S. S. Shupe⁶⁶, S. S. Shupe⁶⁷, S. S. Shupe⁶⁸, S. S. Shupe⁶⁹, S. S. Shupe⁷⁰, S. S. Shupe⁷¹, S. S. Shupe⁷², S. S. Shupe⁷³, S. S. Shupe⁷⁴, S. S. Shupe⁷⁵, S. S. Shupe⁷⁶, S. S. Shupe⁷⁷, S. S. Shupe⁷⁸, S. S. Shupe⁷⁹, S. S. Shupe⁸⁰, S. S. Shupe⁸¹, S. S. Shupe⁸², S. S. Shupe⁸³, S. S. Shupe⁸⁴, S. S. Shupe⁸⁵, S. S. Shupe⁸⁶, S. S. Shupe⁸⁷, S. S. Shupe⁸⁸, S. S. Shupe⁸⁹, S. S. Shupe⁹⁰, S. S. Shupe⁹¹, S. S. Shupe⁹², S. S. Shupe⁹³, S. S. Shupe⁹⁴, S. S. Shupe⁹⁵, S. S. Shupe⁹⁶, S. S. Shupe⁹⁷, S. S. Shupe⁹⁸, S. S. Shupe⁹⁹, S. S. Shupe¹⁰⁰

"Stars in Jar" → The issue of astrophysical plasma opacities

THE ASTROPHYSICAL JOURNAL, 774:25 (13pp), 2013 September 1

doi:10.1088/0004-637X/774/1/25

© 2013. The American Astronomical Society. All rights reserved. Printed in the U.S.A.

OPACITIES AND SPECTRA OF THE r-PROCESS EJECTA FROM NEUTRON STAR MERGERS

DANIEL KASEN^{1,2}, N. R. BADNELL³, AND JENNIFER BARNES^{1,2}

¹ Department of Physics and Astronomy, University of California, Berkeley, CA 94720, USA

² Nuclear Science Division, Lawrence Berkeley National Laboratory, 1 Cyclotron Road, Berkeley, CA 94720, USA

³ Department of Physics, University of Strathclyde, Glasgow G4 0NG, UK

Received 2013 March 5; accepted 2013 June 24; published 2013 August 12

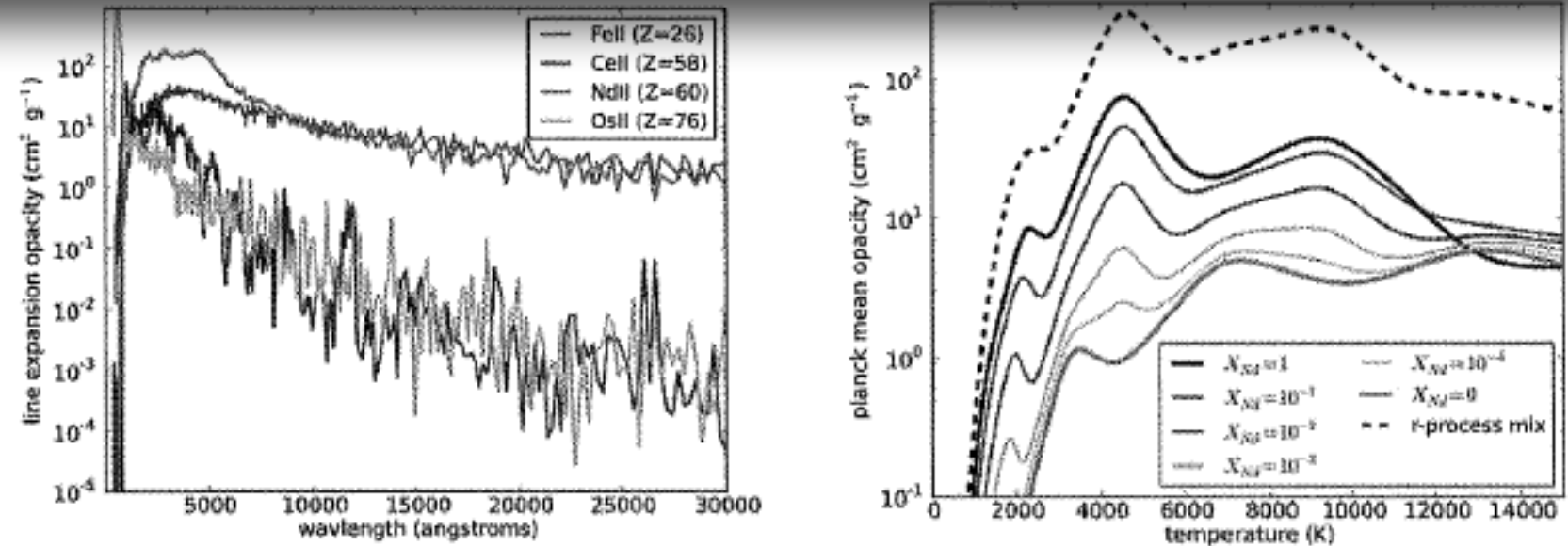
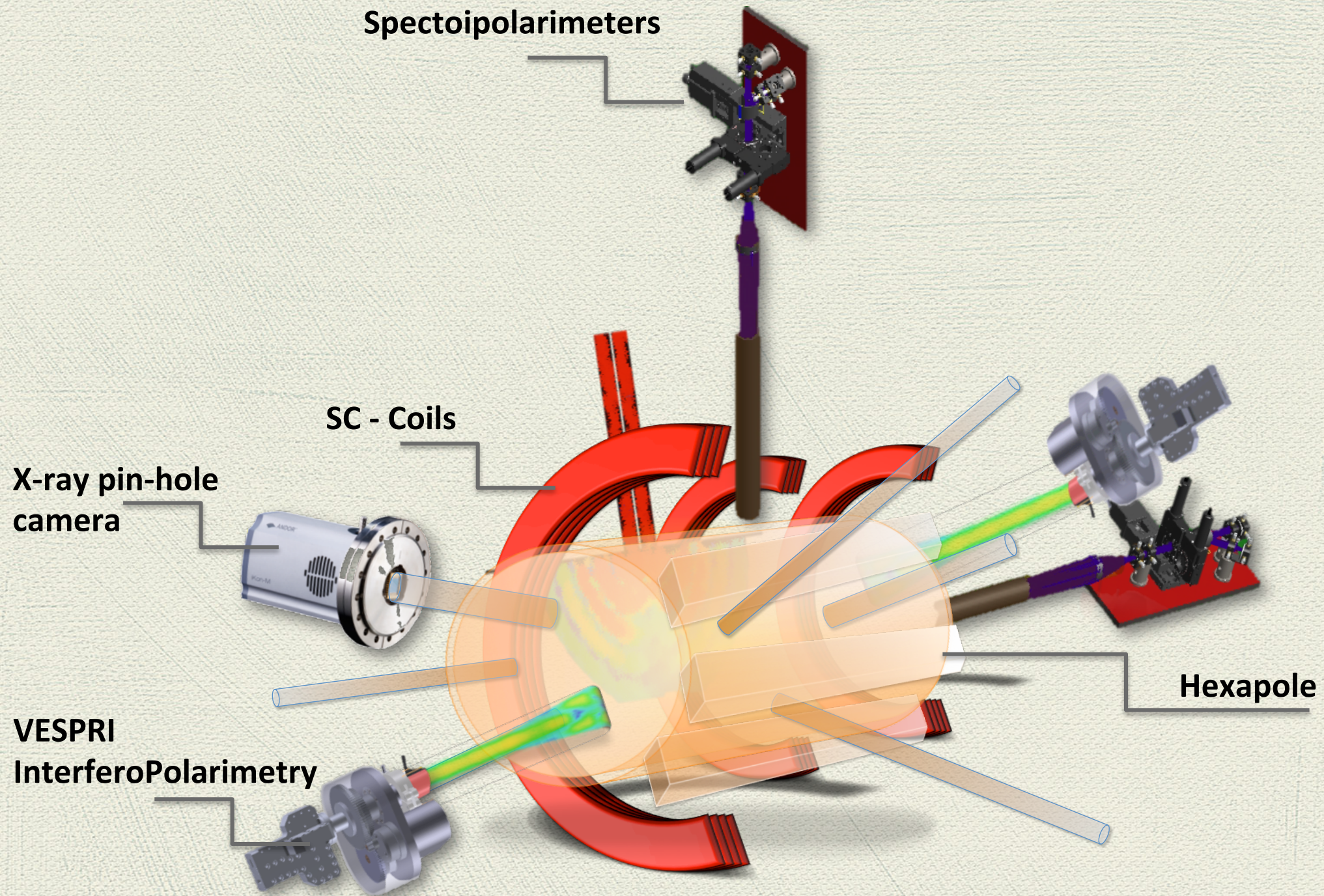


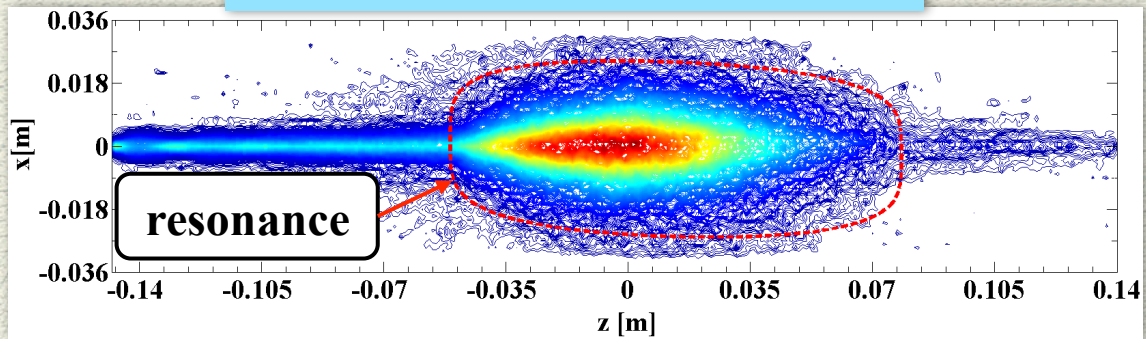
Figure 2: **Left:** Line opacity as a function of wavelength, comparing elements with d-shell valence shell electrons (iron, cerium) to lanthanides with f-shell electrons (e.g. Nd, Os). **Right:** Planck mean opacities, $\kappa_{\text{Pl}} = \frac{\int_0^\infty \kappa_\nu B_\nu(T) d\nu}{\int_0^\infty B_\nu(T) d\nu}$, for ejecta containing different mass fractions of lanthanides X_{Nd} , the remainder being non-lanthanides $X_{\text{Fe}} = 1 - X_{\text{Nd}}$. From Kasen et al. (2013).



PANDORA Multi-Diagnostics approach

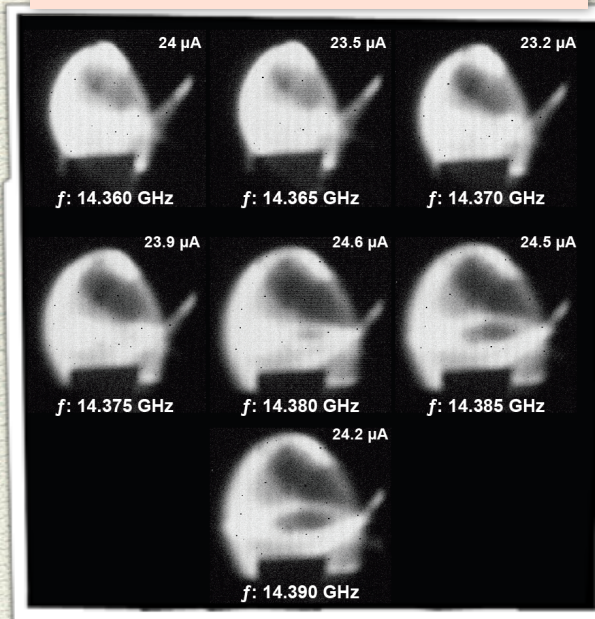


Charge breeding process

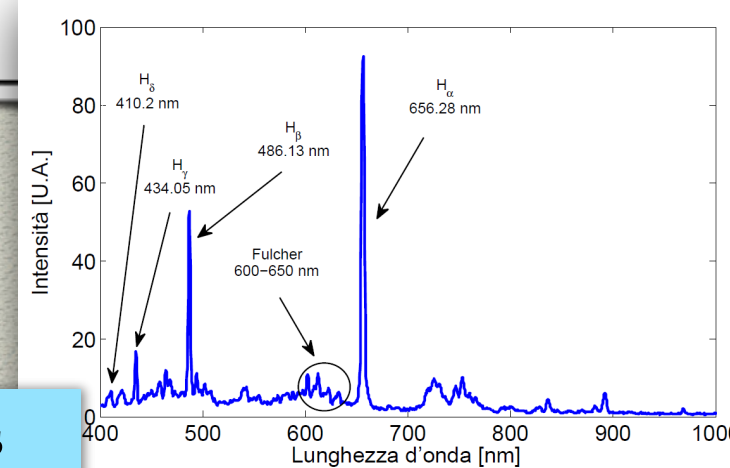
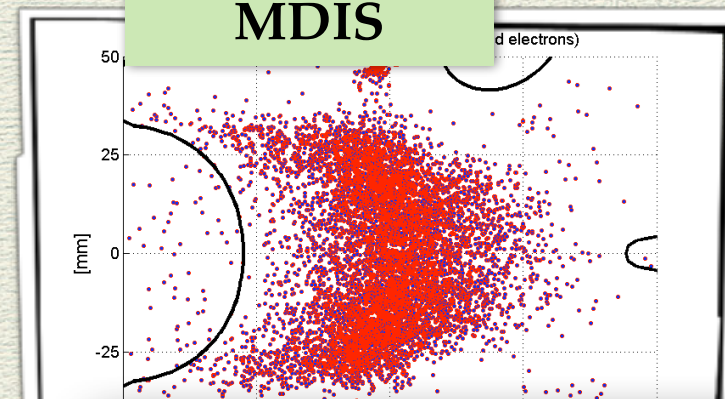


jointly with LNL (A. Galatà)

Beam diagnostics



OES and operations of MDIS



wave-plasma interaction

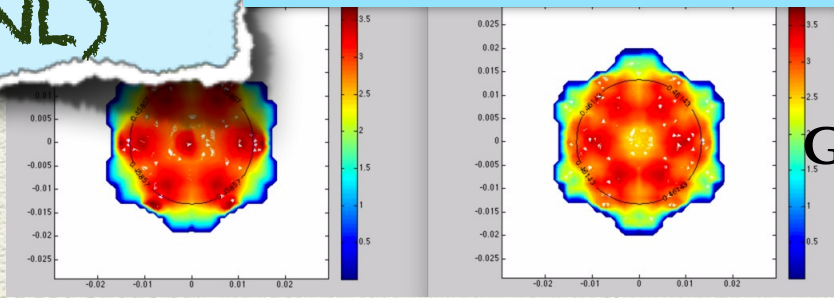


D. Nicolosi, R. Crispino, A. Mazzaglia

G. Castro, M. Mazzaglia, L. Neri

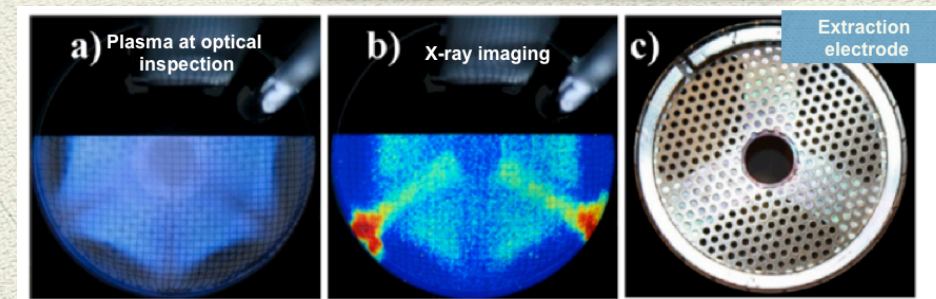
PLASMA
team@LNS
(and LNL)

self-consistent models



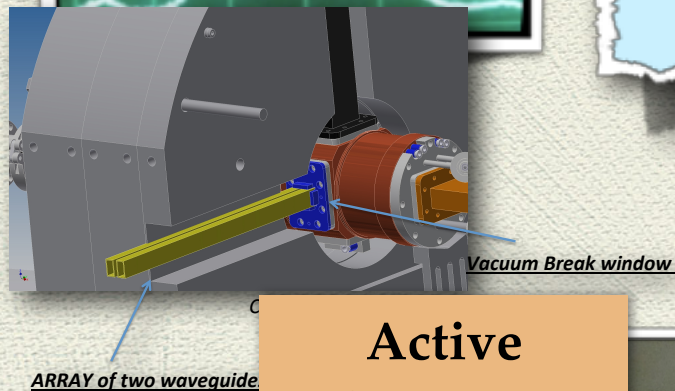
G. Torrissi, A. Galatà

X-ray imaging and spectroscopy



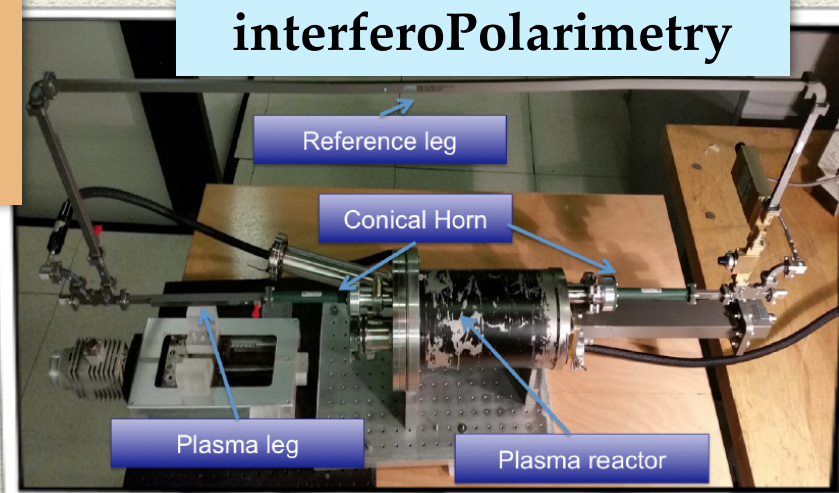
R. Rach, C. Caliri, C. Altana

Active microWaves launching



G. Castro,
G. Torrissi

interferoPolarimetry



G. Torrissi, E Naselli, M. Roccasalva

Many thanks to the LNS plasma & ion source group



The presentation is the results of a collective effort by senior and young colleagues!

Many thanks to Santo Gammino, Luigi Celona, Alessio Galatà, Giuseppe Torrisi, Giuseppe Castro, Lorenzo Neri, Eugenia Naselli, Maria Mazzaglia, Marina Giarrusso, Franco Leone, Carlo Sportato, Tommaso Podestà, Gianluigi Cosentino, Mario Musumeci, Sara Palmerini, Cristian Massimi, Vincenza Bonanno

Thank you for your attention!!





Achievements and Perspectives

• We are now able to see what happens into the plasma and to model through numerical simulations how it could be happen differently (and in a better way)

• Microwave absorption oriented design is needed: Power deposition into the plasma must be done in a highly controlled way

→ Single pass absorption

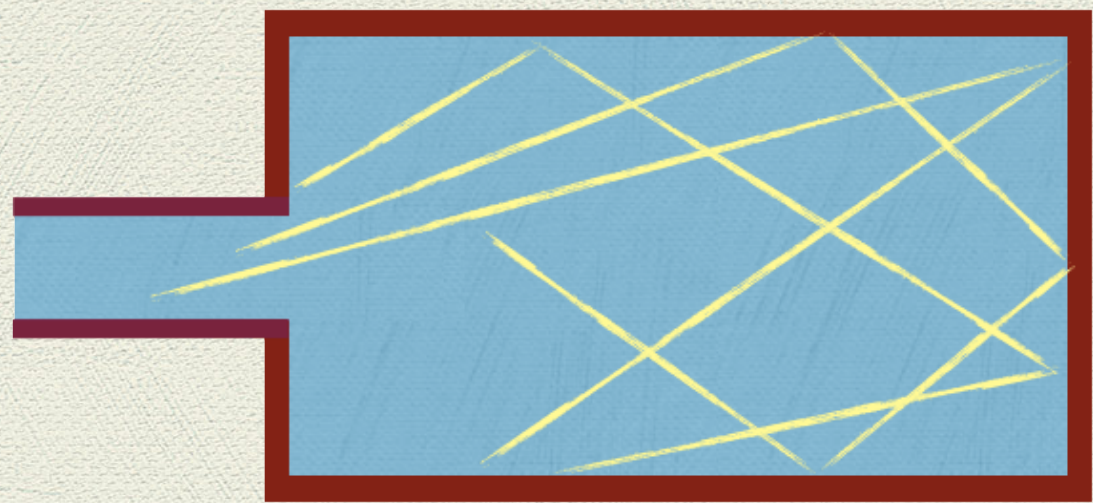


Some ideas



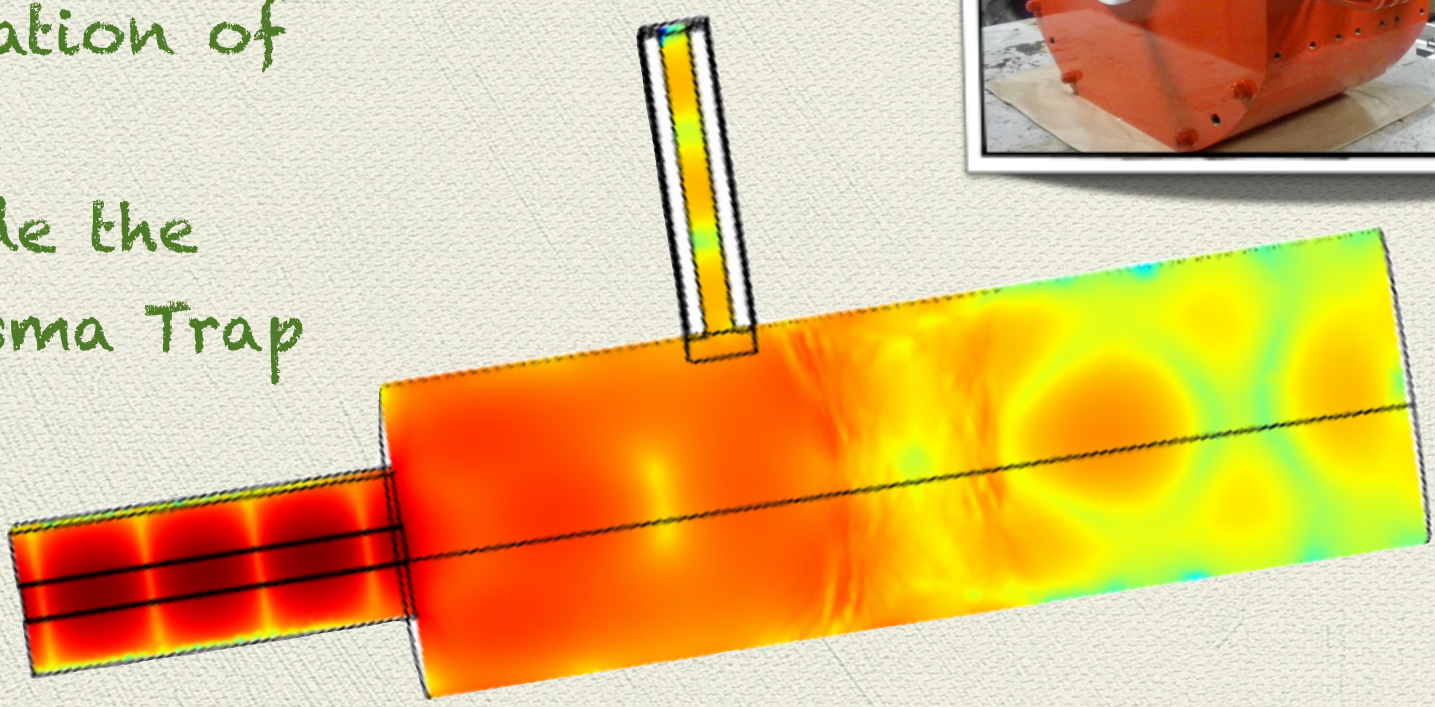
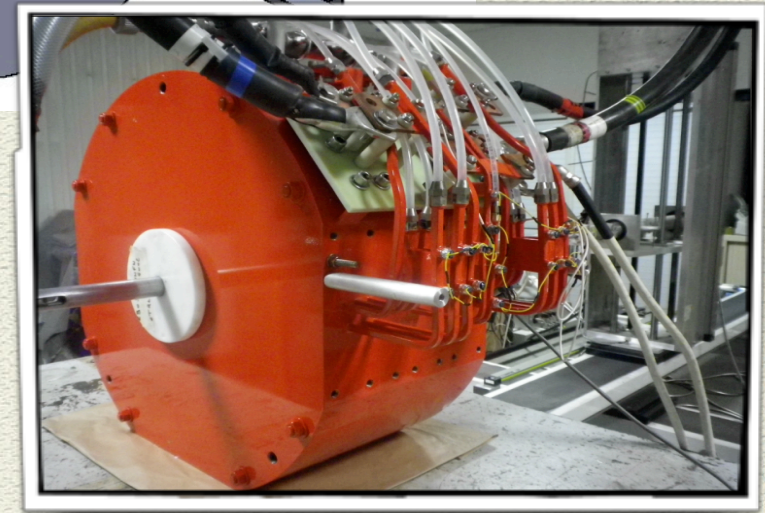
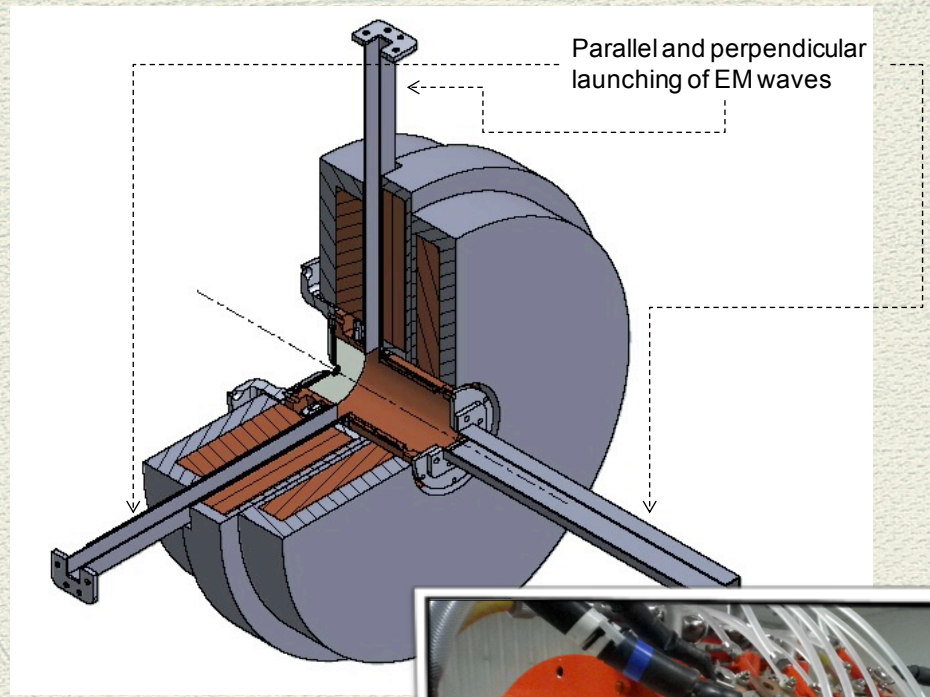
- **STILL IN ECR-heating** paradigm: are cylindrical shapes of the plasma chamber still mandatory?
- **OVERCOMING ECR-heating** paradigm: on-purpose design of launchers

"Microwave-absorption-oriented" design



M.A. + guiding + resonator scheme

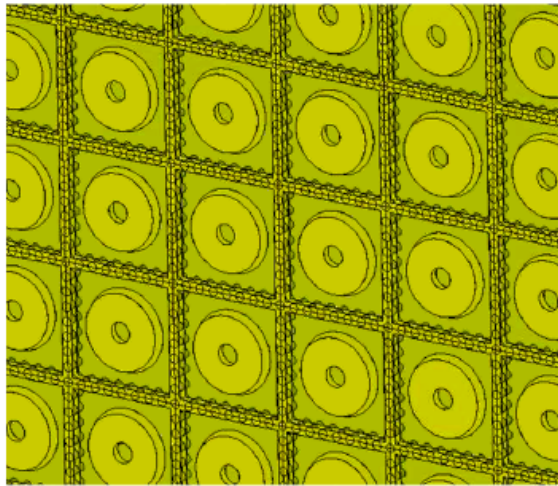
Full-wave calculation of the electric field distribution inside the new Flexible Plasma Trap at INFN-LNS



"Microwave-absorption-oriented" design

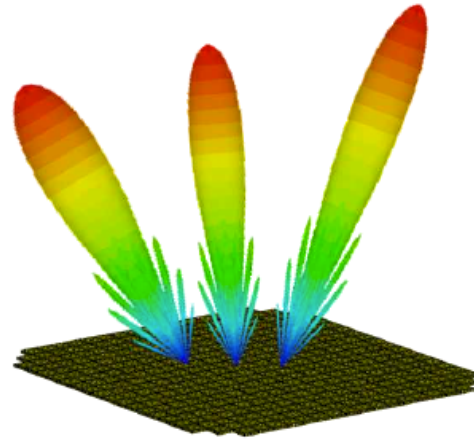
What are they?

Many radiators in close proximity



Why are they used?

Beam control with fixed geometry



16 X 4
waveguides

Plasma chamber

Plasma
heating
@ 7 GHz

Vacuum Break window

Courtesy of S. Passarello

ARRAY of two waveguides as
Alternative plasma heating @ 14 GHz

4.6 GHz / 16x4 GRILL, 1.0 MW net

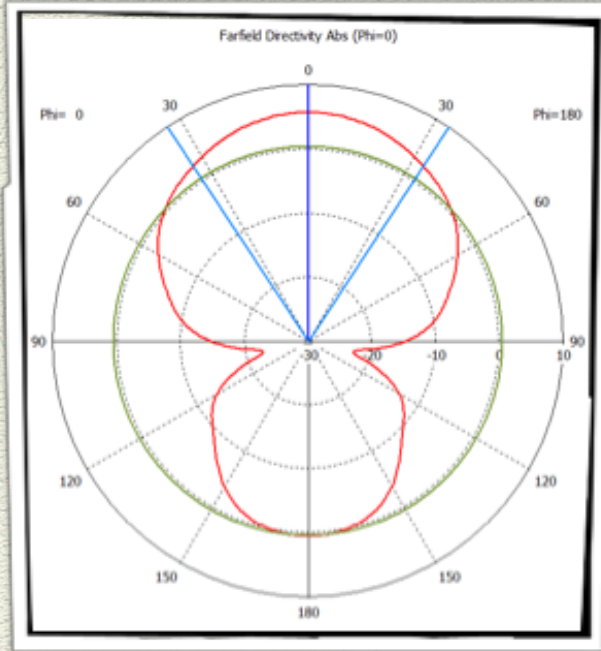
Reflectometer
horns

Langmuir
probes

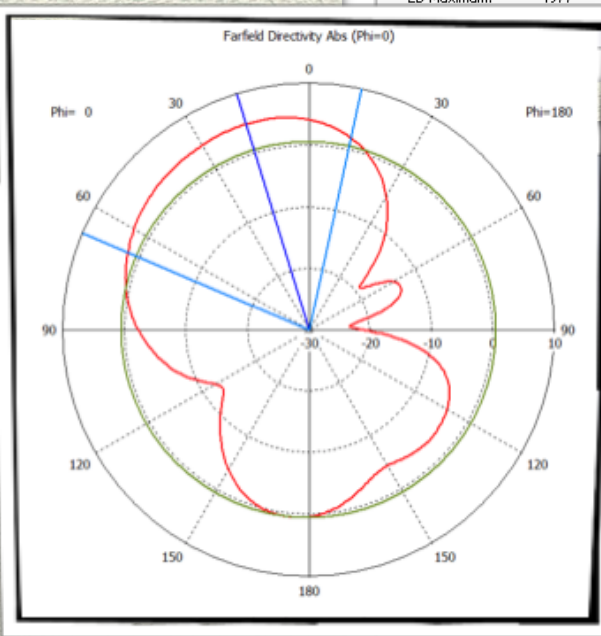
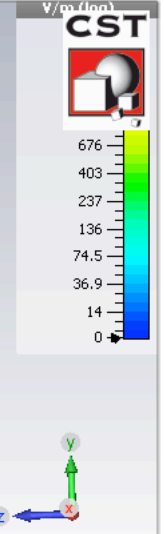
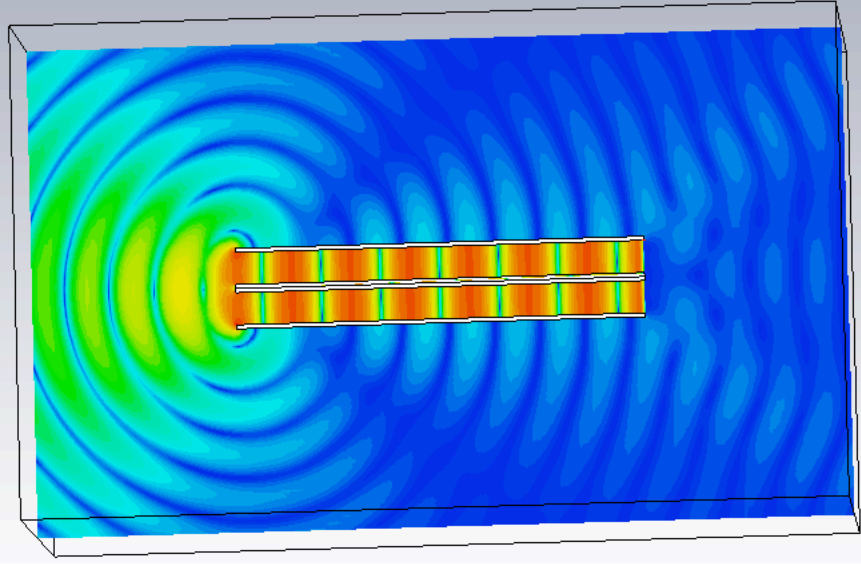
Fixed private limiters

"Microwave-absorption-oriented" design

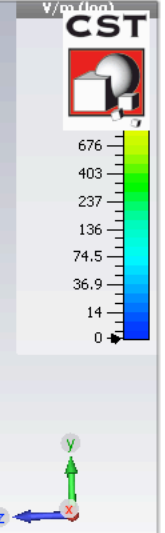
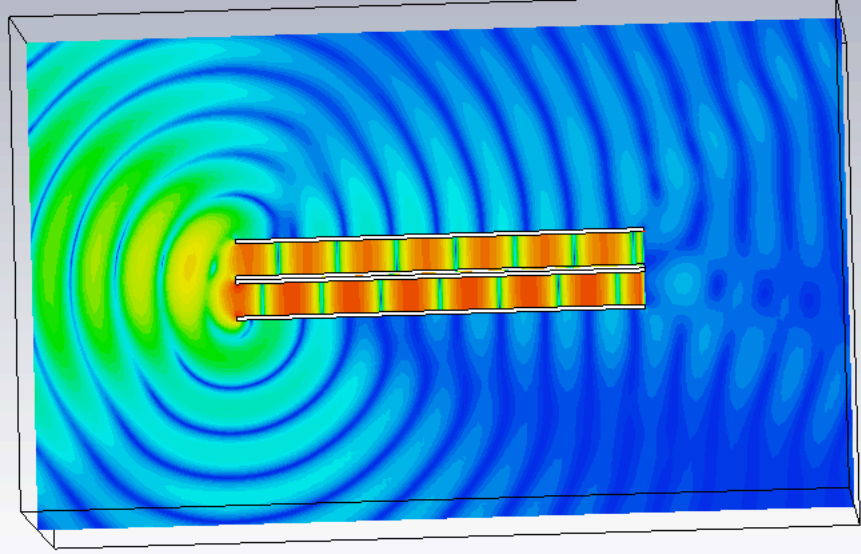
Launcher by "two-waveguides-array": lobe tilt by phase shift for optimizing oblique coupling of O-modes --> modal conversion



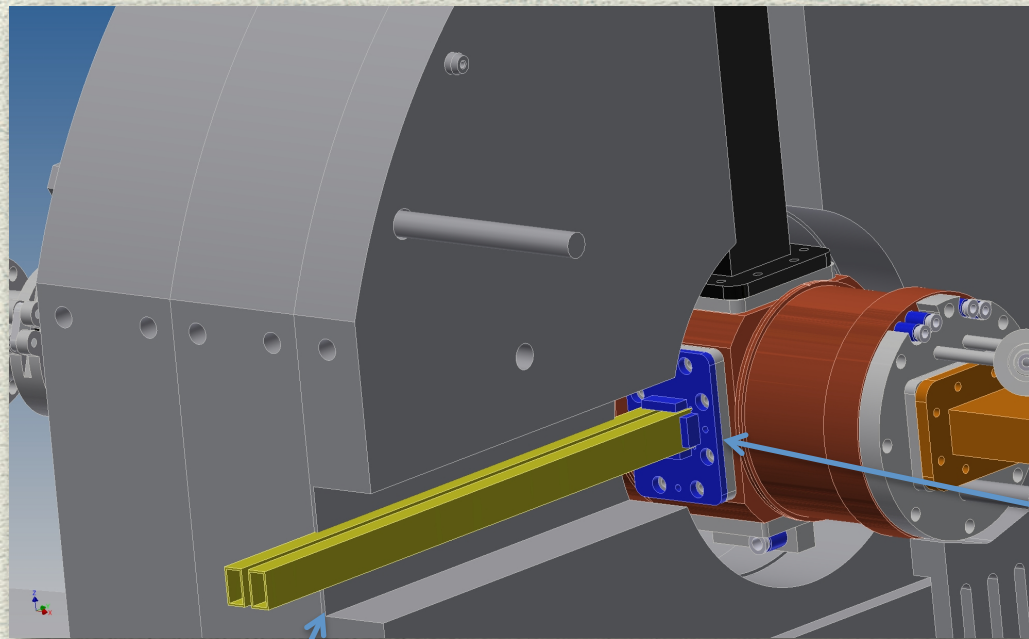
e-field (f=14) [1[1,0]+2[1,0],[15.2]] (peak)
 Cutplane normal: 1, 0, 0
 Cutplane position: 0
 Component: Abs
 2D Maximum: 4977



1,0,45],[15.2]] (peak)
 Cutplane normal: 1, 0, 0
 Cutplane position: 0
 Component: Abs
 2D Maximum: 5031
 Frequency: 14
 Phase: 303.75



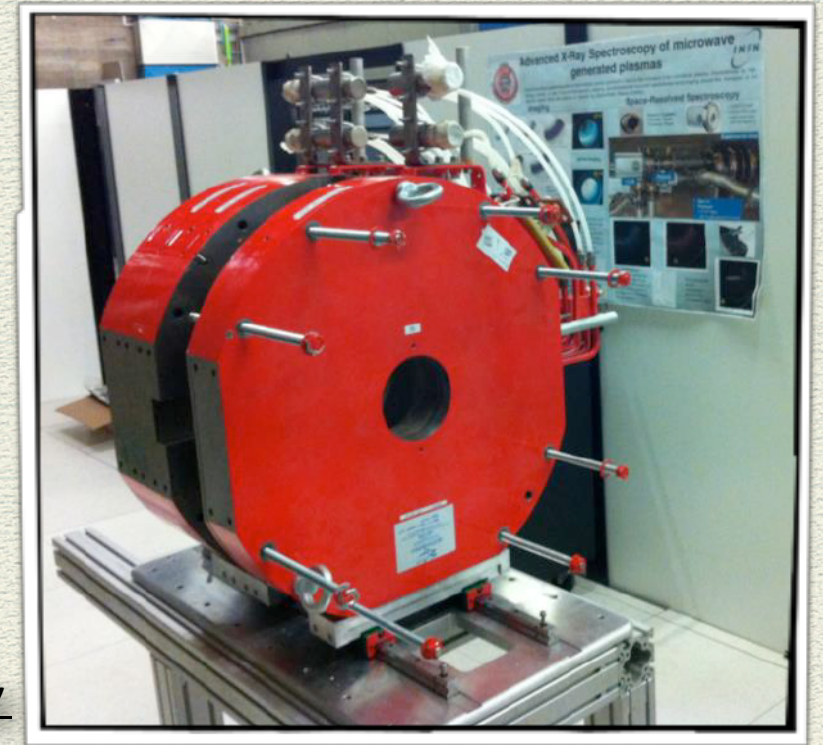
Mechanical Implementation at LNS



Vacuum Break window

Courtesy of S. Passarelo

ARRAY of two waveguides



A new setup developed at LNS for fundamental studies: RF launcher construction is ongoing

